5-9-2007

The Bioinorganic Chemistry Of Copper-Containing Systems: From Type-3 Systems Pertinent To Alzheimer's Disease To Mononuclear Hydrolysis Involved In Biological Development

Giordano Faustini Zimmerer Da Silva
University of South Florida

The Bioinorganic Chemistry Of Copper-Containing Systems: From Type-3 Systems Pertinent To Alzheimer's Disease To Mononuclear Hydrolysis Involved In Biological Development

by

Giordano Faustini Zimmerer Da Silva

A dissertation submitted in partial fulfillment
of the requirements for the degree of
Doctor of Philosophy
Department of Chemistry
College of Arts and Sciences
University of South Florida

Co-Major Professor: Li-June Ming, Ph.D.
Co-Major Professor: Brian T. Livingston, Ph.D.
Steven H. Grossman, Ph.D.
Randy L. Larsen, Ph.D.

Date of Approval:
May 9, 2007

Keywords: kinetics, reactive oxygen species, metallopeptide, amyloid, enzymology, sea urchin, metalloprotease

NOTE TO THE READER

Note to Reader: The original of this document contains color that is necessary for understanding the data. The original dissertation is on file at the USF library in Tampa, FL.

DEDICATION

Although the graduate school experience is highly a personal journey, it would be foolish to believe that I was solely responsible for my accomplishments. I then would like to dedicate this work to all of those who have played a major role in this difficult yet rewarding part of my life. First my grandmother Ermelinda who is the sole reason why I am in the US, my parents Mauricio and Marta for sacrificing the presence of their son, and my sister Marcella for being sibling, friend and parent through part of my formative years. Second I must dedicate this work to the Kelley family for being my parents, brother, and sisters; Moms, Pops, John, Tere, and Abbie, I would not be here today without your love and support. Last and not least I must also dedicate this work to Rachel for being a friend, always in my heart, through difficult and joyous times, for her love and support without which I would have never remained in the US. I truly hope that the rest of my career will make the efforts of all of those herein mentioned worthwhile.

ACKNOWLDGEMENTS

I must acknowledge my friends Bri and Brenda, who were my sisters through the laughter, tears, and often difficult times, and hope to remain life-long friends. I must also acknowledge William and Kash for being brothers in arm, and Vaso for inspiration. I would also like to acknowledge Altan for being a patient mentor during my undergraduate years and believing in my potential. I would like to acknowledge my collaborator Dr. Alexander Angerhofer from UF for his availability and willingness to share his time and effort. Rae Reuille must be acknowledged for her patience and guidance while teaching molecular biology to a chemist. Dr. Randy Larsen and Dr. Steven Grossman must also be acknowledged for their efforts as my committee members and for always being present to discuss matters of science, life, history, and politics. Last and not least I must acknowledge Dr. Li-June Ming and Dr. Brian T. Livingston. In an ever-changing academic world it is often difficult to find mentors who still have a pure scholar's mind. Through their efforts, patience, guidance, and discussions about science and life, I feel prepared to move on to the next stage of the scientific experience. They were teachers, mentors, and friends and I am eternally grateful for their time. I truly hope that the rest of my career will make the efforts of all of those herein mentioned worthwhile.

TABLE OF CONTENTS

LIST OF TABLES

LIST OF FIGURES

LIST OF ABBREVIATIONS

AD:	Alzheimer's disease
Aβ:	Amyloid-β
CuO:	Copper-oxygen intermediate
Hcy:	Hemocyanin
Tyr:	Tyrosinase
ROS:	Reactive Oxygen Species
kDa:	kilo Daltons
APP:	Amyloid Precursor Protein
ADP:	Adenosine 5' diphosphate
ATP:	Adenosine 5' triphosphate
ET:	Electron Transfer
DTT:	Dithiothreitol
EDTA:	Ethylenediaminetetraacetic acid
$NADP^+$:	Nicotinamide adenine dinucleotide phosphate, oxidized form
NADPH:	Nicotinamide adenine dinucleotide phosphate, reduced form
NAD^+:	Nicotinamide adenine dinucleotide, oxidized form

NADH:	Nicotinamide adenine dinucleotide, reduced form
PAGE:	Polyacrylamide gel electrophoresis
SDS:	Sodium dodecyl sulfate
Tris:	Tris(hydroxymethyl)aminomethane
DNA:	Deoxyribonucleic acid
mRNA:	Messenger ribonucleic acid
cDNA:	Complementary DNA
COX:	Cytochrome oxidase activity
CSF:	Cerebral spinal fluid
mtDNA:	Mitochondrial DNA
dsDNA:	Double stranded deoxyribonucleic acid
SOD:	Superoxide dismutase
MnSOD:	Manganese dependent superoxide dismutase
CuZnSOD:	Copper-Zinc dependent superoxide dismutase
PHF:	Paired helical fragments
CNS:	Central nervous system
^{1}H NMR:	Proton nuclear magnetic resonance
CW-EPR:	Continuous wave electron paramagnetic resonance
ESEEM:	Electron spin echo envelope modulation
RAGE:	Receptor for advanced glycation endproducts
ERAB:	Endoplasmic reticulum amyloid- β binding protein
PBN:	*N-tert*-butyl-a-phenylnitrone

PBS: Phosphate buffered saline

MNP: 2-methyl-2-nitrosopropane

PrP: Prion protein

DOPA: 3,4-dihydroxyphenylalanine

XAS: X-ray absorption spectroscopy

EXAFS: Extended X-ray absorption fine structure

DβM: Dopamine β hydroxylating monooxygenase

PHM: Peptidylglycine α-hydroxylating monooxygenase

PPh3: Triphenylphosphine

THB: 1,2,3,-trihydroxybenzene

DMSO: Dimethyl sulfoxide

HEPES: N-(2-hydroxyethyl)-piperazine-N'-2-ethanesulfonic acid

MES: 2-Morpholinoethanesulfonic acid

TAPS: N-Tris(hydroxymethyl)methyl-3-aminopropanesulfonic acid

CAPS: N-Cyclohexyl-3-aminopropanesulfonic acid

MBTH: 3-methyl-2-benzothiazolinone hydrazone

d^6DMSO: Deuterated dimethyl sulfoxide

UV-Vis: Ultraviolet-visible electronic spectroscopy

LMCT: Ligand to metal charge transfer transition

MALDI-TOF: Matrix assisted laser desorption mass spectrometry time of flight

KIE: Kinetic isotope effect

DTC: Di-tertbutyl catechol

DCC:	Dichlorocatechol
CMC:	Critical micelle concentration
GSH:	Reduced glutathione
NQI:	Nuclear quadrupole interactions
BP10:	Blastula Protease 10
CuBP10:	Copper derivative of Blastula protease 10
ZnBP10:	Zinc derivative of Blastula protease 10
BMP-1:	Bone morphogenetic protein 1
EGF:	Epidermal growth factor
ECM:	Extracellular matrix
suBMP:	Sea urchin bone morphogenetic protein 1
TGF-β:	Transformation growth factor β
CUB:	Complement-like domains
Ni-NTA:	Nickel nitrilotriacetic acid
BAPNA:	N-benzoyl-arginine-*p*-nitroanilide
IPTG:	Isopropyl-β-thiogalactopyronoside
PMSF:	Phenylmethyl sulfonyl fluoride
PCR:	Polymerase chain reaction
OD:	Optical density
CD:	Circular dichroism
BCA:	Bicinchoninic acid
APS:	Ammonium persulfate

TEMED:	N,N,N',N'-Tetramethylethylenediamine
OP:	1,10-phenanthroline
Arg-NHOH:	Arginine hydroxamate
MM3:	Molecular mechanics protocol

The Bioinorganic Chemistry of Copper-Containing Systems: from Type-3 Systems Pertinent to Alzheimer's Disease to Mononuclear Hydrolysis Involved in Biological Development

Giordano F.Z. da Silva

ABSTRACT

Although transition metals are essential for life, misregulation of redox-active metal uptake, delivery, storage, and excretion has been linked with a series of neurodegenerative disorders. Alzheimer's disease (AD) is considered an epidemic and is the most widespread of all forms of dementia. Copper ions found in large concentrations localized in amyloid-β plaques in the brain of AD patients have been linked with the generation of reactive oxygen species which are suspected to be the culprits leading to neuronal cell death. Herein a series of mechanistic and spectroscopic studies elucidate the chemistry about the metal-centered oxidation of biomolecules, including catecholamine neurotransmitters and some analogues by copper-complexes of amyloid-β peptide.

Transition metals can also be useful tools for characterization of metalloproteins due to their unique chemical and spectroscopic features. Herein a series of studies of the native Zn^{2+} and Cu^{2+}-derivative of recombinant Blastula Protease 10 (BP10) from the sea urchin *Paracentrotus lividus* are presented in order to elucidate its catalytic mechanism, with the use of enzymology, metal substitution, and electronic absorption spectroscopy.

CHAPTER I. COPPER-DIOXYGEN IN METABOLISM AND CATALYSIS

I. BACKGROUND

The interaction of transition metals with oxygen (O_2, or dioxygen) is of paramount importance in biological systems. The metal-O_2 interaction is ubiquitous in metabolic pathways of aerobic organisms on the earth's crust and it is fundamental to homeostasis by serving as catalysts in redox reactions as well as for the bidning and delivery of O_2 in aerobes.[1] For these purposes, iron and copper are the predominant, albeit not the only, transition metals utilized in metalloproteins and metalloenzymes. Classic examples of iron- containing O_2 transport metalloproteins include hemoglobin,[2] myoglobin,[2] and hemerythrin,[3] while redox-active non-heme iron metalloenzymes involved in O_2 metabolism include methane monooxygenase,[4] and protocatechuate 3,4 dioxygenase.[5] Copper is also well represented in the area of O_2-binding with hemocyanin[6] being the classic example, while catalytic copper-centers include tyrosinase,[6] catechol oxidase,[7] and galactose oxidase.[8]

Of particular interest in the recent years has been the nature of copper-O_2 centered chemistry in metalloenzymes. Several research groups have pursued spectroscopic characterization, crystallography, and biomimetic studies of metalloproteins that contain copper and can interact with O_2 through direct binding or for activation of O_2 in chemical reactions like hydroxylation and oxygenation. These copper metalloenzymes are collectively termed Type-3 copper proteins attributed to the magnetically coupled di-copper center.[6] Although the topic in this review is primarily from a health/disease or a more medicinal perspective, the lessons learned from the investigation of the chemistry of Type-3 copper proteins have some overlap with the area of neurodegeneration involving activated or reduced forms of O_2. The focus of this chapter will be the parallels of what is known about the chemistry of Type-3 copper oxidases and how it may relate to Alzheimer's disease.

The ability of binuclear copper centers in proteins to bind O_2 for transport and to use copper-O_2 (CuO_2) as the catalytic center for O_2 activation has provided a wealth of understanding in both experimental and theoretical chemistry. Understanding the interaction of O_2 with copper has been an intense area of study for bioinorganic chemists, both toward the native molecules and in biomimetic systems.[9,10] Research in this area has utilized the spectroscopic properties of the Type-3 copper proteins, as well as crystal structures when available, to serve as templates toward the synthesis of small model systems that allow the interactions of copper with O_2. Typically, the short-lived CuO_2 intermediates cannot be well resolved in the native systems either due to influence of the size of proteins in spectroscopic techniques that rely in magnetic resonance or because

crystal structures cannot offer a fast enough process in order to catch the transient species responsible for catalysis. Even in small biomimetic compounds, the unstable formation of CuO_2 intermediates has forced the determination of the structure of reactive intermediates at very low temperatures.[11] In fact, a significant effort has been made toward a systematic approach to synthesize biomimetic systems to approximate the chemical and spectroscopic properties of Type-3 copper proteins. The choice of ligands, bridging ligands, solvent systems, and temperature can play a significant role in the elucidation of both redox-activity of model systems and their electronic properties that give rise to the now typical spectroscopic fingerprints of Type-3 oxidases.

In Type-3 metalloprotein biomimetic systems, the coordination environment around the metal ion is typically constituted of strong donor ligands such as the nitrogen atoms of pyridines that can mimic the histidine residues which have been proposed to assist the stabilization of metal-oxygen intermediates for electrophilic substitutions and 2-electron oxidation chemistry. The stabilization of highly electrophilic/nucleophilic CuO_2 intermediates is also assisted by a large hydrophobic environment. However, several factors can influence the reactivity of these compounds; in essence, any alteration on solvent, and coordinated (and bridging) ligands will change the reactivity of these biomimetic compounds.[12] The now classic example of biomimetic O_2-binding copper complexes that mimic the spectroscopic and chemical properties of their natural templates can be traced back to the efforts of Nobumasa Kitajima, Kenneth D. Karlin, and Edward I. Solomon from the late 1980's to today.[13-16]

Although seemingly unrelated, the knowledge gained from investigating copper-O_2 interactions in metalloproteins and enzymes and their biomimetic analogues, may yield significant insight into the possible mechanism for metal-centered generation of reactive oxygen species (ROS). These ROS are generated at a metal center and may either diffuse away and cause damage to redox-sensitive biomolecules or remain bound to the metal and itself be an efficient redox catalyst. The common ground between these two areas of research then can be elucidated as the copper-O_2 interaction. From the detailed spectroscopy of biomimetic compounds and their protein templates, we have a library of diagnostic patterns to elucidate the nature of interactions of redox-active metals and O_2. From the detailed mechanistic investigation of the chemistry catalyzed by the metalloproteins and their model compounds we are now well aware of what reactivity can be expected from different conformations of reactive CuO_2 intermediates. In recent years, a darker side of copper-O_2 chemistry has surfaced in biological studies. As research in the areas of cancer, apoptosis, diabetes, heart disease, and neurodegenerative disorders becomes more focused and detailed, the metal-centered generation of ROS has become a common theme. In fact, much of the focus has been placed on the nature of ROS rather than the interaction of the redox-active metal center with the ROS. These ROS are the radical and reduced forms of oxygen that although present under normal metabolic conditions, could potentially damage oxidizable moieties in their environment if not properly regulated due to the much higher oxidation potential of ROS compared to O_2. ROS alone are able to damage every major type of biological molecule, including membranes (by peroxidation of lipids),[17] proteins (by oxidation of certain residues and

nitration by nitric oxide),[18] DNA (by destruction of the structural stability of the double helix as ribose is oxidized),[19] and smaller molecules such as neurotransmitters.[20] According to recent studies, OH•, $O_2•^-$, and H_2O_2 have been assigned as the culprits in several types of neurological disorders, with a large number of research groups focusing on the role of ROS in the etiology of Alzheimer's disease (AD).[21] However, as chemists further investigate the pathway of ROS generation and the fate of such molecules, it becomes more evident that a redox-active metal is necessary in order for the damaging and often lethal chemical imbalance that is caused by ROS ($E° = -300$ mV for the one electron reduction of O_2) to achieve its full neurodegenerative potential; in other words it is the metallo-ROS interaction that appears to be the culprit in oxidative stress that leads to neurodegeneration, not ROS alone. Recent observations demonstrate that although oxygen radicals and oxidation agents like H_2O_2 cannot achieve high enough concentration in order to be the sole culprits in the neuropathology of AD due to inherent ability of organisms to cope with this oxidative stress, the presence of a metallo-ROS can form a very potent redox catalyst.

Alzheimer's disease is one of several neurodegenerative disorders affecting a large percentage of the population. An estimated 3 million individuals in the United States suffer from the slow, yet aggregate symptoms of AD. The number is expected to double by the year 2030.[22] The progressive nature of AD that has even been called an epidemic,[23] has also dire effects on the families of those diagnosed with the disease. The AD patients are "memory timers", bringing recognition of events and people around them slowly to extinction with each passing day. With the gradual, yet always progressive and

degenerative nature of AD, families are placed under considerable stress while caring for their loved ones and coping with the loss of their existence in the minds of those afflicted by AD. To that end, numerous scientific studies, amounting to tens of thousands, have been published, reflecting the interest in research funding and efforts toward understanding the neuropathology of this disease.

Largely, AD neuropathology concerns the interaction of a 40-42 amino acid peptide splice fragment from the ubiquitous apolipoprotein (or amyloid precursor protein, APP) with a number of intracellular components. These amyloid-β (Aβ) peptides are generated by the cleavage of APP by α, β, and γ secretases.[24] Aβ in the form of insoluble plaques contains up to mM amounts of Zn^{2+}, Cu^{2+}, and Fe^{3+} in the neocortical region of the brain.[25] However, the cause/effect connection of the metallo-Aβ plaques with AD is still under debate.[26] Aβ has been the elusive culprit in AD studies with results ranging from free-radical generation to disruption of mitochondrial cell membrane potential, all hallmarks of oxidative stress. Formation of Aβ plaques in the presence of metals has dominated a large percentage of investigations in correlating the physiology of AD with the metal chelating event (Aβ serving as the ligand) and generation of ROS. The subsequent observations of chemical events once metallo-Aβ is formed have offered numerous hypotheses into the oxidation stress proposed as one of the main causes of AD. Herein we present a compendium of observations that bring together efforts in the area of metal-O_2 chemistry from a catalysis perspective to better understand what role O_2 and its reduced forms may have in disease. Relating the neuropathology of AD with possible

metal-centered pathways is a recent area of focus that help clarify the homeostatic generation of ROS and the possible effects of non-homeostasis ROS generation.

II. METABOLIC GENERATION OF ROS

Electron donors in the tricarboxylic acid cycle in mitochondria (i.e. NADH and succinate) to O_2 are responsible for the generation of ATP for upkeep of cellular processes. Electron transfer (ET) processes rely on a series of molecular complexes to ensure that the transduction of oxidative energy and that the use of proton energy in ATP synthesis is carried out efficiently. The complexes that are functionally connected to mitochondrial energy transduction include: Complex I (NADH:ubiquinone oxido-reductase), Complex II (succinate:ubiquinone oxido-reductase), Complex III (ubiquinol:ferricytochrome c oxido-reductase), Complex IV(ferrocytochrome c:oxygen oxidoreductase), and Complex V (ATP-synthase).[1, 27]

In the inner mitochondrial membrane, within Complexes I, III, and IV the energy transduced from ET is conserved by coupled proton translocation that is responsible for the generation of a membrane electrochemical potential of protons used in ATP synthesis. The whole ET system is reversible and an electron flow can be generated against the current. However, cytochrome aa_3 in Complex IV and O_2, or the final step in ET is irreversible, shifting the equilibrium in the system toward ATP synthesis. Cytochrome aa_3 retains all the partially reduced oxygen intermediates bound to its active sites until the O_2 itself is completely reduced to water. However, through auto-oxidation

that can affect their reduced forms, other elements in the mitochondrial ET chain like ubiquinones and the cytochrome *b* family could transfer the electrons directly to O_2, but do not retain the partially reduced O_2 intermediates in their active sites until the O_2 is completely reduced to water. Because O_2 accepts only one electron at a time, the superoxide radical ($O_2\bullet^-$) is released. In the cytochrome *b* family, it is noteworthy that cytochrome b_{566} is closely involved with the processes of energy transduction in Complex III, wavering continually between a very low potential state of approximately –30 mV and a very high one of approximately 245 mV. The low potential of cytochrome b_{566} could play a primary role in the formation of mitochondrial $O_2\bullet^-$ because of an increase in its redox potential inhibiting the univalent transfer of electrons to oxygen. Therefore, electron leakage from the cytochrome b_{566} would appear to be a real possibility which can thus bring about a continuous release of oxygen free radicals. During aging, the increasing amounts of these radicals that manage to escape the local defense mechanisms (e.g. scavengers, electron-trapping agents, etc.) may lead to multiple changes in the chemical and physical state of the membranes. As a matter of fact, superoxide generation[28,29] is significantly greater in the brain mitochondria of aged rats rather than young rats. This seems to be related to the fact that, with the exception of cytochrome aa_3 in Complex IV, the metabolic levels of the electron carriers does not undergo significant change with aging. However, the decrease in either the amount of cytochrome aa_3 or its catalytic cytochrome oxidase activity (COA)[30-34] in synaptic mitochondria from some cerebral regions (frontal cortex, parieto-temporal cortex, hippocampus, cerebellum, etc.)[35,36] may account for the finding that stoichiometric calculations show aging is

related to an increase in the percentage of ubiquinones and cytochrome *b* family. Although this increase is not dramatic, relatively it does explain how electrons can "escape" the ET sequence from electron donors to O_2. The K_m for cytochrome *c* is constant in aged rats but the V_{max} decreases, suggesting that the COA activity is not related to the functional integrity of mitochondria accompanying senescence.[35] Moreover, the COA activity drops significantly less in cortical synaptic mitochondria from old rats fed a hypocaloric diet,[37] and declines in the homogenate of old rat cerebral cortex[38] and in insect mitochondria.[39]

Electrons can leak from the energy-transduction sequences even in young animals, indicating that the formation of superoxide radicals could be associated with the normal process of mitochondrial respiration.[40] The production of these radicals causes cell damage because of the dismutase reaction in which H_2O_2 is formed and which, with the involvement of low-molecular-weight iron and copper complexes, leads to the highly dangerous hydroxyl radical. The catalytic activity of Complex IV (COA activity) is low in three cortical areas but not in putamen and hippocampus of AD patients compared with age-matched controls.[41,42] There is no correlation between the changes in COA and those of other marker mitochondrial enzymes, such as glutamate dehydrogenase and citrate synthase, leading to the conclusion that the decrease in COA activity is not related to the loss of mitochondria.[41] The decrease in COA activity in cortical areas and in the hippocampus from AD patients[43,44] suggests a primary defect of Complex IV, resulting in more $O_2\bullet^-$ released. A specific decrease in COA in the platelets of AD patients has also been reported[45] but not confirmed.[46] COA is heterogeneously distributed in the cerebral

spinal fluid (CSF).[47] Expression of mRNA for COA in normal human and monkey brain is high in those regions which are most vulnerable to AD pathology and is particularly reduced in the same regions from AD patients.[48, 49] In the mid-temporal gyrus, but not in the primary motor cortex, of AD patients there is a 50-65% decrease in the mRNA levels of the mitochondrial DNA (mtDNA)-encoded COA subunits I and III.[50] However, the mitochondrial-encoded 12S ribosomal RNA (a mitochondrial transcript) does not change, suggesting that the observed reduction of COA I and III mRNA is not due to loss of mitochondria but to a specific alteration of transcriptional regulation. A behavioral study in rats treated with the selective sodium azide COA inhibitor showed significant inhibition of a low-threshold form of hippocampal long-term potentiation and impaired spatial learning.[51] This finding supports the theory that Complex IV alteration is somehow involved in the pathogenesis of AD and also raises the possibility of developing an animal model reflecting this aspect of AD provided it is specific.

III. O_2•$^-$ AND SOD

Superoxide radicals are described as having considerable reactivity, short half-life, and limited diffusion through membranes. However, the latter property has been questioned, as these radicals can appear in the brain extracellular space.[52,53] O_2•$^-$ has a dual effect[54] where it may help protect against infectious microorganisms, but they can also be harmful as it participates in the formation of the very reactive hydroxyl radicals (OH•). Moreover, they can inactivate a number of useful enzymes, such as antioxidat

enzymes (catalase[55] and glutathione peroxidase[56]), enzymes involved in neurotransmission (glutamine synthase[57]), in signal transduction (adenylate cyclase[58]), and in energy transduction (creatine phosphokinase[59] and NADH dehydrogenase and ATPase[60]).

In AD brain and fibroblasts there is evidence of partial uncoupling of mitochondrial oxidation and phosphorylation.[61,62] Apart from the neurodegeneration induced by the impairment of energy metabolism, these oxidative abnormalities could contribute to the accumulation of cytoskeletal material. Addition of an uncoupler to cultured fibroblasts from normal subjects causes the appearance of epitopes recognized by antibodies to paired helical filaments (PHF) and Alz-50 monoclonal antibodies,[61] thus reproducing a pattern that is characteristic of fibroblasts from AD patients.[63]

When O_2 accepts an electron from a reducing agent, the primary product is $O_2\bullet^-$ that, in aqueous environments, is in equilibrium with its protonated form ($\bullet O_2H$). When $O_2\bullet^-$ and $\bullet O_2H$ approach equal molar concentrations, spontaneous dismutation occurs, and H_2O_2 plus $^1O_2$ (singlet oxygen)[64] are generated.

$$2\ O_2\bullet^- + 2H^+ \leftrightarrow H_2O_2 + O_2\ (\text{or } {}^1O_2) \qquad \textbf{Scheme (l)}$$

In scheme 1, $O_2\bullet^-$ can be converted into H_2O_2 catalyzed by superoxide dismutase (SOD) that is present in varying concentrations in neural cells. Thus, the conversion removes $O_2\bullet^-$ and prevents its direct toxic action as well as its interaction with metal ions to increase the production of hydroxyl radicals (Scheme 9 below).

The rate constant for SOD-catalyzed dismutation is approximately four orders of magnitude greater than that for the spontaneous dismutation of $O_2\bullet^-$ at physiological pH. For SOD protection/activity to work properly, it is absolutely vital for other enzymes (e.g., catalase, glutathione peroxidase, etc.) to convert H_2O_2 immediately into H_2O, thus preventing the transformation of H_2O_2 by metal complexes into the highly toxic OH• (Scheme 9 below). In this last case, the intervention of SOD may be dangerous for neuronal cells in spite of what we expect as a beneficial biological scavenging of a highly reactive radical.

The predominant two types of SOD are Mn-dependent and Cu-Zn dependent. The manganese-dependent (Mn-SOD) is located in the mitochondria, where it interacts with the $O_2\bullet^-$ leaking from the ET chain. The copper- and zinc-dependent (Cu,Zn-SOD) is located in the neural cytosol where it carries out a more general catalytic function. Auto-oxidizable electron carriers located on the internal mitochondrial membrane can generate $O_2\bullet^-$ which is enzymatically dismutated to H_2O_2. However, a few reactions catalyzed by some enzymes (e.g., monoamine oxidase and L-aminoacid oxidase) can produce H_2O_2 directly. Thus, H_2O_2 may be generated either as a direct product or from each of the various sources of $O_2\bullet^-$ by auto-oxidation of a variety of low-molecular weight molecules, as byproducts of various enzyme catalyses such as between xanthine and xanthine oxidase, and by the mitochondrial ET system.

The hydroxyl radical is one of the most potent reactive metabolites produced in brain systems derived from O_2. This radical, O_2, and OH^- are all products in the reaction shown in Scheme 2 when H_2O_2 is directly reduced by $O_2\bullet^-$:

$$O_2\bullet^- + H_2O_2 \leftrightarrow O_2 \text{ (or } {}^1O_2) + OH\bullet + OH^- \quad \textbf{Scheme (2)}$$

H_2O_2 can cross cell membranes directly, whereas $O_2\bullet^-$ crosses cell membranes through anion channels. Although H_2O_2 cannot be classified as a radical because it does not contain unpaired electrons, it is still dangerous because it easily permeates cell membranes and can migrate from where it is first generated to other organic compartments. It can interact with the reduced forms of some metal ions (generally, Fe^{2+} and Cu^+) and decompose into the highly reactive OH• and the OH^-, according to:

$$H_2O_2 + Fe^{2+} \leftrightarrow Fe^{3+} + OH\bullet + OH^- \quad \textbf{Scheme (3)}$$

$$H_2O_2 + Cu^+ \leftrightarrow Cu^{2+} + OH\bullet + OH^- \quad \textbf{Scheme (4)}$$

The formation of OH• requires reduced forms of metal ions, such as Fe^{2+} or Cu^+. The superoxide radical $O_2\bullet^-$ can then give rise to Fe^{2+} or Cu^+ by reducing Fe^{3+} or Cu^{2+} according to:

$$O_2\bullet^- + Fe^{3+} \leftrightarrow O_2 + Fe^{2+} \quad \textbf{Scheme (5)}$$

$$O_2\bullet^- + Cu^{2+} \leftrightarrow O_2 + Cu^+ \quad \textbf{Scheme (6)}$$

The reaction in Scheme (2) is slow at physiological pH and would require steady-state concentrations of the reaction partners, which are much higher than those found in cerebral mitochondria to account for detectable amounts of the highly unstable radical.

As shown in Schemes 3-6, metal ions (M^{n+}) accelerate the reaction in Scheme (2) by catalyzing two intermediate reactions:

$$O_2\bullet^- + M^{n+} \leftrightarrow O_2 + M^{(n-l)+} \qquad \textbf{Scheme (7)}$$

$$M^{(n-l)+} + H_2O_2 \leftrightarrow M^{n+} + OH\bullet + OH^- \qquad \textbf{Scheme (8)}$$

$$\text{Overall: } O_2\bullet^- + H_2O_2 + \leftrightarrow O_2 \text{ (or } {}^1O_2) + OH\bullet + OH^- \qquad \textbf{Scheme (9)}$$

In Scheme 9, $O_2\bullet^-$ reduces redox-active transition metals (Fe^{3+}, Cu^{2+}), and generates oxygen or singlet oxygen. The reduced form of the metal subsequently reacts with H_2O_2 to produce the oxidized form of the metal, the hydroxide ion, and the hydroxyl radical. In view of the evidence that in neural systems Scheme 2 proceeds very slowly, the hydroxyl radicals are possibly produced in the presence of a redox-active metal. An additional mechanism by which OH• may be generated is supported by the observation that incubation of H_2O_2 with Fe^{2+} and iodide ions (I^-) can generate a potent reactive molecule that is inhibited by scavengers of the hydroxyl radical (e.g., mannitol[65] and ethanol[66]). Singlet oxygen[63] is generated by the SOD in Scheme 2 or by the interaction with metal ions in Scheme 9 when one of the two unpaired electrons of O_2 acquires sufficient energy to undergo spin inversion or both spin inversion and orbital transition. There are two distinct forms of singlet oxygen, Δ and Σ, which are dependent respectively on whether the excited electron forms an electron pair in the same orbital or remains unpaired in a different orbital. The Δ form of singlet oxygen is more stable than the Σ form. Singlet

Reaction	E° (V)
$O_2 + e^- \rightarrow O_2^{\bullet -}$	–0.33
$O_2^{\bullet -} + e^- + 2\ H^+ \rightarrow H_2O_2$	+ 0.89
$H_2O_2 + e^- + H^+ \rightarrow H_2O + OH$	+ 0.38
$OH + e^- + H^+ \rightarrow H_2O$	+ 2.31
$O_2 + 2e^- + 2\ H^+ \rightarrow H_2O_2$	+ 0.281
$H_2O_2 + 2e^- + 2\ H^+ \rightarrow 2\ H_2O$	+ 1.39
$O_2 + 4\ H^+ + 4\ e^- \rightarrow 2\ H_2O$	+ 0.815

Table 1.1. Standard redox potentials for dioxygen species in water.

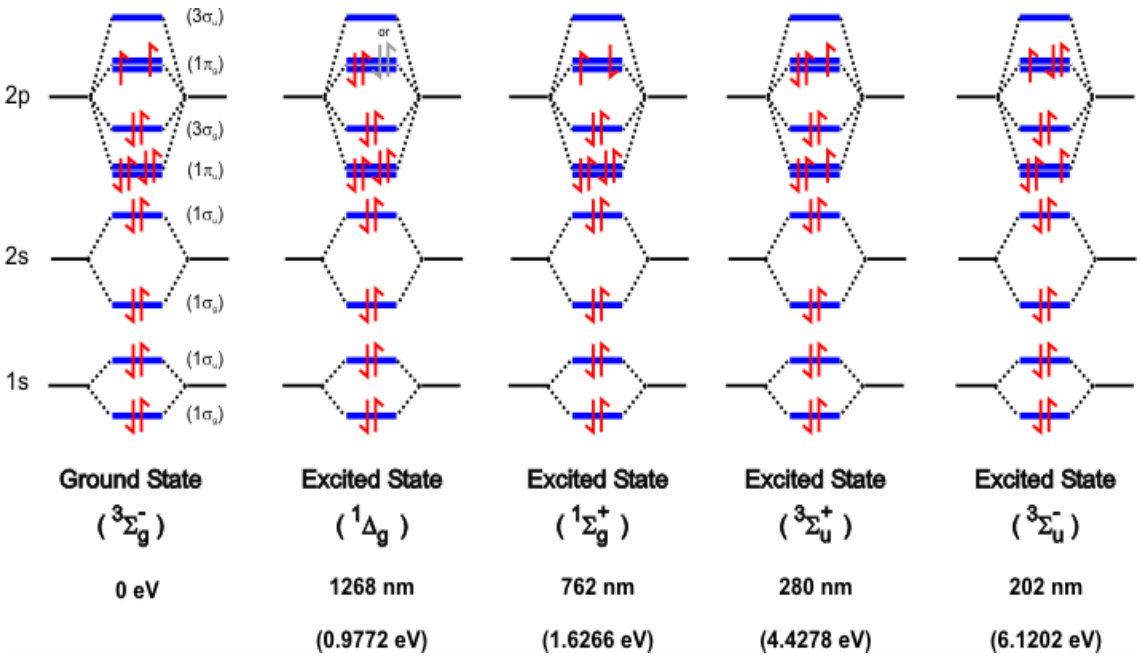

Figure 1.1. Electronic states and standard reduction potentials for O_2. [67]

oxygen is highly electrophilic and can react with electron-rich biomolecules such as tryptophan, methionine, and molecules containing unsaturated double bonds.

The effect of physiological aging on brain SOD is controversial, though most reports describe some age-related decline, mainly of the Cu-Zn form[68,69,70,71,72] probably related to the decline of SOD mRNA. However, other studies report no change of this form and an increase in MnSOD.[73,74] Thus, it would appear that higher levels of SOD are beneficial and lower levels of SOD detrimental. However, if the activity of SOD is increased without a concomitant enhancement of the activity of the enzymes which dispose of H_2O_2 (i.e. glutathione peroxidase) and the concentration of reduced glutathione, then H_2O_2 accumulates and reacts with $O\bullet^-$ and Fe^{3+} and/or reduced metal ions to form the very reactive OH•. Thus the imbalance between SOD and H_2O_2-converting enzymes results in a toxic effect of SOD by OH• generation, inducing DNA fragmentation, protein denaturation, and activation of the autocatalytic process of lipid peroxidation.

Down's syndrome (trisomy 21) has provided some interesting clues on the balance among SOD, ROS, and antioxidants. Human Cu,Zn-SOD is encoded by a gene located on chromosome 21 and Down patients have a 50% increase in the activity of this enzyme secondary to gene dosage effect.[75] The increase in SOD, not accompanied by a concomitant adaptative rise in glutathione peroxidase,[76] might induce oxidative damage to the CNS, including lipid peroxidation and this might explain some of the neurobiological abnormalities found in Down's syndrome, such as accelerated aging and AD-type neuropathology. This is supported by the results in an animal model of gene

dosage effect in transgenic mice carrying the human Cu,Zn-SOD gene.[77,78] Cu,Zn-SOD and its mRNA are preferentially expressed in the large pyramidal neurons of Ammon's horn and granule cells of the dentate gyrus, which are susceptible to degenerative processes in AD.[79] Brain lipid peroxidation is also increased. In seeming contrast with this finding, increased Cu-Zn SOD in transgenic mice makes the hippocampus more resistant to the neurotoxicity induced by amyloid-β.[80]

The levels of Cu,Zn-SOD protein and mRNA in the vulnerable hippocampal neurons of AD patients,[81] their association with neurofibrillar degeneration (PHF),[82] and the observation that the cell distribution of Cu,Zn-SOD mRNA in the human hippocampus is the same as amyloid mRNA[83] suggest that high levels of enzymes for ROS decomposition are needed to remove excess superoxide radicals which indicate that ROS contribute to the degenerative processes leading to neuropathology in AD. Cu,Zn-SOD activity is also upregulated in the temporal cortex and nucleus basalis Meynert[84,85] and in the fibroblasts of AD and Down patients.[86] Cultured skin fibroblasts from both familial and sporadic AD patients are more susceptible to ROS-induced damage then from age-matched controls.[87] Finally, high immunoreactivity for SOD and catalase in the AD brain is associated with some neurofibrillar tangles and senile plaques.[88] This immunoreactivity is absent in tangle-free neurons of AD and all neurons of normal control brains.

IV. METAL-BIDING TO Aβ AND STRUCTURE OF THE COMPLEX

The primary step in understanding metal-centered chemistry is the elucidation of the coordination of metal ions in its complexes. The geometry of metal complexes is often the determinant of reactivity. Once it was determined that transition metals could bind to Aβ from analysis of isolated plaques,[89] more detailed investigation of the nature of the metal-Aβ interaction followed. Through the use of competitive binding in a pH gradient column chromatography, Cu^{2+}, Ni^{2+}, and Zn^{2+} were determined to tightly bind to $A\beta_{1-42}$; shorter fragments ($A\beta_{1-16}$ and $A\beta_{1-28}$) could also be retained in the metal-chelate column but did not bind as tightly.[90] Based on the pK_a of 6.1 determined from the pH gradient elution, His residues were suggested as the ligands responsible for metal-binding. Further pH dependent binding studies using quantitative precipitation and turbidity revealed that Cu^{2+} can induce aggregation of $A\beta_{1-40}$ and $A\beta_{1-42}$. Chemical modification of His residues in the peptide to N-carbethoxyhistidine extinguishes the metal-induced aggregation.[91] These results indicated that His residues were important in metal binding, but did not provide insight into geometry nor the affinity of Aβ toward transition metals. Quantitative precipitation studies suggested that Cu^{2+} binds with an attomolar dissociation constant to $A\beta_{1-42}$.[92] This very low K_d, if correctly measured, would suggest that Aβ could actually remove metal from hemes, some of the tightest binding ligands in biological systems. This result however, erroneously explained the metal-bidning because the combination of multiple molecular events in terms of euqilibrium can yield such a low metal-dissociation constant. Since quantitative

precipitation measures both the metal affinity to Aβ and also the affinity associated with peptide aggregation, the attomolar constant is thus a combination of different constants for the two processes that would not be quantified individually until chemical[93] and spectroscopic[94] methods were used to directly measure metal-peptide interactions in solution. Both methods yielded K_d for metal-binding in the μM range for $A\beta_{1-16}$, $A\beta_{1-20}$,[93] and $A\beta_{1-28}$.[94]

In order to further elucidate the location of metal-binding in metal-Aβ complexes resonance Raman was employed to directly observe metal-peptide interactions.[97] The Raman spectra demonstrate that three His residues in the N-terminal hydrophilic region provide primary metal binding sites and the geometry of the metal-Aβ complex is correlated with the metal binding mode. Zn^{2+} binds to the Nε atom of a His imidazole ring and the peptide was suggested to aggregate through intermolecular His(Nε)-Zn^{2+}-His(Nε) bridges. The Nε-metal ligation also occurs in Cu^{2+}-induced Aβ aggregation at mildly acidic pH.[91] At neutral pH, however, Cu^{2+} was shown to bind to Nδ, the other nitrogen of the His imidazole ring, and to a deprotonated amide nitrogen of the peptide main chain.[95] The studies using electronic absorption spectroscopy and ^{1}H NMR techniques have also shown the nature of the metal-Aβ interaction.[93] The electronic spectrum of Cu^{2+}-$A\beta_{1-20}$ shows a typical tetragonally distorted octahedral environment that is consistent with many Cu^{2+} complexes in solution. Co^{2+} as a paramagnetic shift reagent in ^{1}H NMR experiments revealed that three His resides coordinate all Nε nitrogens from the imidazole rings of His6, His13, and His14. The results of the NMR

study also revealed that neither Tyr10 nor the N-terminus bind to the metal as was previously suggested.[95-97]

Through the use of CW-EPR techniques and line broadening observations in ^{1}H NMR experiments, a model was suggested for the formation of Aβ dimers that resembled the structure of the active site of Cu,Zn-SOD.[96] The suggested structure yields the metal:peptide stoichiometry of 1:1 and that two metal metal centers can be bridged through a third His residue, suggested to be His6.[96] These results were further confirmed by using chemically modified (methylated) His residues and CW-EPR.[98] The broadening of the EPR spectrum was proposed to be due to antiferromagnetically couple Cu^{2+} that could only arise from a bridging ligand interaction or a close proximity of two metal centers. However, the distinct features of Cu,Zn-SOD EPR are well known[99] which do not resemble those of the CuAβ complexes. Indeed, the possibility of bridged metal-centers in CuAβ complexes is not preposterous which can be reasoned as an OH-bridged or even phosphate-bridged Cu centers (being that PBS is the preferred buffers in most of the experiments cited). The interpretation that the broadening of EPR signals in CuAβ samples is likely due to the aggregation of the metallopeptides in solution and not because of magnetic coupling, since the metal-induced aggregation of Aβ is a well known phenomenon.[100-103]

Although the metal-binding properties of Aβ have been widely studied,[25] questions about the correct stoichiometry were until recently not clarified. Recent studies using a number of different physical methods, ranging from ^{1}H NMR to fluorescence and kinetics, have elucidated that each Aβ monomer of varying lengths can only bind one

metal.[93,94,104,105] Recent theoretical studies have shown that the seeds for dimerization occur between residues 16-22, causing β-sheet formation in smaller fragments that can range from dimmer to 16 peptides per fibril.[106,107] It is thus possible for two individual metal centers to be close enough to each other due to dimerization and show binuclear metal-centered catalysis. Such structural motif may well explain the redox chemistry involved in etiology of AD.

V. GENERATION OF ROS BY METALLO-Aβ

The cytotoxic effects of Aβ, which accumulates in the brain in AD, have been studied extensively.[108] Early studies[109] suggested that the aggregation state of Aβ is related to its toxicity. It was shown that freshly solubilized Aβ exhibited little toxicity, whereas Aβ that had been aged for 7 days (forming aggregates in fibrillar states) was cytotoxic.[109] However, the precise molecular mechanism by which Aβ mediates cell death has remained a matter of considerable dispute. There is general agreement that the production of ROS (see section II) and the influx of calcium ions into cells[121] are both involved in toxicity, but it is still unclear how the generation of ROS might be related to Aβ. One possibility is that the aggregated peptide itself may be able to produce ROS directly in the forms of free radicals or H_2O_2.[110,111]

It is generally accepted that Aβ needs to be in aggregated or partially aggregated states before it becomes toxic to cells. However, there is still no clear consensus on the precise nature of the toxic form of the peptide. Dimers, soluble oligomers, protofibrils

and annular protofibrils have all been implicated in amyloid toxicity.[112-117] Furthermore, it is becoming more evident that not all amyloid fibrils are toxic to cultured cells. Recently a synthetic peptide corresponding to amino acid residues 1-15 of Aβ protein (Aβ 1-15) was shown to form amyloid fibrils *in vitro* that are completely non-toxic to cells, even at high concentrations.[118] Some forms of synthetic Aβ are also reported to be non-toxic,[119] as is the Aβ peptide mutant that contains a norleucine in the place of Met35.[120] This leads to yet another area of research that is ongoing and still trying to elucidate which forms of amyloid are toxic. What underlying molecular structures and mechanisms can explain why some amyloids are toxic, whereas others are not.

Various other hypotheses have been put forward to explain the cytotoxic effects of Aβ in addition to the direct production of ROS from the peptide, including the formation of ion calcium channels in cell membranes by Aβ,[121] interactions between Aβ and specific cell surface receptors, such as the RAGE (receptor for advanced glycation endproducts) or scavenger receptors,[122-124] interactions between Aβ and intracellular target molecules such as ERAB (endoplasmic reticulum Aβ binding protein),[125] and non-specific intercalation of aggregated forms of Aβ into membranes.[126] These various interactions may not be related to the idea that the most important aspect of the toxicity of Aβ is due to its ability to generate ROS directly once bound to a redox-active metal. The toxic process could be the result of a combination of binding and/or attachment of Aβ aggregates to cell components, followed by the induction of oxidative damage.

According to the oxidative stress hypothesis, a spontaneous shower of Aβ-derived free radicals is produced upon incubation of Aβ *in vitro*, and it is this phenomenon which

rendered the cytotoxic properties of Aβ.[111] Three main pathways can lead to the formation of free radicals from organic molecules: photolysis, thermal scission, and one-electron redox reactions. Mechanical stress would be a fourth possible route that may apply in some special cases. Of these, photolysis is not relevant to neurodegenerative and amyloid diseases. Thermolysis of most chemical bonds requires temperatures above 450 °C with the exception of peroxides and azo compounds. The temperature at which peroxides undergo unimolecular scission varies with the class of peroxide but can be between about 50 and 150 °C.[127,128] Likewise, nitrogen can be eliminated from certain azo compounds (general structure R-N=N-R) over a similar temperature range.[129,130] However, neither of these classes of bond is present in the parent Aβ peptide molecule. Perhaps the most important redox assisted bond scissions involve a metal ion that readily undergoes a one-electron transfer with one of the best known examples being the Fenton reaction:

$$M^{n+} + H_2O_2 \rightarrow M^{(n+1)} + OH\bullet + OH^-$$

Metal assisted homolysis reactions can take place at much lower temperatures than the corresponding unassisted reaction. While such reactions in peptide molecules cannot be totally discounted at 37 °C, they do not provide an obvious route to the spontaneous generation of peptidyl free radicals from Aβ. However, it has been suggested on purely theoretical studies that peptidyl free radicals might be generated from Aβ by a mechanism involving mechanical stress, i.e physical contact among metallo-Aβ monomers in the plaque.[131]

Electron paramagnetic resonance spectroscopy (EPR) is the preferred technique for the detection of free radicals and geometrical states around paramagnetic transition metal ions with unpaired electrons. EPR is highly sensitive and interpretation of the hyperfine structure associated with each spectrum allows the electronic nature of the radical to be established. However, the high reactivity and short life-time coupled with low steady-state concentrations of nearly all radicals prevent their direct detection in most cases. A simple experimental technique that is coupled with EPR is to employ spin-trapping, in which a reactive radical reacts with a nitrone or a nitroso compound to form a much more stable nitroxyl radical whose concentration rises well above the detection limit of the spectrometer. The selection of the appropriate spin-trap is important and depends upon the nature of the initial radical and on the objectives behind the experiment. Choice of incorrect spin-traps may yield data that are ambiguous and misinterpreted (discussed below).

The suggestion that Aβ itself might spontaneously generate free radicals was first made in 1994 when EPR spectra were observed during 6 hour incubation of Aβ 1-40 at 37 °C in phosphate buffered saline (PBS) in the presence of the spin-trap *N*-*tert*-butyl-α-phenylnitrone (PBN).[111] The observation therein and further EPR spectra employing PBN as a spin-trap[132,133] led to the "molecular shrapnel" hypothesis. The main feature of these EPR spectra was a 4-line pattern, and such a pattern is not characteristic of a true PBN adduct. In a similar experiment, Tomiyama et al.[134] observed a spectrum consisting of the superimposition of 3-line, 4-line, and 6-line patterns during the incubation of Aβ 1-40 in the presence of PBN in deionized water. Again, the 3-line pattern is not characteristic of a

true PBN adduct. Under conditions of good spectral resolution, PBN adducts, without exception, consist of a 6-line pattern.[135] Subsequently, Dikalov et al.[136] reported that they were unable to detect any EPR spectra following the 6 h incubation of Aβ 1-40 and Aβ 25-35 with PBN. When these same peptides were incubated with a less pure sample of PBN they observed both 3-line and 4-line EPR spectra. These spectra were also observed in the absence of peptide, and were attributed to transition metal-catalyzed auto-oxidation of di-*tert*-butylhydroxylamine and *N*-*tert*-butylhydroxylamine, present as impurities within their sample of PBN. It was proposed that these impurities were converted to their corresponding nitroxyls, di-*tert*-butylnitroxide and *tert*-butylhydroaminoxyl. Further there is current evidence that Aβ and α-synuclein can generate ROS directly.[118] The arguments presented herein could apply to proteins associated with some of the other protein conformational diseases mentioned above.

In some recent publications Bush and co-workers have reported that Aβ 1-40 forms H_2O_2 in the presence of both copper and iron and can reduce Fe^{3+} to Fe^{2+} as well as Cu^{2+} to Cu^{+}.[110,137-139] The possible formation of H_2O_2 during the incubation of Aβ in PBS could provide some interesting insights into the chemistry outlined. First, H_2O_2 is a strong oxidizing agent and, if present, would certainly promote the hydrolysis of PBN. Secondly, the presence of both H_2O_2 and Fe^{2+} and/or Cu^{+} would lead to the formation of hydroxyl radicals by Fenton chemistry. It has been found that low concentrations of metals are present even in chelex buffers, and that significant amounts of metals are also bound to the peptide itself.[140] If formed, the hydroxyl radical would be trapped by PBN, but the resulting adduct is unstable and is not directly observed in aqueous solution.

There is good evidence that at pH 7 and above PBN rapidly transforms into the *tert*-butylhydroaminoxyl radical.[141] This could also help to explain the origin of the characteristic 4-line spectrum of the *tert*-butylhydroaminoxyl radical obtained when Aβ is incubated in the presence of PBN. Consequently, it may be that the very weak EPR signals of *tert*- butylhydroaminoxyl observed by Butterfield and co-workers[132,133,142-145] and by Monji *et al*[146,147] are resulted from the formation of H_2O_2 in the presence of low concentrations of Fe and Cu rather than the spontaneous formation of peptide-derived radicals. A second scheme involving reactions of 2-methyl-2-nitrosopropane (MNP) and PBN explains the origins of the 3- and 6-line spectra in the presence of Aβ and ambient laboratory lighting. The possibility that H_2O_2 might be formed in the immediate vicinity of the peptide is interesting since, as noted above, in the presence of the appropriate metal ions it would be readily converted to hydroxyl radicals *via* Fenton chemistry. The hydroxyl radical is a strong oxidant that can attract hydrogen atoms from organic molecules with a rate constant close to the diffusion controlled limit.[148] Because of its high reactivity the hydroxyl radical is very unselective and removes hydrogen atoms from primary, secondary and tertiary carbon atoms with almost equal facility. It also adds to C=C double bonds with a rate close to the diffusion controlled limit. Consequently, immediate oxidative damage would occur to any organic molecule in vicinity of the site of hydroxyl radical.

Bush and co-workers[110, 139] have reported results showing the production of H_2O_2 in systems involving Aβ 1-40, Aβ 1-42 and low concentrations of Fe^{3+} and Cu^{2+} in PBS. Quantitative measurement of the H_2O_2 levels was carried out using the standard

thiobarbituric acid reactive species (TBARS) assay and not spin-trapping. Their results are reasonably convincing, however, not in agreement with other studies where H_2O_2 levels appear to be lower than those reported by Bush, as double integration of DMPO hydroxyl radical adduct signals against calibration standards indicates the concentration of adducts is not higher than about 0.5 mM from 100 mM CuAβ 1-40.

A significant number of the aggregating polypeptides that have been implicated in neurodegenerative disease have been shown to bind to transition metal ions such as iron, zinc, copper or manganese. Another common emerging theme is that some of these polypeptides seem to function normally as antioxidants through structural or activity similarities to the active site of superoxide dismutase. This seems to apply to prion protein (PrP)[149] and the Aβ peptide.[150] When these proteins are in an altered pathological configuration, they could actually become pro-oxidants. If we take the example of Aβ, there is strong evidence supporting that binding of Cu^{2+}, Zn^{2+}, and possibly Fe^{3+} to the peptide involves coordination with the three histidine residues at positions 6, 13 and 14, along with the tyrosine residue at position 10.[150] In the general case of biologically relevant redox-active transition metal ions, binding to peptide molecules would still leave available coordination sites, allowing oxygen to bind, possibly in the form of a peroxo bridge. Such bridges are common in a variety of metal complexes,[5,6,10,11,16] but in this case there is a further issue that should be considered. As the peptide molecules change conformation and begin to aggregate this could have the effect of twisting the bridging oxygens, resulting in a straining of the complex. However, in the dimeric and small polymeric forms of the soluble peptide the possibility of the formation of strong

electrophiles such as the Type-3 copper models (discussed below) cannot be discounted. The conversion of superoxide to H_2O_2 is a well established reaction. It is possible that the superoxide, and subsequently hydrogen peroxide, is formed as a byproduct of the aggregation and fibril assembly process. In other words, the amyloid-induced toxicity could actually be associated with the generation of ROS during the process of fibril extension and growth. In this case, a search for one or more types of special toxic aggregate may yield several variants of toxic intermediates.

It is assumed that Fenton chemistry can occur if peroxide is present in close proximity to Fe^{3+} resulting in the formation of hydroxyl radicals which will react with organic molecules *in situ*, including peptides. In this case a peptidyl radical may be detectable. Yanker and coworkers[151] investigated the neurotoxicity of a range of peptides spanning the entire Aβ 1-40 sequence and concluded that 25-35 was the toxic domain. This report was supported by Pike *et al*[109] who observed the formation of stable aggregates and neurotoxicity in synthetic peptides containing residues 29-35. These results focused attention on the possibility that a particular amino acid residue within this sequence might play a key role. In particular the methionine 35 residue has attracted attention.[145] Substitution of this methionine by aspartate, serine and cysteine all resulted in peptides which were neither aggregated nor neurotoxic.[152] Conversely, substitution by leucine, norleucine, lysine and tyrosine residues resulted in peptides which neither aggregated nor were neurotoxic. Significantly, substitution of the methionine residue by serine or cysteine led to peptides which were at least as neurotoxic as Aβ 25-35 itself suggesting that methionine is not unique in promoting these properties.[152]

VI. TYPE-3 COPPER OXIDASE MODELS AND METALLO-ROS

Because the generation of activated forms of O_2 through metal-centered reactions has been implicated in the etiology of neurodegenerative disorders, it warrants the question: Is the ROS generated and then diffused or does it remain metal bound? Thus, even if the fields of Type-3 copper oxidase biomimetics and neurodegeneration by ROS seem unrelated, at least in terms of goals, they are certainly connected at the chemical level by the drive to understand copper-O_2 interactions.

The oxidation of organic substrates with molecular oxygen under mild conditions is of great interest for industrial and synthetic processes from an economical and environmental point of view.[153] Although the reaction of organic substances with dioxygen is thermodynamically favorable, it is kinetically unfavorable due to the triplet ground state of O_2. In biological systems this problem is overcome by the use of copper- or iron-containing metalloproteins which serve as highly efficient oxidation catalysts.[154-157] Some examples of Cu-oxidases/oxygenases are shown in Figure 1.

The catechol oxidases are Type-3 copper enzymes containing a binuclear copper center.[158,159] Well-known representatives of these Type-3 copper proteins are hemocyanin,[160-162] the O_2 carrier for arthropods and mollusks, and tyrosinase.[163] Catechol oxidase belongs, like tyrosinase, to the polyphenol oxidases which catalyze the oxidation of phenolic compounds to quinone in the presence of O_2. Tyrosinase catalyzes the hydroxylation of tyrosine to DOPA and the oxidation of DOPA to dopaquinone with

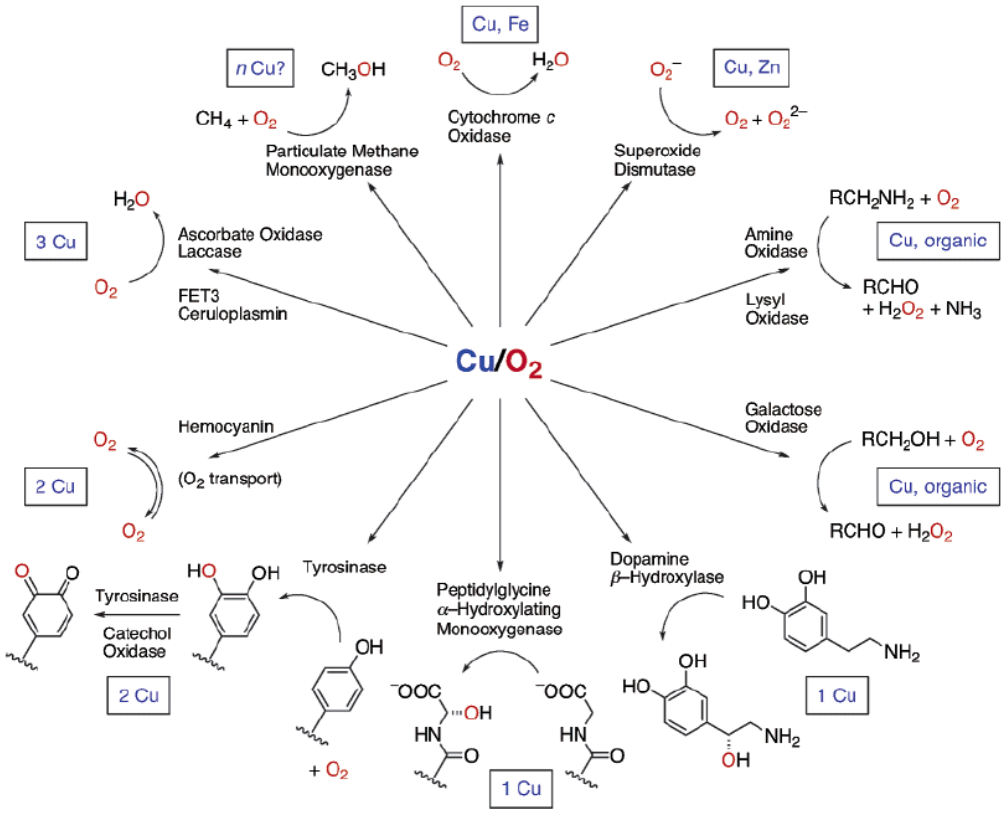

Figure 1.2. Types of enzymes involved in O_2 metabolism.[16]

electron transfer to O_2, while catechol oxidase only catalyzes the oxidation of catechols to quinones.[164] This reaction is of significance in medicine and biology since catecholamine neurotransmitters like epinephrine, norepinephrine, and DOPA are part of the tyrosine metabolic pathway.[165] Secondary reactions like melanin formation are downstream after oxidation of the catechol moiety of catecholamine substrates in the presence of polyphenol oxidases, which are also responsible for the brown color of injured plants.[166]

The copper in isolated catechol oxidases was determined to be EPR-silent due to an antiferromagnetically coupled Cu^{2+}–Cu^{2+} pair.[167] The electronic absorption spectrum of *oxy*-catechol oxidase from *Ipomoea batatas* exhibits an intense absorption band at 343 nm and a weaker band at 580 nm, later found to be due to the peroxo complexes of hemocyanin and tyrosinase. These intense electronic transitions were assigned to a peroxo to Cu^{2+} charge transfer transitions[168,169] with an O–O stretch vibrational band at 749 cm^{-1} indicating a possible μ-η^2:η^2 bridging mode of the peroxo group. X-ray abosorption spectroscopy (XAS) investigations on the native *met* forms of catechol oxidases from *Lycopus europaeus* and *Ipomoeas batatas* have revealed that the active site consists of a dicopper(II) center, in which the metal atoms are coordinated by four N:O donor ligands. Multiple scattering extended x-ray absorption fine structure (EXAFS) calculations have shown high significance for one or two coordinating histidine residues.[170] The short metal–metal distance of 2.9 Å and the results of EPR investigations indicate that a μ-OH bridged dicopper(II) center resides in the active site in the *met* forms of the proteins.[171] Model studies of synthetic analogues have furthered the understanding of the structural and chemical properties of these proteins.[11,16] Current interest is focused

on the elucidation of the mechanism of copper complexes that show catecholase and phenolase activities with different structural and electronic features around the copper ions. In these studies, mono- or multinuclear complexes have been synthesized and the properties of the chelating ligands have been varied with respect to geometry, number, and nature of the donor atoms. There are several structural constraints for proper Type-3 oxidase activity, such as square-planar mononuclear Cu^{2+} complexes exhibit only little catalytic activity while non-planar mononuclear Cu^{2+} complexes show a high activity.[172,173] It was also found that binuclear complexes can also catalyze oxidation reactions if the Cu···Cu distance is less than 5 Å. A steric match between substrate and complex is believed to be one of the determinants for reactivity where two metal centers have to be located in close proximity to facilitate binding of the two hydroxyl oxygen atoms of catechol prior to the electron transfer.[172] This conclusion was supported by the observation that binuclear copper complexes are generally more reactive towards the oxidation of catechols than are the corresponding mononuclear species.[174] It has been particularly challenging to synthesize structures where a substrate bridged compound can be resolved. Thus far only one case is known in which the crystal structure of a catalytically active binuclear Cu^{2+} complex with a coordinated catecholato ligand has been solved.[175] Two other examples of mononuclear square-planar copper complexes[176] were also effective catalysts, demonstrating that geometrical effects are only one aspect of the complex activity. In mechanistic studies, the same authors pointed out that a narrow range of redox potentials for effective catalysis exists between ease of reduction by the substrate and subsequent reoxidation by O_2.[177] Although some general structure-

reactivity patterns have been found, the oxidation chemistry of structurally well-characterized copper complexes is still not fully understood, especially regarding the parameters affecting the catecholase activity. For example, there appears to be no direct correlations between the rates of reaction and the redox potentials of these complexes. Exploration of the oxidation chemistry of well-characterized copper complexes together with a detailed understanding of the function of O_2 activating copper enzymes is expected to provide the basis for new catalytic oxidation systems for synthetic and industrial processes.

Current understanding of the types of copper–dioxygen species or intermediates relevant to O_2-binding to or activation by copper proteins comes from the combination of biochemical/biophysical studies and coordination chemistry efforts, with the latter having played a significant role. Figure 2 on the next page provides a summary of structural types of nearly all now well established reactive intermediates of Cu-O_2 species. These are the starting point for describing the possible conformation of reactive intermediates based on copper chemistry. As seen by the large number of examples (Figure 2), many structural types exist which are perhaps far more than are known for heme or nonheme iron enzymes or complexes.

Synthetic bioinorganic copper(I)–O_2 chemistry has flourished in the last 25 years.[11,16,178-181] These efforts to elucidate fundamental chemical aspects of Type-3 oxidases have been inspired by understanding of the diverse nature of the active-site chemistry of copper-protein O_2-carriers, monooxygenases, and oxidases.[182-185] Enzymes with active sites having one, two, three, or four copper ions are known (Figure 1), and the

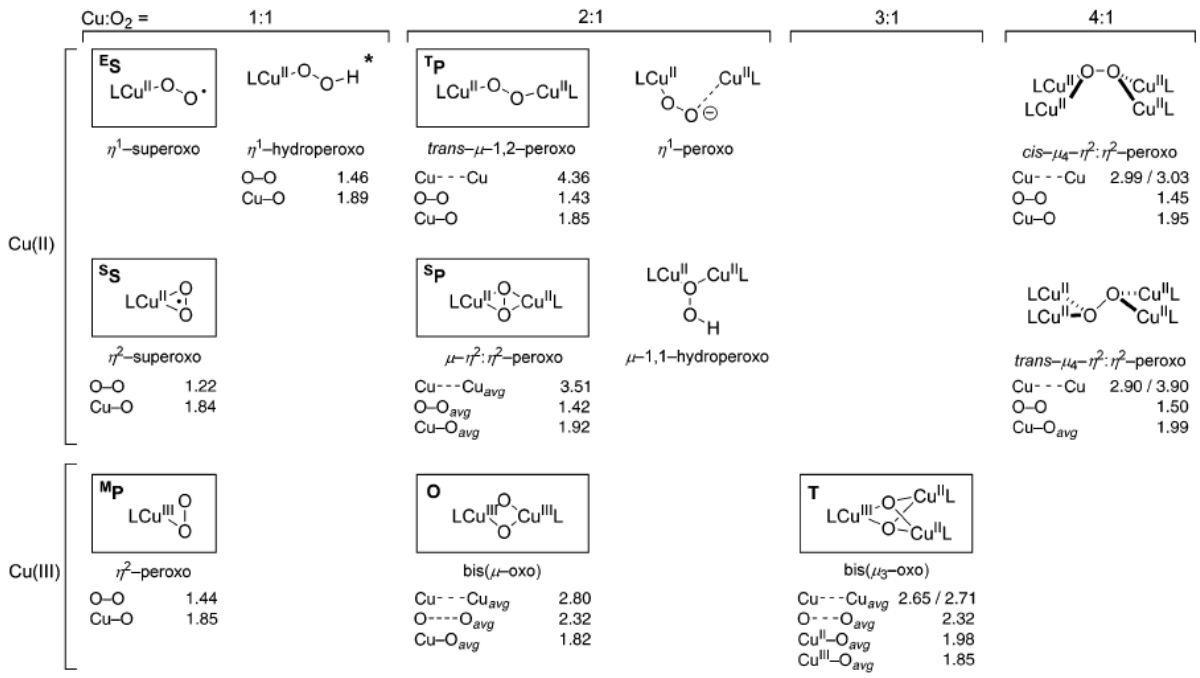

Figure 1.3. Structure of CuO_2 intermediates identified in biomimetic complexes.[16]

variations in ligand environment and reactivity patterns are vast. The prototype for dioxygen binding to copper, and subsequent the primary model for ligand design has been the structure and reversible O_2-binding of arthropodal and molluscan blood oxygen transporting protein, hemocyanin.[185] The dicopper motif, also found in tyrosinase[182]and catechol oxidase,[186] is of considerable interest with respect to the relationship of dioxygen binding and activation. Formation of the copper-dioxygen adducts leads to copper-mediated reduction of O_2 to superoxo (O_2^-), peroxo (O_2^{2-}), or O–O cleaved products (copper-oxo, O^{2-}), which constitute the active species responsible for substrate oxidation. While there is ample literature for oxidative reactions by copper complexes[11,178,179,181,187,188] it is only within the past few years and recent advances in low temperature spectroscopy and reactivity that we have been able to assign a given organic reaction to specific copper-O_2 derived species. In fact, a number of the CuO_2 species can be placed into groups of reactivity types, for example as nucleophilic or electrophilic reactive intermediates. Following is a brief summary of the known reactivity of biomimetic complexes of Type-3 copper oxidases which is the basis for categorizations of different CuO_2 intermediates responsible for reactivity.

The μ-η^2:η^2 peroxo-dicopper(II) (Figure 1.2 ^{S}**P**) complex was first elucidated with x-ray crystallography in a synthetic system by K. Fujisawa and the late N. Kitajima,[189,190] and subsequently confirmed for oxy-hemocyanin.[191] This moiety was also detected in tyrosinase[182]and catechol oxidase[186] with spectroscopic methods. It is likely, and now generally accepted, that the μ-η^2:η^2 peroxo-dicopper(II) core is closely involved in aromatic hydroxylations, both in enzymes like tyrosinase and chemical systems. Notably,

through the research efforts of W.B. Tolman and co-workers there is an established high-valent bis-μ-oxo-dicopper(III) species,[16, 188] (Figure 1.2 **O**) that is thus far not found in biochemistry but only exists as an interesting example of how chemists can elucidate useful new chemical possibilities. A moiety such as this, or even containing more than two copper ions in a different overall redox state, is suggested to be resposnsible for the hydroxylation of methane in particulate methane monooxygenase (p-MMO), a membrane-bound copper-dependent enzyme found in methanogenic bacteria.[192]

Mono and binuclear copper-hydroperoxo reactive intermediates are also known. Cu^{2+}-OOH and more recently Cu^{2+}-superoxide species, were suggested to be present in the copper-containing enzymes dopamine β-monooxygenase (DβM) and peptidylglycine α-hydroxylating monooxygenase (PHM).[183,193,194] While DβM and PHM have two active-site copper ions, they are separated by a large distance (~11 Å) and the oxidative hydrogen-atom chemistry is thought to occur at the CuM site near the substrate binding pocket. The second metal center, dubbed CuH, has been suggested to assist the reaction by serving the role of an electron-transfer center to deliver the proper number of electrons to reduce O_2. The chemistry of Cu-O_2 species is being pursued more heavily as of late and interesting new results from Klinman and co-workers will offer a new insight into both ligand design and mechanistic approaches to studying Type-3 oxidase systems.[195] Binuclear peroxo-dicopper(II) complexes (Figure 1.2 ^{T}P and ^{S}P) were the first to be well characterized.[16,190] In synthetic chemical systems, it is difficult to stabilize the principal reaction product of Cu^{+} and O_2 (Cu-O_2), from coupling with another ligand-copper(I) complex to form a Cu^{2+}-(O_2^{2-})-Cu^{2+} product.[180] These compounds were originally

stabilized at low temperature (–80 °C) in organic solvents. Early examples are $[Cu_2^{2+}(XYLO^-)(O_2)]^+$ which contained an asymmetrical end-on peroxo moiety,[196] a μ-1,2-peroxo complex $[\{(TMPA)Cu^{2+}\}_2(O_2)]^{2+}$, (Figure 1.2 ^TP)[197] and $[Cu_2^{2+}(N_4)(O_2)]^{2+}$ Figure 1.3).[198] Several analogues of $[\{(TMPA)Cu^{2+}\}_2(O_2)]^{2+}$ and $[Cu_2^{2+}(N_4)(O_2)]^{2+}$ have been characterized, showing variable stability and reactivity.[16,199,200] These complexes were used [201] to generate a reactivity profile based on the type of reactive intermediate. It was determined that $[Cu_2^+(XYLO^-)]^+$ reversibly binds O_2 and that the resulting peroxo complex is basic. This means that a catalyst that works through a nucleophilic substitution mechanism. It was also determined that the complex $[Cu_2^+(XYLO^-)O_2]^+$ does not oxygenate triphenylphosphine nor CO, but it releases O_2 and binds PPh3 and CO. The peroxo complex however can be protonated to afford a μ-1,1-hydroperoxo complex, (Figure 1) or it can be acylated to form an analogous μ-1,1-acylperoxo complex. [202] Further, $[Cu_2^{2+}(XYLO^-)(O_2)]^+$ reacts as a nucleophile with CO_2, with the formation of a percarbonato species that thermally decomposes to the carbonato complex $[Cu_2^{2+}(XYLO^-)(CO_3)]^+$. Phenols are not hydroxylated nor oxidatively coupled (forming a dimer product) by $[Cu_2^{2+}(XYLO^-)(O_2)]^+$, but it was the first example of a model system in the area of Type-3 oxidase biomimetics to show reactivity consistent with general acid-general base chemistry. The same nucleophilic chemistry is observed in reactions of $[\{(TMPA)Cu^{2+}\}_2(O_2)]^{2+}$.[201,203] With these preliminary results it became evident that the nature of the intermediate would determine reactivity.

By contrast, the μ-η^2:η^2 side-on peroxo complex $[Cu_2^{2+}(N_4)(O_2)]^{2+}$ reacts differently with the same substrates tested for the end-on peroxo complexes[201] yielding

$O=PPh_3$ in a reaction with PPh_3. Perhaps one of the simplest and most elegant example of a model compound for Type-3 oxidases was synthesized by Stack and co-workers;[204] they showed that a side-on peroxo complex formed from a simple binucleating ligand, namely $[\{(L)Cu\}_2(O)_2]^{2+}$ (L=N,N-di-tert-butyl-N,N'-dimethylethylenediamine Figure 1.4 B), also oxygenates PPh_3. Further, $[Cu_2^{2+}(N_4)(O_2)]^{2+}$ does not protonate, acylate, nor react with CO_2. The peroxo complex oxidizes phenols by H^+ abstraction, leading to catalytic oxidative coupling chemistry under pre-equilibrium conditions (i.e. in the presence of excess phenol and dioxygen). Thus, a side-on peroxo complex is nonbasic or electrophilic in its reactivity toward these substrates. The electrophilic behavior of these model compounds has also been demonstrated in reactions of greater impact, as in hydroxylation of arenes (including phenols); this reactivity can have significant implications toward green chemistry, since phenols and chlorinated phenols are rather stable pollutants which can contaminate soil and water ways. Activation of the peroxo complex $[Cu_2^{2+}(XYLO^-)(O_2)]^+$,[201] was also determined to be electrophilic with H^+ or CO_2, affording $[Cu_2^{2+}(XYLO^-)(O_2H)]^{2+}$ [201] and the percarbonato species $[Cu_2^{2+}(XYLO^-)(CO_4)]^+$, respectively. These, in contrast to the original end-on peroxo complex $[Cu_2^{2+}(XYLO^-)(O_2)]^+$, readily convert PPh_3 to $O=PPh_3$. Thus, in biochemical systems, hydroperoxo-copper complexes are a possible reactive intermediate which may include percarbonato species, since CO_2 as bicarbonate is certainly available in biological media. While carried out for a specific set of peroxo-dicopper(II) compounds, the trends observed in these early reactivity studies of reactive intermediate types in copper-dioxygen chemistry have generally been found to be consistent; however, there are some

exceptions.[190,205,206] The end-on peroxo complexes with nucleophilic behavior have not yet shown oxidative chemistry comparable to the side-on complexes; however, Karlin and co-workers continue to pursue if ths alternative structure can perform useful chemistry, such as in the Baeyer-Villiger oxidation (oxidation of ketones to carboxylic acids in the presence of peracids).

It is now known that binuclear copper enzymes such as tyrosinase and catechol oxidase adopt the side-on μ-η^2:η^2-peroxo structure, as do model compounds like the Kitajima/Fujisawa complex, the Karlin complex $[Cu_2^{2+}(N_4)(O_2)]^{2+}$ and several other analogues.[16] The great number of investigations in copper(I)–dioxygen reactivity have also revealed a novel binding motif in which the peroxo O–O bond is fully cleaved, after receiving 2 electrons from di-Cu^{2+}, resulting in a high-valent dicopper(III) bis-μ-oxo (Cu_2^{3+}-O_2) species (Figure 1.2 **O**), first characterized by Tolman's group,[207] using tridentate substituted triazacyclononane as ligands, and also by Stack and co-workers,[208,188] using ethylenediamine-based donors.[16,188] The two isoelectronic species have dinstinct spectroscopic features and structural differences. The main structural difference is the shortened Cu–Cu distance of ~2.8 Å for the bis-μ-oxo-dicopper(III) species when compared to the side-on peroxo-dicopper(II) Cu–Cu distance of ~3.5 Å. Theoretical calculations haved predicted that there is a small difference in the free energies of the side-on peroxo Cu_2^{2+}-O_2 and the Cu_2^{3+}-O_2 species and a low barrier for interconversion,[209-211] meaning that under experimental conditions (ambient temperature) the two forms are under equilibrium. This is experimentally observed in several systems

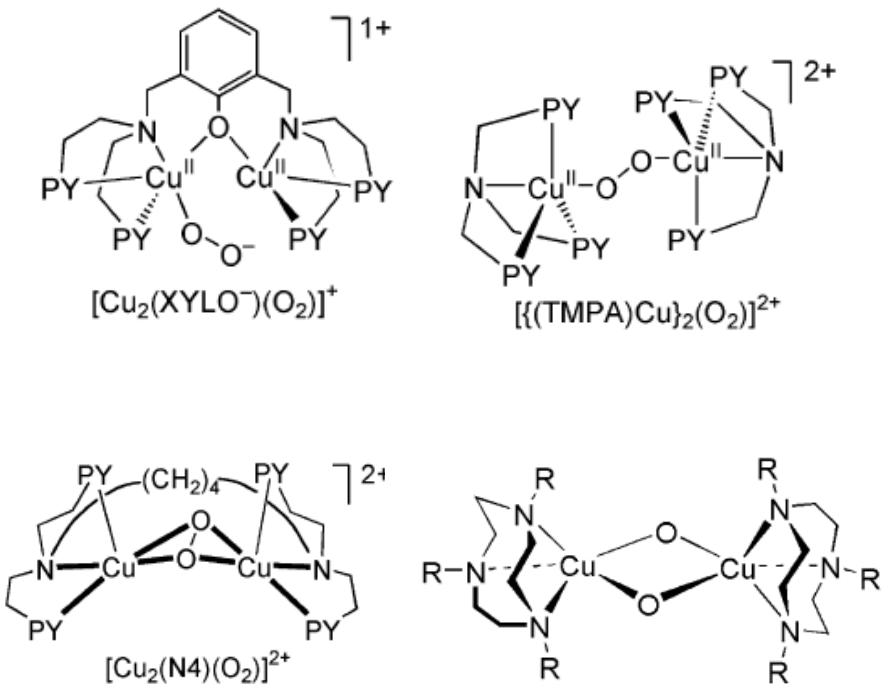

Figure 1.4. Early examples of Type-3 oxidase models by Karlin.[196-198] and Tolman.[207]

where the side-on peroxo-dicopper(II) and bis-μ-oxo-dicopper(III) species are found in a dynamic equilibrium, strongly influenced by the nature of the ligand such as denticity, N-alkyl vs. N-pyridyl donor, and steric effect, as well as reaction conditions, including concentration, counter ion effect, temperature, and solvent.[16,188] These well-characterized

Cu_2O_2-containing synthetic complexes are quite reactive, with oxidative capabilities ranging from alcohol/catechol oxidation, oxo transfer to phosphines and sulfides, to aromatic/aliphatic hydroxylations, and also oxidative N-dealkylations.[11] The existence of two oxidative species coexisting in equilibrium complicates the determination of which form is the true reactive intermediate responsible for the reactivity. A brief summary and comparison of Karlin's and Tolman's effors is discussed below, highlighting preferential reactivity patterns of side-on peroxo-dicopper(II) and bis-μ-oxo-dicopper(III) species.

Karlin's group[212,213] elucidated several examples of copper-promoted dioxygen activation. While stoichiometric in nature, this monooxygenase model system is a rare chemical system where an unactivated C–H bond substrate is rapidly hydroxylated under "very mild" conditions utilizing dioxygen (–80 °C and ≤1 atm O_2).[213,214] The dicopper(I) complex $[Cu_2^{+}(XYL\text{-}H)]^{2+}$ reacts with O_2 to form $[Cu_2^{2+}(XYLO^{-})(OH)]^{2+}$ stoichiometrically. Isotope labeling experiments (using ^{18}O) demonstrate the product phenol O-atom is derived from dioxygen, and the observed O_2-consumption stoichiometry ($Cu:O_2 = 2:1$) is consistent with monooxygenases. Detailed low temperature stopped-flow kinetic studies[180,215] revealed the intermediate

$[Cu_2^{2+}(XYL\text{-}H)(O_2)]^{2+}$. Its peroxo structure was confirmed by utilizing the electron withdrawing R=NO_2 derivative, which results in a decreased k_{on} but even more diminished first order rate constant for the hydroxylation step, thus allowing for spectroscopic investigation.[179,215] In resonance Raman studies, characteristics of $[Cu_2^{2+}(NO_2\text{-}XYL\text{-}H)(O_2)]^{2+}$ are conistent with a $\mu\text{-}\eta^2\text{:}\eta^2$-peroxo moiety, with the O–O vibrational stretch at 747 cm^{-1}.[216] Analysis of spectroscopic and kinetic studies indicates that the side-on peroxo moiety is the reactive species responsible for oxygentation, supported by the observation that the O–O stretching disappears at the same rate as the phenolic C–O bond stretch at 1320 cm^{-1} in $[Cu_2^{2+}(NO_2\text{-}XYLO^-)(OH)]^{2+}$.[216] A number of results support the *m*-xylyl hydroxylation reaction where $[Cu_2^{2+}(R\text{-}XYL\text{-}H)(O_2)]^{2+}$ acts as an electrophile, attacking the π-system of the arene substrate. Side-on peroxo complexes $[Cu_2^{2+}(R\text{-}XYL\text{-}H)(O_2)]^{2+}$ are very similar to $[Cu_2^{2+}(N_4)(O_2)]^{2+}$, shown to be electrophilic. Stopped-flow kinetic studies showed that rate constant for hydroxylation increases as the R substituent becomes more electron donating (Hammett plot $\rho = -2.1$),[179] with deuterium substitution into the 2-H position of the substrate not affecting the first order rate constant for hydroxylation. The lack of a deuterium kinetic isotope effect is consistent with an electrophilic attack on the arene substrate π-system, precluding C–H bond cleavage in the rate-determining step.[179] Methyl substitution into the xylyl 2-position where hydroxylation occurs for the parent compound $[Cu_2^{+}(XYL\text{-}CH_3)]^{2+}$ in a reaction with O_2, results in aromatic hydroxylation followed by a 1,2-migration of the methyl group. The process is similar to the ‘‘NIH shift’’, observed previously in iron hydroxylases via isotope labeling, where a carbonium

ion intermediate is obtained as a result of an electrophilic iron-oxo reactive intermediate, resulting in R migration.[217] Computational studies indicate that the side-on peroxo moiety is indeed electrophilic; the xylyl hydroxylation reaction can be seen as derived from interactions of the empty π*/σ* orbitals of peroxo O–O with the filled pπ orbitals in the arene substrate.[216,218] The favorable proximity of the side-on peroxo moiety to the *m*-xylyl substrate, due to the ligand design and resulting intramolecular O_2 reaction with two copper(I) centers, is certainly important in promoting the aromatic hydroxylation reaction. In this sense, the system resembles reactions at enzyme active sites, where pre-organization of the substrate and reactive species occur.

Since the discovery and characterization of the model monooxygenase system $[Cu_2^+(XYL\text{-}H)]^{2+}+O_2 \rightarrow [Cu_2^{2+}(XYLO^-)(OH)]^{2+}$, a good number of analogous systems have been described.[11,179] Tolman and co-workers,[206] however, have shown that a bis-μ-oxo-dicopper(III) complex is also capable of aromatic hydroxylation. This observation is opposite in trend to the general reactivity patterns establishedthus far, serving to demonstrate the general points that placing a reactive intermediate species in close proximity to a substrate by ligand design greatly enhances the probability of turnover, and that different types of intermedieates will promote certain placements thus promoting different reactivities. Itoh and co-workers[219] have demonstrated the importance of the side-on peroxo-dicopper(II) species as relevant to phenol *o*-hydroxylation both in synthetic systems and in the enzyme tyrosinase.[220] Cresolase activity (*o*-hydroxylation of phenols, i.e cresol) was successfully mimicked with a Cu^+ complex possessing a tridentate ligand *N*,*N*-bis[2-(2-pyridyl)-

ethyl]-R,R-dideuteriobenzylamine (L^{Py2Bz}, Figure 1.4 A) that binds Cu^{+} and reacts with O_2 to generate a low-temperature stable side-on peroxo-dicopper(II) species.[219,220] Addition of lithium salts of *p*-substituted phenols gives the corresponding *o*-hydroxylated catechols in high yields. Neither oxidation to the *o*-quinone nor C–C/C–O coupled dimerization was observed. With the use of ^{18}O isotope labeling experiments, it was confirmed that the incorporated catechol oxygen atom is derived from O_2.[220] Mechanistic studies revealed substrate saturation kinetics, consisent of formation of a phenolate/Cu_2-O_2 complex prior to the rate-determining oxygenation step. An observed increase in reaction rate with increasing electron donating ability of the X substituent (p-XC_6H_4O-Li) coupled with the lack of a deuterium kinetic isotope effect, suggests the side-on peroxo species reacts via an electrophilic aromatic substitution mechanism,[219] similar to that described for the Karlin system,[179] the dicopper-mediated *m*-xylyl aromatic hydroxylation. To compare and contrast, Itoh and co-workers[220] studied the analogous chemistry on tyrosinase. As it was also seen in the model reaction, oxygenation rates increased with increasing *p*-substituted phenol electron donating properties, clearly demonstrating that the enzyme acts as an electrophilic reactive intermediate. Hammett plots of the enzymatic reaction give a ρ value of –2.4, similar to the model reaction (ρ = –1.8) and Karlin's XYL hydroxylation (ρ = –2.1),[179] supporting the hypothesis that the phenolase activity of tyrosinase occurs by an electrophilic attack by a μ-η^2:η^2-peroxo-dicopper(II) species.

Casella and co-workers[221,222] and Sayre and coworkers[223,224] have also contributed in the area of *o*-phenol hydroxylation chemistry and their papers should be noted.

Consistent with the conclusions described above, Casella's group has also concluded that the side-on μ-η^2:η^2-peroxo species is critical in this chemistry.[221] Stack and co-workers[205] showed that a side-on peroxo-dicopper(II) complex with a secondary amine ligand, N,N-di-tert-butylethylenediamine (Figure 1.4 B), also exhibits some phenolase and catecholase activity, producing mixtures of catechol and *o*-benzoquinone from 2,4-di-tert-butylphenolate as substrate. With addition of the neutral phenol, no oxidatively coupled dimer is produced, contrary to Karlin's complex, $[Cu_2^{2+}(N4)(O_2)]^{2+}$. Stack's side-on peroxo complex is also able to perform other electrophilic types of reactions, converting PPh_3 to $O{=}PPh_3$, catechols to quinones, and benzyl alcohol and benzylamine to benzaldehyde and benzonitrile, respectively.[205]

Bis-μ-oxo-dicopper(III) species have been implicated in a number of different reactivities, including alcohol oxidation, phenol coupling, oxidative N-dealkylation, aliphatic hydroxylation, and oxygenation of phosphines or sulfides.[188] Detailed mechanistic studies and theoretical calculations suggested that the bis-μ-oxo core facilitates hydrogen-atom abstraction reactions.[11,210,211,225] Tolman and co-workers[11,226] studied intramolecular N-dealkylation reactions by bis-μ-oxo-dicopper(III) complexes. The electrophilic nature of the bis-μ-oxo core was elucidated by its lack of reactivity towards acids, while it can only act as an outer-sphere reactive intermediate in the presence of acid. The bis-μ-oxo complex decomposes by oxidative N-deakylation, with one of the arms of the tri-substituted triazacyclononane ligand being cleaved, resulting in production of the primary amine and the aldehyde/ketone. Double crossover experiments using labeled $^{18}O_2$ confirm the carbonyl oxygen derives from the high-valent Cu_2^{3+}-O_2

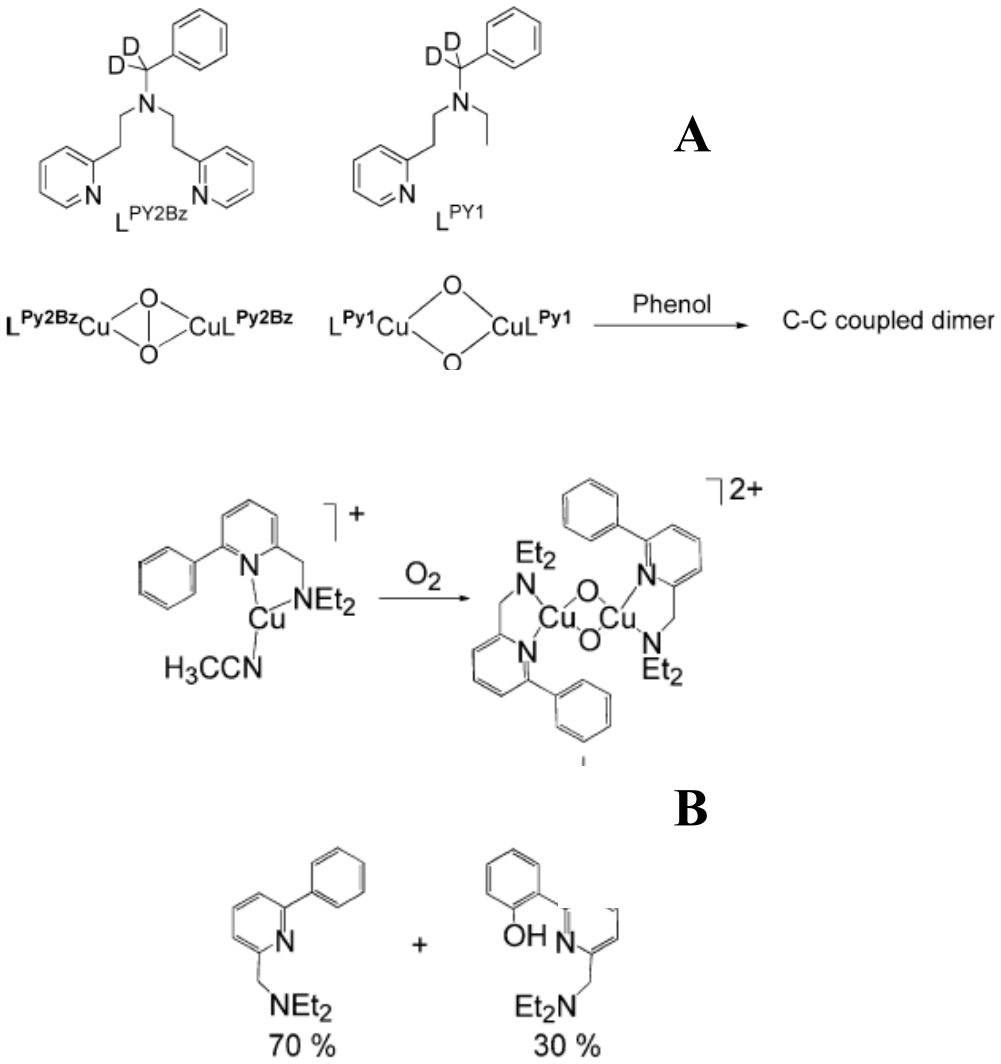

Figure 1.5. Type-3 model systems by Itoh[219] (A) and Stack[204] (B).

core and that the reaction is intramolecular. Primary kinetic isotope effects and Eyring activation parameters revealed that C–H bond cleavage is the rate-determining step. A Hammett study with derivatives of tribenzyl-substituted triazacyclononane ligands demonstrates that reaction rates increase with electron-donating substituents. A small observed negative ρ value of –0.4 suggests the Cu_2^{3+}-O_2 core behaves as an electrophilic radical;[11] similar ρ values were reported for benzylic hydrogen-atom abstraction reactions using free radical reactive intermediates, as well as cytochrome P450 and porphyrin-derived high-valent metal-oxo species. Bis-μ-oxo-dicopper(III) complexes with pyridylalkylamine ligands have been used by Itoh et al.[227] to model benzylic hydroxylation chemistry similar to dopamine-β-monooxygenase (DβM) activity. Their experiments using $^{18}O_2$ confirmed oxygen atom incorporation into the oxygenated alcohol, which in the experiment is trapped by coordinating to copper(II). Deuteration at benzylic positions revealed a large kinetic isotope effect of 35.4 at –80 °C. The activation parameters are consistent with intramolecular rate-determining hydrogen atom abstraction followed by rebound of a copper-bound OH group, analogous to cytochrome P450 monooxygenase chemistry. A Hammett plot based on experiments with varying substituents at the para position gives ρ = –1.48, consistent with benzylic hydrogen atom abstraction reactions. With the tridentate ligand L^{Py2Bz}, benzylic hydroxylation was also observed, but spectroscopic evidence, reveals the low-temperature dioxygen adduct formed is a side-on μ-η^2:η^2-peroxo-dicopper(II) species. For this system, the deuterium kinetic isotope effects are much smaller than expected for a rate-determining hydrogen atom abstraction step, and the rate of hydroxylation is not affected by the *p*-substituent of

the ligand. Instead, the rate of reaction was found to be solvent dependent. From the combined observations, it was proposed that cleavage of the O–O bond to form the high-valent copper(III) bis-μ-oxo core was rate-limiting, which is then responsible for the hydrogen atom abstraction.[228] Karlin and co-workers[229,230] showed that copper(I)/O_2 reactivity with tridentate ligands give rise to mixtures of side-on peroxo-dicopper(II) and bis-μ-oxo-dicopper(III) complexes, in rapid equilibrium at –80 °C. These showed oxidative chemistry towards different substrates. With respect to dimethylaniline oxidative N-dealkylation, mechanistic studies using *p*-substituted and deuterated dimethylanilines suggest the reactive intermediate can operate via either a rate-limiting hydrogen-atom abstraction or electron-transfer pathway, depending on the R group in the complex $[\{Cu(R\text{-}Me\text{-}PY2)\}_2(O_2)]^{2+}$ and the ease of the substrate oxidation.[231]

Itoh and co-workers[232] have been successful in distinguishing the active intermediate for the radical coupling of neutral phenols. According to their spectroscopic features, the Cu_2O_2 adducts are the bis-μ-oxodicopper(III) and the side-on peroxo-dicopper(II) species (Figure 1.2), respectively. Both isomeric species react with neutral phenols to produce solely the C–C coupled dimers. Both Cu_2^{3+}-$(O)_2$ and Cu_2^{2+}-(O_2) species exhibit this same behavior. However, the rate constant for the reaction of the bis-μ-oxo species was two orders of magnitude greater than that for the peroxo complex. This could be due to two reasons: either the bis-μ-oxo is intrinsically a better reactive intermediate than the side-on peroxo because of a difference in redox potentials, or the $(LPY1)_2Cu_2^{3+}$-$(O)_2$ bis-μ-oxo complex is the true reactive intermediate, which would be in much higher concentration than a small amount of bis-μ-oxo isomer present in

equilibrium with the side-on complex $(L^{Py2Bz})_2Cu_2^{2+}$-(O_2). The hypothesis that the bis-μ-oxo is the true reactive species is favored because if the side-on peroxo complex was able to couple phenols via the proton-coupled electron transfer mechanism, then the reaction with phenolates should also occur through an outer-sphere electron transfer mechanism to give the coupled phenol. However, this contradicts previous observations that the μ-η^2:η^2-peroxo-dicopper(II) complex reacts with phenolates to yield solely *o*-catechol products.

In the chemistry described for hydroperoxodicopper(II) (Figure 1.2 μ-1,1 hydroperoxo), enhanced electrophilic reactivity occurs due to protonation of less reactive and nucleophilic peroxo-dicopper(II) complex, at least with respect to triphenylphosphine oxygenation. While the latter reaction is not of great importance due to the ease of PPh_3 oxygenation, protonation of peroxo-copper or other O_2-derived species may be important as a means of peroxo-copper activation.[233-235] In heme enzymes such as cytochrome P450 monooxygenase, protonation of a heme-peroxo leads to O–O heterolytic cleavage and generation of the high-valent ferryl species responsible for electrophilic oxidation reactions like C–H hydroxylation or epoxidation.[236] Activation to an alternate reactive intermediate appears to be present in heme oxygenase, where an O_2-derived heme-hydroperoxo species attacks the porphyrin meso-carbon substrate.[237,238] More unique examples of reactivity for binuclear hydroperoxo complexes which do not have the ArO^- bridging ligands have been reported.[239] Although structural descriptions are not as readily available, kinetic and/or spectroscopic probing shows such Cu^{2+}-$(-O_2H)$-Cu^{2+} intermediates are capable of arene hydroxylation. Thus, Karlin, Zuberbühler, and co-

workers[239] report that reaction of a dicopper(II) complex with ligand XYL-H and hydrogen peroxide also leads to efficient arene hydroxylation. It is likely, according to reactivity, that a μ-η^1:η^1-OOH hydroperoxo-dicopper(II) species facilitates arene hydroxylation. Casella and co-workers[240] reported a compound capable of performing double arene hydroxylation, again in a dicopper(II) plus hydrogen peroxide reaction; not only were kinetic parameters determined for the kinetics of substrate attack by an η^1:η^1-hydroperoxo-dicopper(II) intermediate, but the latter was also characterized by UV-Vis and EPR spectroscopies. Thus, dicopper(II)-hydroperoxo species, with or without an additional phenoxo bridging ligand, which could, be replaced by a water or hydroxo ligand in solution,[240] can effect oxidation reactions, and further exploration of their chemistry should be considered.

The work involved in ligand design and low-temperature techniques leads to stable enough species to be characterized spectroscopically, but may prevent efficient reactivity, especially for hydrocarbon-based substrates. Thus, there is a general caveat in concluding that an observed organic substrate oxidative reaction actually occurs from a well-defined and fairly stable Cu_n-O_2(H) complex. The true reactive intermediate may be something other than what can be observed spectroscopically. It is possible that a transient mononuclear Cu^{3+}-oxide$\leftrightarrow Cu^{2+}$-$O\bullet^-$ species is the most likely candidate for the reaction of Type-3 oxidases both in the native proteins and their biomimetic models.[188]

VII. CONCLUDING REMARKS

Considerable effort in trying to elucidate the nature of the cause of neurodegeneration in AD and the catalytic mechanism through which Type-3 copper oxidases catalyze their chemical transformations has yielded some common threads. First, it is known that oxygen radicals and reduced forms of oxygen collectively termed ROS are generated during normal metabolism. It is also know that the amyloid-β fibrils and plaques can generate those same ROS via a metal-centered mechanism. These activated forms of O_2 are no different than the metal-bound forms associated with Type-3 copper oxidases. It is expected that further analysis of metal complexes of amyloid-β can show that the chemistry proposed as the culprit in the etiology of AD is very much consistent with the reactivity of Type-3 copper oxidases and their biomimetic systems.

VI. LIST OF REFERENCES

1) R.J.P. Williams, J.J.R. Frausto da Silva, *The Biological Chemistry of the Elements: The Inorganic Chemistry of Life*, Oxford University Press, New York, 2001.

2) K. Shikama, Nature of the FeO_2 bonding in myoglobin and hemoglobin: A new molecular paradigm. *Prog. Biophys. & Mol. Biol.* (2006), 91, 83-162.

3) R.E. Stenkamp, Dioxygen and Hemerythrin. *Chem. Rev.* (1994), 94, 715-26.

4) M.-H. Baik, M. Newcomb, R.A. Friesner, S.J. Lippard, Mechanistic Studies on the Hydroxylation of Methane by Methane Monooxygenase. *Chem. Rev.* (2003), 103, 2385-2419.

5) S.J. Lange, L. Que Jr., Oxygen activating nonheme iron enzymes. *Curr. Opinion Chem. Biol.* (1998), 2, 159-172.

6) E.I. Solomon, P. Chen, M.Metz, S.-K Lee, A.E. Palmer, Oxygen binding, activation, and reduction to water by copper proteins. *Angew. Chem. Int. Ed.* (2001), 40, 4570-4590.

7) C. Gerdemann, C. Eicken, B. Krebs, The crystal structure of catechol oxidase : New insight into the function of type-3 copper proteins. *Acc. Chem. Res.* (2002), 35, 183-191.

8) J.W. Whittaker, The radical chemistry of galactose oxidase. *Arch. Biochem. Biophys.* (2005), 433, 227-239.

9) I.A. Koval, P. Gamez, C. Belle, K. Selmeczi, J. Reedijk, Synthetic models of the active site of catechol oxidase: Mechanistic studies. *Chem. Soc. Rev.* (2006), 35, 814-840.

10) A. Decker, E.I. Solomon, Dioxygen activation by copper, heme and non-heme iron enzymes: comparison of electronic structures and reactivities. *Curr. Opinion Chem. Biol.* (2005), 9, 152-163.

11) E.A. Lewis, W.B. Tolman, Reactivity of Dioxygen-Copper Systems. *Chem. Rev.* (2004), 104, 1047-1076.

12) J. Anekwe, A. Hammerschmidt, A. Rompel, B. Krebs, Altering the activity of catechol oxidase model compounds by electronic influence on the copper core. *Zeitschrift fuer Anorganische und Allgemeine Chemie* (2006), 632, 1057-1066.

13) K.D. Karlin, M.S. Haka, R.W. Cruse, G.J. Meyer, A. Farooq, Y. Gultneh, J.C. Hayes, J. Zubieta, Dioxygen-copper reactivity. Models for hemocyanin: Reversible O_2 and CO binding to structurally characterized dicopper(I) complexes containing hydrocarbon-linked bis[2-(2-pyridyl)ethyl]amine units. *J. Am. Chem. Soc.* (1988), 110, 1196-1207.

14) N. Kitajima, K. Fujisawa, C. Fujimoto, Y. Morooka, S. Hashimoto, T. Kitagawa, K. Toriumi, K. Tatsumi, A. Nakamura, A new model for dioxygen binding in hemocyanin. Synthesis, characterization, and molecular structure of the μ-η2:η2 peroxo binuclear copper(II) complexes, [Cu(HB(3,5-R_2pz)$_3$)]2(O_2) (R = isopropyl and Ph). *J. Am. Chem. Soc.* (1992), 114, 1277-1291.

15) M.J. Baldwin, D.E. Root, J.E. Pate, K. Fujisawa, N. Kitajima, E.I. Solomon, Spectroscopic studies of side-on peroxide-bridged binuclear copper (II) model complexes of relevance to oxyhemocyanin and oxytyrosinase. *J. Am. Chem. Soc.* (1992), 114, 10421-10431.

16) L.M. Mirica, X. Ottenwaelder, T.D.P. Stack, Structure and Spectroscopy of Copper-Dioxygen Complexes. *Chem. Rev.* 2004, 104, 1013-1045.

17) G. Stark, Functional Consequences of Oxidative Membrane Damage. *J. Membrane Biol.* (2005), 205, 1-16.

18) M. Valko, H. Morris, M.T.D Cronin, Metals, toxicity and oxidative stress. *Curr. Med. Chem.* (2005), 12, 1161-1208.

19) L.R. Ferguson, M. Philpott, N. Karunasinghe, Oxidative DNA damage and repair: significance and biomarkers. *J. Nutrition.* (2006), 136, 2687S-2689S.

20) M.E. Goetz, M. Gerlach, Formation of radicals. *Brain Damage and Repair* (2004), 135-164.

21) E. Gaggelli, H. Kozlowski, D. Valensin, G. Valensin, Copper Homeostasis and Neurodegenerative Disorders (Alzheimer's, Prion, and Parkinson's Diseases and Amyotrophic Lateral Sclerosis) *Chem. Rev*. (2006), 106, 1995-2044.

22) http://scc.healthcentral.com/bcp/main.asp?page=newsdetail&id=521133&ap=68&brand=30

23) http://www.alzheimersupport.com/library/showarticle.cfm/ID/1352/T/Alzheimers/searchtext/

24) Y. Ling, K. Morgan, N. Kalsheker, *Int. J. Biochem. Cell. Biol*. (2003), 35, 1505-1535.

25) A. I. Bush, The metallobiology of Alzheimer's disease. *Trends Neurosci*. (2003), 26, 207-214.

26) A. Kontush, C. Berndt, W. Weber, V. Akopian, S. Arlt, S. Schippling, U. Beisiegel, *Free Rad. Biol. Med*. (2001), 30, 119-128.

27) R.A. Capaldi, Structural features of the mitochondrial electron-transfer chain. *Curr. Op. Struct. Biol.* (1991), 1, 562-568.

28) M. Sawada, U. Sester, J.C. Carlson, Superoxide radical formation and associated biochemical alterations in the plasma membrane of brain, heart, and liver during the lifetime of the Rat. *J. Cell. Biochem.* (1992), 48, 296-304.

29) R.S. Sohal, L.A. Arnold, B.H. Sohal, Age-related changes in antireactive intermediate enzymes and proreactive intermediate generation in tissues of the rat with special reference to parameters in two insect species. *Free Rad. Biol. Med.* (1990), 10, 495-500.

30) G.M. Abu-Erreish, D.R. Sanadi, Age-related changes in cytochrome concentration of myocardial mitochondria. *Mech. Ageing Dev.* (1978), 7, 425-432.

31) G. Benzi, Enzymatic activities related to energy transduction in the mature rat brain. Interdiscip. *Topics Geront.* (1979), 15, 104-120.

32) G. Benzi, Peroxidation, energy transduction and mitochondria during aging. London, Paris: John Libbey Eurotext, 1990.

33) G. Benzi, O. Pastoris, F. Marzatico, R.F. Villa, F. Dagani, D. Curti, The mitochondrial electron transfer alteration as a factor involved in the brain aging. *Neurobiol. Aging* (1992), 13, 361-368.

34) P.H. Gold, M.W. Gee, B.L. Strehler, Effect of age on oxidative phosphorylation in rat. *J. Gerontol.* (1968), 23, 509-512.

35) D. Curti, G. Benzi, Cytochrome c oxidase activity in discrete brain regions: age-related changes. *Arch. Gerontol. Geriatr. Suppl.* (1991), 2, 549-556.

36) D. Curti, M.C. Giangar, M.E. Redolfi, I. Fugaccia, G. Benzi, Age-related modifications of cytochrome c oxidase activity in discrete brain regions. *Mech. Ageing Dev.* (1990), 55, 171-180.

37) S. Algeri, C. Cafa, A. Cagnotto, F. Marzatico, T. Mennini, L. Raimondi, G. Sacchetti, Calory restriction counteracts some of the neurochemical changes in the cortical neurons of senescent rats. *Neurobiol. Aging* (1992), 31, S134.

38) G. Barja de Quiroga, R. Perez-Campo, M. Lfipez Torres, Antireactive intermediate defences and peroxidation in liver and brain of aged rats. *Biochem. J.* (1990), 272, 247-250.

39) R.S. Sohal, Aging, cytochrome oxidase activity, and hydrogen peroxide release by mitochondria. *Free Rad. Biol. Med*. (1993), 14, 583-588.

40) Q.L. Wang, W. Luo, W. Zheng, Y. Liu, H. Xu, G. Zheng, Z. Dai, W. Zhang, Y. Chen, J. Chen, Iron supplement prevents lead-induced disruption of the blood-brain barrier during rat development. *Toxicol. App. Pharmacol.* (2007), 219, 33-41.

41) S.J. Kish, C. Bergeron, A. Rajput, S. Dozic, F. Mastrogiacomo, L.-J. Chang, J.M. Wilson, L.M. DiStefano, J.N. Nobrega, Brain cytochrome oxidase in Alzheimer's disease. *J. Neurochem.* (1992), 59, 776-779.

42) S.J. Kish, L.M. DiStefano, S. Dozic, J.N. Nobrega, Cerebral cortical but not hippocampal cytochrome oxidase activity is reduced in Alzheimer's disease. *Neurobiol. Aging* (1992),13, suppl. 106.

43) H. Reichmann, S. Flerke, G. Hebenstreit, H. Schrubar, P. Riederer, Analyses of energy metabolism and mitochondrial genome in postmortem brain from patients with Alzheimer's disease. *J. Neurol.* (1993), 240, 377-380.

44) K.J. Reinikainen, L. Paljarvi, T. Halonen, O. Malminen, V.-M. Kosma, M. Laakso, P.J. Riekkinen, Dopaminergic system and monoamine oxidase-β activity in Alzheimer's disease. *Neurobiol. Aging* (1988), 9, 245-252.

45) W.D. Parker Jr., C.M. Filley, Parks, J. K. Cytochrome oxidase deficiency in Alzheimer's disease. *Neurology* (1990), 40, 1302-1303.

46) A.J. Van Zuylen, G.J.C.G.M. Bosman, W. Ruitenbeek, P.J.C. Van Kalmthout, W.J. De Grip, No evidence for reduced thrombocyte cytochrome oxidase activity in Alzheimer's disease. *Neurology* (1992), 42, 1246-1247.

47) M.T.T. Wong-Riley, Cytochrome oxidase: An endogenous metabolic marker for neuronal activity. *Trends Neurosci.* (1989), 12, 94-101.

48) K. Chaudrasekaran, J. Stoll, D.R. Brady, S.I. Rapoport, Distribution of cytochrome oxidase (COX) activity and mRNA in monkey and human brain. COX mRNA distribution correlates with neurons vulnerable to Alzheimer pathology. *Soc. Neurosci. Abstr.* (1992), 18, 557

49) K. Chandrasekaran, J. Stoll, D.R. Brady, S.I. Rapoport, Localization of cytochrome oxidase (COX) activity and COX mRNA in the hippocampus and entorhinal cortex of

the monkey brain: correlation with specific neuronal pathways. *Brain. Res*. (1992), 579, 333-336.

50) K. Chandrasekaran, T. Giordano, D.R. Brady, J. Stoll, L.J. Martin, S.I. Rapoport, Impairments in mitochondrial cytochrome oxidase gene expression in Alzheimer disease. *Mol. Brain Res.* (1994), 24, 336-340.

51) M.C. Bennet, D.M. Diamond, S.L. Stryker, J.K. Parks, W.D. Parker Jr., Cytochrome oxidase inhibition: A novel animal model of Alzheimer's disease. *J. Geriat. Psych. Neurol.* (1992), 5, 93-101.

52) H.A. Kontos, E.P. Wei, E.F. Ellis, L.W. Jenkins, J.T. Povlishock, G.T. Rowe, M.L. Hess, Appearance of superoxide anion radical in cerebral extracellular space during increased prostaglandin synthesis in cats. *Circ. Res.* (1985), 57, 142-151.

53) S. Nakamura, T. Kawamata, I. Akiguchi, M. Kameyama, N. Nakamura, H. Kimura, Expression of monoamine oxidase B activity in astrocytes of senile plaques. *Acta Neuropathol.* (1990), 80, 419-425.

54) M. Valko, D. Leibfritz, J. Moncol, M.T.D. Cronin, M. Mazur, J. Telser, Free radicals and antioxidants in normal physiological functions and human disease. *Intern. J. Biochem. Cell Biol.* (2006), 39, 44-84.

55) Y. Kono, I. Fridovich, Superoxide radical inhibits catalase. *J. Biol. Chem.* (1982), 257, 5751-5754.

56) J. Blum, I. Fridovich, Inactivation of glutathione peroxidase by superoxide radical. *Arch. Biochem. Biophys.* (1985), 240, 500-508.

57) N.F. Schor, Inactivation of mammalian brain glutamine synthetase by oxygen radicals. *Brain Res.* (1988), 456, 17-21.

58) G.C. Palmer, Free radicals generated by xanthine oxidasehypoxanthine damage adenylate cyclase and ATPase in gerbil cerebral cortex. *Metabol. Brain Dis.* (1987), 2, 243-256.

59) J.M. McCord, W.J. Russell, Superoxide inactivate creatine phosphokinase during reperfusion of ischemic heart. In: P.A. Cerutti, I. Fridovich, J.M. McCord, eds. Oxy-radicals in molecular biology and pathology. New York: Alan R. Liss; (1988), 27-35.

60) Y. Zhang, Marcillat, C. Giulivi, L. Ernster, K.J.A. Davies, The oxidative inactivation of mitochondrial electron transport chain components and ATPase. *J. Biol. Chem.* (1990), 265, 16330-16336.

61) J.P. Blass, A.C. Baker, L.-W. Ko, R.S. Black, Induction of Alzheimer antigens by an uncoupler of oxidative phosphorylation. *Arch. Neurol.* (1990), 47, 864-869.

62) N.R. Sims, J.M. Finegan, J.P. Blass, D. M. Bowen, D. Neary, Mitochondrial function in brain tissue in primary degenerative dementia. *Brain Res*. (1987), 436, 30-38.

63) A.C. Baker, L.-W. Ko, J.P. Blass, Systemic manifestations of Alzheimer's disease. *Age* (1988), 11, 60-65.

64) J.N. Kanfer, J.W. Pettegrew, J. Moossy, D.G. McCartney, Alterations in selected enzymes of phospholipids metabolism in Alzheimer's disease brain tissue as compared to nonAlzheimer's demented controls. *Neurochem. Res.* (1993), 18, 331-334.

65) P.J. Benke, H. Levcovitz, J. Paupe, E. Tozman, Scavengers of free radical oxygen affect the generation of low molecular weight DNA in stimulated lymphocytes from

patients with systemic lupus erythematosus. *Metabol. clin. experiment.* (1990), 39, 1278-1284.

66) M. Krenz , M.V. Cohen Michael, J,D. Downey, The protective and anti-protective effects of ethanol in a myocardial infarct model. *Annals N.Y. Acad. Sci.* (2002), 957 103-114.

67) http://www.rsbs.anu.edu.au/ResearchGroups/PBE/Oxygen.html

68) G. Benzi, O. Pastoris, F. Marzatico, R.F. Villa, Cerebral enzyme antireactive intermediate system. Influence of aging and phosphatidylcholine. *J. Cereb. Blood Flow Metabol.* (1989), 9, 373-380.

69) A. Gupta, M. Hasan, R. Chander, N.K. Kapoor, Age-related elevation of lipid peroxidation products: diminution of superoxide dismutase activity in the central nervous system of rats. *Gerontol.* (1991), 37, 305-309.

70) G. Rao, E. Xia, A. Richardson, Effect of age on the expression of antireactive intermediate enzymes in male Fischer F344 rats. *Mech. Ageing Dev.* (1990), 53, 49-60.

71) I. Semsei, G. Rao, A. Richardson, Expression of superoxide dismutase and catalase in rat brain as a function of age. *Mech. Ageing Dev.* (1991), 58, 13-19.

72) A. Vanella, E. Geremia, G. D'Urso, P. Tiriolo, I. Di Silvestro, R. Grimaldi, R. Pinturo, Superoxide dismutase activities in aging rat brain. *Gerontol.* (1982), 28, 108-113.

73) M.C. Carrillo, S. Kanai, Y. Sato, K. Kitani, Age-related changes in antireactive intermediate enzyme activities are region and organ, as well as sex, selective in the rat. *Mech. Ageing Dev.* (1992), 65, 187-198.

74) H. C. Danh, M. Strolin Benedetti, P. Dostert, Differential changes in superoxide dismutase activity in brain and liver of old rats and mice. *J. Neurochem.* (1983), 40, 1003-1007.

75) G. Forloni, β-amyloid neurotoxicity. *Funct. Neurol.* (1993), 8, 211-225.

76) B.W.L. Brooksbank, R. Balazs, Superoxide dismutase, glutathioneperoxidase and lipoperoxidation in Down's syndrome fetal brain. *Dev. Brain Res.* (1984), 16, 37-44.

77) Y. Groner, K.B. Avraham, M. Schickler, R. Yarom, H. Knobler, Down syndrome: Gene dosage and clinical symptoms in transgenic-copper-zinc-SOD mice. *Adv. Mol. Gen.* (1991), 4, 181-211.

78) C.J. Epstein, K.B. Avraham, M. Lovett, S. Smith, O. Elroy-Stein, G. Rotman, C. Bry, Y. Groner, Transgenic mice with increased copper/zinc-superoxide dismutase activity: animal model of dosage effects in Down syndrome. *Proc. Nat. Acad. Sci. U S A* (1987), 84, 8044-8048.

79) I. Ceballos-Picot, A. Nicole, P. Briand, G. Grimber, A. Delacourte, A. Defossez, F. Javoy-Agid, M. Lafon, J.L. Blouin, P.M. Sinet, Neuronal-specific expression of human copper-zinc superoxide dismutase gene in transgenic mice: Animal model of gene dosage effects in Down's syndrome. *Brain Res.* (1991), 552, 198-214.

80) A. L. Friedlich, T.W. Farris, E. Carlson, C.J. Epstein, L.L. Butcher, β-Amyloid protein-induced neurotoxicity in wild type mice and in transgenic mice with elevated CuZn superoxide dismutase activity. *Soc. Neurosci. Abstr.* (1993), 19, 1036.

81) I. Ceballos, F. Javoy-Agid, A. Delacourte, A. Defossez, M. Lafon, E. Hirsch, A. Nicole, P.M. Sinet, Y. Agid, Neuronal localization of copper-zinc superoxide dismutase protein and mRNA within the human hippocampus from control and Alzheimer's disease Brains. *Free Rad. Res. Comm.* (1991), 12-13, 571-580.

82) D. Games, K.M. Khan, F.G. Soriano, I. Lieberburg, S. Sinha, Evidence for altered APP processing following acute head trauma in the rodent. *Soc. Neurosci. Abstr.* (1992), 18, 1437.

83) S. Bahmanyar, G.A. Higgins, D. Goldgaber, D.A. Lewis, J.H. Morrison, M.C. Wilson, S.K. Shankar, D.C. Gajdusek, Localizationof amyloid/3 protein messenger RNA in brains from patients with Alzheimer's disease. *Science* (1987), 237, 77-80.

84) G. Moll, Neurotransmittermetabolismus, Energiestoffwechsel und Radikale in der Pathogenese der Demenz vom Alzheimer-Typ. *Z. Gerontol.* (1991), 24, 212-213.

85) S.S. Panter, M. Scott, Elevated temporal cortex superoxide dismutase in Alzheimer's Disease. *Soc. Neurosci. Abstr.* (1991), 17, 1072.

86) F. P. Zemlan, O.J. Thienhaus, H.B. Bosmann, Superoxide dismutase activity in Alzheimer's disease: Possible mechanism for paired helical filament formation. *Brain Res.* (1989), 476, 160-162.

87) G. Tesco, S. Latorraca, P. Piersanti, S. Piacentini, L. Amaducci, S. Sorbi, Alzheimer skin fibroblasts show increased susceptibility to free radicals. *Mech. Ageing Dev.* (1992), 66, 117-120.

88) M.A. Pappolla, R.A. Omar, K.S. Kim, N.K. Robakis, lmmunohistochemical evidence of antireactive intermediate stress in Alzheimer's disease. *Am. J. Pathol.* (1992), 140, 621-628.

89) R.A.Cherny, J.T. Legg, C.A. McLean, D.P. Fairlie, X. Huang, C.S. Atwood, K. Beyreuther, R.E. Tanzi, C.L. Masters, A.I. Bush, Aqueous dissolution of Alzheimer's disease Aβ amyloid deposits by biometal depletion. *J. Biol. Chem.* (1999), 274, 23223-23228.

90) R. Balakrishnan, R. Parthasarathy, E. Sulkowski, Alzheimer ' s β-amyloid peptide: affinity for metal chelates. *J. Peptide Res.* (1998), 51, 91-95.

91) C.S. Atwood, R.D. Moir, X. Huang, R.C. Scarpa, N.M.E. Bacarra, D.M. Romano, M.A. Hartshorn, R.E. Tanzi, A.I. Bush, Dramatic aggregation of Alzheimer Aβ by Cu(II) is induced by conditions representing physiological acidosis. *J. Biol. Chem.* (1998), 273, 12817-12826.

92) C.S. Atwood, R.C. Scarpa, X. Huang, R.D. Moir, W.D. Jones, D.P Fairlie, R.E. Tanzi, A.I. Bush, Characterization of copper interactions with Alzheimer amyloid β peptides: identification of an attomolar-affinity copper binding site on amyloid β 1-42. *J. Neurochem.* (2000), 75, 1219-1233.

93) G.F.Z. da Silva, W.M. Tay, and L.-J. Ming, Catechol Oxidase-like Oxidation Chemistry of the 1–20 and 1–16 Fragments of Alzheimer's Disease-related β-

Amyloid Peptide: THEIR STRUCTURE-ACTIVITY CORRELATION AND THE FATE OF HYDROGEN PEROXIDE. *J. Biol. Chem.* (2005), 280, 16601-16609.

94) C.D. Syme, R.C. Nadal, S.E.J. Rigby, J.H. Viles, Copper Binding to the Amyloid-β (Aβ) Peptide Associated with Alzheimer's Disease: FOLDING, COORDINATION GEOMETRY, pH DEPENDENCE, STOICHIOMETRY, AND AFFINITY OF Aβ-(1–28): INSIGHTS FROM A RANGE OF COMPLEMENTARY SPECTROSCOPIC TECHNIQUES *J. Biol. Chem.* (2004), 279, 18169-18177.

95) T. Miura, K. Suzuki, N. Kohata, H. Takeuchi, Metal Binding Modes of Alzheimer ' s Amyloid β -Peptide in Insoluble Aggregates and Soluble Complexes. *Biochemistry* (2000), 39, 7024-7031.

96) C. Curtain, F. Ali, I. Volitakis, R.A. Cherny, R.S. Norton, K. Beyreuther, C.J. Barrow, C.L. Masters, A.I. Bush, Alzheimer's Disease Amyloid-β Binds Copper and Zinc to Generate an Allosterically Ordered Membrane-penetrating Structure Containing Superoxide Dismutase-like Subunits. *J. Biol. Chem.* (2001), 276, 20466-20473.

97) T. Miura, K. Suzuki, H. Takeuchi, Binding of iron(III) to the single tyrosine residue of amyloid β-peptide probed by Raman spectroscopy. *J. Mol. Struct.* (2001), 598, 79–84.

98) D.P. Smith, D.G. Smith, C.C. Curtain, J.F. Boas, J.R. Pilbrow, G.D. Ciccotosto, T.L. Lau, D.J. Tew, K. Perez, J.D. Wade, A.I. Bush, S.C. Drew, F. Separovic, C.L. Masters, R. Cappai, K.J. Barnham, Copper-mediated Amyloid-β Toxicity Is

Associated with an Intermolecular Histidine Bridge. *J. Biol. Chem.* (2006), 281, 15145-15154.

99) R.A. Lieberman, R.H. Sands, J.A. Fee, A study of the electron paramagnetic resonance properties of single monoclinic crystals of bovine superoxide dismutase. *J. Biol. Chem.* (1982), 257, 336-44.

100) C.S. Atwood, R.D. Moir, X. Huang, R.C. Scarpa, N.M.E. Bacarra, D.M. Romano, M.A. Hartshorn, R.E. Tanzi, A.I. Bush, Dramatic aggregation of Alzheimer Aβ by Cu(II) is induced by conditions representing physiological acidosis. *J. Biol. Chem.* (1998), 273, 12817-12826.

101) X. Huang, C.S. Atwood, R.D. Moir, M.A. Hartshorn, R.E. Tanzi, A.I. Bush, Trace metal contamination initiates the apparent auto- aggregation , amyloidosis, and oligomerization of Alzheimer ' s Aβ peptides. *J. Biol. Inorg. Chem.* (2004), 9, 954-960.

102) F.E.A. Ali, K.J. Barnham, C.J. Barrow, F. Separovic, Metal -Catalyzed Oxidative Damage and Oligomerization of the Amyloid-β Peptide of Alzheimer's disease. *Australian J. Chem.* (2004), 57, 511-518.

103) D. Drago, M. Folin, S. Baiguera, G. Tognon, F. Ricchelli, P. Zatta, Comparative Effects of Aβ (1-42)-Al Complex from Rat and Human Amyloid on Rat Endothelial Cell Cultures. *J. Alzheimer's Disease* (2007), 11, 33-44.

104) L. Hou, M.G. Zagorski, NMR Reveals Anomalous Copper(II) Binding to the Amyloid Aβ Peptide of Alzheimer's Disease. *J. Am. Chem. Soc.* (2006), 128, 9260-9261.

105) Y. Mekmouche, Y. Coppel, K. Hochgrafe, L. Guilloreau, C. Talmard, H. Mazarguil, P. Faller, Characterization of the Zn(II) binding to the peptide amyloid-β 1-16 linked to Alzheimer's disease. *ChemBioChem.* (2005), 6, 1663-1671.

106) L.O. Tjernberg, A. Tjernberg, N. Bark, Y. Shi, B.P. Ruzsicska, Z. Bu, J. Thyberg, D.J.E. Callaway, Assembling amyloid fibrils from designed structures containing a significant amyloid β -peptide fragment. *Biochem. J.* (2002), 366, 343-351.

107) U.F. Rohrig, A. Laio, N. Tantalo, M. Parrinello, R. Petronzio, Stability and structure of oligomers of the Alzheimer Peptide Aβ 16-22: from the dimer to the 32-mer. *Biophys. J.* (2006), 91, 3217-3229.

108) L.L. Iversen, R.J. Mortishire-Smith, S.J. Pollack, M.S. Shearman, The Toxicity *in-vitro* of β-Amyloid Protein. *Biochem J.* (1995), 311, 1-16.

109) C.J. Pike, D. Burdick, A.J. Walencewicz, C.G. Glabe, C.W. Cotman, Neurodegeneration Induced by β-Amyloid Peptides in vitro: The Role of Peptide Assembly State. *J. Neurosci.* (1993), 13, 1676-1687.

110) X. Huang, C.S. Atwood, M.A. Hartshorn, G. Multhaup, L.E. Goldstein, R.C. Scarpa, M.P. Cuajungco, D.N. Gray, J. Lim, R.D. Moir, R.E. Tanzi, A.I. Bush, The Aβ Peptide of Alzheimer's Disease Directly Produces Hydrogen Peroxide through Metal Ion Reduction. *Biochemistry* (1999), 38, 7609-7616.

111) K. Hensley, J.M. Carney, M.P. Mattson, M. Aksenova, M. Harris, J.F. Wu, R.A. Floyd, D.A.A. Butterfield, A Model for β-Amyloid Aggregation and Neurotoxicity Based on Free Radical Generation by the Peptide: Relevance to Alzheimer Disease. *Proc. Natl. Acad. Sci.USA* (1994), 91, 3270-3274.

112) A.E. Roher, M.O. Chaney, Y.M. Kuo, S.D. Webster, W.B. Stine, L.J. Haverkamp, A.S Woods, R.J. Cotter, J.M. Tuohy, G.A. Krafft, B.S. Bonnell, M. R. Emmerling, Morphology and Toxicity of Aβ-(1-42) Dimer Derived from Neuritic and Vascular Amyloid Deposits of Alzheimer's Disease. *J. Biol. Chem.* (1996), 271, 20631-20635.

113) W.L. Klein, G.A. Krafft, C.E. Finch, Targeting Small Aβ Oligomers: The Solution to an Alzheimer's Disease Conundrum? *Trends Neurosci.* (2001), 24, 219-224.

114) D.M. Hartley, D.M. Walsh, C.P. Ye, T. Diehl, S. Vasquez, P.M. Vassilev, D.B. Teplow, D.J. Selkoe, Protofibrillar Intermediates of Amyloid β-Protein Induce Acute Electrophysiological Changes and Progressive Neurotoxicity in Cortical Neurons. *J. Neurosci.* (1999), 19, 8876-8884.

115) J.D. Harper, S.S. Wong, C.M. Lieber, P.T. Lansbury, Assembly of Aβ Amyloid Protofibrils: An *in vitro*Model for a Possible Early Event in Alzheimer's Disease. *Biochemistry* (1999), 38, 8972-8980.

116) M.S. Goldberg, P.T. Lansbury, Is There a Cause-and effect Relationship Between β-synuclein Fibrillization and Parkinson's Disease? *Nature Cell Biol.* (2000), 2, 115-119.

117) D.R. Howlett, R.V. Ward, L. Bresciani, K.H. Jennings, G. Christie, D. Allsop, C.W. Gray, E.H. Karran, Biological Activity Associated with a High Molecular Weight Form of β-Amyloid. *Alzheimer's Rep.* (1999), 2, 171-177.

118) S. Turnbull, B.J. Tabner, O.M.A. El-Agnaf, S. Moore, Y. Davies, D. Allsop, α-synuclein Implicated in Parkinson's Disease Catalyses the Formation of Hydrogen Peroxide in Vitro. *Free Radical Biol. Med.* (2001), 30, 1163-1170.

119) Y. Fezoui, D.M. Hartley, D.M. Walsh, D.J. Selkoe, J.J. Osterhout, D.B.A. Teplow, A *de novo* Designed Helix-turn-helix Peptide Forms Nontoxic Amyloid Fibrils. *Nature Structural Biol.* (2000), 7, 1095-1099.

120) S. Varadarajan, S. Yatin, D.A. Butterfield, Alzheimer's Amyloid β Peptide (1-42) Fibrils Are Not Always Neurotoxic. *Alzheimer's Rep.* (2000), 3, 71-76.

121) H. Lin, Y.J. Zhu, R. Lal, Amyloid β Protein (1-40) Forms Calcium-permeable, Zn (II)-sensitive Channel in Reconstituted Lipid Vesicles. *Biochemistry* (1999), 38, 11189-11196.

122) S.D. Yan, X.F.J Chen, M. Chen, H. Zhu, A. Roher, T. Slattery, L. Zhao, M. Nagashima, J. Morser, A. Migheli, P. Nawroth, D. Stern, A.M. Schmidt, RAGE and Amyloid-β Peptide Neurotoxicity in Alzheimer's Disease. *Nature* (1996), 382, 685-691.

123) J. El-Khoury, S.E. Hickman, C.A. Thomas, L. Cao, S.C. Silverstein, J.D. Loike, Scavenger Receptor mediated Adhesion of Microglia to β-Amyloid Fibrils. *Nature* (1996), 382, 716-719.

124) D.M. Paresce, R.N. Ghosh, F.R. Maxfield, Microglial Cells Internalize Aggregates of the Alzheimer's Disease Amyloid β-Protein via a Scavenger Receptor. *Neuron* (1996), 17, 553-565.

125) S.D. Yan, J. Fu, C. Soto, X. Chen, H. Zhu, F. Al-Mohanna, K. Collison, A. Zhu, E. Stern, T. Saido, M. Tohyama, S. Ogawa, A. Roher, D. Stern, An Intracellular Protein That Binds Amyloid-β Peptide and Mediates Neurotoxicity in Alzheimer's Disease. *Nature* (1997), 389, 689-695.

126) C.M. Yip, J. McLaurin, Amyloid-β Peptide Assembly: A Critical Step in Fibrillogenesis and Membrane Disruption. *Biophys. J.* (2001), 80, 1359-1371.

127) C. Kosa, I. Lukac, R.G. Weiss, Photochemical Transformation of Benzil Pendant Groups of Polystyrene Copolymers into Benzoyl Peroxide Moieties and Their Subsequent Thermal Decomposition. Cross-Linking or Chain Scission ? *Macromolecules* (2000), 33, 4015-4022.

128) V. Verney, M.A. Vincent. Study of the thermal decomposition of polypropylene peroxides by means of melt rheology. *Poly. Proc. Eng.* (1986), 3, 321-335.

129) T.H. Peterson, B.K. Carpenter, Estimation of dynamic effects on product ratios by vectorial decomposition of a reaction coordinate. Application to thermal nitrogen loss from bicyclic azo compounds. *J. Am. Chem. Soc.* (1992), 114, 766-767.

130) H. Meier, K.P. Zeller, Thermal and photochemical nitrogen cycloelimination. *Angew. Chem.* (1977), 89, 876-890.

131) C.J. Kay, Mechanochemical Mechanism for Peptidyl Free Radical Generation by Amyloid Fibrils. *FEBS Lett.* (1997), 403, 230-235.

132) K. Hensley, M. Aksenova, J.M. Carney, D.A. Butterfield, Amyloid β-Peptide Spin-trapping. 1. Peptide Enzyme Toxicity is Related to Free-radical Spin Trap Reactivity. *NeuroReport* (1995), 6, 489-493.

133) K. Hensley, M. Aksenova, J.M. Carney, D.A. Butterfield, Amyloid β-Peptide Spin-trapping. 2. Evidence for Decomposition of the PBN Spin Adduct. *NeuroReport* (1995), 6, 493-496.

134) T. Tomiyama, A. Shoji, K. Kataoka, Y. Suwa, S. Asano, H. Kaneko, N. Endo, Inhibition of Amyloid β Protein Aggregation and Neurotoxicity by Rifampicin. *J. Biol. Chem.* (1996), 271, 6839-6844.

135) A. Forrester, Nitroxides. In *Magnetic Properties of FreeRadicals*; Fischer, H., Ed.; Springer: Berlin, (1989), 17, 8-71.

136) S.I. Dikalov, M.P. Vitek, K.R. Maples, R.P. Mason, Amyloid β Peptides Do Not Form Peptide-derived Free Radicals Spontaneously, but Can Enhance Metal catalysed Oxidation of Hydroxylamines to Nitroxides. *J.Biol. Chem.* (1999), 274, 9392-9399.

137) A.I. Bush, Metals and Neuroscience. *Curr. Opinion Chem. Biol.* (2000), 4, 184-191.

138) A.I. Bush, X. Huang, D.P. Fairlie, The Possible Origin of Free Radicals from Amyloid β-Peptides in Alzheimer's Disease. *Neurobiol. Aging* (1999), 20, 335-337.

139) X. Huang, M.P. Cuajungco, C.S. Atwood, M.A. Hartshorn, J.D.A. Tyndall, G.R. Hanson, K.C. Stokes, M. Leopold, G. Multhaup, L.E. Goldstein, R.C. Scarpa, A.J. Saunders, J. Lim, R.D. Moir, C. Glabe, E.F. Bowden, C.L. Masters, D.P. Fairlie, R.E. Tanzi, A.I. Bush, Cu(II) Potentiation of Alzheimer Aβ Neurotoxicity - Correlation with Cell-free Hydrogen Peroxide Production and Metal Reduction. *J. Biol.Chem.* (1999), 274, 37111-37116.

140) S. Turnbull, B.J. Tabner, O.M.A. El-Agnaf, L.J. Twyman, D. Allsop, New Evidence that the Alzheimer β- Amyloid Peptide Does Not Spontaneously Form Free Radicals: An ESR Study Using a Series of Spin-traps. *Free Radical Biol. Med.* (2001), 30, 1154-1162.

141) Y. Kotake, E.G. Janzen, Decay and Fate of the Hydroxyl Radical Adduct of β-Phenyl-N-tert-butylnitrone in Aqueous Media. *J. Am. Chem. Soc.* (1991), 113, 9503-9506.

142) S.M. Yatin, S. Varadarajan, C.D. Link, D.A. Butterfield, In Vitro and in Vivo Oxidative Stress Associated with Alzheimer's Amyloid β-Peptide (1-42). *Neurobiol. Aging* (1999), 20, 325-330.

143) D.A. Butterfield, S. Varadarajan, M. Aksenova, C. Link, S.M. Yatin, On Methionine and Alzheimer's Amyloid β-Peptide (1-42)-induced Oxidative Stress. *Neurobiol. Aging* (1999), 20, 339-342.

144) S. Varadarajan, S. Yatin, M. Aksenova, D.A. Butterfield, A Review: Alzheimer's Amyloid β-Peptide-associated Free Radical Oxidative Stress and.Neurotoxicity. *J. Struct. Biol.* (2000), 130, 184-208.

145) S. Varadarajan, S. Yatin. J. Kanski, F. Jahanshahi, D.A. Butterfield, Methionine Residue 35 is Important in Amyloid β-Peptide-associated Free Radical Oxidative Stress. *Brain Res. Bull.* (1999), 50, 133-141.

146) A. Monji, H. Utsumi, I. Yoshida, S. Hashioka, K. Tashiro, N. Tashiro, The Relationship Between Aβ-associated Free Radical Generation and Aβ Fibril

Formation Revealed by Negative Stain Electron Microscopy and Thioflavine-T Fluorometric Assay. *Neurosci. Lett.* (2001), 304, 65-68.

147) A. Monji, H. Utsumi, T. Uedta, T. Imoto, I. Yoshida, S. Hashioka, K. Tashiro, N. Tashiro, The Relationship Between the Aggregated State of the Amyloid-β Peptides and Free Radical Generation by the Peptides. *J. Neurochem*. (2001), 77, 1425-1432.

148) M. Anbar, P.A. Neta, A Compilation of Specific Bimolecular Rate Constants for the Reactions of Hydrated Electrons, Hydrogen Atoms, and Hydroxyl Radicals with Inorganic and Organic Compounds in Aqueous Solution. *Int. J. Appl. Radiat. Isot.* (1967), 18, 493-523.

149) D.R. Brown, B.S. Wong, F. Hafiz, C. Clive, S.J. Haswell, I.M. Jones, Normal Prion Protein Has an Activity Like That of Superoxide Dismutase. *Biochem. J.* (1999), 344, 1-5.

150) L.M. Sayre, G. Perry, M.A. Smith, A. Redox Metals and Disease. Neurodegenerative Disease. *Curr. Opinion Chem. Biol.* (1999), 3, 220-225.

151) B.A. Yanker, L.K. Duffy, D.A. Kirshner, Neurotrophic and Neurotoxic Effects of Amyloid β Protein: Reversal by Tachykinin Neuropeptides. *Science* (1990), 250, 279-282.

152) C.J. Pike, A.J. Walencewicz-Wasserman, J. Kosmoski, D. H. Cribbs, C.G. Glabe, C.W. Cotman, Structure reactivity Analyses of β-Amyloid Peptides: Contributions of the Aβ25-35 Region to Aggregation and Neurotoxicity. *J. Neurochem.* (1995), 64, 253-265.

153) L.I. Simandi, *Catalytic Activation of Dioxygen by Metal Complexes*, Kluwer Academic, Dordrecht, (1992).

154) S.J. Lippard, J.M. Berg, *Principles of Bioinorganic Chemistry*, University Science, Mill Valley, CA, (1994).

155) W. Kaim, B. Schwederski, *Bioinorganic Chemistry*, Wiley, Chichester, UK (1994).

156) R.H. Holm, P. Kennepohl, E.I. Solomon, Structural and Functional Aspects of Metal Sites in Biology. *Chem. Rev*. (1996), 96, 2239-2562.

157) E.I. Solomon, U.M. Sundaram, T.E. Machonkin, Multicopper Oxidases and Oxygenases. *Chem. Rev.* (1996), 96, 2563.

158) K.D. Karlin, Z. Tyeklar (Eds.), Bioinorganic Chemistry of Copper, Chapman & Hall, New York, (1993).

159) E.I. Solomon, K.W. Penfield, D.E. WilCOA, Active sites in copper proteins. An electronic structure overview. *Struct. Bond.* (1983), 53, 1-57.

160) K.A. Magnus, B. Hazes, H. Ton-That, C. Bonaventura, J. Bonaventura, W.G.J. Hol, Crystallographic analysis of oxygenated and deoxygenated states of arthropod hemocyanin shows unusual differences. *Proteins Struct. Funct. Genet*. (1994), 19, 302-309.

161) K.A. Magnus, H. Ton-That, J.E. Carpenter, Recent Structural Work on the Oxygen Transport Protein Hemocyanin. *Chem. Rev.* (1994), 94, 727-735.

162) R.S. Himmelwright, N.C. Eickman, C.D. LuBien, E.I. Solomon, Chemical and spectroscopic comparison of the binuclear copper active site of mollusc and arthropod hemocyanins. *J. Am. Chem. Soc.* (1980), 102, 5378-5388.

163) H.S. Mason, W.L. Fowlks, E. Peterson, Oxygen transfer and electron transport by the phenolase complex. *J. Am. Chem. Soc.* (1955), 77, 2914-2915.

164) M. Tremolieres, J.B. Bieth, Isolation and characterization of the polyphenol oxidase from senescent leaves of black poplar. *Phytochemistry* (1984), 23, 501-505.

165) D. Meiwes, B. Ross, M. Kiesshauer, K. Cammann, H. Witzel, M. Knoll, M. Borchardt, C. Sandermaier, Lab. Med. (1992), 15, 24.

166) K. Lerch, Tyrosinase: molecular and active-site structure. *Enzym. Brown. Prev.* (1995), 600, 64-80.

167) A. Rompel, H. Fischer, K. Büldt-Karentzopoulos, D. Meiwes, F. Zippel, H.-F. Nolting, C. Hermes, B. Krebs, H. Witzel, Structure and magnetism of novel tetranuclear μ-4-oxo-bridged copper(II) complexes. *J. Inorg. Biochem.* (1995), 59, 715-720.

168) N.C. Eickman, R.S. Himmelwright, E.I. Solomon, Geometric and electronic structure of oxyhemocyanin: Spectral and chemical correlations to met apo, half met, met, and dimer active sites. *Proc. Acad. Sci. USA* (1979), 76, 2094-2098.

169) E.I. Solomon, M.J. Baldwin, M.D. Lowery, Electronic structures of active sites in copper proteins: contributions to reactivity. *Chem. Rev.* (1992), 92, 521-542.

170) F. Zippel, F. Ahlers, B. Krebs, S. Behning, K. Büldt-Karentzopoulos, H. Witzel, M. Oversluizen, X-ray absorption studies of the purple acid phosphatase from red kidney beans (native enzyme, metal exchanged form). Daresbury Annual Report, Daresbury Laboratory, Daresbury, UK, (1994:95), 102.

171) B. Krebs, K. Büldt-Karentzopoulos, C. Eicken, A. Rompel, H. Witzel, A. Feldmann, R. Kruth, J. Reim, W. Steinforth, S. Teipel, F. Zippel, S. Schindler, F. Wiesemann, in: DFG Deutsche Forschungsgemeinschaft (Ed.), *Bioinorganic Chemistry: Transition Metals in Biology and their Coordination Chemistry*, D.14, VCH, Weinheim, (1997), p. 616.

172) N. Oishi, Y. Nishida, K. Ida, S. Kida, Reaction between various copper(II) complexes and ascorbic acid or 3,5-di-tert-butylcatechol. *Bull. Chem. Soc. Jpn*. (1980), 53, 2847-2850.

173) S. Kida, H. Okawa, Y. Nishida, in: K.D. Karlin, J. Zubieta (Eds.), *Copper Coordination Chemistry: Biochemical and Inorganic Perspectives*, Adenine, Guilderland, NY, (1983), p. 425.

174) S. Casellato, S. Tamburini, P.A. Vigato, A. de Stefani, M. Vidali, D.E. Fenton, The preparation of binuclear complexes and their catalytic behavior in the oxidation of 3,5-di-tert-butylcatechol. *Inorg. Chim. Acta* (1983), 69, 45-51.

175) K.D. Karlin, Y. Gultneh, T. Nicholson, J. Zubieta, Catecholate coordination to copper: structural characterization of a tetrachloro-o-catecholate-bridged dicopper(II) complex as a model for intermediates in copper-catalyzed oxidation of catechols. *Inorg. Chem.* (1985), 24, 3725-3727.

176) M.R. Malachowski, J. Carden, M.G. Davidson, W.L. Driessen, J. Reedijk, The preparation and catalytic properties of copper(II) complexes derived from a pyrazole containing ligand. X-ray crystal structure of $[Cu(pzmhp)(BF_4)](BF_4)$. *Inorg. Chim. Acta* (1997), 257, 59-67.

177) M.R. Malachowski, H.B. Huynh, L.J. Tomlinson, R.S. Kelly, J.W. Furbee Jr., Comparative study of the catalytic oxidation of catechols by copper(II) complexes of tripodal ligands. *J. Chem. Soc. Dalton Trans.* (1995), 31-36.

178) C.X. Zhang, H.-C. Liang, K.J. Humphreys, K.D. Karlin In: Simandi L (ed) *Catalytic activation of dioxygen by metal complexes*. Kluwer, Dordrecht, The Netherlands, (2003), 79–121.

179) K.D. Karlin, A.D. Zuberbuhler In: Reedijk J, Bouwman E (eds) Bioinorganic catalysis, 2nd edn. Marcel Dekker, New York, (1999), pp 469–534.

180) K.D. Karlin, S. Kaderli, A.D. Zuberbuhler, Kinetics and Thermodynamics of Copper(I)/Dioxygen Interaction. *Accs. Chem. Res* (1997), 30, 139–147.

181) K.D. Karlin, Y. Gultneh, Binding and activation of molecular oxygen by copper complexes. *Prog. Inorg. Chem*. (1987), 35, 219–327.

182) E.I. Solomon, U.M. Sundaram, T.E. Machonkin, Multicopper Oxidases and Oxygenases. *Chem. Rev*. (1996), 96, 2563–2605.

183) J.P. Klinman, Mechanisms Whereby Mononuclear Copper Proteins Functionalize Organic Substrates. *Chem. Rev.* (1996), 96, 2541–2561.

184) E.I. Solomon, P. Chen, M. Metz, S.-K. Lee, A.E. Palmer, Oxygen binding, activation, and reduction to water by copper proteins. *Angew. Chem. Int. Ed.* (2001), 40, 4570–4590.

185) K.A. Magnus, H. Ton-That, J.E. Carpenter, Recent Structural Work on the Oxygen Transport Protein Hemocyanin. *Chem. Rev*. (1994), 94, 727–735.

186) C. Gerdemann, C. Eicken, B. Krebs, The crystal structure of catechol oxidase: New insight into the function of type-3 copper proteins. *Acc. Chem. Res.* (2002), 35, 183–191.

187) H. Gampp, A.D. Zuberbuhler, Copper-catalyzed oxidation and oxygenation. *Metal Ions Biol. Syst*. (1981), 12, 133–189.

188) L. Que Jr., W.B. Tolman, Bis(μ-oxo)dimetal "diamond" cores in copper and iron complexes relevant to biocatalysis. *Angew. Chem. Int. Ed.* (2002), 41, 1114–1137.

189) N. Kitajima, K. Fujisawa, Y. Moro-oka, K. Toriumi, μ-η2:η2-Peroxo binuclear copper complex, $[Cu(HB(3,5\text{-}(Me_2CH)_2pz)_3)]_2(O_2)$. *J. Am. Chem. Soc.* (1989), 111, 8975–8976.

190) N. Kitajima, Y. Moro-oka, Copper-Dioxygen Complexes. Inorganic and Bioinorganic Perspectives. *Chem. Rev.* (1994), 94, 737–757.

191) K.A. Magnus, B. Hazes, H. Ton-That, C. Bonaventura, J. Bonaventura, W.G.J. Hol, Crystallographic analysis of oxygenated and deoxygenated states of arthropod hemocyanin shows unusual differences. *Proteins Struct. Funct. Genet*. (1994), 19, 302–309.

192) S.I. Chan, K.H.C. Chen, S.S.F. Yu, C.L. Chen, S.S.J. Kuo, Polarized ATR-FTIR Spectroscopy of the Membrane-Embedded Domains of the Particulate Methane Monooxygenase. *Biochemistry*, (2004), 43, 4421–4430.

193) J.P. Evans, K. Ahn, J.P. Klinman, Evidence that dioxygen and substrate activation are tightly coupled in dopamine β-monooxygenase: Implications for the reactive oxygen species. *J. Biol. Chem.* (2003), 278, 49691–49698.

194) S.T. Prigge, R.E. Mains, B.A. Eipper, L.M. Amzel, New insights into copper monooxygenases and peptide amidation: structure, mechanism and function. *Cell Mol. Life Sci*. (2000), 57, 1236–1259.

195) J.P. Klinman, G.F.Z. da Silva, unpublished results and personnal communication.

196) K.D. Karlin, R.W. Cruse, Y. Gultneh, J.C. Hayes, J. Zubieta, Peroxide coordination to a dicopper(II) center. Dioxygen binding to a structurally characterized phenoxide-bridged binuclear copper(I) complex. *J. Am. Chem. Soc.* (1984), 106, 3372–3374.

197) R.R. Jacobson, Z. Tyeklar, K.D. Karlin, S. Liu, J. Zubieta, A copper-oxygen (Cu_2-O_2) complex. Crystal structure and characterization of a reversible dioxygen binding system. *J. Am. Chem. Soc.* (1988), 110, 3690–3692.

198) K.D. Karlin, M.S. Haka, R.W. Cruse,Y. Gultneh, Dioxygen-copper reactivity. Reversible oxygen and carbon monoxide binding by a new series of binuclear copper(I) complexes. *J. Am. Chem. Soc.* (1985), 107, 5828–5829.

199) Z. Hu, R.D.Williams, D. Tran, T.G. Spiro, S.M. Gorun, Re-engineering Enzyme-Model Active Sites: Reversible Binding of Dioxygen at Ambient Conditions by a Bioinspired Copper Complex. *J. Am. Chem. Soc.* (2000), 122, 3556–3557.

200) M. Kodera M, Kajita Y, Tachi Y, Katayama K, Kano K, Hirota S, Fujinami S, Suzuki M Synthesis, structure, and greatly improved reversible O_2 binding in a structurally modulated μ-η2:η2-peroxodicopper(II) complex with room-temperature stability. *Angew. Chem. Int. Ed.* (2004), 43, 334–337.

201) P.P. Paul, Z. Tyeklar, R.R. Jacobson, K.D. Karlin, Reactivity patterns and comparisons in three classes of synthetic copper-dioxygen {Cu_2-O_2} complexes: implication for structure and biological relevance. *J. Am. Chem. Soc.* (1991), 113, 5322–5332.

202) K.D. Karlin, P. Ghosh, R.W. Cruse, A. Farooq, Y. Gultneh, R.R. Jacobson, N.J. Blackburn, R.W. Strange, J. Zubieta, Dioxygen-copper reactivity: generation, characterization, and reactivity of a hydroperoxodicopper(II) complex. *J. Am. Chem. Soc.* (1988), 110, 6769–6780.

203) I. Sanyal, P. Ghosh, K.D. Karlin, Mononuclear Copper(II)-Acylperoxo Complexes. *Inorg. Chem.* (1995), 34, 3050–3056.

204) V. Mahadevan, M.J. Henson, E.I. Solomon, T.D.P. Stack, Differential Reactivity between Interconvertible Side-On Peroxo and Bis-μ-oxodicopper Isomers Using Peralkylated Diamine Ligands. *J. Am. Chem. Soc.* (2000), 122, 10249–10250.

205) L.M. Mirica, M. Vance, D.J. Rudd, B. Hedman, K.O. Hodgson, E.I. Solomon, T.D.P. Stack, A Stabilized μ-η2:η2 Peroxodicopper(II) Complex with a Secondary Diamine Ligand and Its Tyrosinase-like Reactivity. *J. Am. Chem. Soc.* (2002), 124, 9332–9333.

206) P.L. Holland, K.R. Rodgers, W.B. Tolman, Is the bis(μ-oxo)dicopper core capable of hydroxylating an arene? *Angew. Chem. Int. Ed.* (1999), 38, 1139–1142.

207) J.A. Halfen, S. Mahapatra, E.C. Wilkinson, S. Kaderli, V.G. Young Jr, L.Que Jr., A.D. Zuberbühler, W.B. Tolman, Reversible cleavage and formation of the dioxygen O-O bond within a dicopper complex. *Science* (1996), 271, 1397–1400.

208) V. Mahadevan, Z. Hou, A.P. Cole, D.E. Root, T.K. Lal, E.I. Solomon, T.D.P. Stack Irreversible Reduction of Dioxygen by Simple Peralkylated Diamine-Copper(I) Complexes: Characterization and Thermal Stability of a $[Cu_2(\mu\text{-}O)_2]^{2+}$ Core. *J. Am. Chem. Soc.* (1997), 119, 11996–11997.

209) C.J. Cramer, B.A. Smith, W.B. Tolman, Ab Initio Characterization of the Isomerism between the μ-η2:η2-Peroxo- and Bis(μ-oxo)dicopper Cores. *J. Am. Chem. Soc.* (1996), 118, 11283–11287.

210) P. Spuhler, M.C. Holthausen, Mechanism of the aliphatic hydroxylation mediated by a bis(μ-oxo)dicopper(III) complex. *Angew. Chem. Int. Ed.* (2003), 42, 5961–5965.

211) M.J. Henson, P. Mukherjee, D.E. Root, T.D.P. Stack, E.I Solomon, Spectroscopic and Electronic Structural Studies of the $Cu(III)_2$ Bis-μ-oxo Core and Its Relation to the Side-On Peroxo-Bridged Dimer. *J. Am. Chem. Soc.* (1999), 121, 10332–10345.

212) K.D. Karlin, P.L. Dahlstrom, S.N. Cozzette, P.M. Scensny, J. Zubieta, Activation of oxygen by a binuclear copper(I) compound. Hydroxylation of a new xylyl binucleating ligand to produce a phenoxy-bridged binuclear copper(II) complex; x-ray crystal structure of $[Cu_2\{OC_6H_3[CH_2N(CH_2CH_2py)_2]_2\text{-}2,6\}(OMe)]$ (py = 2-pyridyl). *J. Chem. Soc. Chem. Commun.* (1981), 881-882.

213) K.D. Karlin, Y. Gultneh, J.C. Hayes, R.W. Cruse, J.W. McKown, J.P. Hutchinson, J. Zubieta, Copper-mediated hydroxylation of an arene: model system for the action of copper monooxygenases. Structures of a binuclear copper(I) complex and its oxygenated product. *J. Am. Chem. Soc.* (1984), 106, 2121–2128.

214) M.S. Nasir, B.I. Cohen, K.D. Karlin, Mechanism of aromatic hydroxylation in a copper monooxygenase model system. 1,2-Methyl migrations and the NIH shift in copper chemistry. *J. Am. Chem. Soc.* (1992), 114, 2482–2494.

215) K.D. Karlin, M.S. Nasir, B.I. Cohen, R.W. Cruse, S. Kaderli, A.D. Zuberbühler, Reversible Dioxygen Binding and Aromatic Hydroxylation in O_2-Reactions with Substituted Xylyl Binuclear Copper(I) Complexes: Syntheses and Low-Temperature Kinetic/Thermodynamic and Spectroscopic Investigations of a Copper Monooxygenase Model System. *J. Am. Chem. Soc.* (1994), 116, 1324–1336.

216) E. Pidcock, H.V. Obias, C.X. Zhang, S.D. Karlin, E.I. Solomon, Investigation of the reactive oxygen intermediate in an arene hydroxylation reaction performed by xylyl-bridged binuclear copper complexes. *J. Am. Chem. Soc.* (1998), 120, 7841–7847.

217) M.S. Nasir, B.I. Cohen, K.D. Karlin, Mechanism of aromatic hydroxylation in a copper monooxygenase model system. 1,2-Methyl migrations and the NIH shift in copper chemistry. *J. Am. Chem. Soc.* (1992), 114, 2482–2494.

218) E. Pidcock, H.V. Obias, M. Abe, H.-C. Liang, K.D. Karlin, E.I. Solomon, Spectroscopic and Theoretical Studies of Oxygenated Dicopper(I) Complexes Containing Hydrocarbon-Linked Bis[2-(2-pyridyl)ethyl]amine Units: Investigation of a Butterfly $[Cu_2(\mu\text{-}\eta2\text{:}\eta2)(O_2)]^{2+}$ Core. *J. Am. Chem. Soc.* (1999), 121, 1299–1308.

219) S. Itoh, H. Kumei, M. Taki, S. Nagatomo, T. Kitagawa, S. Fukuzumi, Oxygenation of phenols to catechols by a (μ-η2:η2-peroxo)dicopper(II) complex: mechanistic

insight into the phenolase activity of tyrosinase. *J. Am. Chem. Soc.* (2001), 123, 6708–6709.

220) S.-I. Yamazaki, S. Itoh, Kinetic evaluation of phenolase activity of tyrosinase using simplified catalytic reaction system. *J. Am. Chem. Soc.* (2003), 125, 13034–13035.

221) G. Battaini, M. De Carolis, E. Monzani, F. Tuczek, L. Casella, The phenol ortho-oxygenation by mononuclear copper(I) complexes requires a binuclear μ-η2:η2-peroxodicopper(II) complex rather than mononuclear CuO2 species. *Chem. Commun.* (2003), 726–727.

222) L. Santagostini, M. Gullotti, E. Monzani, L. Casella, R. Dillinger, F. Tuczek, Reversible dioxygen binding and phenol oxygenation in a tyrosinase model system. *Chem. Eur. J.* (2000), 6, 519–522.

223) S. Mandal, D. Macikenas, J.D. Protasiewicz, L.M. Sayre, Novel tert-Butyl Migration in Copper-Mediated Phenol Ortho-Oxygenation Implicates a Mechanism Involving Conversion of a 6-Hydroperoxy-2,4-cyclohexadienone Directly to an o-Quinone. *J. Org. Chem.* (2000), 65, 4804–4809.

224) L.M. Sayre, D. Nadkarni, Direct Conversion of Phenols to o-Quinones by Copper(I) Dioxygen. Questions Regarding the Monophenolase Activity of Tyrosinase Mimics. *J. Am. Chem. Soc.* (1994), 116, 3157–3158.

225) S. Mahapatra, J.A. Halfen, E.C. Wilkinson, G. Pan, X. Wang, V.G. Young Jr., C.J. Cramer, L. Que Jr., W.B. Tolman, Structural, Spectroscopic, and Theoretical Characterization of Bis(μ-oxo)dicopper Complexes, Novel Intermediates in

Copper-Mediated Dioxygen Activation. *J. Am. Chem. Soc.* (1996), 118, 11555–11574.

226) S. Mahapatra, J.A. Halfen, W.B. Tolman, Mechanistic Study of the Oxidative N-Dealkylation Reactions of Bis(μ-oxo)dicopper Complexes. *J. Am. Chem. Soc.* (1996), 118, 11575–11586.

227) S. Itoh, M. Taki, H. Nakao, P.L. Holland, W.B. Tolman, L. Que Jr., S. Fukuzumi, Aliphatic hydroxylation by a bis(μ -oxo)dicopper(III) complex. *Angew. Chem. Int. Ed.* (2000), 39, 398–400.

228) S. Itoh, H. Nakao, L.M. Berreau, T. Kondo, M. Komatsu, S. Fukuzumi, Mechanistic Studies of Aliphatic Ligand Hydroxylation of a Copper Complex by Dioxygen: A Model Reaction for Copper Monooxygenases. *J. Am. Chem. Soc.* (1998), 120, 2890–2899.

229) C.X. Zhang, H.-C. Liang, E.-I. Kim, J. Shearer, M.E. Helton, E. Kim, S. Kaderli, C.D. Incarvito, A.D. Zuberbuhler, A.L. Rheingold, K.D. Karlin, Tuning Copper-Dioxygen Reactivity and Exogenous Substrate Oxidations via Alterations in Ligand Electronics. *J. Am. Chem. Soc.* (2003), 125:634–635.

230) M.J. Henson, M.A. Vance, C.X. Zhang, H.-C. Liang, K.D. Karlin, E.I. Solomon, Resonance Raman Investigation of Equatorial Ligand Donor Effects on the $Cu_2O_2^{2+}$ Core in End-On and Side-On μ-Peroxo-Dicopper(II) and Bis-μ-oxo-Dicopper(III) Complexes. *J. Am. Chem. Soc.* (2003), 125, 5186–5192.

231) J. Shearer, C.X. Zhang, L.Q. Hatcher, K.D. Karlin, Distinguishing Rate-Limiting Electron versus H-Atom Transfers in $Cu_2(O_2)$-Mediated Oxidative N-Dealkylations:

Application of Inter- versus Intramolecular Kinetic Isotope Effects. *J. Am. Chem. Soc.* (2003), 125, 12670–12671.

232) T. Osako, K. Ohkubo, M. Taki, Y. Tachi, S. Fukuzumi, S. Itoh, Oxidation Mechanism of Phenols by Dicopper-Dioxygen (Cu_2/O_2) Complexes. *J. Am. Chem. Soc.* (2003), 125, 11027–11033.

233) D.E. Root, M. Mahroof-Tahir, K.D. Karlin, E.I. Solomon, Effect of Protonation on Peroxo-Copper Bonding: Spectroscopic and Electronic Structure Study of $[Cu_2(UN\text{-}O\text{-})(OOH)]^{2+}$. *Inorg. Chem.* (1998), 37, 4838–4848.

234) P. Chen, K. Fujisawa, E.I. Solomon, Spectroscopic and Theoretical Studies of Mononuclear Copper(II) Alkyl- and Hydroperoxo Complexes: Electronic Structure Contributions to Reactivity. *J. Am. Chem. Soc.* (2000), 122, 10177–10193.

235) P. Chen, E.I. Solomon, Frontier molecular orbital analysis of Cu_n-O_2 reactivity. *J. Inorg. Biochem.* (2002), 88, 368–374.

236) M. Sono, M.P. Roach, E.D. Coulter, J.H. Dawson, Heme-Containing Oxygenases. *Chem. Rev.* (1996), 96, 2841–2887.

237) R. Davydov, V. Kofman, H. Fujii, T. Yoshida, M. Ikeda-Saito, B.M. Hoffman, Catalytic Mechanism of Heme Oxygenase through EPR and ENDOR of Cryoreduced Oxy-Heme Oxygenase and Its Asp 140 Mutants. *J. Am. Chem. Soc.* (2002), 124, 1798–1808.

238) P.R. Ortiz de Montellano, EPR Spin-Trapping of a Myeloperoxidase Protein Radical. *Curr. Opin. Chem. Biol.* (2000), 4, 221–227.

239) R.W. Cruse, S. Kaderli, C.J. Meyer, A.D. Zuberbühler, K.D. Karlin, Copper-mediated hydroxylation of an arene: kinetics and mechanism of the reaction of a dicopper(II) m-xylyl-containing complex with H_2O_2 to yield a phenoxodicopper(II) complex. *J. Am. Chem. Soc.* (1988), 110, 5020–5024.

240) G. Battaini, E. Monzani, A. Perotti, C. Para, L. Casella, L. Santagostini, M.M. Gullotti, R. Dillinger, C. Nather, F.A. Tuczek, A Double Arene Hydroxylation Mediated by Dicopper(II)-Hydroperoxide Species. *J. Am. Chem. Soc.* (2003), 125, 4185–4198.

CHAPTER II. Cu^{2+}-AMYLOID-β COMPLEXES AS A REDOX-ACTIVE CATALYST TOWARD THE OXIDATION OF 1,2,3-TRIHYDROXY BENZENE‡

I. INTRODUCTION

Abnormal metal-ion homeostasis has been closely associated with several neurodegenerative diseases, including Parkinson's, amyotrophic lateral sclerosis, Creutzfeldt-Jakob disease (i.e. mad cow disease), and Alzheimer's disease (AD).[1–3] Because high cytoplasmic concentrations of free metal ions are toxic and potentially lethal, intricate physiological pathways have evolved to transport and distribute metal ions to their targets which include enzymes and proteins.[4] With aging, physiological processes responsible for accurate delivery of metal ions break down and "leakage" of free metal ions can cause toxic effects to cells.[5,6] Divalent ions of redox-active transition metals have often been associated with oxidative stress and closely involved in the

This work has been published: ‡ G.F.Z. da Silva, W.M. Tay, L.-J. Ming, Catechol Oxidase-like Oxidation Chemistry of the 1–20 and 1–16 Fragments of Alzheimer's Disease-related β-Amyloid Peptide: THEIR STRUCTURE-ACTIVITY CORRELATION AND THE FATE OF HYDROGEN PEROXIDE, *J. Biol. Chem.* (2005), 280, 16601-16609.

chemistry of reactive oxygen species (ROS), including hydrogen peroxide and superoxide and hydroxyl radicals.[7] Because increases in intracellular concentrations of metal ions is closely related to the effects of aging, oxidative stress, and AD, there is considerable interest in investigating the connection between malfunction of regulatory processes such as metal transport and the presence of ROS with the pathology of AD.

The chemistry of redox-active metal complexes of β-amyloid peptide (Aβ) has been an area of intense focus in the study of AD. The aggregation of Aβ within the neocortex is closely related to the pathology of AD and has been shown to be induced by metal binding.[8,9] The Aβ peptides are generated by the cleavage of the ubiquitous amyloid precursor protein (APP) by α, β, and γ secretases.[10] Aβ in the form of insoluble plaques contains up to mM amounts of Zn^{2+}, Cu^{2+}, and Fe^{3+} in the neocortical region of the brain;[7] however, the cause/effect connection of the metallo-Aβ plaques with AD is still under debate.[11] The metal coordination environment of the 1–40 and 1–42 peptides has been previously studied and their pH dependent aggregation reported.[9,12] The results showed the metal binding seemed to be non-stoichiometric with approximately 3.5 metal ions per pair of aggregated peptides and a cooperative binding pattern as the amount of aggregates increases.[7] Since $A\beta_{1\text{-}42}$ and $A\beta_{1\text{-}40}$ have been shown to bind Zn^{2+} and Fe^{3+} with nM and Cu^{2+} with aM apparent dissociation constants by means of quantitative determination of the metal-complex precipitates,[7] understanding of the metal-binding domain and its structure may shed light on the chemistry related to the neuropathology of AD.

Though the coagulation of the peptide plaques leaves little doubt that interaction with cytoplasmic molecules is unlikely, smaller fragments of the amyloid peptide are soluble and Aβ fibrils extend across membranes, exposing them to the cytoplasm. Recently, insulin degrading enzyme (IDE) has been shown to digest the longer Aβ peptides (40–42 amino acids) into smaller soluble fragments.[13] Moreover, the cleavage of APP by α and β- secretases produces the $A\beta_{1\text{-}16}$ fragment of APP.[14] These soluble fragments and intra-membrane spanning fibrils still possess possible metal binding sites such as histidines, glutamate, aspartate, and tyrosine within the 1-20 fragment of Aβ in the sequence $DAEFR_5\,HDSGY_{10}\,EVHHN_{15}\,KLVFF_{20}$. Redox chemistry of Aβ has been previously reported, wherein Met_{35} was suggested as a "built-in" reducing agent required for the redox cycling hypothesis.[15] The lack of sufficient data on the redox chemistry of and the oxidative stress caused by metallo-Aβ and the discrepancies in previous studies such as the presence or absence of free-radicals and the nature of the metal-Aβ interaction seem often to be the shortcoming in Aβ research. Understanding of the chemical processes associated with metallo-Aβ may provide insight into the upstream and/or downstream regulatory processes that lead to AD. Herein, we describe the oxidation chemistry of CuAβ in the presence and absence of H_2O_2, showing conclusive metal-centered pre-equilibrium kinetics toward the oxidation of a simple substrate and the oxidative cleavage of double-stranded plasmid DNA.

II. EXPERIMENTAL

The 1-20 and 1-16 fragments of Aβ were purchased from Aldrich (St. Louis, MO) or synthesized at the Peptide Center of the University of South Florida. The identities of the peptides have been confirmed with a Bruker MALDI-TOF mass spectrometer. The substrate 1,2,3-trihydroxylbenzene (THB) was obtained from Sigma -ldrich, 3-methyl-2-benzothiazolinone hydrazone hydrochloride monohydrate from Acros (Fairlawn, NJ), the plasmid pQE30Xa from Quiagen (Valencia, CA), EDTA, DMSO, mannitol, H_2O_2, $Cu(NO_3)_2$, $ZnCl_2$, and $Ni(SO_4)$ from Fisher (Swanee, GA), and $CoCl_2$ from Mallickrodt (Paris, KY). All plastic ware was demetallized with EDTA and extensively rinsed with 18.0-MΩ water to remove the chelator. The water used for the studies of DNA cleavage was autoclaved to remove ubiquitous nucleases.

DNA cleavage assay: The metal derivatives of Aβ were prepared by dissolving the peptide in 18.0-MΩ water and separated into aliquots followed by addition of corresponding metal ions at 1:1 stoichiometric ratio, which was further diluted into aliquots of working concentrations. The metal-complexes were freshly prepared in all experiments. A typical reaction toward DNA cleavage contained 150 ng of plasmid DNA, 4.0%, 2.0%, or 0.2% H_2O_2, and 5.0 μM of metallo-Aβ derivatives in 100 mM HEPES at pH 7.00 in a volume of 15.0 μL. A time-course experiment was performed and analyzed in a 1.0 % agarose gel stained with ethydium bromide, and then photographed on a transilluminator.

THB oxidation assay: Several concentrations of THB ranging from 0.10 to 5.0 mM were incubated with 7.5 μM of CuAβ and 1.60, 3.20, 16.20, 32.3 or 70.0 mM H_2O_2 and

buffered with 100 mM HEPES at pH 7.00 in a final volume of 1.0 ml. The formation of product was monitored at 420 nm (ε = 4,583 M^{-1} cm^{-1}) on a Varian CARY50 Bio-UV-Vis spectrophotometer for 5 minutes, and the rates determined by the change in absorbance over time. The background oxidation of THB was conducted in the same manner without CuAβ in the assay solution. Rates were fitted to appropriate rate laws and rate constants determined by the use of SigmaPlot 8.0.

The dependence of H_2O_2 on THB oxidation by CuAβ was determined by measuring the oxidation rate at several different concentrations of hydrogen peroxide with saturating concentration of THB (6.0 mM). The initial rates were determined and then fitted as a function of [H_2O_2] to an appropriate rate law to reveal the rate constant. Alternatively, the catechol oxidase assay was performed as previously reported with minor changes to fit current studies.[16] Same molar concentrations of THB and 3-methyl-2-benzothiazolinone hydrazone (which serves as an *ortho*-quinone indicator) were mixed in 100 mM HEPES at pH 7.00 in the presence of 3.5 μM CuAβ. The red-adduct of the *ortho*-quinone product was monitored at 500 nm (ε = 32,500 $M^{-1}cm^{-1}$) and rates calculated. Auto-oxidation of THB was determined under the same conditions without Cu-Aβ.

Metal Titration: Apo-Aβ was dissolved in 100 mM HEPES at pH 7.00 to a final concentration of 1.0 mM. Cu^{2+} binding was monitored by titrating the metal into the apo-Aβ solution and the electronic spectra collected after each addition of the metal. Cu^{2+} binding was also determined through the activity of CuAβ complex toward THB. In this case, Cu^{2+} was titrated into a fixed amount of the peptide in 100 mM HEPES at pH 7.00

in the presence of 10.0 mM of THB and 70.0 mM H_2O_2. The oxidation rates were determined as a function of [Cu^{2+}], then fitted to a simple equilibrium of metal:peptide = 1:1 or a cooperative binding pattern using the Hill equation.

NMR Spectroscopy: All the NMR spectra were acquired on a Bruker DPX250 spectrometer at ^1H resonance of 250 MHz. The metal-binding was monitored through the changes in the NMR spectra. The peptides $A\beta_{1-16}$ and $A\beta_{1-20}$ and the paramagnetic shift reagent Co^{2+} were prepared in d^6-DMSO. The metal ion was gradually titrated into the peptide and the paramagnetically shifted ^1H NMR signals detected. A typical spectrum showing the paramagnetically shifted ^1H NMR signals consists of ~80,000 transients from accumulation of several spectra of 10,000–20,000 transients with a recycle time of ~50 ms and a spectral window of ~250 ppm. Solvent exchangeable signals were determined by adding a drop of D_2O into the sample which disappear after the addition.

Molecular mechanics: The primary sequence of $A\beta_{1-16}$ peptide was entered into BioCAChe 6.0 (Fujitsu, Beaverton, Oregon) and the energy of its structure under solvation using a simulated water droplet was minimized with the MM3 molecular mechanics method. Histidine side chains were considered the ligands in the calculations on the basis of the NMR data.

III. RESULTS AND DISCUSSION

Oxidative Double-Stranded DNA Cleavage: Though the bulk of the amyloid plaques in AD brain is membrane bound, proteolytic processing of amyloid has been shown to yield soluble fragments.[12] It has also been demonstrated that the neuropathology of AD

may directly affect DNA, eventually leading to apoptosis.[17] As metal ions are involved in the formation of amyloid plaques, the oxidative activity of metallo-Aβ complexes against plasmid DNA was probed *in vitro* with gel electrophoresis. The oxidative activities of the Zn^{2+}, Ni^{2+}, and Cu^{2+} complexes of $A\beta_{1-20}$ ($ZnA\beta_{1-20}$, $NiA\beta_{1-20}$, and $CuA\beta_{1-20}$) toward the cleavage of plasmid DNA were determined by incubating several different concentrations of the complexes with plasmid DNA in the presence of 4.0 % H_2O_2 at room temperature for 30 minutes (Figure 2.1). Here, $ZnA\beta_{1-20}$ serves as the control since Zn^{2+} is oxidative inactive. The plasmid in the presence of metallo-$A\beta_{1-20}$ at lower concentrations shows a middle band that is not present in the reference (Lane R, Figure 2.1). Comparing the middle band with the DNA ladder gives an approximate size of 3.5 kbp, consistent with the size of linearized plasmid from the manufacturer. The activities of the derivatives follow the trend $CuA\beta_{1-20} > NiA\beta_{1-20} > ZnA\beta_{1-20}$, demonstrating the involvement of metal in the oxidative cleavage of dsDNA.

One interesting result is shown in the H_2O_2 + DNA and the H_2O_2 + DNA + $A\beta_{1-20}$ control experiments. The 4.0 % H_2O_2 shows a significant damage toward plasmid dsDNA (Lanes 1, Figure 2.1), whereas $A\beta_{1-20}$ decreases the H_2O_2 damage of plasmid dsDNA and perhaps acts as a scavenger of ROS species (Lane 2, Figure 2.1). The role of Aβ as an antioxidant has been previously reported,[18] wherein the presence of Met_{35} was proposed to prevent lipid peroxidation while the M35L mutant showed reduced antioxidant activity. In a similar study, $A\beta_{1-40}$ was found to prevent the oxidation of the lipoproteins from cerebral spinal fluid and plasma.[11] Moreover, $A\beta_{1-42}$ was shown to exhibit an

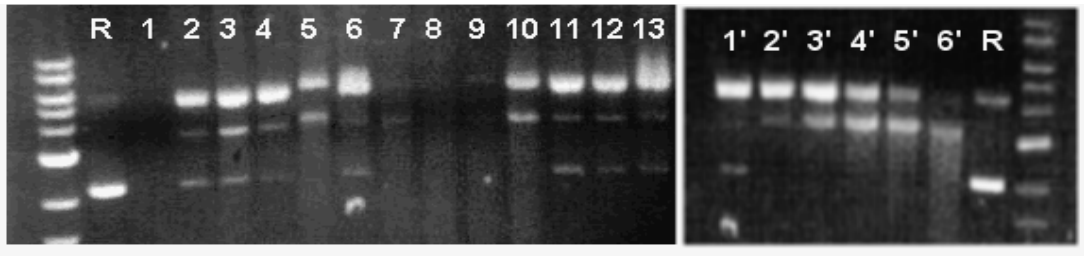

Figure 2.1. Concentration and metal-dependent assay of dsDNA cleavage. R is the reference plasmid DNA which shows supercoiled band (bottom) and nicked circular band (top); lane 1, DNA + 4% H_2O_2; lane 2, DNA + apo-A$\beta_{1\text{-}20}$ (200 μM) + 4% H_2O_2; lanes 3–6, ZnA$\beta_{1\text{-}20}$ (40, 80, 100, and 200 μM, respectively) + 4% H_2O_2; lanes 7–13, NiA$\beta_{1\text{-}20}$ (5, 10, 20, 40, 80, 100, and 200 μM, respectively) + 4% H_2O_2; CuA$\beta_{1\text{-}20}$ (at 5, 10, 20, 40, 80, 100, and 200 μM) + 4% H_2O_2 shows complete DNA cleavage ("blank" gel, not shown). All assays were incubated for 30 minutes. The middle band is the linearized plasmid detected at 3.5 kbp position, consistent with that obtained from the sequence of the plasmid pQE30Xa (Qiagen). Lanes 1'–6' show the plasmid cleavage by Cu^{2+} ions (5 μM) + 3.6% H_2O_2 at 10, 20, 40, 60, 90, 120 min. The standard DNA ladder starts with 1 kbp from the bottom with 1 kbp increment upward.

antioxidant activity more effective than ascorbate in cerebral spinal fluid.[19] The antioxidant activity of Aβ was also demonstrated in the decrease of cytoplasmic amounts of 8-hydroxyguanosine, a major product of nucleic acid oxidation present in elevated amounts in the brains of AD patients.[20] These observations implied that the production of Aβ could be related to prevention of oxidative stress. We have demonstrated here that even shorter fragments of Aβ without a Met can serve as a protective agent against oxidative damage of DNA, corroborating with some previous reports[11,19,20] and supporting the hypothesis that apo-Aβ might be an effect of the oxidative stress in AD brains and might serve a specific purpose to scavenge ROS. This antioxidant activity is also observed in all concentrations of $ZnA\beta_{1\text{-}20}$ (Lanes 3–6, Figure 2.1), consistent with the lack of redox chemistry of Zn^{2+} and a protection role against dsDNA cleavage as in the case of apo-$A\beta_{1\text{-}20}$.

Although Ni^{2+} is redox active and some of its complexes have been shown to exhibit oxidative damage toward DNA,[21] $NiA\beta_{1\text{-}20}$ does not show such "chemical nuclease" activity, probably attributed to its low redox potential. Conversely, like apo-Aβ and $ZnA\beta_{1\text{-}20}$ discussed above, $NiA\beta_{1\text{-}20}$ shows a concentration-dependent *protection* against oxidative damage of dsDNA by H_2O_2, with better protection at higher concentrations while no significant protection at [$NiA\beta_{1\text{-}20}$] < 80 μM (Lanes 7–12, Figure 2.1). NiAβ has not been shown to be associated with AD pathology; however, it may serve as a structural and mechanistic probe in future studies of metallo-Aβ or similar systems.

The activity of 5.0 μM $CuA\beta_{1\text{-}20}$ (Lane 14, Figure 2.1) is exceedingly higher than that of $ZnA\beta_{1\text{-}20}$ at all concentrations tested in the presence of 4.0% H_2O_2 (Lanes 3-6, Figure

2.1) which effectively oxidizes the entire dsDNA plasmid sample into fragments that are too small to be resolved with the agarose gel electrophoresis (empty lanes not shown). Cu^{2+} ion has been demonstrated in the literature to be active toward DNA cleavage in the presence of H_2O_2.[22] The use of Cu^{2+} (5.0 μM) in the presence of 3.6% H_2O_2 as control shows a much slower cleavage rate as the plasmid is not completely digested after 2 hours of incubation. In order to monitor the catalytic activity of $CuA\beta_{1-20}$ toward plasmid dsDNA, the concentration of H_2O_2 was reduced to 2.0% and a time course experiment conducted (Figure 2.2). $CuA\beta_{1-20}$ completely oxidizes plasmid DNA within 5.0 minutes in the presence of 2.0% H_2O_2, leaving only a faint streak in the gel (Lane 7, Figure 2.2). The ability of apo-$A\beta_{1-20}$ to act as a protector against oxidation of dsDNA in the presence of H_2O_2 is once again demonstrated here. Further reducing the concentration of H_2O_2 to 0.2% allows a clearer monitoring of plasmid cleavage patterns (Figure 2.3). Within 10 minutes of incubation, 5.0 μM of $CuA\beta_{1-20}$ shows double-stranded DNA cleavage as evident in the appearance of a middle band approximately 3.5 kbp (Lane 6, Figure 2.3). Within 20-30 minutes, complete conversion of the supercoiled plasmid into linear and nick-circular conformations is observed, evident in the changes in the intensity of the different forms of the plasmid compared to the reference (Lanes 3 and 4, respectively, Figure 2.3). After 30 minutes, plasmid is cleaved into small pieces leaving a streak of oligonucleotide products (Lanes 1, 2, and 3). The different and quite opposite activities between apo-$A\beta_{1-20}$ and $CuA\beta_{1-20}$ toward dsDNA damage may hint a physiological role of small fragments of apo-Aβ.

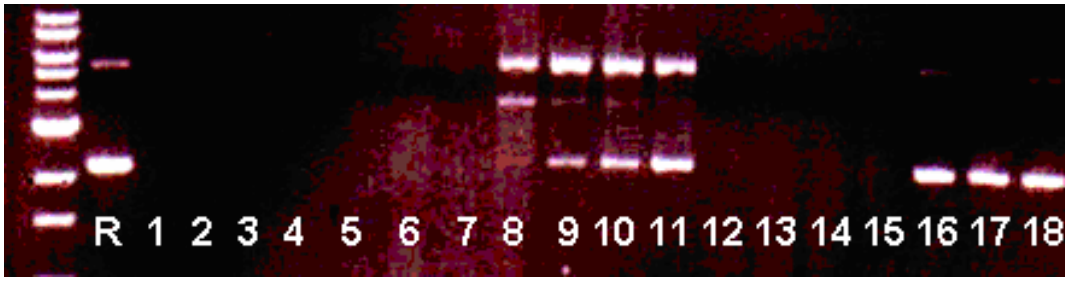

Figure 2.2. Time course reactivity assay of dsDNA cleavage. R is the reference plasmid DNA; lanes 1–7, DNA + 5.0 μM $CuA\beta_{1\text{-}20}$ + 2% H_2O_2 (60, 50, 40, 30, 20, 10, 5 min, respectively); lanes 8-11, DNA + $A\beta_{1\text{-}20}$ (metal free) + 2% H_2O_2 (60, 40, 20, 10 min, respectively); lanes 12–15, DNA + 2% H_2O_2 (60, 40, 20, 10 min, respectively); and lanes 16–18, DNA + $A\beta_{1\text{-}20}$ (metal free, peroxide free). The standard DNA ladder starts with 1 kbp from the bottom with 1 kbp increment upward.

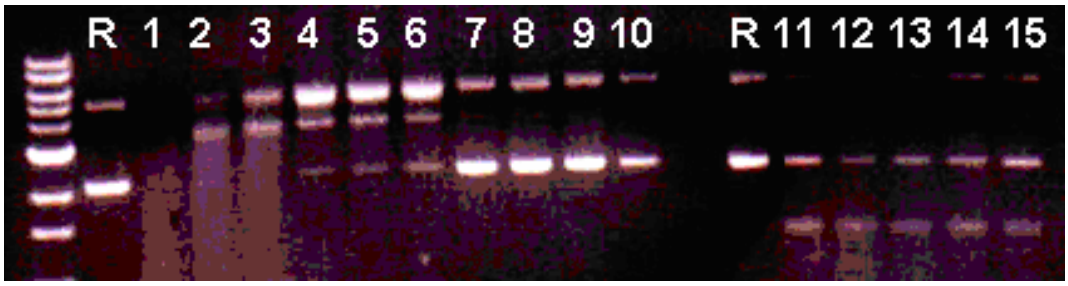

Figure 2.3. Time course reactivity assay toward the cleavage of 150 ng dsDNA. R is the reference DNA; lanes 1–6, DNA + 5.0 μM $CuA\beta_{1\text{-}20}$ + 0.2% H_2O_2 (60, 40, 30, 20, 15, 10 min, respectively); lanes 7-10, DNA + 5.0 μM $CuA\beta_{1\text{-}20}$ (peroxide free 60, 40, 20, 10 min, respectively); and lanes 11-15, DNA + 0.2% H_2O_2 (40, 30, 20, 15, 10 min, respectively). The standard DNA ladder starts with 1 kbp from the bottom with 1 kbp increment upward. The cleavage of plasmid by 5.0 μM Cu^{2+} ions and 3.6% H_2O_2 is shown in Fig. 1, which exhibits a much lower activity.

To determine the role of the oxidizing agent in these reactions, the same concentration of $CuA\beta_{1-20}$ was incubated with the plasmid in the absence of H_2O_2 up to 60 minutes, which shows negligible cleavage (Lane 7, Figure 2.3). The low activity of $CuA\beta_{1-20}$ without H_2O_2 indicates a metal-centered activation of peroxide, such as the formation of a Cu_2-peroxo center found in many Cu complexes[23,24] which subsequently results in oxidative damage to dsDNA. To distinguish the reaction pathways of oxidative DNA cleavage by H_2O_2 in the presence and absence of $CuA\beta_{1-20}$, a time-course experiment was established (Lanes 11-15, Figure 2.3). The reaction patterns of dsDNA cleavage in these two cases are clearly different. In the absence of $A\beta_{1-20}$, dsDNA is cleaved into small fragments without formation of a linear intermediate as evident by the faint band at 2.0 kbp. The nature of the band is not clear at this stage and is not associated with Aβ. The dsDNA cleavage by $CuA\beta_{1-20}$ in the presence of H_2O_2 is conformation-dependent, most active toward supercoiled dsDNA as evident by the accumulation of nicked-circular and linear forms with time in the reaction, likely due to the structural constraints of the supercoiled form. The accumulation of the linearized form (middle bands) is indicative of double-stranded DNA cleavage, rather than a random single-stranded cleavage, which is a key trigger that can result in cell apoptosis.[25] The linearization of the plasmid via cleavage of double-stranded (ds) DNA is also characteristic of the cleavage pattern by DNA-recognizing agents such as Cu-bleomycin.[26]

False regulation of metal homeostasis and ROS physiology is closely related to aging and oxidative stress,[6] wherein apo-$A\beta_{1-20}$ seems to serve as a scavenger of metal ions due

to its large affinity constant with metal ions and a protective agent against oxidative damage of biological macromolecules by H_2O_2 based on the observations in this and other studies.[27, 28] However, the presence of H_2O_2 can result in severe damage toward dsDNA and presumably other redox-sensitive biomolecules as well by metallo-Aβ when the metal ions are redox active as demonstrated herein.

Kinetics and Mechanism of Oxidative Catalysis by CuAβ: To gain further insight into the mechanism for the oxidation activity of $CuA\beta_{1\text{-}20}$ and its interaction with H_2O_2, the catechol analogue 1,2,3-trihydroxylbenzene (THB) was utilized to provide detailed kinetic information owing to its easily accessible oxidation state which also has been utilized for investigation of oxidative activities of metal complexes.[29] The oxidation rate of THB by 7.5 μM $CuA\beta_{1\text{-}20}$ was determined at different values of [THB] in the presence of H_2O_2 at various concentrations (Figure 2.4), which reached saturation at high THB

$$v_O = v_{backgrond} + \frac{k_{cat}[CuA\beta][THB]}{K'_{app}+[THB]} \qquad (1)$$

concentrations. This saturation pattern suggests a possibility of pre-equilibrium kinetics. The rate law for this reaction mechanism can be expressed as in Eq. (1), assuming that the concentration of the intermediate THB-$CuA\beta_{1\text{-}20}$ complex is much lower than that of

the unbound THB in which $K'_{app} = (k_{-1} + k_{cat})/k_1$ is the virtual dissociation constant and k_1 and k_{-1} are the rate constants for the formation and dissociation, respectively, of the THB-CuAβ complex. The data can be well fitted to Eq. (1), yielding $k_{cat} = 0.00767\ s^{-1}$ and $K'_{app} = 1.67$ mM, and a second-order rate constant k_{cat}/K'_{app} of $4.59\ M^{-1}\ s^{-1}$ for the

reaction in the presence of 16.0 mM (0.0544%) H_2O_2. This represents a 724 fold increase in terms of the first-order rate constant when compared to the auto-oxidation of THB under the same reaction conditions in the absence of CuA$\beta_{1\text{-}20}$ (determined to be $k_0 = 1.06 \times 10^{-5}$ s^{-1}). A plot of k_{cat} as a function of [H_2O_2] from Figure 2.4 shows that k_{cat} reaches a plateau at high H_2O_2 concentrations (inset, Fig. 1.4). However, the k_{cat} value does not reach zero at 0% H_2O_2 that is higher than k_0 of the auto-oxidation of the substrate. The oxidation reaction in the absence of H_2O_2 was further explored and discussed in a later section below. The plot seems slightly sigmoidal which indicates a possible presence of either a consecutive or a cooperative binding of H_2O_2 to the active center. Since catechol oxidation involves 2-electron transfer which matches with the two-electron reduction of H_2O_2 to yield two oxides, a consecutive mechanism is not fundamentally necessary for the reaction to take place. The data were fitted to the Hill equation to extract the Hill coefficient θ of 2.09 and k_{cat} value of 0.00731 s^{-1} at 0% H_2O_2 (close to the value of 0.0065 s^{-1} directly measured in the absence of exogenous H_2O_2 discussed later), indicative of the presence of weak cooperativity and H_2O_2-independent oxidative catalysis.

Interestingly, the smaller fragment CuA$\beta_{1\text{-}16}$ showed more than 4-folds higher k_{cat} of 0.0340 s^{-1} for the reaction with the same concentration of H_2O_2. However, its catalytic efficiency is only twice higher than the larger fragment in terms of the second order rate constant k_{cat}/K'_{app} (10.5 M^{-1} s^{-1}), which suggests a participation of the last four C-terminal hydrophobic residues (LVFF) in the reaction pathway. The hydrophobic C-terminus may influence substrate binding and product release as reflected by the higher

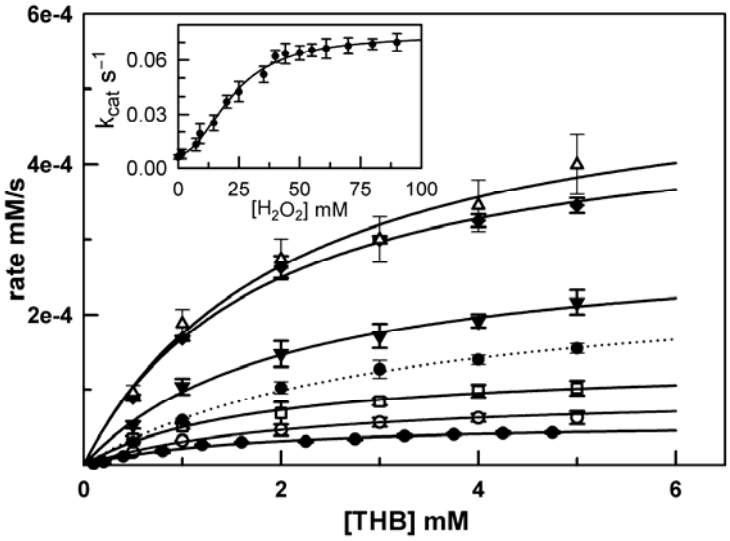

Figure 2.4. Effect of peroxide concentrations on the rate of THB oxidation in the presence of 7.5 μM of CuA$\beta_{1\text{-}20}$ in the presence of 1.6 (●), 3.2 (○), 16.2 (□), 32.3 (▼), 64.6 (♦), and 70.0 (Δ) mM H_2O_2 (HEPES buffer of 100 mM at pH 7.0 and 25.0 °C). The dotted line is CuA$\beta_{1\text{-}16}$ in the presence of 16.2 mM H_2O_2. The inset shows the first order rate constant k_{cat} as a function of hydrogen peroxide, wherein the solid trace is a fitting of the data to the Hill equation by taking into consideration of an activity at 0% H_2O_2.

K'_{app} and k_{cat} values for CuA$\beta_{1\text{-}16}$ (K'_{app} = 3.23 mM). This observation suggests that the C-terminus is close enough to the metal center to influence THB binding or a transition-state conformational change that affects both the binding of THB and the turnover of the reaction.

It has previously been documented that H_2O_2 and other ROS generated by metallo-Aβ may play a role in the pathology of AD.[27,28,30] Since the local concentration of metallo-Aβ in an AD brain can reach sub-mM range,[7] the above observation implies that a significant rate acceleration in redox reactions can be expected at a location where H_2O_2 is produced. This rate enhancement in the brains of AD patients can be metabolically catastrophic. In the studies shown here, I have further specified the fate of H_2O_2 in metallo-Aβ-associated redox reactions.

To further analyze the role of H_2O_2 in the reaction pathway, a saturation profile was constructed with a fixed amount of the substrate THB at 6.0 mM. Under such conditions, the reaction reaches plateau at [H_2O_2] near 70.0 mM or 0.238% (Figure 2.5). The results can be well fitted to a pre-equilibrium kinetics (Eq. 2). This kinetics further corroborates a metal-centered mechanism as described above.

$$v_O = v_{background} + \frac{k_{cat}[CuA\beta][H_2O_2]}{K'_{\alpha app} + [H_2O_2]} \qquad (2)$$

The rate of acceleration against the background oxidation of THB at saturating [H_2O_2] is approximately 6,000 folds (background rate constant $k_o = 1.14 \times 10^{-5}$ s^{-1}) with k_{cat} =

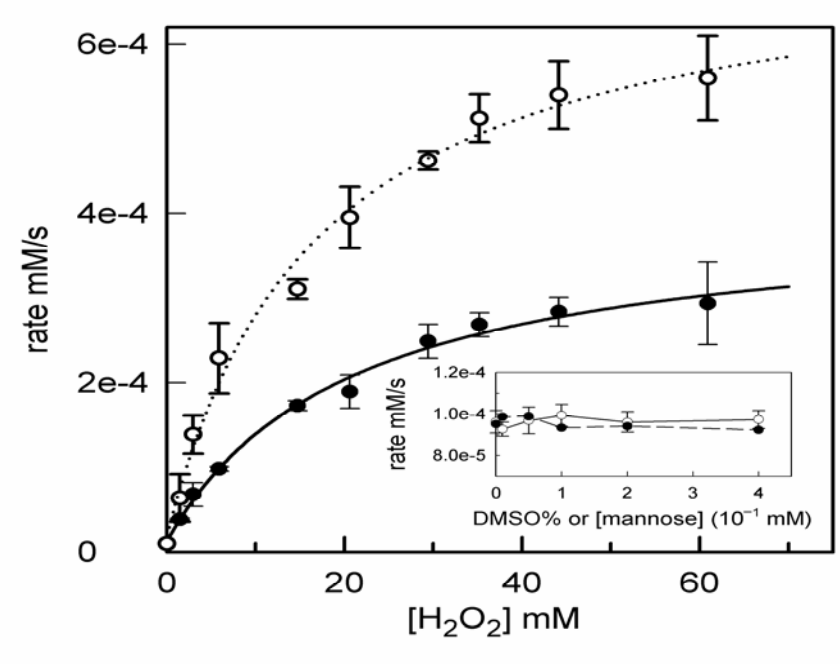

Figure 2.5. H_2O_2 saturation profile of $CuA\beta_{1\text{-}16}$ (○) and $CuA\beta_{1\text{-}20}$ (●) activity at a fixed [THB] of 6.0 mM (HEPES buffer of 100 mM at pH 7.0 and 25.0 °C). The inset shows that DMSO (○) and mannitol (●) do not inhibit the oxidation of THB by CuAβ.

0.066 s^{-1} and k_{cat}/K'_{app} = 37.2 M^{-1} s^{-1}. The hydrophobicity at the C-terminus does not affect the binding of H_2O_2 as reflected by the similar apparent virtual dissociation constant K'_{app} between CuAβ_{1-20} and CuAβ_{1-16} (17.3 and 16.6 mM, respectively). Qualitatively, since the k_{cat} value is small, the K'_{app} value is expected to be closer to the dissociation of the CuAβ-THB complex. The binding of each H_2O_2 molecule in this case may not yield a complete turnover, suggesting that formation of the intermediate Cu-peroxo active center is not favorable under the experimental conditions which may well be the rate-determining step. This result corroborates with chemical model studies of catechol oxidase and tyrosinase in that a dinuclear Cu-peroxo intermediate is often short-lived and thermodynamically unstable.[24,31]

Because the involvement of free radicals in the redox chemistry of metallo-Aβ had been implicated in previous reports,[7] different amounts of DMSO and mannitol, two common scavengers for superoxide free radical and hydroxyl free radical,[37,32] were added to the reaction solution separately with saturating concentrations of H_2O_2 and THB. No noticeable effect on the reaction rates was observed under the experimental conditions (Figure 2.5, inset). However, this does not discount possible free radical generation since the free radicals may well be metal-centered and free-radical oxidation in solution may not be the predominant pathway in the oxidation of THB catalyzed by CuAβ_{1-20}. We have established here a metal-centered oxidative catalysis by CuAβ_{1-20} and CuAβ_{1-16} which can not only generate H_2O_2 as noted previously[30] but also activate H_2O_2 for possible oxidation of biomolecules.[33]

Since both H_2O_2 and THB can interact with the metal center and are considered "substrates" for CuAβ, it is imperative to further narrow down the mechanism about how these two substrates interact individually with the metal center. For this purpose, the redox indicator 3-methyl-2-benzothiazolinone hydrazone (MBTH) was used to probe the oxidation product of THB *in the absence of* H_2O_2. MBTH is a common indicator used in catechol oxidase assay which forms a red adduct with the *o*-quinone products instantaneously.[16] The rate for the oxidation of a catechol into its corresponding *o*-quinone can thus be easily monitored colorimetrically as the oxidation is the rate-limiting step. The rate for the oxidation of THB by $CuA\beta_{1\text{-}20}$ in the absence of H_2O_2 as a function of [THB] is not linear which can be well fitted to pre-equilibrium kinetics to give k_{cat} = 0.0065 s^{-1} and K'_{app} = 2.0 mM. The first order rate acceleration of THB oxidation here is 650 folds with respect to the auto-oxidation (i.e. k_{cat}/k_o; $k_o = 1.06 \times 10^{-5}$ s^{-1}). This oxidative reaction is much less significant in terms of rate acceleration than that in the presence of a saturating amount of H_2O_2 described above. Here, catechol is possibly oxidized by CuAβ in form of a dinuclear Cu^{2+} center via 2-electron transfer to afford $2Cu^+$ and *o*-quinone product. The reduced $2Cu^+$ in turn can bind O_2 to form a dinuclear Cu^{2+}-peroxo center and follow the catalytic pathway as the CuAβ/H_2O_2 system discussed above. Because a bi-substrate mechanism was implied from our results (i.e. both THB and H_2O_2 show saturation), further analysis of the data was performed. The Hanes analysis was used to minimize the error across the concentration range (Figure 2.6A).[34] The virtual dissociation constant K'_{app} for both substrates cannot be resolved only from the primary nonlinear fitting without analyzing their combined effects.[35] It is thus

important to determine the rates at varying amounts of H_2O_2 when holding THB constant and vice versa. The data in Figure 2.4 were fitted to a two-substrate random-binding mechanism according to Equation 3 (Figure 2.6A),[34] wherein the binding of THB and H_2O_2 to CuA$\beta_{1\text{-}20}$ was assumed to be random and in rapid-equilibrium with a subsequent ordered product release. Under these conditions, a simple conversion to a secondary plot

$$\frac{[THB]}{v_O} = \frac{\left(1 + K'/[H_2O_2]\right)}{V_{\max}}[THB] + \frac{K'_{\alpha}}{V_{\max}}\left(1 + \frac{K_i}{[H_2O_2]}\right) \qquad (3)$$

of the slope (slope = $(1+ K'/[H_2O_2])/V_{max}$) and the y-intercept (y intercept = $(K'_{app}/V_{max})*(1+ K_i/[H_2O_2])$ in Figure 2.6B versus $1/[H_2O_2]$ yields K' and K'_{α}, the true values for the virtual dissociation of H_2O_2 and THB, respectively, and the intrinsic affinity constant of H_2O_2 K_i. Moreover, if any cooperativity is present in this bi-substrate reaction mechanism, it would be revealed by the ratio of K'_{app}/K'. For a random equilibrium mechanism a ratio of K'_{app}/K' between 1 and 5 would suggest little cooperativity.[35] In the oxidative catalysis by CuA$\beta_{1\text{-}20}$, the K'_{app}/K' ratio is 2.85 for THB oxidation and $K'_{\alpha app}/K'_{\alpha}$ is 1.62 for H_2O_2 which indicates little cooperativity. It is important to note that based on the data alone it is difficult to distinguish between an ordered sequential-binding mechanism and the mechanism herein proposed.[34] However, a random equilibrium phase is a sound assumption since both THB and H_2O_2 can interact with the metal centers separately.

In our proposed reaction mechanism, only when both THB and H_2O_2 substrates bind to the metal-center can productive turnover be observed with second-order rate constants of 8.66 and 15.6 $M^{-1}s^{-1}$ for the oxidation of THB by CuA$\beta_{1\text{-}20}$ and CuA$\beta_{1\text{-}16}$, respectively, in

the presence of H_2O_2 (whereas molecular O_2 serves as the second substrate in the absence of H_2O_2). This pathway differs from the previously proposed mechanism in the redox cycling of metallo-Aβ wherein the presence of the thioether group of Met_{35} was accounted for the reduction of the metal center.[7] The results presented here indicate substrate-mediated reduction of the metal center (since Met is absent in the studies) as well as oxidation of the substrate by metal-activated H_2O_2. However, our data do not discount the possibility of the involvement of Met in the reductive pathway in $A\beta_{1\text{-}40/42}$. Regardless, the redox chemistry of CuAβ presented here shows an important mechanism for possible destructive actions in Alzheimer's disease.

Taken together, the metal-centered redox cycle of CuAβ action in this study seems to match the mechanism of the dinuclear Cu-containing catechol oxidase, wherein the oxidation of the substrate takes place both in the presence and absence of H_2O_2.[38,39] Since the oxidation of catechols is a two-electron transfer process, the involvement of a dinuclear Cu center is thus a preferred pathway as in the case of the enzyme. In the presence of THB and H_2O_2, the dinuclear $\mu\text{-}\eta^2,\eta^2$-peroxo-$Cu^{2+}{}_2$-THB transition state is eventually formed by assembling two metal centers together via the bridging peroxo as in the case of many mononuclear Cu^{2+} complexes[23,24] (Figure 2.7, steps **A–C**), which is followed by 2-electron transfer from the bound peroxide to the bound catechol (likely through the metal center) to yield $Cu^{2+}{}_2$-μ-OH and *o*-quinone to complete a catalytic cycle (step **D**). Here, the complexes oxy-$Cu^{+}{}_2$, $Cu^{2+}{}_2$-μ-(η^2,η^2-peroxo), $Cu^{2+}{}_2$-μ-(η^1,η^1-

.

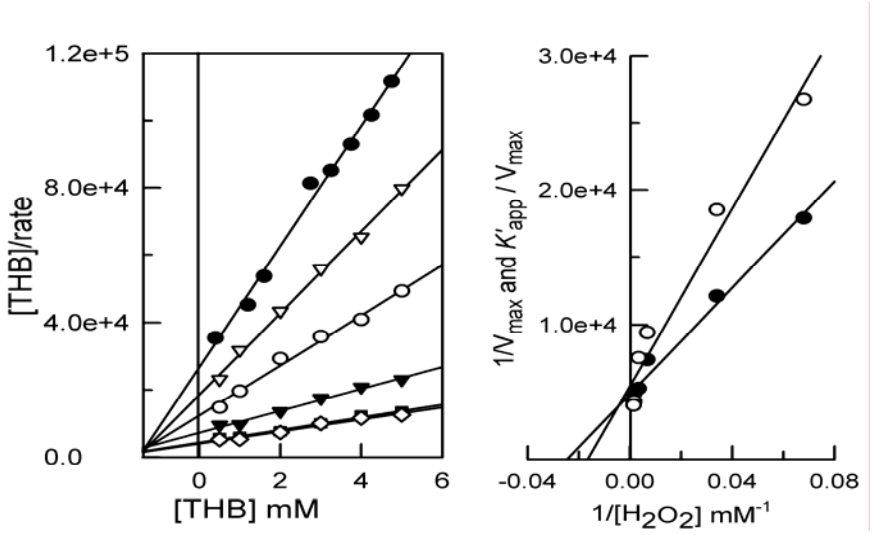

Figure 2.6. Hanes analysis of the kinetic data from Figure 4. The plots in **A** yield the apparent virtual dissociation constant for THB. The re-plot of the slope (●)and y-intercept (○) from **A** reveals dissociation constants for THB (K'_{α} = 0.41 mM) and H_2O_2 (K_i = 17.3 mM) in a bi-substrate reaction.

peroxo), and Cu^{3+}_2-(μ-oxo)$_2$ (**B**) are isoelectronic[24] which are not distinguishable in our study. In the absence of H_2O_2, the oxidation of the bound THB is achieved by 2-electron transfer to the dinuclear Cu^{2+}_2 center to yield Cu^{+}_2 (steps **F–G**) which is followed by O_2 and THB binding to regenerate the THB-Cu^{2+}_2-η^2-peroxo transition state (steps **H**, **B**, and **C**). The binary and the ternary complexes then follow the same pathway as the case in the presence of H_2O_2 for another turnover. H_2O_2 is also generated according to this mechanism under reducing conditions (steps **E** and **I**), which has been previously observed[30] and can serve as a competing reaction pathway toward the oxidation of catechols (steps **C**, **D**).

The mechanism of oxidative "chemical nucleases" has been thoroughly studied and reviewed.[36] According to the studies of some simple chemical nucleases such as Cu-1,10-phenanthroline, a reduced state of the metal center (by a reducing agent) is required for catalysis in the presence of O_2. In our experiments, however, the absence of a reducing agent to convert Cu^{2+} to Cu^{+} and the use of H_2O_2 as the oxidation agent suggest a different oxidative pathway. Moreover, the free radical scavenger[37] dimethyl sulfoxide (DMSO) did not inhibit the reaction, suggesting the absence of free radicals to induce the oxidative damage. On the basis of the results shown here, we propose a η^2-peroxo-bridged dinuclear Cu^{2+} active center for CuA$\beta_{1\text{-}20}$ as observed in a number of chemical model systems[23] and in catechol oxidase, tyrosinase, and hemocyanin.[38,39] The nature of this transient η^2-peroxo species and its attack on the substrates, although thoroughly

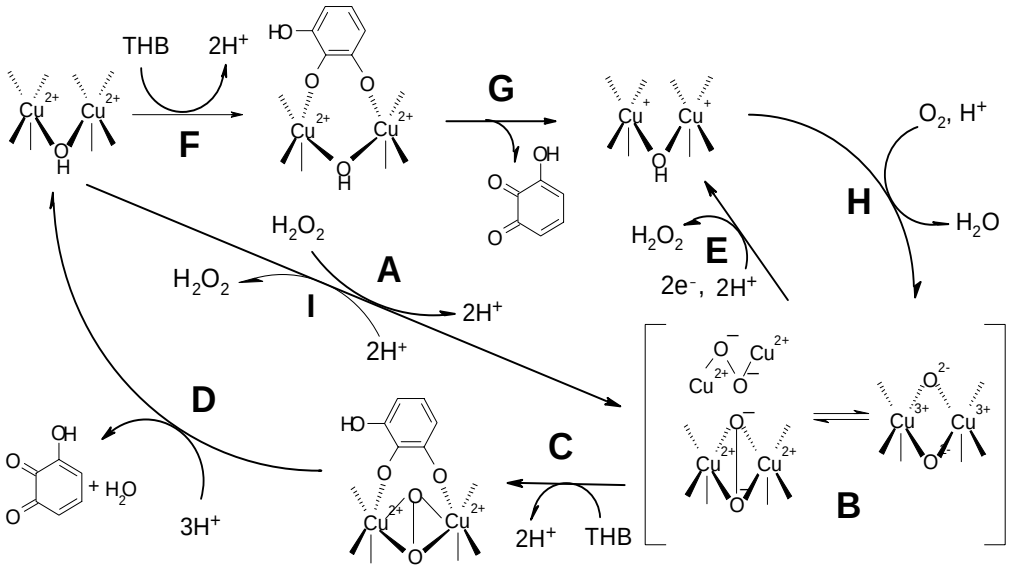

Figure 2.7. Proposed mechanism for the oxidation of THB by CuAβ in the presence (steps **A–D**) and absence of H_2O_2 (steps **F–H** and **B–D**). The production of H_2O_2 under reduction conditions (steps **E**) is also consistent with this mechanism.

studied, still has key mechanistic questions to be answered, such as the true structure of reaction intermediates, the role of substrate in the reaction mechanism, rate determining steps in catalysis, and specificity of metal cofactor for the function of enzymes like catechol oxidase, tyrosinase, peptidylglycine monooxygengase, methane monooxygenase, fatty acid desaturase, and ribonucleotide reductase.[40–42]

It has been proposed that substrate accessibility in the active site after O_2 binding plays a key role in the action of these proteins.[40,43] Consequently, a reversible O_2 binding has been demonstrated in hemocyanin because of the lack of substrate accessibility, wherein bulky substrates such as aromatic systems and the ribose moiety of DNA may not easily gain access to the O_2-binding active center of the proteins. However, studies of catechol oxidase and tyrosinase have shown the production of hydroxylated phenols and *ortho*-quinones, reflecting that substrates bind directly to the dinuclear Cu_2-η^2-O_2 active center which enables a direct attack on the substrates by the peroxo unit.[44,24]

Metal Binding and Structure: Detailed information about the metal-binding ligands and geometry of the metal site is needed to gain further insight into the metal-centered redox chemistry and to elucidate any structure-function correlation important for the action of metallo-Aβ. Since activity is an excellent probe for monitoring reaction mechanism, it is thus chosen as a probe for the determination of the metal-binding stoichiometry of metallo-Aβ. Upon introduction of Cu^{2+} to Aβ, oxidative activity can be measured as described above. It is evident from the data that metal binding reaches saturation at slightly above 1:1 ligand-to-metal ratio (Figure 2.8). Despite a previous

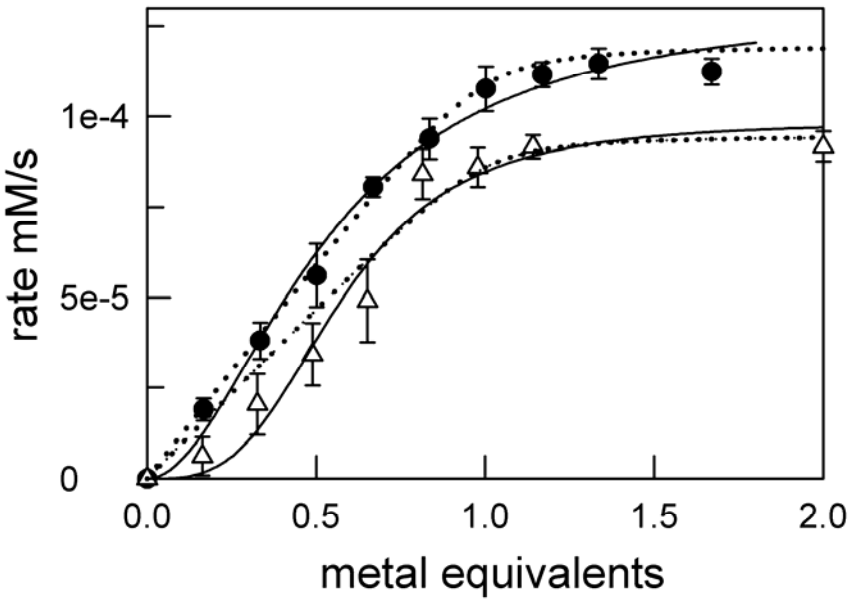

Figure 2.8. Cu^{2+} titration toward $A\beta_{1\text{-}20}$ (△) and $A\beta_{1\text{-}16}$ (●) monitored with their oxidation activities (100 mM HEPES buffer at pH 7.0 and 25.0 °C). The dotted curves show the best fittings to a noncooperative M+L ↔ ML equilibrium. Solid curves are the nonlinear fittings to the Hill Equation which yield Hill coefficients of 1.94 and 3.27 for Cu^{2+} binding to $A\beta_{1\text{-}16}$ and $A\beta_{1\text{-}20}$, respectively.

EPR study which indicate the binding of two Cu^{2+} ions to Aβ,[45] our result indicates the active species is a 1:1 CuAβ complex. Both a noncooperative binding equilibrium (a quadratic pattern) and a cooperative equilibrium (a sigmoidal pattern) were used to fit the data. It is evident from the fitting that the shorter $CuA\beta_{1-16}$ fits equally well to both binding patterns with a metal-to-ligand stoichiometry of 1 to 1, whereas $CuA\beta_{1-20}$ seems to fit better the cooperative binding pattern. The binding of Cu^{2+} to $A\beta_{1-16}$ gives a Hill coefficient θ of 1.94, while the binding to $A\beta_{1-20}$ shows a higher cooperativity with θ of 3.27. This result is consistent with previous reports of cooperative metal binding to the entire Aβ determined on the basis of quantitative precipitation.[46] The results presented here further indicate the presence of cooperativity in the oxidative activity as well as metal-binding. The higher C-terminal hydrophobicity of $A\beta_{1-20}$ may influence intermolecular interactions, resulting in a more apparent cooperativity. The data were also analyzed to determine whether or not there were possible inactive dimer conformations of this metallopeptide by plotting activity as function of the square root of metal ion concentration as previously described.[47] However, the data do not reflect the existence of such equilibrium in this reaction pathway, adding supporting evidence to the dinuclear metal-centered redox mechanism herein proposed. Dissociation constants (K_d) for metal binding to Aβ can be extrapolated from both fits with values of 3.96 and 4.30 μM for $CuA\beta_{1-16}$ and $CuA\beta_{1-20}$, respectively. Since activity serves as the probe here, the values obtained above are thus the intrinsic dissociation constants attributable to the active CuAβ complexes and are not affected by coagulation equilibrium for Aβ. The intrinsic dissociation constant for metal binding in $CuA\beta_{1-40}$ is likely to be in the same

range of ~4 μM for $CuA\beta_{1\text{-}20}$ and $CuA\beta_{1\text{-}16}$ owing to their probably similar metal-binding configuration. Indeed, dissociation constants in the range of ~0.1 μM for $CuA\beta_{1\text{-}28}$ and ~2 μM for $CuA\beta_{1\text{-}40}$ and $CuA\beta_{1\text{-}42}$ were determined with ligand-competition[45] and direct fluorescence measurement.[48] An apparent dissociation constant $K_{d\text{app}}$ of 0.50 pM for Cu^{2+} binding to$A\beta_{1\text{-}40}$ was determined based on the formation of $CuA\beta_{1\text{-}40}$ coagulates,[46] which can be dissected into the intrinsic metal dissociation constant K_{Cu} of ~4 μM and the dissociation constant of $CuA\beta_{1\text{-}40}$ coagulates K_{co} ~0.13 μM (i.e., $K_{d\text{app}} = K_{Cu} \times K_{co}$). The much smaller dissociation constant of 6.3 aM for Cu^{2+} binding to$A\beta_{1\text{-}42}$ would thus afford an apparent dissociation constant of $CuA\beta_{1\text{-}40}$ coagulates in the range of 1.6 pM. A recent report indicates that trace amounts of metal ions can significantly affect Aβ coagulation, it is thus suspected that the dissociation constants may be under estimated based on the coagulation.[49] I report in this dissertation a direct and reliable means for the determination of metal binding to soluble Aβ fragments which is not complicated by the formation of the coagulation as previously observed[46] that can be influenced by other factors, such as trace amount of metal ions.[49]

To further investigate the metal-coordination environment, the electronic spectrum of $CuA\beta_{1\text{-}20}$ was obtained (Figure 2.9). The spectrum reveals a typical type-2 copper center with d-d transitions showing λ_{max} at 610 nm (107 M^{-1} cm^{-1}), clearly distinguishable from the near IR absorption at 820 nm for aqueous Cu^{2+} solutions. This absorption is consistent with that of the "CuH_2L" species of acetyl-$A\beta_{1\text{–}16}$ with three coordinated His side chains in a potentiometric study[50] (617 nm and 117 M^{-1} cm^{-1}) and another study[45] (610 nm and ~50 M^{-1} cm^{-1} which seems to be too low an absorptivity[51]). The result

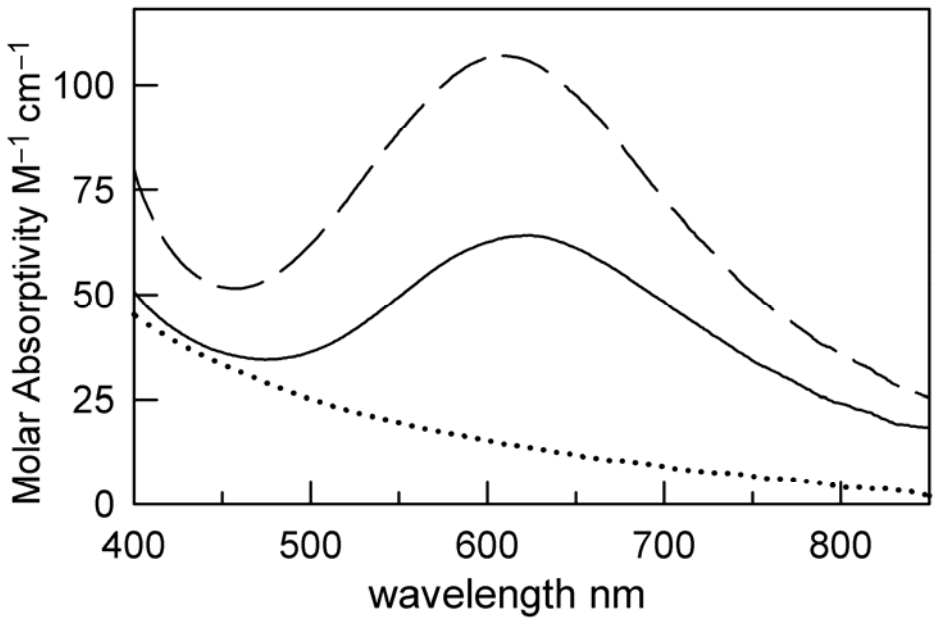

Figure 2.9. Electronic spectra of $A\beta_{1\text{-}20}$ with 0.5 equivalents (solid trace) and 1.0 equivalent Cu^{2+} (dashed trace) referenced against apo $A\beta_{1\text{-}20}$ (100 mM HEPES buffer at pH 7.0). The dotted trace is the difference spectra of 1.4 and 1.0 equivalents of Cu^{+2} in $A\beta_{1\text{-}20}$, showing no further increase in the d-d transition after the binding of one equivalent of Cu^{2+}.

agrees well with a tetragonally distorted octahedral environment[51,52] for the Cu^{2+} in $CuA\beta_{1-20}$. Upon addition of more than one equivalent of metal, the spectrum does not change. This is consistent with the results when activity is used as the probe to monitor metal binding (Fig. 2.8), wherein one equivalent Cu^{2+} is determined to bind to one peptide. It is also worth noting that there are no intense transitions in the near-UV range that can be possibly assigned to Tyr-to-Cu^{2+} charge-transfer transitions as observed in the Cu^{2+}-substituted proteases astacin and serralysin.[53]

The metal coordination chemistry was also investigated by the use of Co^{2+} as an NMR probe. Co^{2+} has been well demonstrated to be an excellent probe for the investigation of metal-binding sites in a number of metalloproteins, including Zn and Cu proteins.[54,55] Although $A\beta_{1-20}$ has four additional hydrophobic amino acids on the C-terminus, the conformations of the two peptides in d^6-DMSO are similar as they show nearly identical ^1H NMR spectra (Figure 2.10). The signals due to $L_{16}VFF_{20}$ side chains in $A\beta_{1-20}$ are clearly observed when compared with the spectrum of $A\beta_{1-16}$, wherein LV are seen at ~0.6 ppm and FF ~7.2 ppm. This similarity reflects their similar configuration. There are two solvent exchangeable signals in the 14–16 ppm range (imidazole N-H signature chemical shifts[56]) with a 1:2 ratio in intensity, corresponding to the three His side chains (insets, Figure 2.10 A and B).

Upon Co^{2+} titration, the intensities of these solvent exchangeable His-imidazole signals gradually decreased which was accompanied by the appearance of three far-downfield paramagnetically shifted signals in the region of 40–80 ppm as shown here for $A\beta_{1-20}$ (Figure 2.10C). These far-shifted signals are also solvent exchangeable and

correspond to the chemical shift of the solvent exchangeable signal of a paramagnetic Co^{2+}-bound imidazole group of a histidine residue (which cannot be due to dipolar shift of unbound His residues since the octahedral Co^{2+} center is expected not to possess magnetic anisotropy) as observed in many Co^{2+}-substituted metalloproteins.[54,55] These three solvent exchangeable NH signals further confirms the involvement of all three histidine residues in $A\beta_{1-20}$ for metal binding, consistent with previous Raman spectroscopic studies,[9] and is indicative of the absence of a bridging histidyl imidazole (in contrast to previously suggested[9,12]) which would result in the loss of an imidazole NH signal.

Tyr_{10} was suggested to be a possible ligand for Cu^{2+} and Fe^{3+} binding,[9,12,57] but was suggested not to be a ligand in other studies.[50] The ^1H NMR signals of Tyr_{10} (the two asterisked doublets centered at ~6.7 ppm in Figure 2.10 do not show any noticeable change upon the addition of the paramagnetic Co^{2+} ion. The binding of a Tyr-phenol group to Co^{2+} is expected to exhibit paramagnetically shifted ^1H NMR signals of the bound phenol group outside the diamagnetic region as previously observed.[58] This result indicates that this Tyr is not a metal-binding ligand, consistent with the lack of charge-transfer transitions for a possible Tyr-Cu^{2+} binding as described above. Our results also do not support the binding of the N-terminal amino group to the metal as previously suggested.[45] This binding mode for paramagnetic Co^{2+} would show far upfield-shifted NH_2 signal(s), a downfield-sifted $C_\alpha H$ proton, and slightly upfield-shifted $C_\beta H_2$ protons owing to spin polarization, which were not observed.[55]

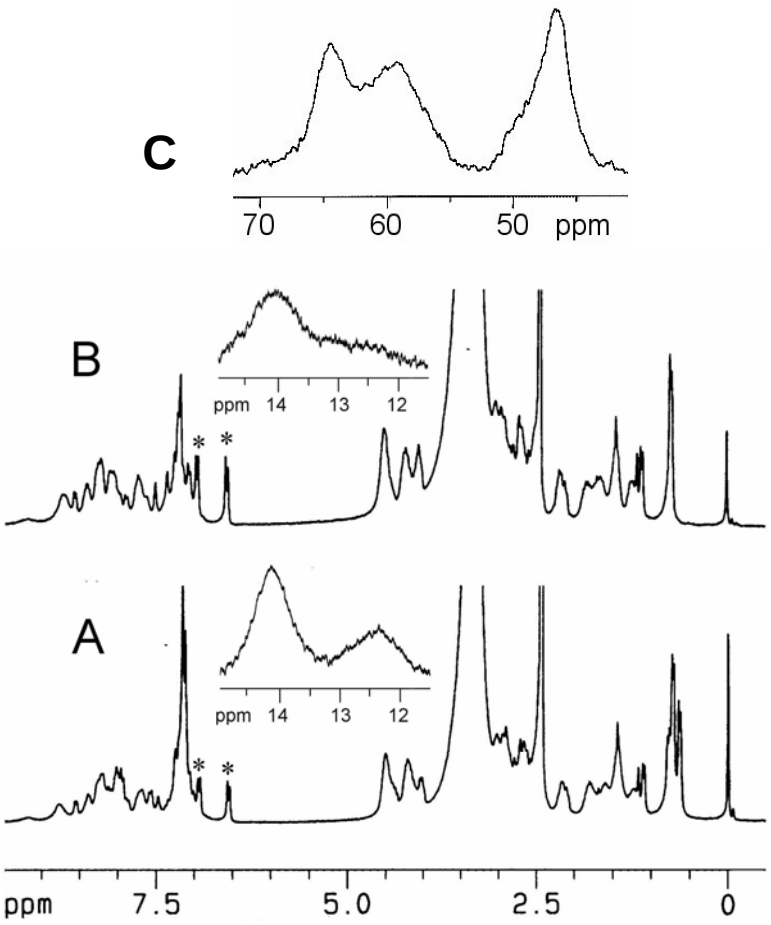

Figure 2.10. ^{1}H NMR spectra of $A\beta_{1-20}$ (A) and $A\beta_{1-16}$ (B) in DMSO. The insets show the imidazole N-H solvent exchangeable signals of His which disappear upon addition of a drop of D_2O (remain intact with same amount of H_2O). These signals disappear upon addition of paramagnetic Co^{2+}, with concomitant appearance of three solvent exchangeable hyperfine-shifted signals in the far-downfield region as shown here for Co-$A\beta_{1-20}$ (C). The asterisked signals in A and B are due to Tyr ring protons which remain the same upon Co^{2+} binding.

Molecular mechanical calculations have been applied to determine the structure of $A\beta_{1-16}$ and its metal-binding domain. The energies for different metal-binding modes have been calculated by the use of the MM3 force field and a simulated water droplet to solvate the peptide. Binding of Cu^{2+} to His_{13} and His_{14} yields the lowest energy of –385 kcal/mol as compared to all other possible binding modes in the peptide. The binding to all three His side chains yields a distorted octahedral geometry (with 3 open coordination sites presumably occupied by water molecules) and a slightly higher energy at –363 kcal/mol (Figure 2.11). The energy difference between these two metal-binding modes may be low enough to be easily overcome at room temperature. Extensive H-bonding are observed in this calculated structure, particularly Glu3-Arg5-Asp7 H-bonding interactions may stabilize the structure to a great extend (dotted lines in Fig. 2.11). The energies for Cu^{2+} binding to $His_{6/13}$ and $His_{6/14}$ are much higher at –125 and –210 kcal/mol, respectively, and are not likely to be the metal binding modes for Aβ. A histidine-bridged dimer form of the peptide previously proposed[12] was also calculated which gave an unacceptably high overall energy of 52,500 kcal/mol. The binding of Tyr_{10} along with the histidine residues is also highly unfavorable which puts undue stress on the phenol ring causing it to pucker and the peptide backbone to distort, with a high overall energy of 570 kcal/mol. The recently suggested N-terminal binding mode (along with the binding of the 3 histidines) has also been calculated to give an unfavorable overall energy of 147 kcal/mol. Since Cu^{+} can easily adopt a trigonal coordination sphere,[52] a calculation with a fixed trigonal coordination was performed which yielded an energy of –318 kcal/mol. The low energy difference between octahedral and trigonal

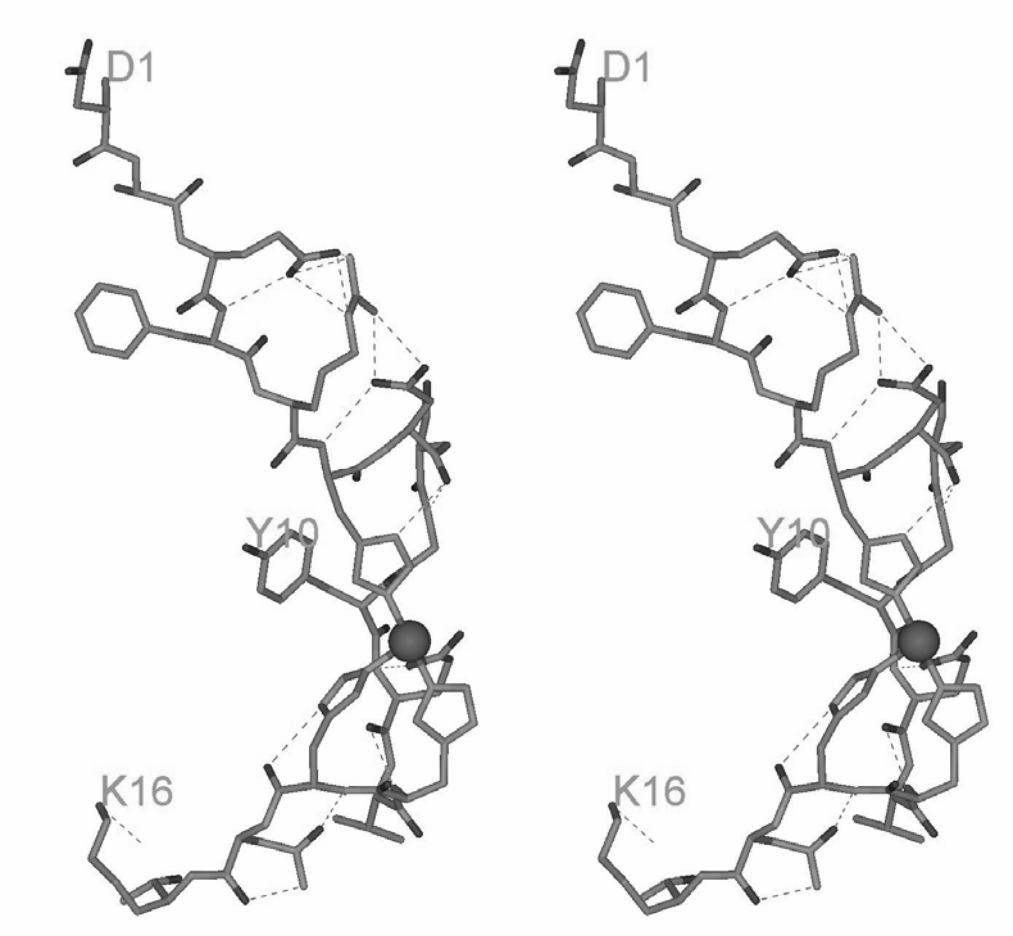

Figure 2.11- Proposed metal coordination and solution structure of $CuA\beta_{1\text{-}16}$ in a relaxed-eye stereo view based on NMR study of Co^{2+} binding and molecular mechanics calculations. According to the molecular mechanical calculations both the two-histidine (H13/H14) and three-histidine binding patterns are stable, whereas NMR study suggests the latter binding pattern. The dotted lines are H-bonds, which may prevent further bending of the peptide to allow the binding of the N-terminus to the metal as recently reported.[45]

geometries rationalizes the redox cycle of the Cu center in the catalysis of catechol oxidation. The binding of the 3 His side chains to the metal renders one side of the metal center to have an open coordination sphere which can possibly bind H_2O_2 or O_2 to form the dinuclear bridging η^2-peroxo center described above.

IV. CONCLUDING REMARKS

The results presented here have added further insight and support to the structure and chemistry of metallo-Aβ which may assist better understanding of the neuropathology of Alzheimer's disease. A complete redox cycle for the action of CuAβ has been proposed from the kinetic studies which is consistent with the mechanism proposed for the dinuclear Cu catechol oxidase. The results in this report, however, do not resolve the cause/effect debate about the role of Aβ in AD, but add more information to the chemistry of metallo-Aβ. As a cause for AD, I have shown and quantified redox chemistry of CuAβ in this dissertation which can serve as a catalyst both in the absence and presence of H_2O_2 to cause severe oxidative damages in the brains of AD patients. As an effect of AD, Aβ can be reasoned to be present as a regulator toward metal ion homeostasis due to its considerable metal affinities and its protective property toward oxidative DNA damage in the absence of Cu^{2+}. In the latter case, abnormal homeostasis of redox-active metal ions can leach the metal ions to yield metallo-Aβ that can undergo redox destruction of biomolecules. I have presented data herein to revise the redox chemistry of the methionine-centered hypothesis by showing a metal-centered catalysis

as a significant contribution to the oxidative damage in the pathology of the neurodegenerative AD. The fate of H_2O_2 generated by CuAβ in the presence of a reducing agent previously observed or an electron-donating substrate shown here has also been established and quantified with exogenous addition of this oxidant. Further studies currently under way that focus on the structure-activity relationship of metallo-Aβ are expected to shed light on the roles of metal ions and Aβ in AD and with hope to provide useful information for treatment and prevention of Alzheimer's disease.

IV. LIST OF REFERENCES

1) (a) S.R. Paik, H.J. Shin, J.H. Lee, C.S. Chang, J. Kim, Copper(II)-induced self-oligomerization of alpha-synuclein. *Biochem. J.* (1999), 340, 821-828. (b) S.R. Paik, H.J. Shin, J.H Lee, Metal-catalyzed oxidation of alpha-synuclein in the presence of Copper(II) and hydrogen peroxide. *Arch. Biochem. Biophys.* (2000), 378, 269-277.

2) A.G. Estevez, J.P. Crow, J.B. Sampson, C. Reiter, Y. Zhuang, G.J. Richardson, M.M. Tarpey, L. Barbeito, J.S. Beckman, Induction of nitric oxide-dependent apoptosis in motor neurons by zinc-deficient superoxide dismutase. *Science* (1999), 286, 2498-2500.

3) D. Mckenzie, J. Bartz, J. Mirwald, D. Olander, R. Marsh, J. Aiken, J. Reversibility of scrapie inactivation is enhanced by copper. *J. Biol. Chem*. (1998), 273, 25545-25547.

4) V.C. Culotta, L.W.J. Komp, J. Strain, R.L.B. Casareno, B. Krems, J.D. Gitlin, The copper chaperone for superoxide dismutase. *J. Biol. Chem.* (1997), 272(38), 23469-23472.

5) E. Roche, D. Romero-Alvira, Oxidative stress in some dementia types. *Med. Hypot.* (1993), 40, 342-50.

6) L.A. Shinobu, M.F. Beal, in J.R. Conner, J. R. Ed. *Metals in Oxidative Damage in Neurological Disorders*; Plenum, New York (1997).

7) A.I. Bush, The metallobiology of Alzheimer's disease. *Trends Neurosci*. (2003), 26, 207-214.

8) A.I. Bush, W.H. Pettingell, G. Multhaup, M. Paradis, J. Vonsattel, J.F. Gusella, K. Beyreuther, C.L. Masters, R.E. Tanzi, Rapid induction of Alzheimer Aβ amyloid formation by zinc. *Science* (1994), 265, 1464-1467.

9) T. Miura, K. Suzuki, N. Kohata, H. Takeuchi, Metal binding modes of Alzheimer's amyloid beta-peptide in insoluble aggregates and soluble complexes. *Biochemistry* (2000), 39, 7024-7031.

10) Y. Ling, K. Morgan, N. Kalsheker, Angiotensinogen: molecular biology, biochemistry and physiology. *Int. J. Biochem. Cell. Biol*. (2003), 35, 1505-1535.

11) A. Kontush, C. Berndt, W. Weber, V. Akopian, S. Arlt, S. Schippling, U. Beisiegel, Amyloid-β is an antioxidant for lipoproteins in cerebrospinal fluid and plasma. *Free Rad. Biol. Med*. (2001), 30, 119-128.

12) C. Curtain, F. Ali, I.Volitakis, R.A. Cherny, R.S. Norton, K. Beyreuther, C.J. Barrow, C.L. Masters, A.I. Bush, Alzheimer's disease amyloid-β binds copper and zinc to generate an allosterically ordered membrane-penetrating structure containing superoxide dismutase-like subunits. *J. Biol. Chem*. (2001), 276, 20466-2073.

13) G. Evin, A. Weidemann, Biogenesis and metabolism of Alzheimer's disease Aβ amyloid peptides. *Peptides* (2001), 23, 1285-1297.

14) G. Evin, A. Zhu, D. Holsinger, C.L. Masters, Q. Li, Proteolytic processing of the Alzheimer's disease amyloid precursor protein in brain and platelets. *J.Neurosci. Res.* (2003), 74, 386-392.

15) C. Schőneich, D. Pogocki, G.L. Hug, K. Bobrowski, Free Radical Reactions of Methionine in Peptides: Mechanisms Relevant to β-Amyloid Oxidation and Alzheimer's Disease. *J. Am. Chem. Soc*. (2003*)*, 125, 13700-13713.

16) S.G. Srivatsan, P. Nigam, M.S. Rao, S. Verma, Phenol oxidation by copper-metallated 9-allyladenine-DVB polymer: reaction catalysis and polymer recycling. *Applied Catal. A: General* (2001), 209, 327-334.

17) J.H. Jang, Y.J. Surh, beta-Amyloid induces oxidative DNA damage and cell death through activation of c-Jun N terminal kinase. *Ann. NY Acad. Sci*. (2002), 973, 228-236.

18) M.F. Walter, P.E. Mason, R.P. Mason, Alzheimer's disease amyloid β peptide 25-35 inhibits lipid peroxidation as a result of its membrane interactions. *Biochem. Biophys. Res. Comm*. (1997), 233, 760-764.

19) K. Lonrot, K.T. Metsa, G. Molnar, J.P. Ahonen, M. Latvala, J. Peltola, T. Pietila, H. Alho, The effect of ascorbate and ubiquinone supplementation on plasma and CSF total antioxidant capacity. *Free Rad. Med. Biol*. (1996), 21, 211-217.

20) A. Nunomura, G. Perry, J. Zhang, T. Montine, A. Takeda, S. Chiba, M.A. Smith, RNA oxidation in Alzheimer's and Parkinson's diseases. *J. Anti-Aging Med*. (1999), 2, 227-230.

21) C.J. Burrows, V. Lepentsiotis, J. Domagala, I. Grgic, R. van Eldik, J.G. Muller, Mechanistic information on the redox cycling of nickel(II/III) complexes in the

presence of sulfur oxides and oxygen. Correlation with DNA damage experiments. *Inorg. Chem.* (1999), 38, 3500-3505

22) (a) O.I. Aruoma, B. Halliwell, E. Gajewski, M. Dizdaroglu, Copper-ion-dependent damage to the bases in DNA in the presence of hydrogen peroxide. *Biochem. J.* (1991), 273, 601–604; (b) J. Sagripanti, K.H. Kraemer, Site-specific oxidative DNA damage at polyguanosines produced by copper plus hydrogen peroxide. *J. Biol. Chem.* (1989), 264 1729–1734; (c) S.-M. Chiu, L.-Y. Xue, L.R. Friedman, N.L. Oleinick, Differential Dependence on Chromatin Structure for Copper and Iron Ion Induction of DNA Double-Strand Breaks. *Biochemistry* (1995), 34, 2653-2661; (d) K. Yamamoto, S. Kawanishi, Site-specific DNA damage induced by hydrazine in the presence of manganese and copper ions. The role of hydroxyl radical and hydrogen atom. *J. Biol. Chem.* (1991), 266, 1509–1515; (e) K. Yamamoto, S. Kawanishi, Hydroxyl free radical is not the main active species in site-specific DNA damage induced by copper(II) ion and hydrogen peroxide. *J. Biol. Chem.* (1989), 264, 15435–15440.

23) N. Kitajima, T. Koda, Y. Iwata, Y. Morooka, Reaction aspects of a μ-peroxo binuclear copper(II) complex. *J. Am. Chem. Soc.* (1990), 112, 8833-8839.

24) (a) E.A. Lewis, W.B. Tolman, Reactivity of Dioxygen-Copper Systems. *Chem. Rev.* (2004), 104, 1047-1076. (b) W.B. Tolman, Making and Breaking the Dioxygen O-O Bond: New Insights from Studies of Synthetic Copper Complexes. *Acc. Chem. Res.* (1997) 30, 227–237.

25) M. Stanulla, J. Wang, D.S. Chervinsky, S. Thandla, P.D. Aplan, DNA cleavage within the MLL breakpoint cluster region is a specific event which occurs as part of higher-order chromatin fragmentation during the initial stages of apoptosis. *Mol. Cell. Biol.* (1997), 17, 4070–4079.

26) G.M. Ehrenfeld, L.O. Rodriguez, S.M. Hecht, Copper(I)-bleomycin: structurally unique complex that mediates oxidative DNA strand scission. *Biochemistry* (1985), 24, 81-92.

27) K. Zou, J.S. Gong., K. Yanagisawa, M. Michikawa, A novel function of monomeric amyloid β -protein serving as an antioxidant molecule against metal-induced oxidative damage. *The J. Neurosci.* (2002), 22, 4833-4841

28) A. Kontush, Amyloid-β : an antioxidant that becomes a pro-oxidant and critically contributes to Alzheimer's disease. *Free Rad. Med. Biol.* (2001), 31, 1120-1131.

29) K. J. Humphreys, A. E. Johnson, K. D. Karlin, S. E. Rokita, Oxidative strand scission of nucleic acids by a multinuclear copper(II) complex. *J. Biol. Inorg. Chem*. (2002), 7, 835-842.

30) C. Opazo, X. Huang, R.A. Cherny, R.D. Moir, A.E. Roher, A.R. White, R. Cappai, C.L. Masters, R.E. Tanzi, N.C. Inestrosa, A.I. Bush, Metalloenzyme-like activity of Alzheimer's disease β -amyloid. *J. Biol. Chem*. (2002), 277, 40302-40308.

31) V. Mahadevan, M.J. Henson, E.I. Solomon, T.D.P. Stack, Irreversible Reduction of Dioxygen by Simple Peralkylated Diamine-Copper(I) Complexes: Characterization

and Thermal Stability of a [Cu2(μ -O)2]2+ Core. *J. Am. Chem. Soc.* (2000), 122, 10249-10250.

32) D. Bagchi, A. Garg, R.L. Krohn, M. Bagchi, M.X. Tran, S.J. Stohs, Oxygen free radical scavenging abilities of vitamins C and E, and a grape seed proanthocyanidin extract in vitro. *Res. Comm. Mol. Pathol. Pharmacol.* (1997), 95, 179-89.

33) See Chapter IV.

34) V. Leskovac, Comprehensive Enzyme Kinetics, Kluwer/Plenum, Boston, MA (2002).

35) J.R. Florini, C.S. Vestling, Graphical determination of the dissociation constants for two-substrate enzyme systems. *Biochim. Biophys. Acta*. (1957), 25, 575-578.

36) D.S. Sigman, A. Mazumder, D. Perrin, Chemical nucleases. *Chem. Rev*. (1993), 93, 2295-2316.

37) P.S. Rao, J.M. Luber, J. Milinowicz, P. Lalezari, H.S. Mueller, Specificity of oxygen radical scavengers and assessment of free radical scavenger efficiency using luminol enhanced chemiluminescence. *Biochem. Biophys. Res. Comm*. (1988), 150, 39-44.

38) I. Bertini, S.J. Lippard, H.B. Gray, J.S. Valentine, Eds. *Bioinorganic Chemistry*, University Science Books, Sausalito, CA. (1994) Chapters 4 & 5.

39) C. Gerdemann, C. Eicken, B. Krebs, The crystal structure of catechol oxidase: New insight into the function of type-3 copper proteins. *Acc. Chem. Res.* (2002), 35, 183-191.

40) N.J. Blackburn, F.C. Rhames, M. Ralle, S. Jaron, Major changes in copper coordination accompany reduction of peptidylglycine monooxygenase: implications

for electron transfer and the catalytic mechanism. *J. Biol. Inorg. Chem.* (2000), 5, 341-353.

41) L. Que Jr., W.B. Tolman, Bis(μ -oxo)dimetal "diamond" cores in copper and iron complexes relevant to biocatalysis. *Angew. Chem.* (2002), 41, 1114-1137.

42) S.Y. Seo, V.K. Sharma, N. Sharma, Mushroom tyrosinase: Recent prospects. *J. Agric. Food Chem.* (2003), 51, 2837-2853.

43) P. Chen, E.I. Solomon, Oxygen Activation by the Noncoupled Binuclear Copper Site in Peptidylglycine β -Hydroxylating Monooxygenase. Reaction Mechanism and Role of the Noncoupled Nature of the Active Site. *J. Am. Chem. Soc.* (2004), 15, 4991-5000.

44) S. Yamazaki, S. Itoh, Kinetic evaluation of phenolase activity of tyrosinase using simplified catalytic reaction system. *J. Am. Chem. Soc.* (2003), 125, 13034-13035.

45) C.D. Syme, R.C. Nadal, S.E.J. Rigby, J.H. Viles, Copper Binding to the Amyloid-β (Aβ) Peptide Associated with Alzheimer's Disease: Folding, coordination Geometry, pH Dependence, Stoichiometry, and Affinity of Aβ -(1-28): Insights from a Range of Complementary Spectroscopic Techniques. *J. Biol. Chem.* (2004), 279, 18169–18177.

46) C.S. Atwood, R.C. Scarpa, X. Huang, R.D. Moir, W.D. Jones, D.P. Fairlie, R.E. Tanzi, A.I. Bush, Characterization of copper interactions with Alzheimer amyloid β peptides: identification of an attomolar-affinity copper binding site on amyloid β 1-42. *J. Neurochem*. (2000), 75, 1219-33.

47) E.L. Hegg, S.H. Mortimore, C.L. Cheung, J.E. Huyett, D.R. Powell, J.N. Burstyn, Structure-Reactivity Studies in Copper(II)-Catalyzed Phosphodiester Hydrolysis. *Inorg. Chem.* (1999), 38, 2961-2968.

48) W. Garzon-Rodriguez, A.K. Yatsimirsky, C.G. Glabe, Binding of Zn(II), Cu(II), and Fe(II) ions to Alzheimer's Aβ peptide studied by fluorescence. *Bioorg. Med. Chem. Lett.* (1999), 9, 2243-2248

49) X. Huang, C.S. Atwood, R.D. Moir, M.A. Hartshorn, R.E. Tanzi, A.I. Bush, Trace metal contamination initiates the apparent auto-aggregation, amyloidosis, and oligomerization of Alzheimer's Aβ peptides. *J. Biol. Inorg. Chem.* (2004), 9, 954-960.

50) T. Kowalik-Jankowska, M. Ruta, K. Wiśniewska, L. Łankiewicz, Coordination abilities of the 1-16 and 1-28 fragments of β -amyloid peptide towards copper(II) ions: a combined potentiometric and spectroscopic study. *J. Inorg. Biochem.* (2003), 95, 270–282.

51) A.B.P. Lever, *Inorganic Electronic Spectroscopy*, 2nd ed. Elsevier, (1986).

52) F.A. Cotton, G. Wilkinson, *Advanced Inorganic Chemistry,* 5th Ed., Wiley, New York, NY (1988).

53) H.I. Park, L.-J. Ming, Mechanistic studies of the astacin-like Serratia metalloendopeptidase serralysin: highly active (>2000%) Co(II) and Cu(II) derivatives for further corroboration of a "metallotriad" mechanism. *J. Biol. Inorg. Chem*. (2002), 7, 600-610.

54) I. Bertini, C. Luchinat, High spin cobalt(II) as a probe for the investigation of metalloproteins. *Adv. Inorg. Biochem.*, (1984), 6, 71-111.

55) L.-J. Ming, Nuclear Magnetic Resonance of Paramagnetic Metal Centers in Proteins and Synthetic Complexes In *Physical Methods in Bioinorganic Chemistry, Spectroscopy and Magnetism*, Que, L., Jr., Ed.; University Science Books, (2000).

56) A.R. Burger, S. J. Lippard, M.W. Pantoliano, J.S. Valentine, Nuclear magnetic resonance study of the exchangeable histidine protons in bovine and wheat germ superoxide dismutases. *Biochemistry* (1980), 19, 4139-4143.

57) T. Miura, K. Suzuki, H. Takeuchi, Binding of iron(III) to the single tyrosine residue of amyloid β -peptide probed by Raman spectroscopy. *J. Mol. Struct*. (2001), 598, 79–84.

58) H.I. Park, L.-J. Ming, The mechanistic role of the coordinated tyrosine in astacin. *J. Inorg. Biochem.* (1998), 72, 57-62.

CHAPTER III. CATECHOL OXIDASE AND PHENOL MONOOXYGNEASE ACTIVITIES OF CuAβ_{1-20}[‡]

I. INTRODUCTION

Over the past few years an enormous effort has been directed toward the investigation of the metal-dependent mechanisms that lead to the neuropathology of Alzheimer's disease (AD).[1] The self-assembled metallo-β-amyloid (Aβ) peptide fibrils are the hallmark of this disease[2] and have been attributed to Fe^{III} and Cu^{II}-centered generation of H_2O_2 under reducing conditions which has been postulated to be of significant importance in connection with neuropathy in AD.[3,4] However, an area of oversight has been the detailed chemical processes associated with the neuropathology of AD, besides the general acclaimed "ROS" (reactive oxygen species, including H_2O_2) assault.[5] Hence,

[‡] This work has been published: G.F.Z. da Silva, L.-J. Ming, Alzheimer's Disease Related Copper(II)-β-Amyloid Peptide Exhibits Phenol Monooxygenase and Catechol OxidaseActivities. *Angew. Chem. Int. Ed.* (2005), 44, 5501-5504.

a better understanding of metal-centered redox chemistry and the mechanism for the generation of ROS and their fate can provide insight into potential strategies for prevention and treatment of AD.

Several examples of redox chemistry in biological systems are known to be associated with di- or multi-nuclear "Type-3" Cu oxidases,[6] which might be related to the redox activity of Cu^{II}-Aβ.[1–4] A number of chemical model systems targeting Type-3 copper centers have successfully been demonstrated to contain highly active isoelectronic copper-dioxygen species (i.e. Cu^{II}_2-μ-η^1:η^1-peroxo, Cu^{II}_2-μ-η^2:η^2-peroxo, and Cu^{III}_2-bis-μ-oxo) responsible for copper-dependent oxidation and hydroxylation reactions.[6–9] Despite the extensive modeling studies, peptide mimics of these enzymes have apparently been excluded from the studies. Cu^{II}-Aβ seems to fill the gap since it is a natural-occurring Cu-peptide complex demonstrated to exhibit oxygen-associated redox chemistry,[1–4] although details about its oxygen binding and activation mechanisms is lacking. I present herein results which bring together two distinct fields of research, AD and Type-3 copper centers. The results elucidate that the Cu^{II} complex ($CuA\beta_{1\text{-}20}$) of the icosapeptidyl metal-binding domain of Aβ ($DAEFR^5\,HDSGY^{10}\,EVHHN^{15}\,KLVFF^{20}$) exhibits metal-centered redox chemistry consistent with the mechanisms of the Type-3 copper enzymes phenol monooxygenase (e.g., tyrosinase) and catechol oxidase.

II. EXPERIMENTAL

Phenol Monooxygenase assay: Phenol hydroxylation and oxidation and catechol oxidation were performed as previously reported[10] with minor changes to fit current studies. Same molar concentrations of phenol or catechol and 3-methyl-2-benzothiazolinone hydrazone (MBTH, which serves as an *ortho*-quinone indicator) were mixed in 100 mM HEPES at pH 7.00 in the presence of 5.0 μM (phenol hydroxylation/oxidation) or 0.50 μM $CuA\beta_{1\text{-}20}$ (catechol oxidation). The red-adduct of the *ortho*-quinone product was monitored at 500 nm (ε = 32,500 $M^{-1}cm^{-1}$; cf. Figure 3.1) Auto-oxidation of phenol and catechol were determined under the same conditions without $CuA\beta_{1\text{-}20}$. The 1-20 fragment of Aβ was synthesized at the Peptide Center of the University of South Florida. The identity of the peptide has been confirmed with a Bruker MALDI-TOF mass spectrometer.

The rates were determined on a Varian CARY50 spectrophotometer equipped with a temperature controller. The rate law for pre-equilibrium kinetics (Eq. 1), which Cu^{II}-Aβ follows, is shown in Eq. 2, where k_{cat} and K'_{app} are the first-order rate constant and virtual dissociation constant, respectively, S is the substrate and $v_{background}$ is the auto-oxidation rate.

$$Cu^{II}\text{-}A\beta + S \underset{k_{-1}}{\overset{k_1}{\rightleftharpoons}} A\beta\text{-}Cu^{II}\text{-}S \xrightarrow{k_{cat}} Cu^{II}\text{-}A\beta + Prod. \qquad (1)$$

$$v = v_{background} + \frac{k_{cat}[CuA\beta][S]}{K'_{app} + [S]} \qquad (2)$$

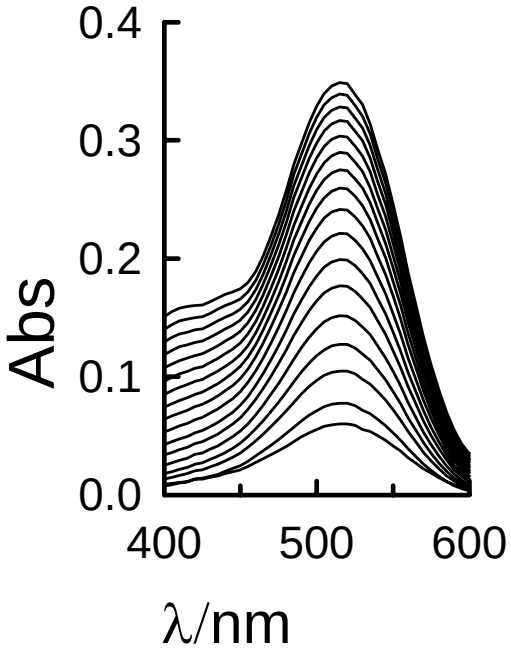

Figure 3.1. The production of *o*-quinone from phenol in the absence of H_2O_2 is monitored by the increase in the absorption due to its adduct with MBTH.

The Hill equation can serve as a general model for cooperativity as reflected by the Hill coefficient θ which deviates from one in the presence of cooperativity (Eq. 3), wherein K_x is the intrinsic dissociation constant.

$$\frac{V_o}{V_{\max}} = \frac{[\text{CuA}\beta]^{\theta}}{K_x + [\text{CuA}\beta]^{\theta}} \tag{3}$$

In case of a bi-substrate catalysis, such as phenol hydroxylation/oxidation and catechol oxidation in the presence of H_2O_2, both substrates can interact with the metal center independently. The data are fitted to the Hanes plot (Eq. 4) to yield true values of substrate dissociation constants *K'*.[19]

$$\frac{[S]}{v_0} = \frac{\left(1 + K'_{\alpha} / [H_2O_2]\right)}{V_{\max}}[S] + \frac{K'}{V_{\max}}\left(1 + \frac{K_i}{[H_2O_2]}\right) \tag{4}$$

III. RESULTS AND DISCUSSION

Catechol Oxidase activity: The metal-centered redox chemistry of $\text{CuA}\beta_{1\text{-}20}$ was probed using catechol and the much more inert phenol as substrates.[10] The oxidation of catechol under aerobic conditions reaches a plateau at low-mM concentrations (Fig. 3.2). This saturation profile fits nicely to pre-equilibrium kinetics (Eqs. 1 and 2), affording k_{cat} = 0.154 s^{-1}, K'_{app} = 0.35 mM and a significant second-order rate constant k_{cat}/K'_{app} = 440 M^{-1} s^{-1} (● Fig. 3.2). Since the formation of quinone from catechol is a two-electron oxidative process, the reaction is expected to follow the two-electron dinuclear reaction pathway for catechol oxidase,[11] wherein the binding of catechol to the active-site di-Cu^{II}

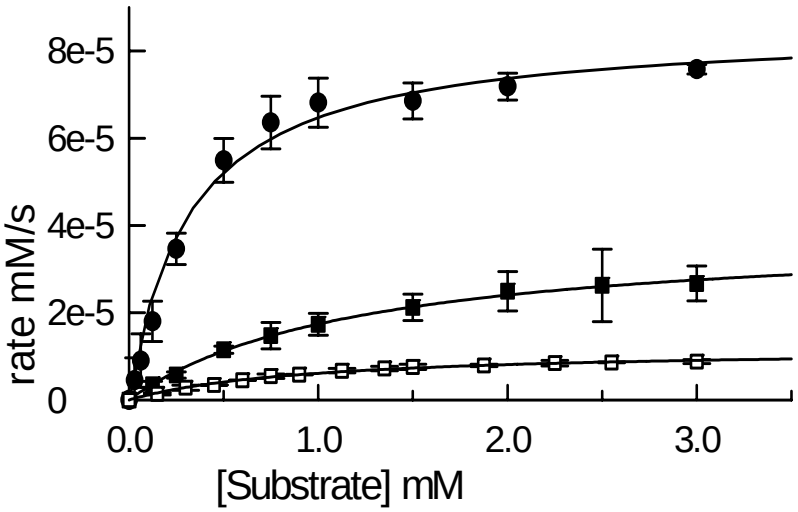

Figure 3.2. Saturation profile for the oxidation of phenol (solid square), deuterated phenol (square), and catechol (solid circle) in the absence of H_2O_2.

center results in the reduction of the center to yield di-Cu^{I} with concomitant production of *o*-quinone. The reduced di-Cu^{I} center can bind dioxygen to afford the active peroxo-bridged di-Cu^{II} center, which can further oxidize a subsequently bound substrate. H_2O_2 can also be generated in this reaction pathway from the peroxo-bridged di-Cu^{II} center in the presence of a reducing agent, such as the substrate itself. This H_2O_2 production pathway under reduction conditions is consistent with previous observations in AD studies.[3] This catechol oxidase-like mechanism has also been observed in kinetic studies in several chemical model systems[12] and in polyphenol oxidation by $CuA\beta_{1\text{-}20}$.[13] It is noteworthy that recent density functional theory (DFT) results reported mixed valence Cu^{II}-Cu^{I} transition states,[14] corroborating with the reduction pathway for the Cu center.

Zn^{2+} dilution: I show in Chapter II that the Cu^{II}:$A\beta_{1\text{-}20}$ stoichiometry to be in 1:1 ratio for oxidative activity with three N_ε-coordinated imidazole histidine rings as metal-binding ligands.[13] Since activity is an excellent probe for determining stoichiometry, gradual replacement of Cu^{II} in $CuA\beta_{1\text{-}20}$ with redox-inactive Zn^{II} can serve as a practical method for addressing the nature of the metallo-active center by virtually "silencing" the active sites through the dilution with Zn^{II}. A linear correlation between the activity and the extent of of Cu^{II} in the Zn^{II} dilution should be observed for simple 1:1 metal binding if there is no cooperativity and/or interactions between the active site Cu^{II} from different Aβ strands. Conversely, a sigmoidal activity profile was observed as a function of mole fraction of Cu^{II} in $A\beta_{1\text{-}20}$ toward the oxidation of the catechol derivative 3,5-di-*tert*-butyl catechol (DTC, $k_{cat} = 0.411\ s^{-1}$ and $K'_{app} = 0.781$ mM) which can be nicely fitted to the Hill equation (Eq. 3) with a Hill coefficient θ of 2.40 and $r^2 = 0.99$ (Figure 3.3A, solid

trace). The data clearly cannot be fitted well to a quadratic equation for 1:1 non-cooperative binding mode ($r^2 = 0.91$; dashed trace, Figure 3.3A). These results imply a possible presence of a cooperative dinuclear active Cu^{II} center during the catalytic oxidation of catechol by $CuA\beta_{1\text{-}20}$, consistent with the catalytic cycle of catechol oxidase.[11]

Effect of H_2O_2: The presence of the ROS H_2O_2 (25 mM) significantly enhances the turnover and catalytic efficiency of $CuA\beta_{1\text{-}20}$ toward catechol oxidation (Figure 3.4), yielding $k_{cat} = 0.531\ s^{-1}$ and $K'_{app} = 0.342$ mM and a significant second-order rate constant $k_{cat}/K' = 1.51 \times 10^3\ M^{-1}s^{-1}$ from the Hanes plot (to give K'; Eq. 4, Figure 3.5A)[15] for a random bi-substrate reaction, wherein the bindings of the two substrates H_2O_2 and catechol are independent of each other. It is worth noting that the second-order rate constant for catechol oxidation is only about 20 times lower than that of the catechol oxidase from gypsywort.[16] This pathway is consistent with the "peroxide shunt" in the action of catechol oxidase in the presence of H_2O_2, wherein a Cu^{II}_2-μ-η^2:η^2-peroxo intermediate is proposed to be the active species (cf. Fig. 2.7 A-D).[6] The oxidation of catechol to form *o*-quinone in the absence and presence of H_2O_2 exhibits remarkable 3.25×10^5 and 1.12×10^6 folds, respectively, rate acceleration in terms of the first-order rate constant k_{cat} compared to that of aerobic auto-oxidation of catechol without $CuA\beta_{1\text{-}20}$ determined to be $k_o = 4.74 \times 10^{-7}\ s^{-1}$.

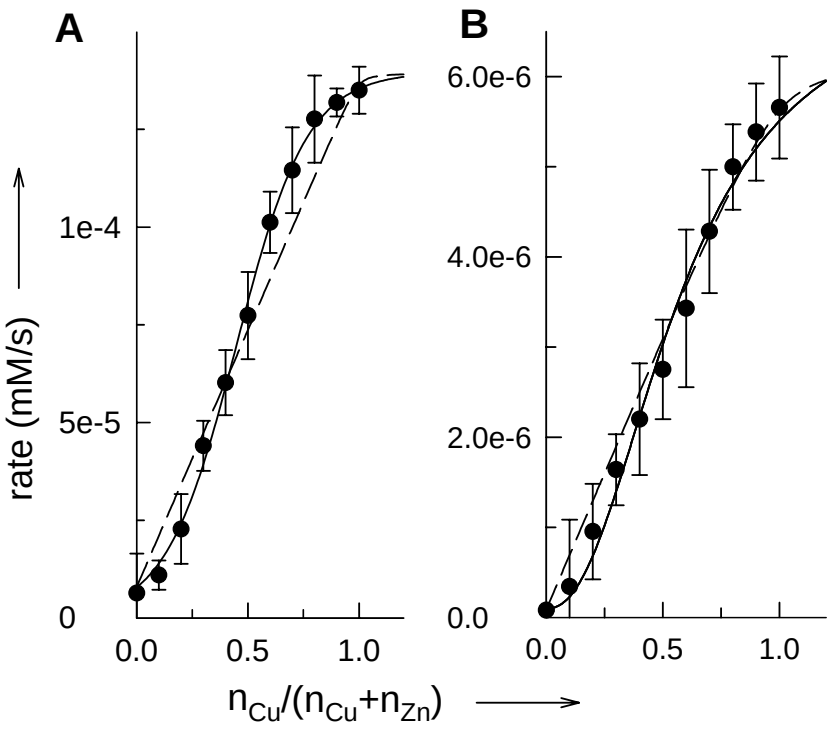

Figure 3.3. Oxidative activity of $CuA\beta_{1\text{-}20}$ toward the oxidation of DTC (**A**) and phenol (**B**) in the absence of H_2O_2 as a function of Cu^{II} mole fraction with a constant $Cu^{II} + Zn^{II}$ at pH 7.0 and 25 °C. The solid traces are fittings to the Hill equation and the dotted traces are fittings to a quadratic binding pattern with metal:ligand = 1:1.

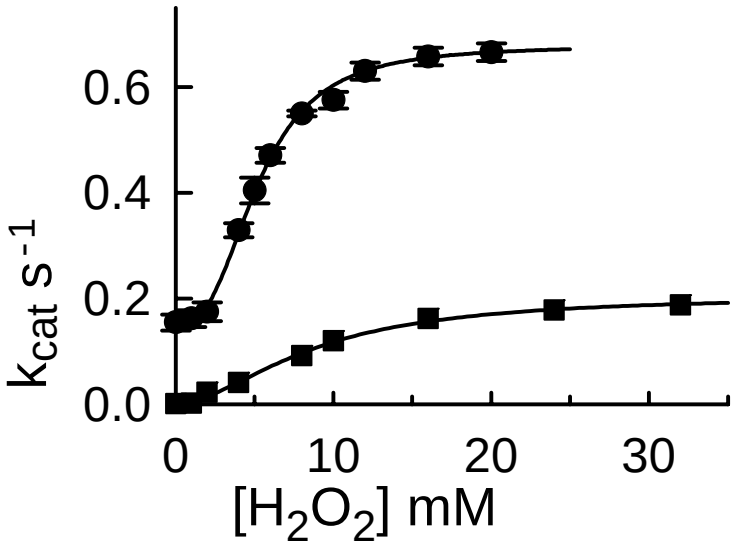

Figure 3.4. . The effect of H_2O_2 on the first order rate constant k_{cat} toward the oxidation of phenol (solid square) and catechol (solid circle).

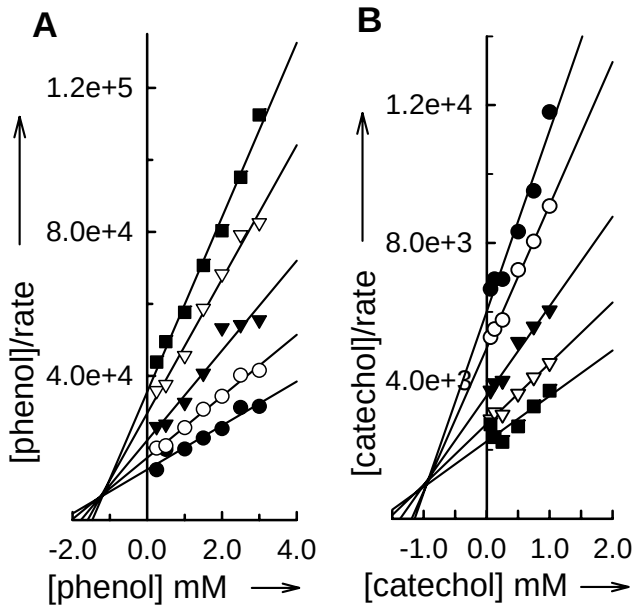

Figure 3.5. Hanes plot analysis of kinetic data from Figure 3.4.

Phenol hydroxylation: Owing to their inertness, metal-centered hydroxylation of phenol and derivatives, particularly polychlorophenols, poses some challenging tasks in chemical synthesis and ensvironmental detoxification and remediation[17] and may provide further insight into the action of those metalloenzymes for arene monooxygenation.[8,18] In addition to catechol oxidation described above, phenol was observed to be hydroxylated and oxidized by $CuA\beta_{1\text{-}20}$ in the presence of saturating amount of H_2O_2 (> 50.0 mM), wherein the formation of *o*-quinone exhibits rate constants of $k_{cat} = 0.213\ s^{-1}$ and $K'_{app} =$ 1.31 mM, and $k_{cat}/K' = 457\ M^{-1}s^{-1}$ from the Hanes plot (Figs. 3.1and 3.2). This result represents a remarkable rate acceleration of 4.6×10^6 folds for the ydroxylation/oxidation of phenol to form *o*-quinone in terms of k_{cat} compared to that of aerobic auto-oxidation of phenol (measured to be $k_o = 4.6 \times 10^{-8}\ s^{-1}$). This reaction is expected to take place following a similar dinuclear mechanism as in the action of the di-Cu enzyme tyrosinase toward hydroxylation and oxidation of tyrosine, wherein the active center is believed to contain dinuclear $\mu\text{-}\eta^2\text{:}\eta^2$-peroxo-$Cu^{II}_2$ on the basis of spectroscopic studies.[8,14]

Cooperativity for the oxidation of both catechol and phenol in terms of k_{cat} is observed upon titration of H_2O_2 as reflected in the sigmoidal activity profile with respect to H_2O_2 (Figure 3.4). The data from the oxidation of catechol and phenol by H_2O_2 fit nicely to the Hill equation (Eq. 3), yielding Hill coefficients $\theta = 2.23$ and 1.78, respectively. Moreover, fitting of the rates to a random bi-substrate reaction mechanism yields corrected *K'* values and a cooperativity index based on the ratio K'_{app}/K' (Fig. 3.5 B), wherein a ratio of 1.70 for H_2O_2 in both phenol and catechol oxidations and 2.07 and

2.10 for phenol and catechol, respectively, also suggest a small cooperativity and their independent binding to the active center.

Of particular interest is the observation of scarcely reported[19] Cu^{II}-centered hydroxylation and oxidation of phenol *aerobically without* H_2O_2. The production of *o*-quinone from phenol catalyzed by $CuA\beta_{1\text{-}20}$ follows pre-equilibrium kinetics, yielding $k_{cat} = 3.90 \times 10^{-3}$ s^{-1} and $K'_{app} = 1.23$ mM (Figure 3.2) which represents a first-order rate acceleration of 8.67×10^4 folds with respect to aerobic auto-oxidation of phenol. The k_{cat} value is lower than that for catechol oxidation, indicating that the hydroxylation step here must be the rate-limiting step. Otherwise, these two reactions would have similar k_{cat} values attributed to the oxidation of a bound catechol upon hydroxylation of a bound phenol. Moreover, the use of deuterated phenol as substrate shows significant kinetic isotope effect (KIE), wherein k_{cat} values of 1.12×10^{-3} and 0.0442 s^{-1} are obtained in the absence (□ Fig. 3.2) and presence of 100 mM H_2O_2 which represent KIE of 3.46 and 4.77, respectively. The results indicate that hydroxylation and breakage of the *o*-C–H bond of phenol is the rate-limiting step, which is followed by a faster step to form *o*-quinone. The different KIE values for phenol hydroxylation in the presence and absence of H_2O_2 suggest that the rate-determining step in these two cases may be different and/or possibly involve additional pathways. The K'_{app} values are not significantly different between phenol and deuterated phenol (1.31 and 1.23 mM for the latter in the presence and absence of H_2O_2, respectively), suggesting that k_{cat} does not significantly contribute to the magnitude of K'_{app} and that they may have a similar binding mode. The mechanistic reasoning (Figure 3.6) for the conversion of phenol to *o*-quinone may be

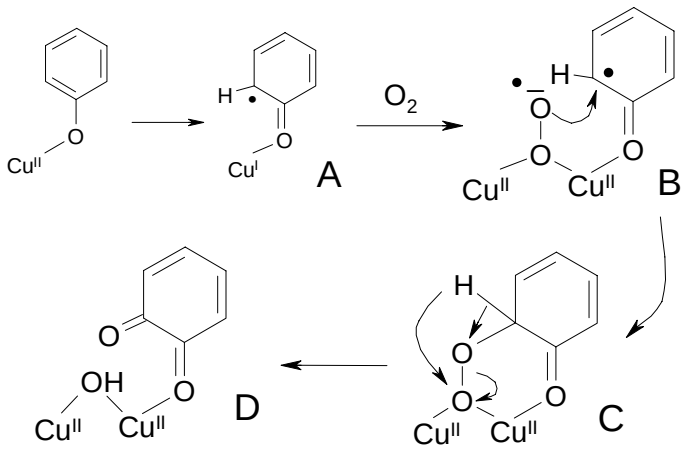

Figure 3.6. Proposed mechanism for aerobic hydroxylation and oxidation of phenol in the absence of H_2O_2, wherein the binding of phenol and reduction of the metal center is a key step (**A**). The binding of dioxygen and formation of superoxide (**B**) is proposed to be assisted by a dinuclear center.

attributed to that the $Cu^{II/I}$ redox equilibrium can be achieved upon phenol binding, followed by electron transfer to afford Cu^{I} and phenol radical which was suggested to be stabilized through resonance structure with the free radical situated at the *ortho* and *para* positions[19a] (step **A**). This intermediate is then attacked by dioxygen followed by electron transfer to possibly form a Cu^{II}-superoxide center which may be further stabilized by a dinuclear center (step **B**). The free radical was proposed previously to be attached directly by triplet dioxygen,[19a] which however is not symmetrically favorable. Coupling between the bound phenol radical and superoxide radical at an *ortho* position can then be expected to be a favorable step (step **C**), which is followed by transfer of electrons and an oxygen atom to afford the final quinone product (step **D**). An involvement of a dinuclear center for the catalysis is possible as discussed below. Since the hydroxylation and oxidation of phenol is a multi-electron transfer process, the involvement of two metal centers is suspected. An activity profile is obtained for phenol oxidation similar to the case of the "Zn^{II} dilution" experiment for catechol oxidation. The data can be fitted equally well to the Hill equation (Eq. 3) to afford θ value of 1.80 (r^2 = 0.98) and a quadratic equation for single metal-binding (r^2 = 0.98), consisting with either a mononuclear oxidation[19] or a cooperative mechanism involving a dinuclear center,[14] or a combination of both pathways.

DCC optical titration: To monitor substrate binding, a slow substrate 4,5-dichlorocatechol (DCC which is approximately 200 times slower in terms of k_{cat} than catechol) was titrated to 0.2 mM CuAβ_{1-20} in the presence or absence of 100 mM H_2O_2 and the electronic spectrum collected at 25 °C and pH 7.0 (Figure 3.4). Similar spectra

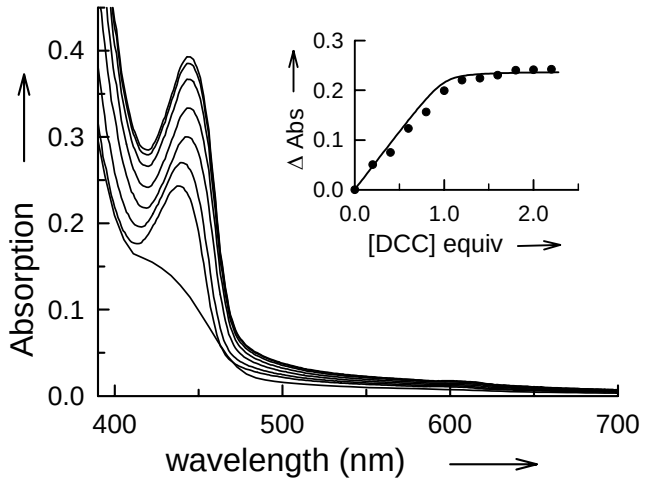

Figure 3.7. Optical titration of DCC to 0.2 mM CuAβ in the presence of 100.0 mM H_2O_2 in 100 mM HEPES at pH 7.0. Analogous spectra were obtained in the absence of H_2O_2. The inset shows the change in absorbance at 437 nm as a function of equivalents of DCC added, consisting with the formation of a 1:1 adduct.

were obtained, indicating that H_2O_2 was not involved in DCC binding to $Cu^{II}A\beta$ under the experimental conditions. The absorption at 437 nm increases upon addition of DCC and reaches saturation at >1.2 equivalents of its addition, which can be nicely fitted to single-substrate binding mode to yield a dissociation constant of 0.24 mM. The result provides a direct evidence for catechol binding to the metal center, consistent with the observation in a chemical model[20] and the mechanism proposed above.

IV. CONCLUDING REMARKS

In conclusion, we have established the catalytic activities of $CuA\beta_{1-20}$ toward the *relatively inactive* (according to their k_o values) catechol and phenol in the presence and absence of H_2O_2 in aqueous solutions near physiological conditions. The reaction patterns are consistent with the mechanisms carried out by Type-3 copper centers as observed in catechol oxidase and tyrosinase and their dinuclear model systems.[8,18] These results are unique thus far in metal-centered redox chemistry related to Alzheimer's disease, and expected to offer further insight into the neuropathology of this disease since it has been suspected to connect with, in addition to many other factors, the oxidation of mono- and diphenol-containing neurotransmitters such as dopamine, epinephrine, norepinephrine, and serotonin.[21,22] Furthermore, the connection of this highly reactive Cu-oxygen chemistry with Alzheimer's disease can better define the role of metallo-Aβ in the neuropathology of this disease and possibly lead to different treatment strategies toward this disease.

V. LIST OF REFERENCES

1) A. I. Bush, The metallobiology of Alzheimer's disease *Trends Neurosci.* (2003), 26, 207-214.

2) B. Tseng, M. Kitazawa, F.M. LaFerla, Amyloid β -peptide: The inside story. *Curr. Alzheimer Res.* (2004), 1, 231-239

3) X. Huang, C. S. Atwood, M. A. Hartshorn, G. Multhaup, L. E. Goldstein, R. C. Scarpa, M. P. Cuajungco, D. N. Gray, J. Lim, R. D. Moir, R. E. Tanzi, A. I. Bush, Characterization of copper interactions with Alzheimer amyloid β peptides: identification of an attomolar-affinity copper binding site on amyloid β 1-42. *Biochemistry* (1999), 38, 7609-7616.

4) C. Opazo, X. Huang, R.A. Cherny, R.D. Moir, A. E. Roher, A. R. White, R. Cappai, C. L. Masters, R. E. Tanzi, N.C. Inestrosa, A. I. Bush, Metalloenzyme-like activity of Alzheimer's disease β -amyloid. *J. Biol. Chem*. (2002), 277, 40302-40308.

5) K. G. Manton, S. Volovik, A. Kulminski, ROS effects on neurodegeneration in Alzheimer's disease and related disorders: On environmental stresses of ionizing radiation. *Curr. Alzheimer Res*. (2004), 1, 277-293.

6) T. E. Machonkin, U. M. Sundaram, E. I. Solomon, Multicopper Oxidases and Oxygenases.*Chem. Rev.* (1996), 96, 2563-2605.

7) W. B. Tolman, L. Que Jr., Bis(μ -oxo)dimetal "diamond" cores in copper and iron complexes relevant to biocatalysis. *Angew. Chem. Int. Ed.* (2002), 41, 1114-1137.

8) a)E. A. Lewis, W. B. Tolman, Reactivity of Dioxygen-Copper Systems. *Chem. Rev.* (2004), 104, 1047-1076; b) W. B. Tolman, Making and Breaking the Dioxygen O-O

Bond: New Insights from Studies of Synthetic Copper Complexes *Acc. Chem. Res.* (1997), *30*, 227–237.

9) L. M. Mirica, X. Ottenwaelder, D. P. Stack, Structure and Spectroscopy of Copper-Dioxygen Complexes. *Chem. Rev.* (2004), 104, 1013-1045.

10) S. G. Srivatsan, P. Nigamb, M. S. Raob, S. Verma, Phenol oxidation by copper-metallated 9-allyladenine-DVB polymer: reaction catalysis and polymer recycling. *Appl. Catal. A: General* (2001), 209, 327–334.

11) A. Rompel, H. Fischer, D. Meiwes, K. Büldt-Karentzopoulos, R. Dillinger, F. Tuczek, H. Witzel, B. Krebs, Structure and magnetism of novel tetranuclear μ-4-oxo-bridged copper(II) complexes. *J. Biol. Inorg. Chem.* (1999), 4, 56–63.

12) a) C. T. Yang, M. Vetrichelvan, X. Yang, B. Moubaraki, K. S. Murray, J. J. Vittal, Syntheses, structural properties and catecholase activity of copper(II) complexes with reduced Schiff base N-(2-hydroxybenzyl)-amino acids. *J. Chem. Soc. Dalton Trans* (2004), 113–121; b) A. Granata, E. Monzani, L. Casella, Mechanistic insight into the catechol oxidase activity by a biomimetic dinuclear copper complex. *J. Biol. Inorg. Chem.* (2004), 9, 903-913; c) R .Than, A. A. Feldmann, B. Krebs, Structural and functional studies on model compounds of purple acid phosphatases and catechol oxidases. *Coord. Chem. Rev.* (1999), 182, 211–241.

13) G. F. Z da Silva, W. T. Tay, L. -J. Ming, Catechol Oxidase-like Oxidation Chemistry of the 1–20 and 1–16 Fragments of Alzheimer's Disease-related β-Amyloid Peptide: Their Structure-Activity Correlation and the Fate of Hydrogen Peroxide *J. Biol. Chem*. (2005), 280, 16601-16609.

14) P. E. M. Siegbahn, The catalytic cycle of tyrosinase: peroxide attack on the phenolate ring followed by O-O bond cleavage. *J. Biol. Inorg. Chem.* (2003), 8, 567-576.

15) V. Leskovac, *Comprehensive Enzyme Kinetics*, Kluwer/Plenum, Boston, 2002, p.119.

16) A. Rompel, H. Fischer, D. Meiwes, K. Buëldt-Karentzopoulos, A. Magrini, C. Eicken, C. Gerdemann, B. Krebs, Substrate specificity of catechol oxidase from Lycopus europaeus and characterization of the bioproducts of enzymic caffeic acid oxidation. *FEBS Lett.* (1999), 445, 103–110.

17) M. Maumy, P. Capdevielle, Copper-catalyzed ortho-oxidation of phenols by dioxygen (tyrosinase mimics) do yields catechols as primary products. *J. Mol. Catal., A: Chem.* (1996), 113, 159-166.

18) K. D. Karlin, S. Kaderli, A. D. Zuberbühler, Kinetics and Thermodynamics of Copper(I)/Dioxygen Interaction. *Acc. Chem. Res.* (1997), 30, 139-147.

19) a) K. -Q. Ling, Y. Lee, D. Macikenas, J. D. Protasiewicz, L. M. Sayre, Copper(II)-Mediated Autoxidation of tert-Butylresorcinols. *J. Org. Chem.* (2003), 68, 1358-1366; b) S. R. Starck, J. -Z. Deng, S. M. Hecht, Naturally Occurring Alkylresorcinols That Mediate DNA Damage and Inhibit Its Repair. *Biochemistry* (2000), 39, 2413-2419.

20) S. Torelli, C. Belle, S. Hamman, J. P. Pierre, Substrate Binding in Catechol Oxidase Activity: Biomimetic Approach. *Inorg. Chem.* (2002), 41, 3983-3989.

21) H. Umegaki, N. Tamaya, T. Shinkai, A. Iguchi, The metabolism of plasma glucose and catecholamines in Alzheimer's disease. *Gerontology* (2000), 35, 1373-1382.

22) W. Fu, H. Luo, S. Parthasarathy, M. P. Mattson, Catecholamines potentiate amyloid β -peptide neurotoxicity: involvement of oxidative stress, mitochondrial dysfunction, and perturbed calcium homeostasis. *Neurobiol. Disease* (1998), 5, 229-243.

CHAPTER IV. METALLO-ROS IN ALZHEIMER'S DISEASE: METAL-CENTERED OXIDATION OF NEUROTRANSMITTERS BY Cu^{2+}-β-AMYLOID PROVIDES AN ALTERNATIVE PERSPECTIVE FOR THE NEUROPATHOLOGY OF ALZHEIMER'S DISEASE[‡]

I. INTRODUCTION

The generation of reactive oxygen species (ROS), including superoxide, peroxide, and free radicals, is associated with normal redox metabolic pathways as side-tracks which can be regulated through the action of superoxide dismutase, catalase, and some reducing agents under homeostasis.[1,2] However, long-term effects of such oxidative chemical imbalance in normal and disease states can be expected. ROS are often considered the culprits responsible for the devastating effects of oxidative stress,[3] concerning cancer, aging, heart diseases, arthritis, diabetes, and the etiology of neurodegenerative disorders such as Parkinson's disease and Alzheimer's disease (AD).[4] AD affects primarily the elderly which causes considerable distress of the patients and emotional sufferings of their families and close friends. One mechanism

[‡] This work has been published: G.F.Z. da Silva, Ming L.-J, "Metallo-ROS" in Alzheimer's Disease: Metal-Centered Oxidation of Neurotransmitters by CuII-β-Amyloid Provides an Alternative Perspective for the Neuropathology of Alzheimer's Disease. *Angew. Chem. Int. Ed.* (2007), 46, in press.

proposed for the neurodegeneration in AD focuses on amyloid-β peptides (Aβ) and their metal complexes through formation of plaques and fibrils and generation of the ROS H_2O_2 and free-radicals.[5–9]

Aggregation of Aβ of 40 or 42 amino acids (DAEFR HDSGY[10] EVHHQ KLVFF[20] AEDVG SNKGA[30] IIGLM VGGVV[40] IA) in the brain is the hallmark in AD neuropathology induced by metal binding[10–12] and is usually found as metal-containing plaques and insoluble fibrils. Similar pathological effects are also found in transgenic mouse models with human Aβ.[13,14] Moreover, soluble fragments of Aβ can be generated *in vivo* by insulin degrading enzyme as well as α and β-secretases.[15,16] Nevertheless, the cause or effect connection of the metallo-Aβ plaques with AD is still under debate.[17–19] Despite immense endeavor in Aβ research, the potential risk of metal-centered oxidative catalyses by metallo-Aβ has been overlooked.[20] The Cu^{II} complexes of metal-binding domains of Aβ (CuAβ) have recently been demonstrated to exhibit metal-centered oxidative catalysis, consistent with Type-3 copper oxidases.[21,22] To verify the bio-relevance of this metal-centered catalysis, we have determined the oxidation of several catecholamine and indoleamine neurotransmitters catalyzed by $CuA\beta_{1–40}$ and two metal-binding N-terminal fragments $CuA\beta_{1–16}$ and $CuA\beta_{1–20}$ under various biomimetic conditions. The studies described herein are expected to provide chemical basis for better understanding the etiology of AD.

II. EXPERIMENTAL

The peptides $A\beta_{1–16(20)}$ were synthesized at the Peptide Center of the University of South Florida, and confirmed with a Bruker MALDI-TOF mass spectrometer. $A\beta_{1–40}$ was purchased from Biopeptide Co., LLC (San Diego, CA). The Cu^{II} complex

of $A\beta_{1-40}$ was prepared according to literature procedures[23] and concentration determined with a standard BCA assay. The CuAβ stock solutions were quickly aliquoted to prevent concentration deviations caused by aggregation.

Kinetic assays: Kinetic measurements were performed and analyzed as previously described [21,22] by the use of MBTH as a o-quinone indicator ($\varepsilon_{product}$ = 32,500 M^{-1} cm^{-1} for phenol and catechol[24] and 28,900, 27,200, and 27,500 $M^{-1}cm^{-1}$ for Dopa, dopamine, and epinephrine/norepinephrine, respectively,[25] and 35,200 $M^{-1}cm^{-1}$ for serotonin and 5-hydroxytriptophan). The data are analyzed with the bi-substrate Hanes plot for experiments in the presence of H_2O_2 to yield the apparent K_S and intrinsic K_{Si} dissociation constants for the neurotransmitters and H_2O_2.[37]

III. RESULTS AND DISCUSSION

Dopamine has been directly linked to the neurodegenerative Parkinson's disease.[26] Moreover, symptoms of Parkinson's disease have also been recognized in AD patients.[27] Thus, disturbance of dopamine metabolism may be closely associated with AD. Dopamine is effectively oxidized aerobically to dopaquinone by $CuA\beta_{1-40}$ at pH 7.0, reaching saturation at high dopamine concentrations (Fig. 4.1; Table 1) which is consistent with pre-equilibrium-like kinetics. There is an apparent cooperativity in the catalysis that is not usually expected in simple monomeric systems, which may be due to the tendency of the peptide to coagulate and/or the formation of a dinuclear center during catalysis. Fitting the results to the Hill equation gives kinetic constants $k_{cat} = 7.48 \times 10^{-4}$ s^{-1} and $k_{cat}/K' = 2.77$ M^{-1} s^{-1} and a Hill coefficient $\theta = 1.48$. This reaction shows 85-fold rate enhancement relative to

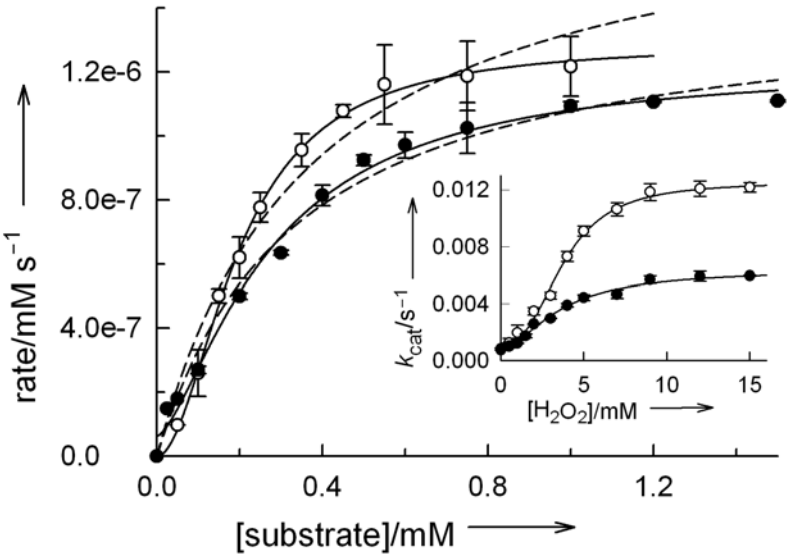

Figure 4.1. Oxidation of catechol (o) and dopamine (•) by 1.47 μM $CuA\beta_{1\text{-}40}$ in 100 mM HEPES at pH 7.0 and 25° C. Dashed traces are fittings to simple pre-equilibrium kinetics while the solid traces are the fitting to the Hill equation. The inset shows the effect of H_2O_2 on k_{cat} which also show the presence of cooperativity.

CuAβ	k_{cat} (10^{-3} s^{-1})	K' (mM)	k_{cat}/K'_1 ($M^{-1}s^{-1}$)	k_{rel}
1–40	0.748	0.27	2.77	85
1–20	11.6	0.90	12.9	1,320
1–16	28.0	0.31	90.3	3,180
1–40[b]	5.61	0.27	21	312
1–20[b]	99.0	0.52	190	5,530
1–16[b]	230	0.68	339	12,700

Table 2. Kinetic parameters for dopamine oxidation by Aβ[a] in 100 mM HEPES buffer at pH 7.0 and 25 °C. b in the presence of 20 mM H_2O_2

auto-oxidation of dopamine. The shorter CuAβ_{1-20} and CuAβ_{1-16} do not exhibit the apparent cooperativity and exhibit 16 and 37-fold, respectively, higher activity than CuAβ_{1-40} toward dopamine oxidation in terms of k_{cat}. Catechol oxidation shows the same catalytic trend (Fig. 4.1; Table 1), with CuAβ_{1-40} showing cooperativity (θ = 2.7) and CuAβ_{1-16} exhibiting the highest activity. The results herein indicate that the soluble CuAβ fragments may be more severe in causing oxidative stress in the brain of AD patients than the coagulation-prone CuAβ_{1-40}. Recent studies also suggested pathological significance of soluble forms of Aβ.[28]

Collectively termed catecholamines, dopamine, epinephrine, norepinephrine, and Dopa are catechol-containing neurotransmitters (whereas serotonin and its precursor 5-hydroxytryptophan are indole-containing) which are involved in cognitive, behavioral, physical, physiological, and psychological functions.[29] Oxidation of these molecules may cause severe alteration in bioactivity, eventually leading to neuronal death.[30] Metabolic malfunctions of neurotransmitters are known phenomena in the physiology of AD[31,32] and have also been suggested to be related to the neuropathology of this disease.[31–34] However, a chemical mechanism for the neurotransmitter malfunction in AD is still unknown. These catecholamine neurotransmitters are found to be effectively oxidized aerobically to their respective *o*-quinone products by CuAβ_{1-20} (Fig. 4.2, Table 1). Herein, CuAβ_{1-20} is shown to significantly accelerate aerobic oxidation rate of these neurotransmitters by 333–2,420 times in terms of k_{cat} relative to auto-oxidation rate constant k_o.

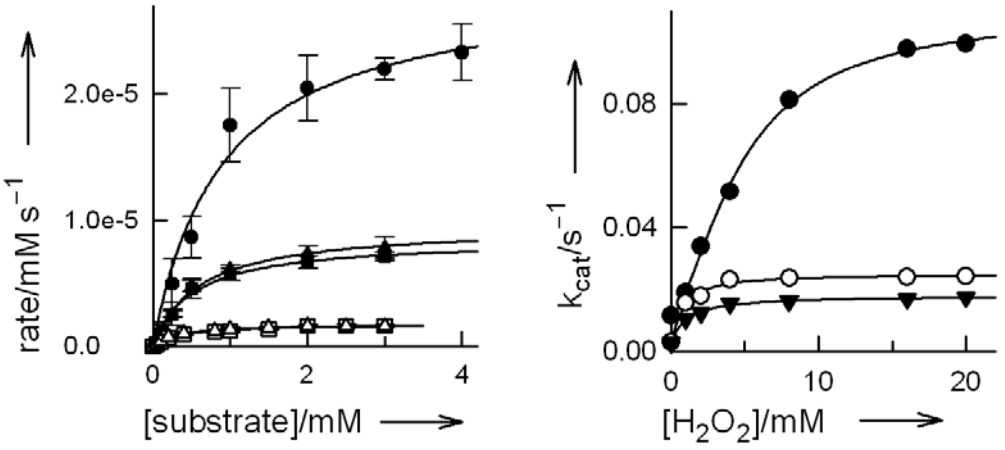

Figure 4.2. a) Catecholamine oxidation by 2.5 μM CuA$\beta_{1\text{-}20}$ in the absence of H_2O_2 toward dopamine (●), (+/–)epinephrine (▲) and (–)norepinephrine (■), L-DOPA (○) and D-DOPA (□). The solid lines are the best fit to an enzyme-like pre-equilibrium kinetics). b) The dependence of the first-order rate constant on H_2O_2 toward the oxidation of dopamine (●), (+/–)epinephrine (○), and (–) norepinephrine (▼).

Compared to that of catechol, the auto-oxidation rates of these neurotransmitters are faster by nearly 10 times in terms of k_o. However, their oxidation rates by CuAβ are ~130–980-fold slower than that of catechol, reflecting their higher resistance to oxidation by CuAβ by ~10^3–10^4-fold relative to catechol oxidation. The relatively higher stability against oxidative damage entitles these molecules better suited for the purpose of neurotransmission. Dopa shows a lower reactivity than other catecholamines, likely due to the inductive effect of the carboxyl group on the side chain. Chirality of these neurotransmitters does not appear to play a role in this oxidation chemistry (Table 2).

The ROS H_2O_2 has been commonly suggested to be a culprit causing the oxidative stress in AD.[4,6] However, this ROS alone at 50.0 mM does not significantly affect the oxidations of neurotransmitters (footnote b, Table 2). Conversely, oxidations of these neurotransmitters by CuAβ in the presence of >15 mM (>0.051%)[35] H_2O_2 under the same conditions exhibit significant rate enhancement (k_{rel}, Table 2; Fig. 4.3), e.g., 312-fold relative to auto-oxidation rate constant k_o for dopamine oxidation by CuAβ_{1-40} with k_{cat} = 0.0056 s^{-1} and k_{cat}/K' = 21 M^{-1} s^{-1}. The oxidation of dopamine is dependent on H_2O_2 and reaches a plateau at H_2O_2 > 15 mM with θ = 3.57 (Fig. 1, inset), which indicates that the ROS H_2O_2 can bind to CuAβ to afford a "metallo-ROS" in a cooperative manner. Oxidation of catechol without the side chain by Cu-Aβ_{1-40} exhibits a similar kinetic pattern (Fig. 4.1; Table 2), confirming the cooperative nature of this oxidative catalysis.

The results conclude that "metallo-ROS" is much more reactive than free ROS alone as far as H_2O_2 is concerned. Once again, the shorter CuA$\beta_{1-16(20)}$ fragments exhibit higher activity than CuAβ_{1-40} toward dopamine oxidation in the presence of

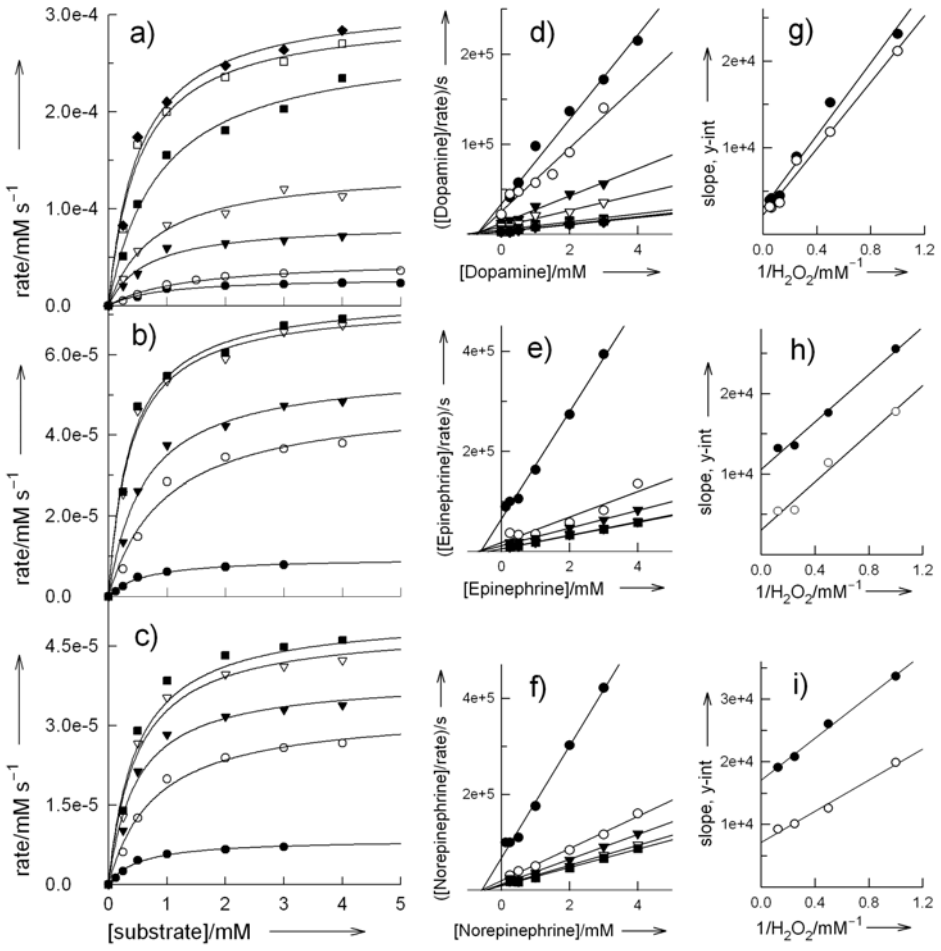

Figure 4.3. H_2O_2 effect on oxidation of dopamine (a), (+/–)epinephrine (b), and (–)norepinephrine (c) catalyzed by 3.15 μM CuA$\beta_{1\text{-}20}$ in the presence of H_2O_2 (from bottom, 0, 1.0, 2.0, 4.0, 8.0, 16.0, and 20.0 mM). (d–f) Hanes plot analysis of catecholamine oxidation in the presence of H_2O_2 (from plots a–c). The lines are the best fits to a bi-substrate mechanism (g–i) Secondary plots of the Hanes plots from d–f which reveal apparent and intrinsic dissociation constants *K*' values, by plotting of the slope (•) and y-intercept (o) from plots d–f as a function of 1/H_2O_2.

H_2O_2 (Table 1). This observation once again suggests pathological significance of soluble Aβ fragments in AD. Herein, $CuA\beta_{1\text{-}20}$ is able to significantly accelerate oxidation rates of catechol and catecholamine neurotransmitters by 1,350 to 2.24×10^5 times in terms of k_{cat} relative to k_o (Table 2). It is worth noting that k_{cat}/K' of 1,690 M^{-1} s^{-1} for catechol oxidation by $CuA\beta_{1-16}$ approaches enzyme-like catalytic efficiency which is 5.3% of the activity of the catechol oxidase (32,000 M^{-1} s^{-1}) from gypsywort (*Lycopus europaeus*).[36]

Since both H_2O_2 and the neurotransmitters can bind to the metal active-center, the data are analyzed with a two-substrate random-binding mechanism according to the Hanes equation (Fig. 4.3)[37] to afford the apparent and intrinsic dissociation constants K_S and $K_{i(S)}$ (0.34 and 0.23 for catechol and 0.52 and 0.22 for dopamine, respectively). The ratios of $K_S/K_{i(S)}$ are greater than one, indicating that the neurotransmitters and H_2O_2 are affecting the binding of each other in this bi-substrate reaction mechanism.[37,38]

Influence of micelles: $A\beta_{1-40}$ and fragments are found in various cellular environments, including soluble forms in the cytosol and insoluble forms as membrane-bound plaques. Herein, the detergent sodium dodecyl sulfate (SDS) is used to approximate the amphiphilic nature of cell membrane. Structures of short Aβ fragments in the presence of SDS differ considerably from that in the absence of this micelle-forming surfactant.[39] The activities of CuAβs in the presence of micelles may offer insight into the nature of the structure and activity of Aβ. The rate constant k_{cat} of $CuA\beta_{1-20}$ for the oxidation of dopamine is largely affected by the soluble form of SDS (4.5 times) and noticeably influenced (80%) by micelles with the critical micelle concentration (CMC) of SDS

Substrate	$k_{cat}(10^{-3}\ s^{-1})$	K' (mM)[a]	k_{cat}/K' ($M^{-1}s^{-1}$)	k_{rel}[b]	k_{cat} ($10^{-3}\ s^{-1}$) sat. H_2O_2	k_{cat}/K' ($M^{-1}s^{-1}$)[c] sat. H_2O_2	k'_{rel}[d] sat. H_2O_2
Catechol[e]	154	0.35	440	3.25×10^5	531	1,510	2.24×10^5
(by $A\beta_{1-16}$)	280	0.31	900	5.92×10^5	1,150	1,690	7.64×10^5
(by $A\beta_{1-40}$)[f]	0.87	0.19	4.6	1,850	11.2	28	1.96×10^4
dopamine	11.6	0.90	13	1,320	99	190	5,530
(by $A\beta_{1-16}$)	28	0.31	90	3,180	230	340	1.27×10^4
(by $A\beta_{1-40}$)[f]	0.75	0.27	2.8	85	5.61	11	312
(±) Epinephrine	3.1	0.60	5.2	2,420	24	34	9,420
(–) Epinephrine	2.9	0.61	4.8	2,270	22	54	8,630
(–) Norepi.	2.7	0.52	5.2	1,330	17	32	6,940
(+) Norepi.	2.8	0.57	4.9	1,380	18	39	7,350
(–) Dopa	1.1	0.34	3.2	333	9.11	27	1,360
(+) Dopa	1.2	0.32	3.8	364	9.03	28	1,350
Phenol[e]	3.9	1.23	3.2	8.67×10^4	213	170	4.16×10^6
(by $A\beta_{1-16}$)	6.4	0.59	11	1.41×10^5	340	58	6.64×10^6
(by $A\beta_{1-40}$)[f]	0.44	1.25	0.35	9.54×10^3	1.43	1.14	2.79×10^4
5-hydroxy-Trp	6.4	0.45	14	8.25×10^3	43.9	97.5	5.64×10^4
serotonin	6.7	1.47	4.5	7.75×10^3	30.4	67.6	3.28×10^4
(by $A\beta_{1-16}$)	26	0.63	41	3.03×10^4	250	380	2.69×10^5
(by $A\beta_{1-40}$)[f]	0.28	0.33	0.84	324	7.8	24.4	8.41×10^3

Table 3. Kinetic parameters for the oxidation of catecholamines to *o*-quinone by $A\beta_{1-20}$, except those indicated. Intrinsic dissociation constant for the CuAβ-S complex. b The background self-oxidation rate constant k_o is calculated based on the MBTH detection of *o*-quinone formation in the absence of CuAβ at 25 °C in 100.0 mM HEPES pH 7.0 under aerobic conditions.

around 8 mM (Fig. 4.4);[xl] whereas that of CuAβ_{1-40} is slightly influenced by soluble SDS (2-fold) and greatly affected by micellar SDS (8-fold).

Under our experimental conditions, SDS micelles do not influence the self-oxidation rates of neurotransmitters. The shortest CuAβ_{1-16} is only slightly affected (85% enhancement) in the presence of saturating amount of SDS and shows only 14% enhancement in correspondence with CMC. The results indicate that the plaque-forming CuAβ_{1-40} is expected to exhibit more significant oxidation chemistry when it is "solubilized" and incorporated into a hydrophobic environment; whereas the soluble CuAβ_{1-16} and CuAβ_{1-20} are already more powerful oxidation agents than CuAβ_{1-40} in aqueous environments (Table 1). The results seem to also corroborate the "opposing activities" proposal for neuroprotection via proteolysis and aggregation,[xli] wherein the highly active small A$\beta_{1-16(20)}$ fragments are supposed to be eliminated by the former process whereas the activity of Aβ_{1-40} is much decreased by the latter process by forming aggregates. The local concentrations of metallo-Aβ plaques can reach mM range,[4] which can cause significant oxidative damages of proximal areas on the brain. Consequently, the devastating metallo-ROS chemistry due to CuAβ_{1-40} and fragments in the brain of AD patients can have a widespread effect in different cellular environments, particularly in hydrophobic membranes that significantly enhance the metal-centered oxidative activities as demonstrated herein.

Influence by reducing agents: The NAD(P)$^+$/NAD(P)H ratios vary according to changes in metabolism and is species/tissue-dependent,[xlii] thus are expected to affect the redox property of CuAβ in vivo. Changes in the homeostatic levels in terms of NAD(P)$^+$/NAD(P)H may reflect the neurochemical status under oxidative stress.[xliv] Metabolic changes have been

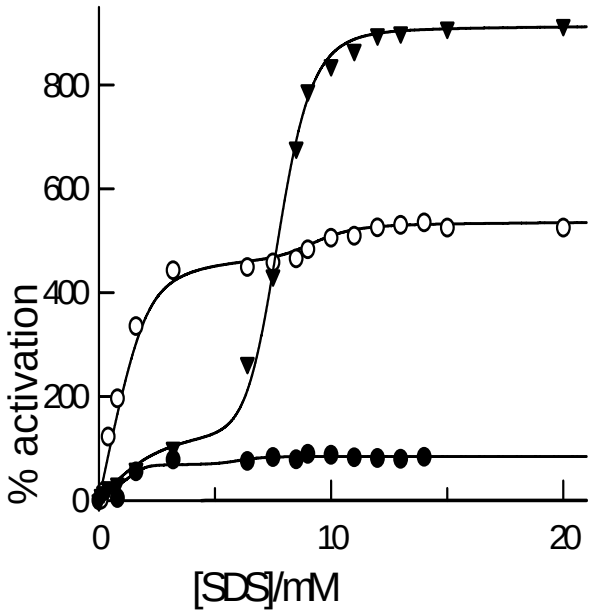

Figure 4.4. Effect of SDS on the oxidative activity of $CuA\beta_{1-16}$ (●), $CuA\beta_{1-20}$ (o), and $CuA\beta_{1-40}$ (▼) in 100.0 mM HEPES pH 7.0 and 25 °C. The data show influence of the activity by both the monomeric and the micellar forms of SDS with CMC of 8 mM.

noted to be associated with several age-associated diseases, including neurodegenerative diseases.[xliii] It has been previously reported that these ratios are managed according to spatial and temporal constraints in the brain under oxidative stress.[xliv] The oxidation activity of CuA$\beta_{1\text{-}20}$ is lowered by NAD(P)H. As the ratios of $NAD(P)^+$/NAD(P)H decrease, the activity in terms of k_{cat} toward dopamine oxidation decreases by 2.4 and 1.9 times, respectively (Fig. 4.5). Based on the proposed mechanism for catechol oxidation by Cu-A$\beta_{1\text{–}20}$,[21] the inhibitory effect of NAD(P)H is due to shifting in equilibrium toward H_2O_2 generation under reducing conditions.[21,xlii] The more pronounced inhibition caused by NADPH as compared to NADH might be attributed to the phosphate group in NADPH. Indeed, phosphate has been observed to be a competitive inhibitor toward the oxidation of dopamine, showing K_i = 4.7 mM (Fig. 4.6). The ratio of free NAD^+/NADH has been under debate which nevertheless has recently been suggested[xlv] to be around 600, consistent with the value based on potentiometric measurement.[xlvi] The relatively smaller availability of free form of NADH suggests that this biological reducing agent may not significantly influence the metal-centered oxidative catalysis of CuAβ under physiological conditions.

To reveal the mechanism of the full-length A$\beta_{1\text{–}40}$, the slow substrate 4,5-dichlorocatechol (DCC) was titrated into a solution of CuA$\beta_{1\text{–}40}$. The observation of a charge transfer transition at 438 nm (Fig. 4.7) is indicative of DCC binding to the Cu^{II} center (with an affinity constant of 6.4×10^5 M^{-1}, dotted trace; Fig. 4.6) analogous to its binding to the soluble CuA$\beta_{1\text{–}20}$.[22] Cooperativity is apparent in DCC binding (solid

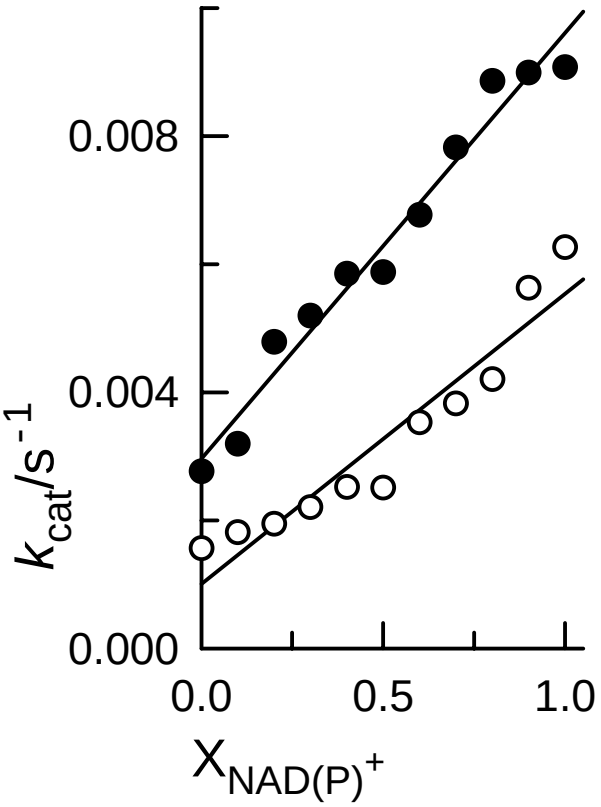

Figure 4.5. Influence of $NAD(P)^+$ (o) and NAD^+ (●) on the oxidative activity of $CuA\beta_{1-20}$ toward dopamine oxidation with a fixed total concentration of $NAD(P)^+$ + NAD(P)H = 10.0 mM.

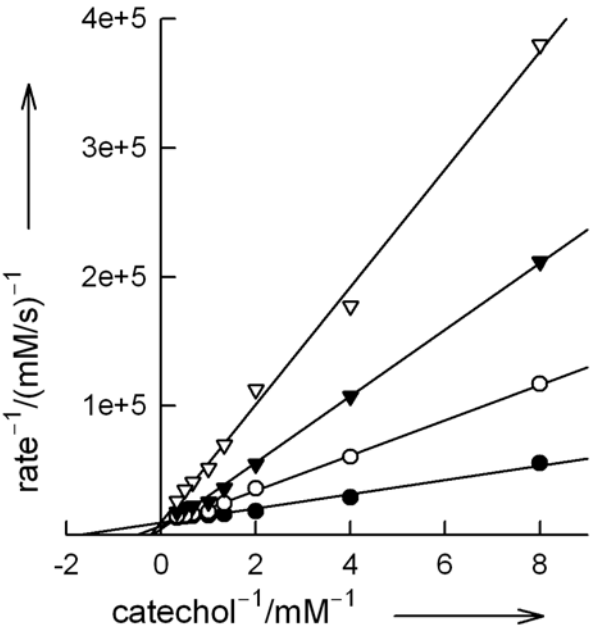

Figure 4.6. Phosphate inhibition toward catechol oxidation by CuAβ_{1-20} in 100 mM HEPES at pH. 7.0. Phosphate concentrations are 0, 10, 20, and 40 mM (from bottom).

trace; Fig. 4.7), probably due to the coagulation nature of $A\beta_{1-40}$. The stoichiometry of DCC:$CuA\beta_{1-40}$ = 1:2 verifies the dinuclear nature of the catalysis. The activation profile during Cu^{II} titration to $A\beta_{1-40}$ is sigmoidal with a Hill coefficient θ =2.68 (Fig. 4.8) which further support a dinuclear catalysis. Cooperativity is not usually expected in mononuclear catalysis, wherein a linear correlation of the activity with Cu^{II} is expected until one equivalent is reached.

The oxidation of catecholamine neurotransmitters by $CuA\beta_{1-20}$ and the stoichiometry for DCC binding are consistent with the action of dinuclear catechol oxidase.[21] The mechanism of this enzyme thus serves as a working model for the metal-centered oxidation of catecholamines by CuAβ. Under aerobic conditions, the catechol moiety binds to a di-Cu^{II} center (Fig. 4.9) and is oxidized via 2-electron transfer to afford di-Cu^{I} and *o*-quinone product (**B**). Di-Cu^{+} then binds O_2 to form the metallo-ROS μ-peroxo-Cu_2 center (**C** and **D**) after 2-electron transfer from di-Cu^{2+} to O_2, which may bind (**E**) and oxidize (**F**) another substrate. In the presence of an electron donor such as NAD(P)H (**H**), the oxidation of neurotransmitters is inhibited. Herein, H_2O_2 is formed to certain extents which can produce other types of ROS and may exacerbate the oxidative destruction by going through the peroxide shunt (**G**) upon forming the highly reactive metallo-ROS μ-peroxo-di-Cu^{II} intermediate. The metal-bound H_2O_2 as a metallo-ROS in equilibrium of three possible iso-electronic species[xlvii] (**D**) has been demonstrated herein to be a more potent oxidative agent than H_2O_2 alone to cause neurodegeneration.

The full-length plaque-forming $CuA\beta_{1-40}$ also shows significant metal-centered oxidative activity toward the relatively more inert phenol (Fig. 4.10; Table 2),

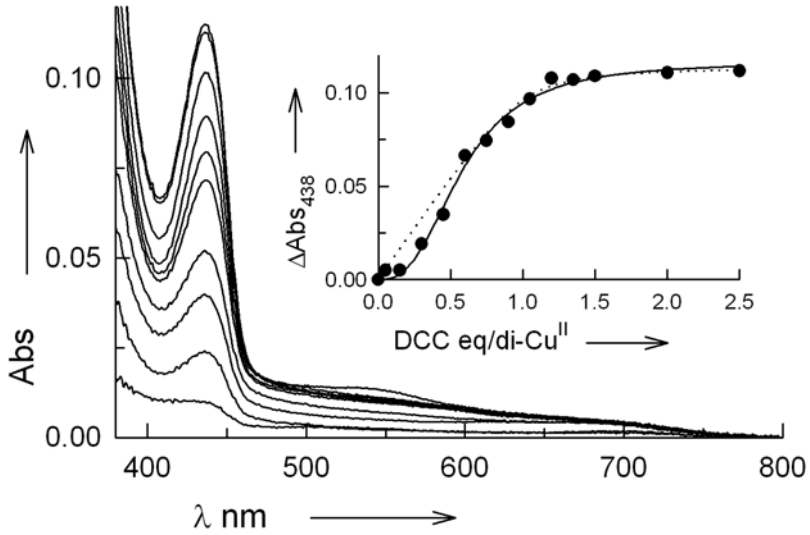

Figure 4.7. a) Optical titration of DCC into 0.05 mM CuAβ_{1-40}. Inset shows change of intensity at 438 nm upon DCC binding to a di-Cu^{II} center. Both were in 100.0 mM HEPES at pH 7.0.

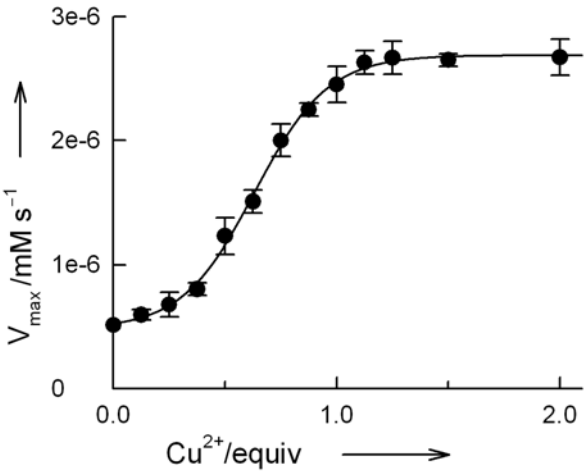

Figure 4.8. Activity titration of Cu^{II} into 2.5 micro-M $A\beta_{1-40}$ under saturating conditions of catechol.

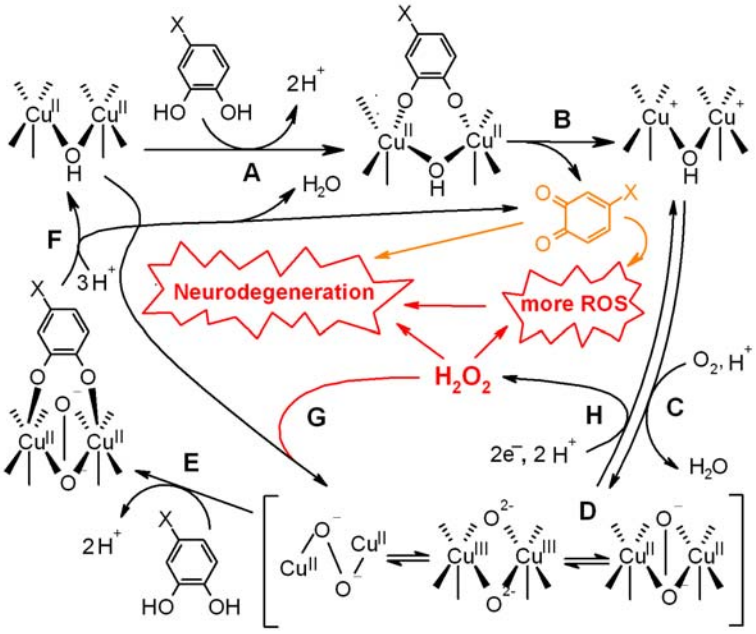

Figure 4.9. Mechanism for the oxidation of catecholamine neurotransmitters and the cause of neurodegeneration by CuAβ. The metal-bound H_2O_2 as a metallo-ROS is shown in **D**.

showing k_{cat} = 0.439 and 1.43 s^{-1} (with a small cooperativity θ = 1.6) and k_{cat}/K' = 0.351 and 1.14 M^{-1} s^{-1}, respectively, in the absence and presence of 50.0 mM H_2O_2. The activity reaches saturation at high H_2O_2 (Fig. 4.10), reflecting binding of H_2O_2 to the metal to afford metallo-ROS. Phenol hydroxylation and oxidation exhibits the same trend of reactivity with the shortest CuAβ_{1-16} showing the highest activity (Table 2). Herein, oxidation of phenol is dramatically enhanced by 6.64 × 10^6 and 1.41 × 10^5 times by CuAβ_{1-16} with and without 50.0 mM H_2O_2, respectively.

Serotonin can be hydroxylated and oxidized by CuA$\beta_{1-(16,20,40)}$ into its quinone form with significant rate enhancements ranging from 324 to 3.03 × 10^4 and 8.41 × 10^3 to 2.69 × 10^5-fold, respectively, relative to k_o in the absence and presence of a saturating amount of H_2O_2 (Fig. 4.11; Table 2). As in the case of catecholamine oxidation, the oxidation of serotonin by CuAβ_{1-40} is slower than that by CuA$\beta_{1-(16,20)}$. Moreover, the precursor of serotonin 5-hydroxy-Trp can also be effectively hydroxylated and oxidized by CuAβ_{1-20} (Table 2). The apparent and intrinsic dissociation constants K_S and $K_{i(S)}$ for phenol are determined to be 1.23 and 0.54 mM, respectively, from the Hanes plots, indicating H_2O_2 binding to the metal center decreases the binding of serotonin. The reactions may follow the tyrosinase mechanism[xlviii] for the hydroxylation and oxidation of phenol, serotonin, and 5-hydroxy-Trp. However, Cu^{II}-Aβ is still highly active without H_2O_2 in hydroxylation reaction, whereas the di-Cu^{II} met-form of tyrosinase is not. The large oxidation enhancements of the two indoleamines by CuAβ suggest that their oxidation possibly taking place in the brain of AD patients may alter serotonin-mediated physiological functions, including sleep disorder, mood change, and anxiety often associated with AD patients.[xlix]

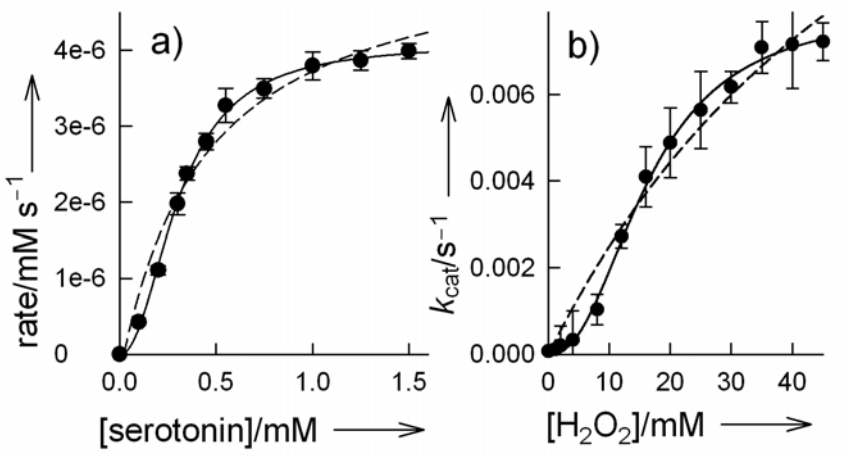

Figure 4.10. (a) Aerobic oxidation of serotonin by 1.47 μM CuA$\beta_{1\text{-}40}$ in 100.0 mM HEPES at pH 7.0 and 25 °C. Dashed traces are fittings to a pre-equilibrium kinetics while the solid traces are fittings to the Hill equation, showing the presence of cooperativity. (b) Oxidation of serotonin by CuA$\beta_{1\text{–}40}$ in the presence of H_2O_2 as in (a).

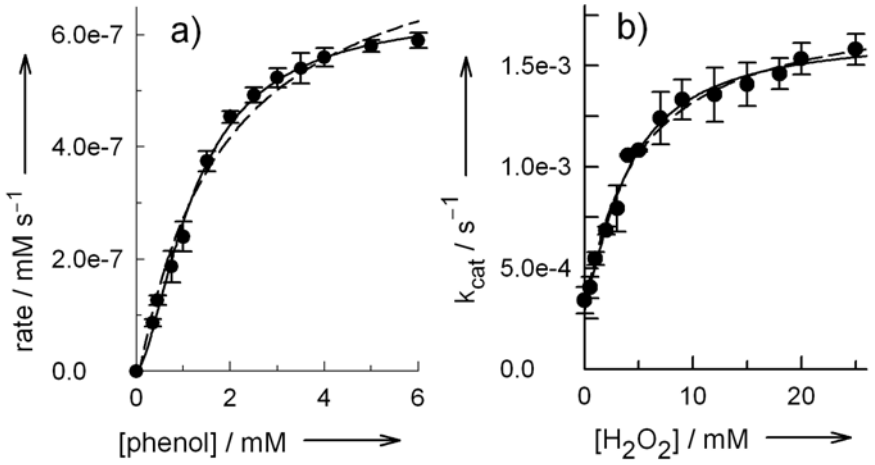

Figure 4.11. (a) Saturation profile of phenol oxidation by 1.47 μM CuA$\beta_{1\text{-}40}$ in 100.0 mM HEPES at pH 7.0 and 25°C. Dashed line is the fitting to a pre-equilibrium kinetics while the solid line is the fitting to the Hill equation ($k_{cat} = 4.39 \times 10^{-4}$, $K_m = 1.25$ mM, $k_{cat}/K_m = 0.35$ $M^{-1}s^{-1}$, $\theta = 1.60$). (b) The effect of H_2O_2 on the first order rate constant k_{cat}. Cooperativity is not very apparent in this case, showing $\theta = 1.33$.

Cell culture experiments reveal that catecholamines can exacerbate the oxidative stress caused by Aβ.[l] However, the metal-centered oxidative catalysis has been overlooked.[20] Oxidation of catecholamines is known to generate neurotoxic quinone products[li] that are involved in protein modification (e.g., covalent modification of dopamine transporter[lii]) and polymerizing tau protein into fibrils.[liii] Age-related deficits of both dopamine and norepinephrine have been implicated in the vulnerability of noradrenergic neurons in the hippocampus,[liv] which suffers significant damage in AD. Moreover, loss of noradrenergic neurons is linked to degradation of the locus ceruleus, which is rich in dopaminergic neurons that shows severe lesion in AD.[lv] Hence, a possible mechanism for reduction in neurotransmitter-regulated alertness response, delay-period activity, sleep cycle, mood stabilization, short-term memory, cognition, attention and problem solving capability, satisfaction feeling, and coordination of physical movement experienced by AD patients[31–34] may be due to excessive oxidation of neurotransmitters, hinting at a possible neuropathological role of metallo-ROS associated with CuAβ.

IV. CONCLUDING REMARKS

In conclusion, the full-length plaque-forming $CuA\beta_{1-40}$ found in the brain of AD patients has been demonstrated to exhibit significant activities toward the oxidation of neurotransmitters with or without H_2O_2 which can be further enhanced by interacting with membranes. The results suggest that imbalance of neurotransmitter metabolism

can be created near $A\beta_{1-40}$ plaques in AD. Moreover, the smaller fragments $CuA\beta_{1-(16,20)}$ show higher activities than $CuA\beta_{1-40}$ toward the oxidation of neurotransmitters. This observation suggests that small fragments of Aβ, due to their soluble nature, can significantly disturb neurotransmission in a more systematic manner in the brain of AD patients and thus may play an important role in neuropathology of this devastating disease.

IV. LIST OF REFERENCES

1) K. Schuessel, S. Leutner, N.J. Cairns, W.E. Mueller, A. Eckert, Impact of gender on upregulation of antioxidant defense mechanisms in Alzheimer's disease brain. *J. Neural Trans.* (2004), 111, 1167-1182.

2) J. Apelt, M. Bigl, P. Wunderlich, R. Schliebs, Aging-related increase in oxidative stress correlates with developmental pattern of beta-secretase activity and beta-amyloid plaque formation in transgenic Tg2576 mice with Alzheimer-like pathology. *Inter. J. Develop. Neurosci.* (2004), 22, 475-484.

3) (a) A.J. Núñez-Sellés, Antioxidant therapy: Myth or reality? *J. Braz. Chem. Soc.* (2005), 16, 699-710. (b) M. Valko, M. Izakovic, M. Mazur, C.J. Rhodes, J. Telser, Role of oxygen radicals in DNA damage and cancer incidence. *Mol. Cell. Biochem.* (2004), 266, 37-56. (c) A.C. Maritim, R.A. Sanders, J.B. Watkins, nfluence of treatment of diabetic rats with combinations of pycnogenol, β -carotene, and γ-lipoic acid on parameters of oxidative stress. *J. Biochem. Mol. Toxicol.* (2003), 17, 24-38. (d) A. Spector, Review: oxidative stress and disease. *J. Ocul. Pharmacol. Ther.* (2000), 16, 193-201.

4) (a) A.I. Bush, The metallobiology of Alzheimer's disease *Trends Neurosci*. (2003), 26, 207-214. (b) D.A. Butterfield, Amyloid β -peptide (1-42)-induced oxidative stress and neurotoxicity: implications for neurodegeneration in Alzheimer's disease brain. A review. *Free Rad. Res.* (2002), 36, 1307-1313.

5) M.J. Del Rio, C. Velez-Pardo, The hydrogen peroxide and its importance in Alzheimer's and Parkinson's disease. *Curr. Med. Chem. Cent. Nerv. Syst. Agen.* (2004), 4, 279-285.

6) C. Opazo, X. Huang, R.A. Cherny, R.D. Moir, A.E. Roher, A.R. White, R. Cappai, C.L. Masters, R.E. Tanzi, N.C. Inestrosa, A.I. Bush, Metalloenzyme-like activity of Alzheimer's disease β -amyloid. *J.Biol. Chem.* (2002), 277, 40302-40308.

7) R. Sultana, S. Newman, H. Mohmmad-Abdul, J.N. Keller, D.A Butterfield, Protective effect of the xanthate, D609, on Alzheimer's amyloid β-peptide (1-42)-induced oxidative stress in primary neuronal cells. *Free Rad. Res.* (2004), 38, 449-458.

8) H. Engelberg, Pathogenic Factors in Vascular Dementia and Alzheimer's Disease. *Demen. Geriat. Cogn. Disord.* (2004), 18, 278-298.

9) D.A Butterfield, Amyloid β-peptide 1-42-associated free radical-induced oxidative stress and neurodegeneration in Alzheimer's disease brain: Mechanisms and consequences. *Curr. Med. Chem.* (2003), 10, 2651-2659.

10) A.I. Bush, W.H. Pettingell, G. Multhaup, M. Paradis, J. Vonsattel, J.F. Gusella, K. Beyreuther, C.L. Masters, R.E. Tanzi, Rapid induction of Alzheimer Aβ amyloid formation by zinc. *Science* (1994), 265, 1464-1467.

11) T. Miura, K. Suzuki, N. Kohata, H. Takeuchi, Alzheimer's amyloid beta-peptide in insoluble aggregates and soluble complexes. *Biochemistry* 2000, *39*, 7024-7031.

12) R.E. Tanzi, L. Bertram, Twenty years of the Alzheimer's disease amyloid hypothesis: a genetic perspective. *Cell* (2005), 120, 545-555.

13) I.H. Cheng, J.J. Palop, L.A. Esposito, N. Bien-Ly, F. Yan, L. Mucke, Aggressive amyloidosis in mice expressing human amyloid peptides with the Arctic mutation. *Nat. Med.* 2004, *10*, 1190-1192.

14) K. Jin, V. Galvan, L. Xie, X. M. Ou, O.F. Gorostiza, D.E. Bredesen, D.A. Greenberg, *Proc. Natl. Acad. Sci. USA* Enhanced neurogenesis in Alzheimer's disease transgenic (PDGF-APPSw,Ind) mice. (2004), 101, 13363-13367.

15) G. Evin, A. Weidemann, Biogenesis and metabolism of Alzheimer's disease Aβ amyloid peptides. *Peptides* (2002), 23, 1285-1297.

16) G. Evin, A. Zhu, D. Holsinger, C.L. Masters, Q. Li, . Proteolytic processing of the Alzheimer's disease amyloid precursor protein in brain and platelets. *J.Neurosci. Res.* (2003), 74, 386-392.

17) A. Kontush, C. Berndt, W. Weber, V. Akopian, S. Arlt, S. Schippling, U. Beisiegel, Amyloid-β is an antioxidant for lipoproteins in cerebrospinal fluid and plasma. *Free Rad. Biol. Med*. (2001), 30, 119-128.

18) Y. Luo, P. Butko, Amyloid-β peptide, a therapeutic target for Alzheimer's disease? *Oxid. Stre. Dis.*(2006), 22, 395-408.

19) J. Hardy, Has the amyloid cascade hypothesis for Alzheimer's disease been proved? *Curr. Alzhei. Res.* (2006), 3, 71-73.

20) (a) D.P. Smith, D.G. Smith, C.C. Curtain, J.F. Boas, J.R. Pilbrow, G.D. Ciccotosto, T.-L. Lau, D.J.Tew, K. Perez, J.D. Wade, A.I. Bush, S.C. Drew, F. Separovic, C.L Masters, R. Cappai, K.J. Barnham, Copper-mediated Amyloid-β Toxicity Is Associated with an Intermolecular Histidine Bridge. *J. Biol. Chem.* (2006), 281, 15145-15154; (b) F.E. Ali, F.B. Separovic, C.J. Barrow, R.A. Cherny, F. Fraser, A.I. Bush, C.L. Masters, K.J. Barnham, Methionine regulates copper/hydrogen

peroxide oxidation products of Aβ *J. Peptide Sci.* (2005), 11, 353-360. (c) P.I. Moreira, K.Honda, Q. Liu, M.S. Santos, C.R. Oliveira, G. Aliev, A. Nunomura, Z. Akihiko, X. Zhu, M.A. Smith, G.Perry, Oxidative stress mechanisms and potential therapeutics in Alzheimer disease. *J. Neur. Trans.* (2005), 112, 921-932.

21) G.F.Z. da Silva, W.M. Tay, L.-J. Ming, Catechol Oxidase-like Oxidation Chemistry of the 1–20 and 1–16 Fragments of Alzheimer's Disease-related β-Amyloid Peptide: Their Structure-Activity Correlation and the Fate of Hydrogen Peroxide. *J. Biol. Chem.* (2005), 280, 16601-16609.

22) G.F.Z. da Silva, L.-J. Ming, Alzheimer s Disease Related Copper(II)-β-Amyloid Peptide Exhibits Phenol Monooxygenase and Catechol Oxidase Activities *Angew. Chem. Int. Ed.* (2005), 44, 5501-5504.

23) X. Huang, C.S. Atwood, R.D. Moir, M.A. Hartshorn, J.P. Vonsattel, R.E. Tanzi, A.I. Bush, Zinc-induced Alzheimer's Aβ 1-40 aggregation is mediated by conformational factors. *J. Biol. Chem.* (1997), 272, 26464-26470.

24) S. G. Srivatsan, P. Nigamb, M. S. Raob, S. Verma, Phenol oxidation by copper-metallated 9-allyladenine-DVB polymer: reaction catalysis and polymer recycling. *Appl. Catal. A* (2001), 209, 327–334.

25) J.N. Rodríguez-López, J. Escribano, F. García-Cánovas, A continuous spectrophotometric method for the determination of monophenolase activity of tyrosinase using 3-methyl-2-benzothiazolinone hydrazone. *Anal. Biochem.* (1994), 216, 205-212.

26) D.B. Calne, J.W. Langston, Aetiology of Parkinson's disease. *Lancet* (1983), 322, 1457-1459.

27) (a) Ditter, S. M.; Mirra, S. S. Neuropathologic and clinical features of Parkinson's disease in Alzheimer's disease patients. *Neurology* (1987), 37, 754-760. (b) Masliah E, Rockenstein E, Veinbergs I, Sagara Y, Mallory M, Hashimoto M, Mucke L β - amyloid peptides enhance α-synuclein accumulation and neuronal deficits in a transgenic mouse model linking Alzheimer's disease and Parkinson's disease. *Proc. Nat. Acad. Sci. USA* (2001), 98, 12245-12250.

28) (a) K. Heinitz, M. Beck, R. Schliebs, J.R. Perez-Polo Toxicity mediated by soluble oligomers of β-amyloid(1-42) on cholinergic SN56.B5.G4 cells. *J. Neurochem.* (2006), 98, 1930-1945. (b) R. Kayed, E. Head, J.L. Thompson, T.M. McIntire, S.C. Milton, C.W. Cotman, C.G. Glabe, Common Structure of Soluble Amyloid Oligomers Implies Common Mechanism of Pathogenesis. *Science* (2003), 300, 486–489.

29) (a) A.F. Arnsten, B.M. Li, Neurobiology of Executive Functions: Catecholamine Influences on Prefrontal Cortical Functions. *Biol. Psych.* (2005), 57, 1377-1384. (b) S.F. Leibowitz, G.F. Weiss, G. Shor-Posner, pharmacological, biochemical, and behavioral analyses of its feeding-suppressive action. *Clin. Neuropharm.* (1988), 11, S51-S71.

30) E.B. Larson, W.A. Kukull, R.L. Katzman, R.L. Cognitive impairment: dementia and Alzheimer's disease. *Ann. Rev. Pub. Heal.* (1992), 13, 431-49.

31) J.B. Friedman, D.N. Adler, K.L. Davis, Diffusion tensor imaging in schizophrenia. *Biol. Psychiatry* (1999), 46, 1243-1252.

32) H. Umegaki, N. Tamaya, T. Shinkai, A. Iguchi, The metabolism of plasma glucose and catecholamines in Alzheimer's disease. *Exp. Gerontol.* (2000), 35, 1373-1382.

33) R.J. Gruen, J. Ehrlich, R. Silva, J.W. Schweitzer, A.J. Friedhoff, Cognitive factors and stress-induced changes in catecholamine biochemistry. *Psychia. Res.*, (2000), 93, 55-61.

34) J. Li, M. Zhu, A.B. Manning-Bog, D.A. Di Monte, A.L. Fink, Dopamine and L-dopa disaggregate amyloid fibrils: implications for Parkinson's and Alzheimer's disease. *FASEB* (2004), 18, 962-964

35) The off-the-shelf H_2O_2 solution in the U.S. is 3%.

36) A. Rompel, H. Fischer, D. Meiwes, K. Buëldt-Karentzopoulos, A. Magrini, C. Eicken, C. Gerdemann, B. Krebs, Substrate specificity of catechol oxidase from Lycopus europaeus and characterization of the bioproducts of enzymic caffeic acid oxidation. *FEBS Lett.* (1999), 445, 103–110.

37) V. Leskovac, *Comprehensive Enzyme Kinetics*, Kluwer, Boston, (2002), p.119.

38) J.R. Florini, C.S. Vestling, Graphical determination of the dissociation constants for two-substrate enzyme systems. *Biochim. Biophys. Acta*. (1957), 25, 575-578.

39) C. Morgan, M. Colombres, M.T. Nunez, N.C. Inestrosa, Structure and function of amyloid in Alzheimer's disease. *Prog. Neurobiol.* (2004), 74, 323-349.

xl) (a) G.W. Buchko, A. Rozek, D.W. Hoyt, R.J. Cushley, M.A. Kennedy, The use of sodium dodecyl sulfate to model the apolipoprotein environment. Evidence for peptide-SDS complexes using pulsed-field-gradient NMR spectroscopy. *Biochim. Biophys. Acta.* (1998), 1392, 101-108. (b) P. C. Griffiths, J. A. Roe, B. L. Bales, A. R. Pitt, A. M. Howe, Paramagnetic Resonance and Small-Angle Neutron Scattering Studies of Mixed Sodium Dodecyl Sulfate and (Tetradecylmalono)bis(N-methylglucamide) Surfactant Micelles. *Langmuir* (2000), 16, 8248-8254.

xli) E. Cohen, J. Bieschke, R. M. Perciavalle, J. W. Kelly, A. Dillin, Opposing Activities Protect Against Age-Onset Proteotoxicity. *Science* (2006), 313, 1604-1610.

xlii) S.-J. Lin, L. Guarente, Longevity determinant genes: what is the evidence? What's the importance? Panel discussion. *Curr. Opin. Cell Biol.* (2003), 15, 241–246.

xliii) (a) F. Garcia Soriano, L. Virag, P. Jagtap, E. Szabo, J.G. Mabley, L. Liaudet, A. Marton, D.G. Hoyt, K.G. Murthy, A.L. Salzman, G.J. Southan, C. Szabó, Diabetic endothelial dysfunction: the role of poly(ADP-ribose) polymerase activation. *Nature Med.* (2001), 7, 108-113. (b) Q. Zhang, D.W. Piston, R.H. Goodman, Regulation of corepressor function by nuclear NADH. *Science* (2002), 295, 1895-1897.

xliv) L.K. Klaidman, S.K. Mukrherjee, J.D. Adams Jr., Oxidative changes in brain pyridine nucleotides and neuroprotection using nicotinamide. *Biochim. Biophys. Acta* (2001), 1525, 136-148.

xlv) Q. Zhang, D.W. Piston, R.H. Goodman, *Science* (2002), 295, 1895-1897.

xlvi) H. Sies, *Metabolic Compartmentation* Academic Press, London, (1982).

xlvii) L.M Mirica, X. Ottenwaelder, T.D.P. Stack, Structure and Spectroscopy of Copper-Dioxygen Complexes. *Chem. Rev.* (2004), 104, 1013-45.

xlviii) A. Sánchez-Ferrer, J.N. Rodriguez-López, F. García-Cánovas, F. García-Carmona, Tyrosinase: a comprehensive review of its mechanism. *Biochim. Biophys. Acta* (1995), 1247, 1-11.

xlix) L. Volicer, M.Z. Wrona, W. Matson, G. Dryhurst, Neurotoxic oxidative metabolite of serotonin: possible role in Alzheimer's disease. *Bioimag. Neurodegen.* (2005), 85-93.

l) W. Fu, H. Luo, S. Parthasarathy, M.P. Mattson, Catecholamines potentiate amyloid β-peptide neurotoxicity: involvement of oxidative stress, mitochondrial dysfunction, and perturbed calcium homeostasis. *Neurobiol. Dis.* (1998), 5, 229-243.

li) (a) D.G. Graham, Oxidative pathways for catecholamines in the genesis of neuromelanin and cytotoxic quinones. *Mol. Pharmacol.* (1978), 14, 633-643. (b) D.G. Graham, S.M. Tiffany, W.R Bell Jr. W.F. Gutknecht, Autoxidation versus covalent binding of quinones as the mechanism of toxicity of dopamine, 6-hydroxydopamine, and related compounds toward C1300 neuroblastoma cells in vitro. *Mol. Pharmacol.* 1978, *14*, 644-653. (c) T.G. Hastings, *J. Neurochem.*, (1995), 64, 919-924.

lii) S.B. Berman, M.J. Zigmond, T.G. Hastings, Enzymatic oxidation of dopamine: the role of prostaglandin H synthase. *J. Neurochem.* (1996), 67, 593-600.

liii) (a) M.J. LaVoie, T.G. Hastings, Peroxynitrite- and nitrite-induced oxidation of dopamine: implications for nitric oxide in dopaminergic cell loss. *J. Neurosci.* (1999), 19, 1484-1491. (b) I. Santa-Maria, F. Hernandez, M.A. Smith, G. Perry, J. Avila, F.J. Moreno, eurotoxic dopamine quinone facilitates the assembly of tau into fibrillar polymers. *Mol. Cell. Biochem.* (2005), 278, 203-212.

liv) A.J. Nazarali, G.P. Reynolds, Monoamine neurotransmitters and their metabolites in brain regions in Alzheimer's disease: a postmortem study. *Cell. Mol. Neurobiol.* (1992), 12, 581-587.

lv) M.A. Miller, P.E. Klob, J.B Levernz, E.R. Peskind, M.A. Raskind Preservation of noradrenergic neurons in the locus ceruleus that coexpress galanin mRNA in Alzheimer's disease. *J. Neurochem.* (1999), 73, 2028-2036.

CHAPTER V. METHIONINE-35 IS NOT A REDUCING AGENT FOR THE METAL-CENTERED OXIDATION CHEMISTRY OF Cu^{2+}-β-AMYLOID– KINETIC AND EPR STUDIES

I. INTRODUCTION

Oxidative stress[1] has been a key topic of research concerning cancer, aging, heart diseases, arthritis, diabetes, and neurodegenerative disorders such as Parkinson's and Alzheimer's diseases[2] (AD). Mechanisms proposed for the neurodegeneration in AD brains generally focus on the amyloid-β peptide (Aβ),[2] a proteolytic product of 40–42 amino acids of the ubiquitously distributed amyloid precursor protein (APP), and its interaction with redox-active metal ions. The recent "Aβ cascade hypothesis" suggested that Aβ aggregates trigger a complex pathological cascade which leads to neurodegeneration in AD,[3] including generation of H_2O_2,[4,5] free-radical induced oxidation,[6–8] and the involvement of Met35 as a reducing agent[9] in the redox chemistry of metallo-Aβ. A central focus of the neuropathology of AD thus has been the effects of

redox-active transition metal ions and reactive oxygen species (ROS), such as superoxide, hydroxyl free radical, and H_2O_2.[2] Although physiological processes responsible for dealing with ROS can be up-regulated to tackle variations in oxidative stress,[10,11] long-term negative effects of such oxidative chemical imbalance such as that taking place in the brains of AD patients can be expected. Some AD treatment strategies have targeted the metal center in Aβ to prevent peptide aggregation and ROS generation.[12–14] However, comparatively little effort has been focused on the metal-centered chemistry associated with the bound metal ions, such as the detailed coordination chemistry and the reactivity of the metal–bound ROS in CuAβ.

Transgenic mouse models with human Aβ show similar effects as AD patients, including Aβ aggregation and loss of memory.[15,16] Rodent Aβ has been shown to exhibit redox activity *in vitro* that was attributed to ROS generation via Met35,[17] even though the metal-binding domain was mutated in rodent Aβ (i.e., His13→Arg). Since Aβ activity and aggregation in AD brains is sequence-specific and metal-dependent,[2] it is a priority to establish the targets of redox activity that can contribute to the physiological and cognitive effects of AD. I have shown in Chapters II-IV that the Cu^{2+} complexes of Aβ and its soluble fragments ($Aβ_{1-16}$ and $Aβ_{1-20}$) showed considerable activities toward the oxidation of phenol, polyphenol, catechol, and neurotransmitters to form *o*-quinones which challenges the redox role of Met35 that is not present in the fragments.[18,19,20] The capability of Aβ to bind copper[21] with subsequent H_2O_2 generation under reduction conditions[5] and catechol oxidation[18–20] hint at the possible formation of a reactive μ-η^2:η^2-peroxo-di-Cu^{2+} species (or its isoelectronic counterparts, oxy-di-Cu^{+}, μ-η^1:η^1-

peroxo-di-Cu^{2+}, and bis-μ-oxo-di-Cu^{3+})[22] which is the active species in action of the type-3 dinuclear copper oxidases[23] such as catechol oxidase.

In this chapter I present kinetic and spectroscopic investigations of the oxidation chemistry of CuA$\beta_{1\text{-}20}$ and the influence of methionine and reducing agents on the oxidation chemistry. The results support metal-centered oxidative stress and shed light on the mechanistic role of Met35 and reducing agents in the redox chemistry of CuAβ.

II. EXPERIMENTAL

The 1-20 fragment of Aβ was synthesized by the use of the Fmoc chemistry at the Peptide Center of the University of South Florida, and the identity of the peptide confirmed with a Bruker MALDI-TOF mass spectrometer. Dopamine, ascorbic acid, and glutathione (GSH) were obtained from Sigma-Aldrich (St. Louis, MO), 3-methyl-2-benzothiazolinone hydrazone hydrochloride monohydrate (MBTH) from Acros (Fairlawn, NJ), and H_2O_2, EDTA, L-methionine, and $Cu(NO_3)_2$ from Fisher Scientific (Swanee, GA). All plastic ware and glassware were demetallized with EDTA and extensively rinsed with 18.0-MΩ deionized water.

The catechol oxidase assay toward dopamine was performed as previously reported.[20,24] Same equivalent of a substrate dopamine and the *o*-quinone indicator MBTH were mixed in 100 mM HEPES at pH 7.00 in a final volume of 1.0 mL. The MBTH-adduct of *o*-quinone was monitored at 505 nm (ε = 27,200 M^{-1} cm^{-1}) and 25 °C for 5–10 minutes with a Varian CARY50 Bio-UV-Vis spectrophotometer equipped with

a CARY PCB-150 Water Peltier temperature regulation system, and the rates determined by the change in absorbance over time. Rates were fitted to appropriate rate laws and rate constants determined with non-linear regression (SigmaPlot 8.0), such as the enzymatic Michaelis-Menten-like kinetics.[25] The effects by H_2O_2, ascorbate, GSH, and L-Met were determined similarly in the presence of different amounts of the corresponding reagent and the inhibition/dissociation constants determined accordingly. Binding of L-Met to CuAβ_{1-20} was performed by direct titration of Met into CuAβ_{1-20} in 100 mM HEPES at pH 7.0 and monitored with the CARY50 spectrophotometer.

Electron paramagnetic resonance (EPR) experiments were performed on a Bruker Elexsys E580 cw/pulsed X-band spectrometer at the University of Florida with professor Alexander Angerhofer. For a typical cw EPR spectrum, the field was set wide enough to reveal a possible low-field transition for magnetically coupled systems with a microwave frequency of 9.4 GHz, field modulation typically around 2 G, and time constant of 40-80 ms at ~5–6 K. The g and A tensors were obtained with numerical fittings using the "easyspin" toolbox for Matlab.[26] Electron relaxation times were measured with the standard two-pulse Hahn's spin-echo method or the inversion-recovery methods, wherein the signal intensity as a function of time is fitted to simple or double exponential decay to obtain the relaxation time. ESEEM (electron spin echo envelope modulation) spectra were recorded with the usual $\pi/2$-τ- $\pi/2$-T- $\pi/2$ pulse sequence with a $\pi/2$ pulse of 20 ns in order to study ^{14}N and ^{2}H nuclei in the ligand sphere. A typical ESEEM trace consisted of 1024 points taken at time intervals of 8 ns. The transient was first base-line corrected by subtracting the ordinary T_1 exponential decay function and any remaining constant

baseline offset, then zero-appended to 2048 points. A Hamming window function was then applied to the time-domain spin-echo envelope, followed by Fourier transformation to afford the frequency-domain spectrum.

An ESEEM spectrum can reveal those nuclei having super-hyperfine coupling with the Cu^{2+} center, including coordinated His side chains and water, which can thus serve as a very useful tool for the investigation of the Cu^{2+} center in CuAβ. The theoretical background[27] of ESEEM is summarized herein. In the case of coordinated His side chains, the super-hyperfine coupling arises from the electron-nuclear interactions and the nuclear quadrupole interactions (NQI) of the remote non-coordinated nitrogen (^{14}N, I = 1) on the imidazole ring of coordinated His side chains. At X-band, three zero-field nuclear quadrupole resonance lines $\nu_{\pm}$ and ν_o are observed which can be determined from the NQI lines in the ESEEM spectrum (Eq. 1 and 2), wherein e^2qQ is the quadrupole coupling constant and η the asymmetry parameter (η = 0 for a complete axial symmetry and 1 for a pure rhombic symmetry).

$$\nu_{\pm} = {}^1/_4(e^2qQ)(3 \pm \eta) \qquad (1)$$

$$\nu_o = {}^1/_2(e^2qQ)\eta \qquad (2)$$

The e^2qQ and η values can thus be obtained from the NQI lines in the ESEEM spectra since $(\nu_+ - \nu_o/2)/3 = {}^1/_4(e^2qQ)$. In the case of coordinated water, the super-hyperfine coupling arises from the electron-nuclear interactions and the NQI of the coordinated water molecules upon deuteration. The deuterium Zeeman interaction at X-band is much

larger than the isotropic component of the electron-nuclear coupling. Thus, the deuterium peak in the ESEEM spectrum is found at the deuterium Zeeman frequency and split slightly by the electron-nuclear coupling.

III. RESULTS

Dopamine is oxidized by $CuA\beta_{1-20}$ in the absence of H_2O_2 with rate constant of k_{cat} = 0.0104 s^{-1} and K_m = 0.89 mM (trace •, Fig. 5.1), consistent with the observations discussed in Chapter IV.[20] Addition of L-Met to the reaction solution significantly increases the activity (Fig. 5.2). The reaction in the presence of saturating amount of Met seems to induce slight cooperativity which can be fitted to the Hill equation with a Hill's coefficient θ = 2.3 (Solid trace Figure 5.1). The activity reaches a plateau at high [Met] (Fig. 5.1), indicating direct Met binding to the active center of CuAβ. Fitting of the k_{cat} values as a function of [Met] to a simple equilibrium of [CuAβ + Met $\rightleftharpoons$ Met-CuAβ] gives an affinity constant of 1,900 M (K_d = 0.53 mM). Met follows a non-essential activation pattern toward dopamine oxidation by $CuA\beta_{1-20}$ as shown in the Lineweaver-Burk plot (Fig. 5.1), i.e., both CuAβ-substrate and Met-CuAβ-substrate complexes are active. From the data, the dissociation constant for the activation K_A can be obtained to be 0.087 mM, and the dissociation constant for the ternary [$CuA\beta_{1-20}$-Met-dopamine] complex K_{TS} is 0.125 mM. In the presence of H_2O_2, the activity is further

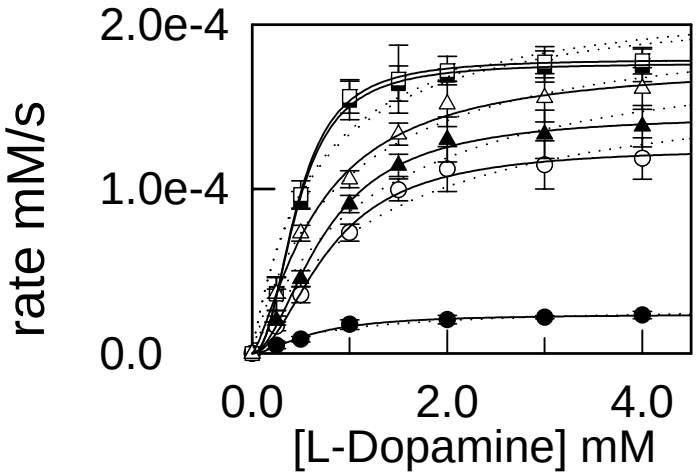

Figure 5.1. Saturation kinetics curves of dopamine oxidation by CuAβ fitted with Michaelis-Menten kinetics (dotted traces) and with Hill equation (solid traces).

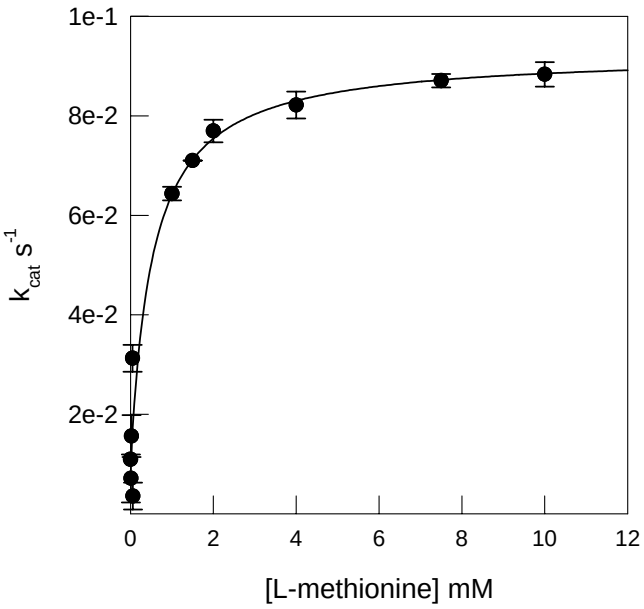

Figure 5.2. Effect of L-Met on the the first order rate constant toward dopamine oxidation.

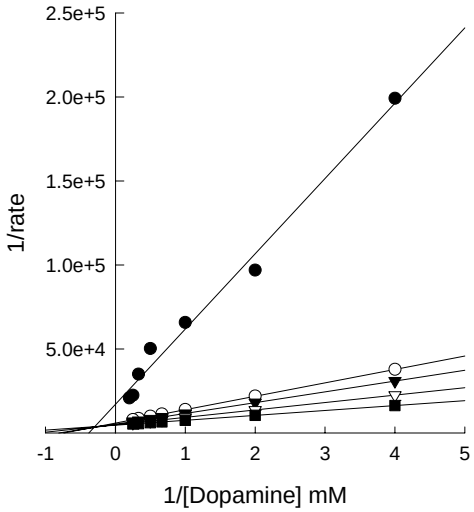

Figure 5.3. Lineweaver-Burk plot of showing the non-essential activation pattern for L-Met toward dopamine oxidation by CuAβ

enhanced. Herein, both Met and H_2O_2 can activate dopamine oxidation which are not exclusive of each other and show a combined effect, i.e., the k_{cat} value of 0.180 s^{-1} in the presence of saturating amount of Met and H_2O_2 (Fig. 5.4) is a combination of those in the saturating amount of Met (0.088 s^{-1} for Met activation) and H_2O_2 (0.099 s^{-1} for H_2O_2 activation), indicating their independent activation mechanisms. As opposed to Met, the reducing agents ascorbic acid and GSH act as inhibitors toward dopamine oxidation by CuAβ (Fig. 5.5), with the former being a competitive inhibitor (K_i = 66 μM) while GSH a non-competitive inhibitor (K_i = 53 μM).

The electronic spectrum of CuAβ exhibits an intense charge-transfer transition at 316 nm upon addition of Met (Fig. 5.6), indicative of direct Met binding to the Cu^{2+} center. Such charge-transfer transition is not observed in $CuA\beta_{1–40}$, suggesting that Met35 does not interact with the Cu^{2+} center. The d-d transition of $CuA\beta_{1-20}$ at 600 nm is not significantly affected in the presence of saturating amounts of Met (Fig. 5.6; inset). The change in the intensity of the charge transfer transition as a function of [Met] can be fitted to the 1:1 binding pattern of [CuAβ + Met $\rightleftharpoons$ Met-CuAβ] to yield a dissociation constant K_d = 0.25 mM. This value is comparable to that obtained from the activity profile discussed above, indicating that direct Met binding to the Cu^{2+} center affords the enhancement of CuAβ activity.

The coordination of CuAβ and its binding with Met have been investigated with EPR spectroscopy. The EPR spectrum of $CuA\beta_{1–20}$ (Figure 5.7) can be attributed to a typical tetragonally distorted Cu^{2+} center, i.e., an elongation along the z axis due to the Jahn-

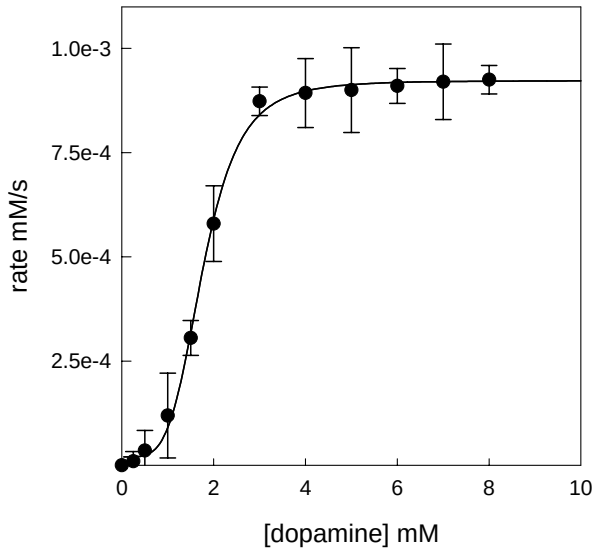

Figure 5.4. Rate of dopamine oxidation by $CuA\beta_{1\text{-}20}$ in the presence of saturating amounts of L-Met and H_2O_2.

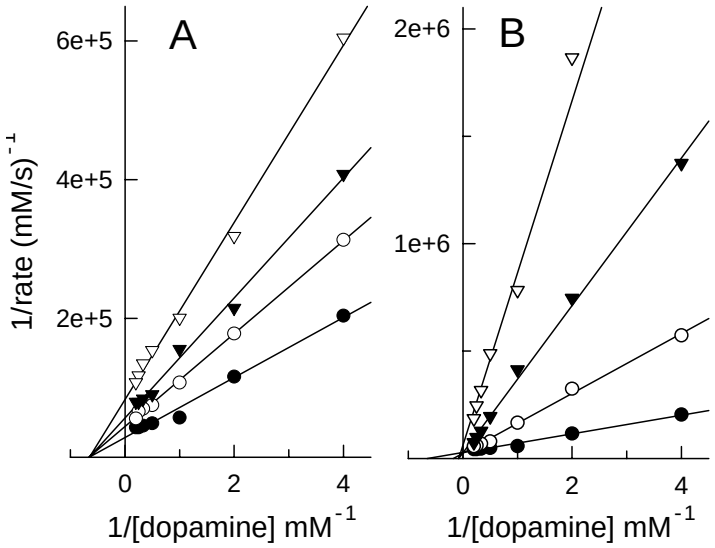

Figure 5.5. (A) Glutathione (10.0 μM, 20.0 μM, and 40.0 μM from bottom) inhibition and (B) ascorbic acid inhibition (0.0, 0.12, 0.55, and 0.95 mM from bottom) toward dopamine oxidation by Cu-Aβ_{1-20} in 100.0 mM HEPES pH 7.0.

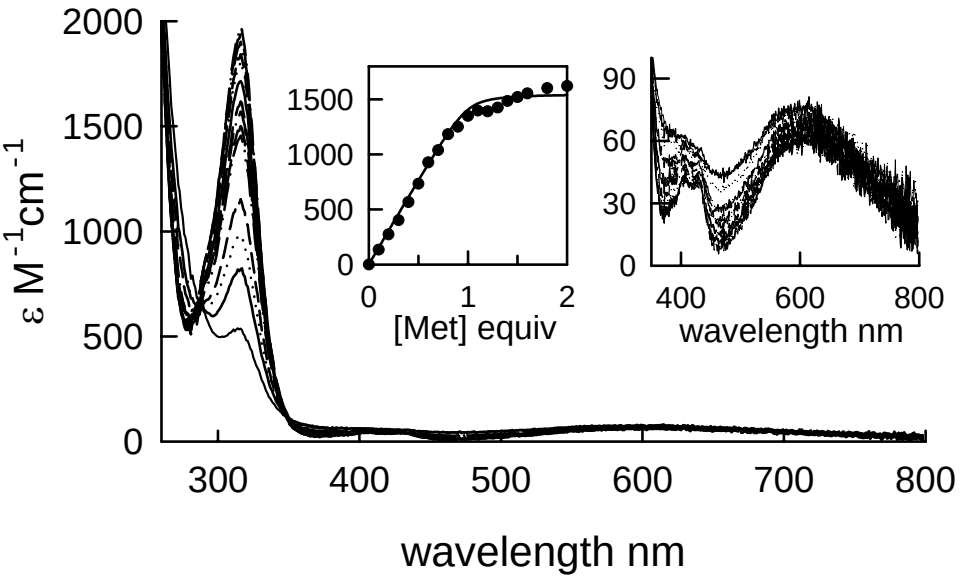

Figure 5.6. Optical titration of L-methionine to 0.2 mM CuAβ. The insets show the low energy d-d transition and the saturation curve fitted to 1:1 ligand:metal stoichiometry.

Teller effect, which can be slightly better fitted to a rhombic than an axial magnetic g_z = 2.266, g_x = 2.057, and g_y = 2.080 and A_z = 547, A_x = 30.6, and A_y = 51.1 MHz (Fig. 5.7) or $g_{//}$ = 2.268, $g_{\perp}$ = 2.064, $A_{//}$ = 547, and $A_{\perp}$ = 51.1 MHz. These values are consistent with those reported for several Cu^{2+} complexes of Aβ and fragments,[28] i.e., $g_{//}$ = 2.265–2.269, $g_{\perp}$ = 2.059–2.062, and $A_{//}$ = 465–577 MHz (from 166-206 G). Upon addition of Met, the EPR spectrum changes only slightly to g_z = 2.257, g_x = 2.055, and g_y = 2.072 and A_z = 564.9, A_x = 35.8, and A_y = 46.0 MHz (Fig. 4A) or $g_{//}$ = 2.257, $g_{\perp}$ = 2.059, $A_{//}$ = 565, and $A_{\perp}$ = 35.8 MHz, as opposed to the dramatic change in the electronic spectrum.

The Cu^{2+} center in $CuA\beta_{1-20}$ and its interaction with Met are further investigated with pulsed EPR. The X-band ESEEM spectrum of $CuA\beta_{1-20}$ (Fig. 5.8) reveal three ^{14}N NQI lines at ν_o = 0.33, ν_- = 1.11 (shoulder), and ν_+ = 1.45 MHz (Eqs. 1 and 2), the double-quantum transitions at ~4 Mz, and the combination lines at 2.33, 2.95, and 3.45 MHz. From which, e^2qQ is obtained to be 1.71 MHz, a value typical of a coordinated His,[27] and η calculated to be 0.39 (Eqs. 1 and 2). The ν_- line (a shoulder) can be better determined once the values of e^2qQ and η are determined from ν_o and ν_+. At least one coordinated water is also revealed which attributes to the deuterium modulation at 2.29 MHz when the spectrum was acquired from a sample in D_2O buffer excited at 3391 G (dashed trace, Fig. 5.8), consistent with ^2H resonance of 2.21 MHz at this field. This small discrepancy may be attributed to the presence of a small super-hyperfine coupling. An ESEEM spectrum for Met-bound CuAβ in D_2O buffer was acquired under the same conditions (dotted trace, Fig. 5.8) to investigate the status of the coordinated water upon

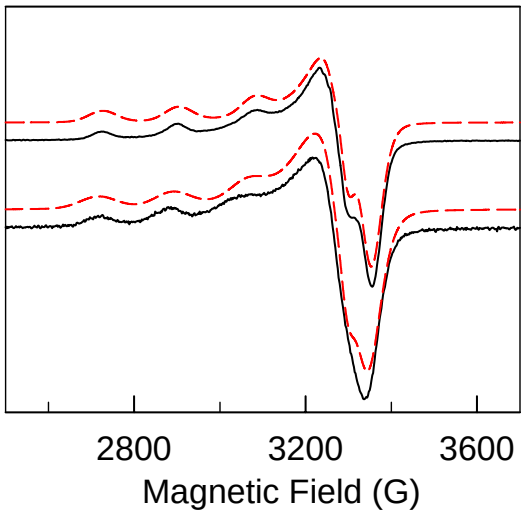

Figure 5.7. X-band EPR spectra of $CuA\beta_{1\text{-}20}$ in the presence and absence of L-Met and simulated spectra with rhombic g tensors (dashed traces).

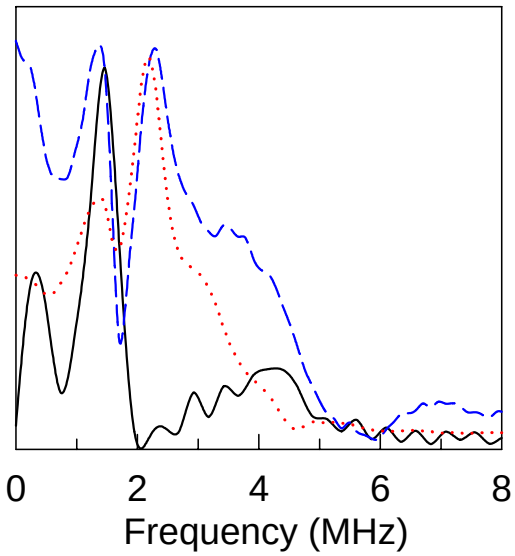

Figure 5.8. ESEEM spectra of 1.0 mM CuAβ_{1-20} in 100.0 mM HEPES buffer in H_2O (solid trace) and in D_2O (dashed trace) at pH(D) 7.0 and after addition of 8.0 equivalents Met (dash-dot trace).

Met binding. The ^{14}N NQI lines change only slightly upon Met binding, found at ν_o = 0.15, ν_- = 1.22 (shoulder), and ν_+ = 1.37 MHz which afford e^2qQ = 1.73 MHz and a small η = 0.17. Upon Met binding, the deuterium line is observed at 2.19 MHz when excited at 3351 G, right at the ^2H resonance frequency at this field which reflects a negligible super-hyperfine coupling.

IV. DISCUSSION

The oxidation of catechol and phenol and their derivatives by CuAβ in the presence and absence of H_2O_2 was demonstrated to be consistent with the mechanism of type-3 copper oxidases such as di-Cu catechol oxidase (Fig. 5.9).[19] Therein, the catechol-containing substrate like dopamine binds to a di-Cu^{2+} active center (step ***i***) under aerobic conditions and is oxidized via 2-electron transfer to afford a di-Cu^+ active center (**C**) and *o*-quinone product (step ***ii***). The reduced di-Cu^+ can bind O_2 (step ***iii***) to form a μ-peroxo-Cu^{2+}_2 center (**D**) as demonstrated in both enzyme and chemical model systems, which may bind a substrate and followed by oxidation of the substrate (steps ***iv*** and ***v***). The presence of a reducing agent such as ascorbic acid (or Met35 as previously suggested[9]) can thus facilitate the aerobic pathway to yield the di-Cu^+ active center (**C**) ready for O_2 binding. In the meantime, a reducing agent can also result in H_2O_2 production through the reduction of the μ-peroxo-Cu^{2+}_2 center (step ***vi***). An alternative "short-cut" route, also known as the "peroxide shunt" pathway in heme-containing peroxidase,[29] for the oxidation to take place is to form the μ-peroxo-Cu^{2+}_2 intermediate

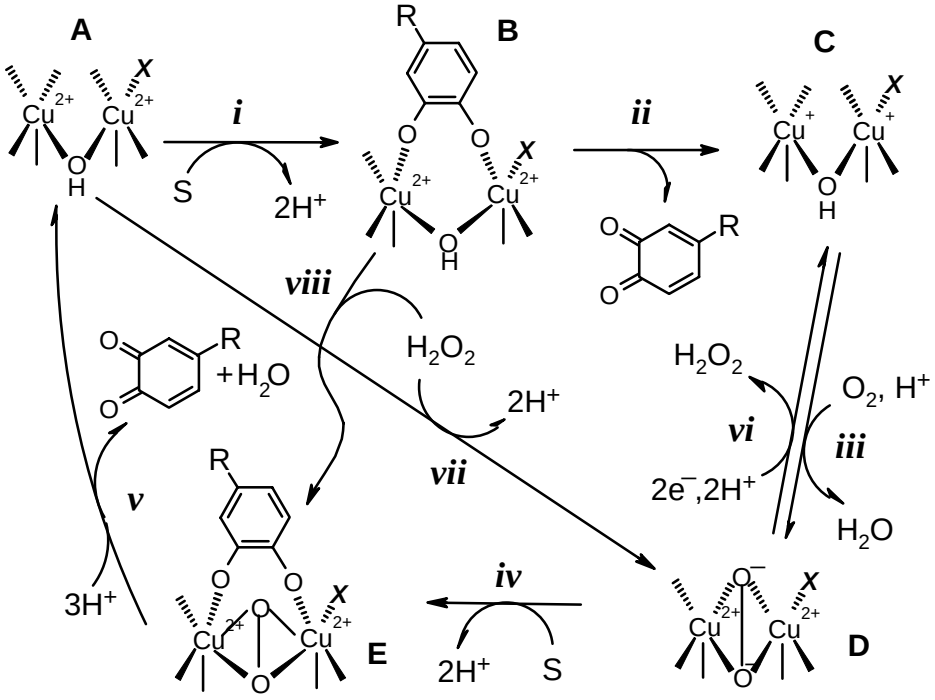

Figure 5.9. Proposed mechanism for the catechol oxidase-like activity of CuAβ toward the oxidation of dopamine. X indicates an endogenous ligand or a bound Met.

by direct binding of H_2O_2 to the di-Cu^{2+} center (step ***vii***), followed by substrate binding (step ***iv***) to form the μ-peroxo-$Cu^{2+}{}_2$-substrate ternary complex (**E**) which then undergoes oxidation. The ternary complex **E** can also be formed upon H_2O_2 binding to the substrate-bound intermediate (**B**; step ***viii***), representing a random bi-substrate mechanism.

Met_{35} in Aβ has been suggested to be a reducing agent[9] responsible for the initiation of the redox cycling of the Cu^{2+} center in CuAβ and leads to H_2O_2 production (i.e., step ***vi***).[5] The oxidation of the thioether moiety of Met to its sulfoxide form in Aβ has been implicated in aggregation, lipid peroxidation, and redox chemistry in association with the metal center.[9] The activity profile of [Met] (Fig. 5.1) and the optical spectrum (Fig. 5.6) indicate direct Met binding to CuAβ, rather than outer-sphere interaction, which potentially can reduce the Cu^{2+} center as proposed previously. Herein, the amount of di-Cu^{+} (**C**) increases which in turn forms a larger amount of the μ-peroxo-$Cu^{2+}{}_2$ center upon O_2 binding (**D**; step ***iii***), but fewer amount of di-Cu^{2+} (**A**) would be present for substrate binding as it is reduced by Met. However, once CuAβ (**A)** is reduced, it cannot follow the peroxide shunt pathway anymore. The observation that H_2O_2 can still significantly enhance the activity in the presence of a saturating amount of Met (Fig. 5.2) suggests the Cu^{2+} center is not significantly reduced by Met, which is demonstrated by the detection of the S = 1/2 EPR features (Fig. 5.7). Moreover, the difference in electrode potentials between Cu^{2+}-Aβ and Met is 0.71 V,[30] which gives a dramatic 68.5 kJ Gibbs free energy that is equivalent to a negligibly small equilibrium constant of 9.8×10^{-13} for one-electron reduction of Cu^{2+}-Aβ by Met at 298 K.

The non-exclusive nature of Met and H_2O_2 binding and their additive activations indicate that there are two pathways for the oxidation of dopamine in the presence of Met and H_2O_2, presumably the pathways ***i–v*** and ***vii–iv–v*** with a bound Met (the "X" ligand in Fig. 5.9), wherein the enhancement of the activity with Met alone is supposed to be due to a non-redox mechanism that fine-tunes the reduction potential of the Cu^{2+} to favor the oxidative catalysis. The sigmoidal activity profiles for dopamine oxidation in the presence of Met (Fig. 5.1) and from the concerted action of both H_2O_2 and Met (Fig. 5.4) reflect possible presence of cooperativity, such as the formation of the dinuclear active center **D**. Despite the lack of a Met and any redox-active amino acid, the fragments $CuA\beta_{1-16}$ and $CuA\beta_{1-20}$ exhibit significant metal-centered oxidative activity[18–20] which indicates the redox role of Met35 might have been overstretched.

The oxidation state of the Cu center in $CuA\beta_{1-20}$ upon Met binding can be concluded from the electronic and EPR spectra, wherein the remaining d-d transition at 600-nm (Fig. 5.6) and EPR features (Fig. 5.7) indicate that Cu^{2+} is not reduced by Met as opposed to previous suggestions for the reductive role of Met35 in $CuA\beta_{1-40}$.[9] Moreover, the charge transfer transition is consistent with a thio-to-Cu^{2+} charge-transfer transition observed in Cu^{2+}-methionine complexes.[31] The well resolved EPR spectral features at g~2 (Fig. 5.7) upon Met binding confirm the d^9 electron configuration of the Cu^{2+} center with S = 1/2. The lack of $\Delta M_S = \pm 2$ transition (i.e., between the $M_S = -1$ and +1 levels in an antiferromagnetically coupled di-Cu^{2+} center) in the EPR spectrum at low field indicates magnetic coupling between the Cu^{2+} centers may not exist. Thus, the previously proposed His-bridged dinuclear Cu,Zn-superoxide dismutase center for

$CuA\beta_{1-28}$[32] is not present in the case herein. The small change in the EPR spectrum upon Met binding indicates the charge transfer transition must be due to the binding of the thioether of Met through the non-magnetic d_{z^2} orbital at an axial position of $CuA\beta_{1-20}$. Otherwise, more significant changes in the g and A tensors would be observed as reported for the binding of thio-groups to Type-2 Cu proteins.[33]

The ESEEM spectrum of $CuA\beta_{1-20}$ (Fig. 5.8) confirms the binding of Cu^{2+} to Aβ through His side chains via the magnetic $d_{x^2-y^2}$ orbital in equatorial positions which gives rise to the quadrupole coupling with the remote non-coordinated ^{14}N on the coordinated His imidazole ring. There are at least two coordinated His side as reflected by the combination lines since a single coordinated His does not give rise to these lines.[33g,34] The small η values indicate that the Cu^{2+} center is only slight rhombic, which has already been observed in the CW EPR spectra (Fig. 5.7). The detection of a deuterium line at 2.29 MHz suggests the presence of coordinated water (as D_2O), presumably in an equatorial position via the magnetic $d_{x^2-y^2}$ orbital.[27] This signal is not much affected upon Met binding, once again suggesting Met binding to an axial position. It is interesting to note that the double-frequency peak at 4.6 MHz vanishes upon Met binding. This indicates that at least one of the weakly coupled deuterium atoms in the vicinity of the Cu^{2+} is replaced by the Met ligand.

Since the binding of Met to CuAβ does not reduce the Cu^{2+} center, the enhancement in activity must be attributed to a change in the reduction potential of the Cu^{2+} center. The axially coordinated Met ligand in blue copper proteins has been suggested to play a role in controlling the reduction potential of the protein since mutation of this Met results

in a significant change in the potential.[35] Based on the results herein, I propose the binding of methionine to Cu^{2+} in CuAβ may modulate the Cu^{2+}/Cu^{+} potential to favor the redox catalysis, yet is not necessarily involved directly in the redox chemistry as a reducing agent as previously proposed.[9] The oxidation of Met35 previously observed may follow the metal-centered mechanism as a catechol or phenol substrate via the reactive di-Cu^{2+}-peroxo intermediate to result in oxygenation reaction, ie., the coordinated Met "X" serves as a substrate via step ***iv*** and ***v*** in the mechanism without the catechol substrate (Fig. 5.9).

The catalytic pathway of CuAβ is altered under reduction conditions (Fig. 5.9), wherein the reaction is locked into a H_2O_2-producing cycle (***iii*** and ***vi***). The competitive inhibition of ascorbate toward the oxidation of dopamine by CuAβ (Fig. 5.5A) may be because of possible chelation and reduction of the Cu^{2+} center by ascorbate. GSH may bind to and reduce the Cu^{2+} center as a monodentate ligand which does not prevent substrate from binding to the Cu^{2+} center to form the inactive inhibitor-CuAβ-substrate complex, thus exhibiting non-competitive pattern (Fig. 5.5B). The inhibitory effect of the reducing agents toward metal-centered catalysis is consistent with the proposed mechanism wherein H_2O_2 is generated (step ***vi***), also reported previously.[5] Thus, the ability of CuAβ to oxidize biologically relevant molecules such as dopamine is highly dependent on the redox state of its environment. Although reducing agents can potentially inhibit the oxidation of neurotransmitters by CuAβ, the production of H_2O_2 may still exacerbate the situation of oxidative stress.

Metabolic malfunctions of catecholamines neurotransmitters have been suggested to be related to the neuropathology of AD.[36] Of these neurotransmitters, dopamine has been directly linked to the neurodegenerative Parkinson's disease[37] and has been proposed to be associated with adult neurogenesis in the subventricular zone.[38] I discuss in chapter IV that CuAβ can catalyze oxidation of catecholamine neurotransmitters such as dopamine[20] to generate neurotoxic quinone products.[39] Dopamine quinone can result in polymerization of tau protein into fibrils[40] and covalent modification of dopamine transporter which directly affects dopamine uptake.[41] A possible mechanism for reduction in the delay-period activity and short-term memory, lack of attention, and change in mood and motivation experienced by AD patients may probably be partially due to long-term oxidation of dopamine by CuAβ. Hence, the acceleration of dopamine oxidation via metal-centered mechanism that can be modulated by small molecules such as reducing agents, H_2O_2, and Met may well hint at the significant role of CuAβ in oxidative stress in the brain of AD patients.

V. CONCLUDING REMARKS

Taken together, the results herein present more structural information about the metal center and further support for metal-oxygen/peroxo-centered redox chemistry of CuAβ and provide additional mechanism for the oxidative stress in the brain of AD patients. The role of Met35 has been redefined and the dual mechanistic character of reducing agents (i.e., inhibition and H_2O_2 generation) in the redox cycle of CuAβ is

clearly defined. The overall picture of AD neuropathology is likely to be composed of the pieces of information uncovered thus far, including generation of ROS, metal-dependent aggregation of Aβ, and the largely overlooked metal-centered degradation of biomolecules. Treatment and prevention strategies hence must address all of these pathways, including inhibitions toward H_2O_2 production and oxidative damage of neurotransmitters and other biomolecules by the di-copper-peroxo active center.

VI. LIST OF REFERENCES

1) (a) A.J. Núñez-Sellés, Antioxidant therapy: Myth or reality? *J. Braz. Chem. Soc.* (2005), 16, 699-710. (b) M. Valko, M. Izakovic, M. Mazur, C.J. Rhodes, J. Telser, Role of oxygen radicals in DNA damage and cancer incidence *Mol. Cell. Biochem.* (2004), 266, 37-56. (c) A.C. Maritim, R.A. Sanders, J.B. Watkins, Diabetes, oxidative stress, and antioxidants: A review *J. Biochem. Mol. Toxicol.* (2003), 17, 24-38. (d) L. Kruidenier, H.W. Verspaget, Review article: oxidative stress as a pathogenic factor in inflammatory bowel disease—radicals or ridiculous? *Alim. Pharmacol. Therap.* (2002), 16, 1997-2015. (e) A. Spector, Review: Oxidative stress and disease *J. Ocul. Pharmacol. Ther.* (2000), 16, 193-201.

2) (a) A.I. Bush, The Metallobiology of Alzheimer's Disease. *Trends Neurosci.* (2003), 26, 207-214. (b) D.A. Butterfield, Amyloid beta-peptide (1-42)-induced oxidative stress and neurotoxicity: Implications for neurodegeneration in Alzheimer's disease brain: A review. *Free Rad. Res.* (2002), 36, 1307-1313.

3) T.E. Golde, D. Dickson, M. Hutton, Filling the gaps in the Aβ cascade hypothesis of Alzheimer's disease. *Curr. Alzhei. Dise.* (2006), 3, 421-430.

4) M.J. Del Rio, C. Velez-Pardo, The hydrogen peroxide and its importance in Alzheimer's and Parkinson's disease**.** *Curr. Med. Chem.* (2004), 4, 279-285.

5) C. Opazo, X. Huang, R.A. Cherny, R.D. Moir, A.E. Roher, A.R. White, R. Cappai, C.L. Masters, R.E. Tanzi, N.C. Inestrosa, A.I. Bush, Metalloenzyme-like activity of Alzheimer's disease β-amyloid. *J. Biol. Chem.* (2002), 277, 40302-40308.

6) R. Sultana, S. Newman, H. Mohmmad-Abdul, J.N Keller, D.A. Butterfield, Protective effect of the xanthate, D609, on Alzheimer's amyloid β-peptide (1-42)-induced oxidative stress in primary neuronal cells. *Free Rad. Res.* (2004), 38, 449-458

7) H. Engelberg, Pathogenic Factors in Vascular Dementia and Alzheimer's Disease. *Demen. Geriat. Cogn. Disord.* (2004), 18, 278-298.

8) D.A. Butterfield, Amyloid β-peptide [1-42]-associated free radical-induced oxidative stress and neurodegeneration in Alzheimer's disease brain: Mechanisms and consequences. *Cur. Med. Chem.* (2003), 10, 2651-2659.

9) (a) G.D. Ciccotosto, K.J. Barnham, R.A. Cherny, C.L. Masters, A.I. Bush, C.C. Curtain, R. Cappai, D. Tew, Methionine oxidation: Implications for the mechanism of toxicity of the β-amyloid peptide from Alzheimer's disease. *Lett. Pept. Sci.* (2003), 10, 413-417. (b) M.E. Clementi, G.E. Martorana, M. Pezzotti, B. Giardina, F. Misiti, Methionine 35 oxidation reduces toxic effects of the amyloid β-protein fragment (31-35) on human red blood cell. *Int. J. Biochem. Cell Biol.* (2004), 36, 2066-2076. (c) C. Schőneich, D. Pogocki, G.L. Hug, K. Bobrowski, Free Radical Reactions of Methionine in Peptides: Mechanisms Relevant to β-Amyloid Oxidation and Alzheimer's Disease. *J. Am. Chem. Soc.* (2003), 125, 13700-13713. (d) F.E. Ali , F. Separovic, C.J. Barrow, R.A. Cherny, F. Fraser, A.I. Bush, C.L. Masters, K.J. Barnham, Methionine regulates copper/hydrogen peroxide oxidation products of Aβ**.** *J. Pep. Sci.* (2005), 11, 353-360. (e) F.E. Ali, K.J. Barnham, C.J. Barrow, F. Separovic, Copper catalysed oxidation of amino acids and Alzheimer's disease. *Lett.*

Pep. Sci. (2003), 10, 405-412. (f) D.A. Butterfield, A.I. Bush, Alzheimer's amyloid beta-peptide (1-42): involvement of methionine residue 35 in the oxidative stress and neurotoxicity properties of this peptide**.** *Neurobiol. Aging.* (2004), 25, 563-568.

10) K. Schuessel, S. Leutner, N.J. Cairns, W.E. Mueller, A. Eckert, Impact of gender on upregulation of antioxidant defense mechanisms in Alzheimer's disease brain. *J. Neural Trans.* (2004), 111, 1167-1182.

11) J. Apelt, M. Bigl, P. Wunderlich, R. Schliebs, Aging-related increase in oxidative stress correlates with developmental pattern of beta-secretase activity and beta-amyloid plaque formation in transgenic Tg2576 mice with Alzheimer-like pathology. *Inter. J. Develop.l Neurosci.* (2004), 22, 475-484.

12) J.T. Rogers, D.K. Lahiri, Metal and inflammatory targets for Alzheimer's disease. *Curr. Drug Targets* (2004), 5, 535-551.

13) D.R. Richardson, Novel chelators for central nervous system disorders that involve alterations in the metabolism of iron and other metal ions. *Ann. N.Y. Acad. Sci.* (2004), 1012, 326-341.

14) N.G.N. Milton, Role of hydrogen peroxide in the etiology of Alzheimer's disease: implications for treatment. *Drugs & Aging* (2004), 21, 81-100.

15) I.H. Cheng, J.J. Palop, L.A. Esposito, N. Bien-Ly, F. Yan, L. Mucke, Aggressive amyloidosis in mice expressing human amyloid peptides with the Arctic mutation. *Nature Med.* (2004), 10, 1190-1192.

16) K. Jin, V. Galvan, L. Xie, X.O. Mao, O.F. Gorostiza, D.E. Bredesen, D.A. Greenberg, Enhanced neurogenesis in Alzheimer's disease transgenic (PDGF-APPSw,Ind) mice. *Proc. Natl. Acad. Sci. USA* (2004), 101, 13363-13367.

17) D. Boyd-Kimball, R. Sultana, H. Mohmmad-Abdul, D.A. Butterfield, Rodent A beta(1-42) exhibits oxidative stress properties similar to those of human A beta(1-42): Implications for proposed mechanisms of toxicity. *J. Alzheimer's Dis.* (2004), 6, 515-525.

18) G.F.Z. da Silva, L.-J. Ming, Alzheimer's Disease-Related Copper(II)-β-Amyloid Peptide Exhibits Phenol Monooxygenase and Catechol Oxidase Activities. *Angew. Chem. Int. Ed.* (2005), 44, 5501-5504.

19) G.F.Z. da Silva, W.T. Tay, L.-J. Ming, Catechol Oxidase-Like Oxidation Chemistry of the 1-20 and 1-16 Fragments of Alzheimer's Disease-Related β-Amyloid Peptide: Their Structure-Activity Correlation and the Fate of Hydrogen Peroxide. *J. Biol. Chem.* (2005), 280, 16601-16609.

20) G.F.Z. da Silva, Ming L.-J, "Metallo-ROS" in Alzheimer's Disease*:* Metal-Centered Oxidation of Neurotransmitters by CuII-β-Amyloid Provides an Alternative Perspective for the Neuropathology of Alzheimer's Disease. *Angew. Chem. Int. Ed.* (2007), 46, in press.

21) C.D. Syme, R.C. Nadal, S.E.J. Rigby, J.H. Viles, Copper Binding to the Amyloid-β (Aβ) Peptide Associated with Alzheimer's Disease. Folding, Coordination Geometry, pH Dependence, Stoichiometry, and Affinity of Aβ(1–28): Insights from a Range of

Complementary Spectroscopic Techniques. *J. Biol. Chem*. (2004)**,** 279, 18169–18177.

22) (a) E.A. Lewis, W.B. Tolman, Reactivity of dioxygen-copper systems. *Chem. Rev.* (2004), 104, 1047-1076. (b) W.B. Tolman, Making and breaking the dioxygen O–O bond: New insights from studies of synthetic copper complexes. *Acc. Chem. Res.* (1997), 30, 227–237.

23) C. Gerdemann, C. Eicken, B. Krebs, The crystal structure of catechol oxidase: New insight into the function of type-3 copper proteins. *Acc. Chem. Res.* (2002), 35, 183-191.

24) S.G. Srivatsan, P. Nigam, M.S. Rao, S. Verma, Phenol oxidation by copper-metallated 9-allyladenine-DVB polymer: reaction catalysis and polymer recycling. *Applied Catal. A: General* (2001), 209, 327-334.

25) Leskovac V. Comprehensive Enzyme Kinetics. Kluwer/Plenum, Boston, MA (2002).

26) S. Stoll, A. Schweiger, EasySpin, a comprehensive software package for spectral simulation and analysis in EPR**,** *J. Mag. Res.* (2006), 178, 42.

27) N.D. Chasteen, P.A. Snetsinger, ESEEM and ENDOR Spectroscopy In Physical Methods in Bioinorganic Chemistry, Spectroscopy and Magnetism, L. Que Jr. Ed.; University Science Books, (2000).

28) J.W. Karr, H. Akintoye, L.J. Kaupp, V.A. Szalai, N-Terminal Deletions Modify the Cu^{2+} Binding Site in Amyloid-β. *Biochemistry* (2005), 44, 5478 – 5487.

29) J.S. Valentine J.S. in Bioinorganic Chemistry (I. Bertini, H.B. Gray, S.J. Lippard, J.S. Valentine Eds.) pp. 253-313, University Science Books, Mill Valley, CA (1994).

30) C. Schöneich, Methionine oxidation by reactive oxygen species: reaction mechanisms and relevance to Alzheimer's disease. *Biochim. Biophys. Acta* (2005), 1703, 111-119.

31) K. Várnagy, B. Bóka, I. Sóvágó, D. Sanna, P. Marras, G. Micera, Potentiomentric and spectroscopic studies on the copper(II) and nickel(II) complexes of tripeptides of methionine. *Inorg. Chim. Acta.* (1998), 275-276, 440-446.

32) C.C. Curtain, F. Ali, I. Volitakis, R.A. Cherny, R.S. Norton, K. Beyreuther, C.J. Barrow, C.L. Masters, A.I. Bush, K.J. Barnham, Alzheimer's disease amyloid-β binds copper and zinc to generate an allosterically ordered membrane-penetrating structure containing superoxide dismutase -like subunits. *J. Biol. Chem.* (2001), 276, 20466-20473.

33) (a) D.M. Dooley, C.E. Coté, Inactivation of beef plasma amine oxidase by sulfide.*J. Biol. Chem.* (1984), 259, 2923-2926. (b) L. Morpurgo, A. Desideri, A. Rigo, R. Viglino, G. Rotilio, Reaction of N,N-diethyldithiocarbamate and other bidentate ligands with Zn, Co and Cu bovine carbonic anhydrases. Inhibition of the enzyme activity and evidence for stable ternary enzyme-metal-ligand complexes. *Biochim.Biophys. Acta* (1983), 746, 168-175. (c) S. Suzuki, T. Sakurai, A. Nakahara, O. Oda, T. Manabe, T. Okuyama, Copper binding site in serum amine oxidase treated with sodium diethyldithiocarbamate. *Chem. Lett.* (1982), 487-490. (d) L. Morpurgo, G. Rotilio, A. Finazzi Agrò, B. Mondovi, Anion complexes of copper(II) bovine carbonic anhydrase. *Arch. Biochem. Biophys.* (1975), 170, 360-367. (e) L. Morpurgo, A. Finazzi Agrò, G. Rotilio, B. Mondovi, Anion complexes of copper(II) and cobalt(II) bovine carbonic anhydrase as models for the copper site of blue copper

proteins. *Eur. J. Biochem.* (1976), 64, 453-457. (f) J. Peisach, W.E. Blumberg, Structural implications derived from the analysis of electron paramagnetic resonance spectra of natural and artificial copper proteins. *Arch. Biochem. Biophys*. (1974), 165, 691–708. (g) F. Jian, J. Peisach, L.-J. Ming, L. Que Jr., V.J. Chen, Electron Spin Echo Envelope Modulation Studies of the Cu(II)-Substituted Derivative of Isopenicillin N Synthase, a Structural and Spectroscopic Model. *Biochemistry* (1991), 30, 11437–11445.

34) S.S. Eto, J. Dubach, G.R. Eaton, G. Thurman, D.R. Ambruso, Electron Spin Echo Envelope Modulation Evidence for Carbonate Binding to Fe(III) and Cu(II) Transferrin and Lectoferrin. *J. Biol. Chem.* (1990), 265, 7138–7141.

35) (a) H. Li, S.P. Webb, J. Ivanic, J.H. Jensen, Determinants of the relative reduction potentials of type-1 copper sites in proteins. *J. Am Chem. Soc.* (2004), 126, 8010-8019. (b) J.F. Hall, L.D. Kanbi, R.W. Strange, S.S. Hasnain, Role of the axial ligand in type 1 Cu centers studied by point mutations of Met148 in rusticyanin. *Biochemistry* (1999), 38, 12675-12680.

36) (a) W. Fu, H. Luo, S. Parthasarathy, M.P. Mattson, Catecholamines potentiate amyloid β-peptide neurotoxicity: involvement of oxidative stress, mitochondrial dysfunction, and perturbed calcium homeostasis. *Neurobiol. Disease* (1998), 5, 229-243. (b) J.I. Friedman, D.N. Adler, K.L. Davis, The role of norepinephrine in the pathophysiology of cognitive disorders: potential applications to the treatment of cognitive dysfunction in Schizophrenia and Alzheimer's disease. *Biol. Psychiatry* (1999), 46, 1243-1252. (c) R.J. Gruen, J. Ehrlich, R. Silva, J.W. Schweitzer, A.J.

Friedhoff , Cognitive factors and stress-induced changes in catecholamine biochemistry. *Psychiatry Res.* (2000), 93, 55-61. (d) H. Umegaki, N. Tamaya, T. Shinkai, A. Iguchi, The metabolism of plasma glucose and catcholamines in Alzheimer's disease. *Experiment. Gerontol.* (2000), 35, 1373-1382.

37) D.B. Calne, J.W. Langston, Aetiology of Parkinson's disease. *Lancet* (1983), 322, 1457-1459.

38) (a) N. Ohtani, T. Goto, C. Waeber, P.G. Bhide, Dopamine modulates cell cycle in the lateral ganglionic eminence. *J. Neurosci*. (2003), 23, 2840–2850. (b) A. Borta, G.U. Höglinger, Dopamine and adult neurogenesis. *J. Neurochem.* (2007), 100, 587–595.

39) (a) Graham, D.G. (1978) Oxidative pathways for catecholamines in the genesis of neuromelanin and cytotoxic quinones. *Mol. Pharmacol*. 14, 633-643. (b) Graham D.G., Tiffany S.M., Bell W.R.Jr., Gutknecht W.F. (1978) Autooxidation versus covalent binding of quinones as the mechamism of toxicity of dopamine, 6-hydroxydopamine and related compounds toward C1300 neuroblastoma cells *in vitro. Mol. Pharmacol.* 644-653. (c) Hastings T.G. (1995) Enzymatic oxidation of dopamine: the role of prostaglandin H synthase. *J. Neurochem.b* 919-924.

40) (a) M.J. LaVoie, T.G. Hastings, Dopamine quinone formation and protein modification associated with the striatal neurotoxicity of methamphetamine: Evidence against a role for extracellular dopamine. *J. Neurosci.* (1999), 19, 1484-1491. (b) I. Santa-Maria, F. Hernandez, M.A. Smith, G. Perry, J. Avila, F.J. Moreno, Neurotoxic dopamine quinone facilitates the assembly of tau into fibrillar polymers. *Mol. Cell. Biochem.* (2005), 278, 203-212.

41) S.B. Berman, M.J. Zigmond, T.G. Hastings, Modification of dopamine transporter function: effect of reactive oxygen species and dopamine. *J. Neurochem*. (1996), 67, 593-600.

CHAPTER VI. THE ASTACIN FAMILY OF ENDOPEPTIDASES AND EMBRYOGENESIS

I. INRODUCTION

The astacin family of zinc-dependent endopeptidases is a class of enzymes ubiquitously distributed across all phyla and part of the superfamily of metzincins.[1] Approximately thirty members of the astacin family have been characterized at the protein level, including meprins, bone morphogenetic protein-1 (BMP-1), and tolloid while several others have been identified through gene sequencing, including a large number in *Caenorhabditis. elegans*.[2] The signature active site sequence for this family of enzymes is **H**EXX**H**GXX**H**EXXRXDR (Figure 6.1), where one Zn^{2+} atom coordinates to three histidines, a tyrosine, and a water molecule (Figure 6.2).[3] Most members share common expression features such as the pre- and pro-enzyme sequences immediately located NH_2-

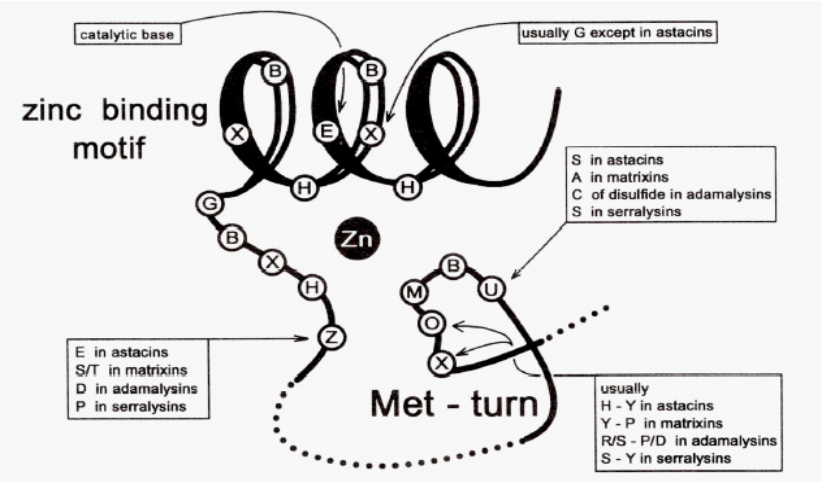

Figure 6.1. Active site motif common to all astacins.[2]

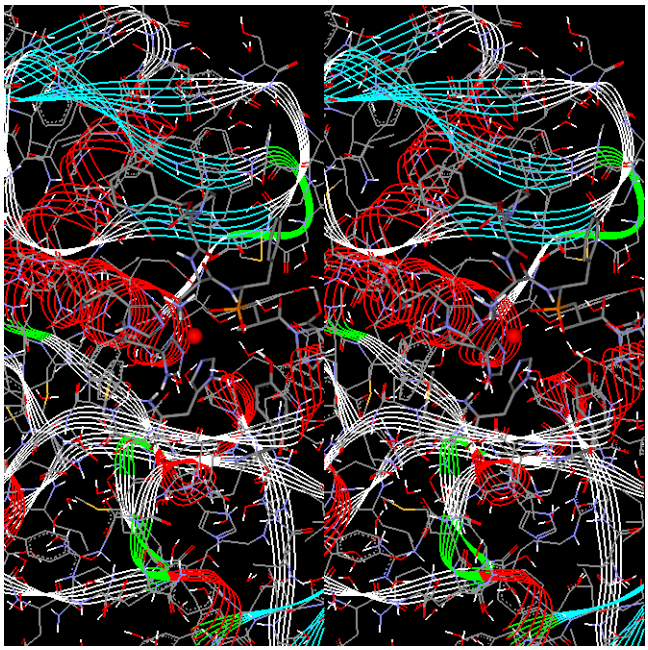

Figure 6.2. Relaxed eye stereo view of the active-site structure of astacin with transition state analogue (PDB ID 1QJI).

terminal to the protease domain. Several members contain one or two copies of epidermal growth factor EGF-like domains, and complement-like domains (Clr, Cls) near the COOH-terminus. The shuffling of different domains in relation to the catalytic (protease or astacin) domain creates a variety of proteins with several different structures and functions.

Embryo development is an area which remains unresolved in a number of more complex animals, including human embryogenesis and other representatives of sub-phylum vertebrata due to the inherent complexities of deuterostome embryogenesis. The challenge of resolving proteolytic signaling, that is likely responsible for modification of the extra cellular matrix (ECM), important in embryogenesis events, has partially been due to the lack of convenient model systems; a particular challenge is the isolation of ECM components in pure form in mice and human models. Sea-urchins hence are a good model system for the study of morphogenesis due to the facility of isolation of pure and large amounts of protein components of the ECM.[4] Another advantage of the sea-urchin model is that its genome has recently been sequenced which will facilitate the connection of upstream genetic events with its downstream message and proteolytic mechanisms. The presence of several astacin family enzymes in the development of the sea-urchin embryo (i.e. suBMP, SpAN, envelysin, and BP10) makes it a target to study similar proteolytic processes in higher organisms, especially those containing enzymatic processes analogous to tolloid and BMP-1, two enzymes proposed to be similar to BP10 in structure.[5,6] BP10 is an interesting enzymatic model system because it contains similar

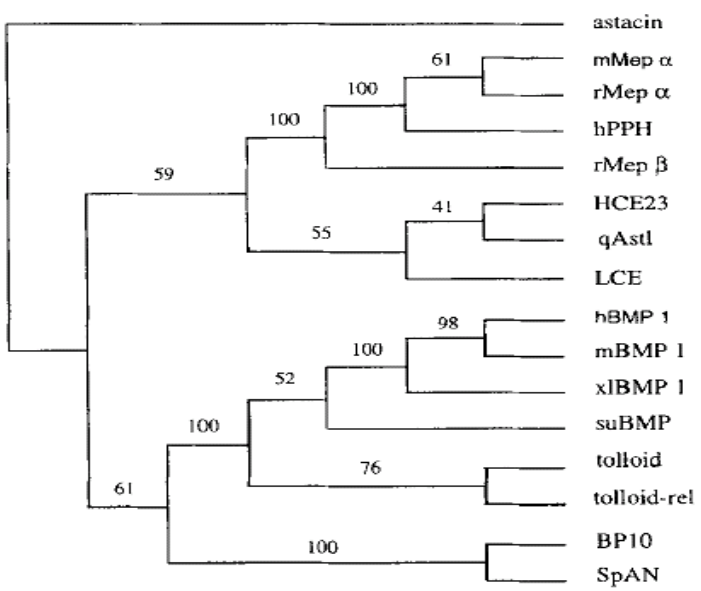

Figure 6.3. Phylogeny of the astacin family catalytic domains.[6]

domains as other complex astacins such as tolloid and BMP-1, but is unique in domain arrangement which will be discussed further.[5]

Originally characterized by the use of immunoblotting techniques and sequence analysis of the gene and m-RNA transcript,[5, 6] BP10 has remained an unstudied member of this class of enzymes. The focus of research has shifted to other members of the astacin class of enzymes (astacin itself being a crayfish digestive enzyme and hence only a novel prototype in catalytic mechanism) such as BMP-1 and tolloid due to their potential role in unraveling developmental information about human embryos (BMP-1) and the facility of handling a well established model system (tolloid from *Drosophila*). However, from an evolution standpoint, echinoderms (Echinodermata, the deuterostomes) are more closely related to humans than a fruitfly (Arthropoda, the ecdysozoans).[7] BP10 hence is a good candidate as a functional model system of BMP-1 and tolloid. The transcription of the BP10 gene is transiently activated around the 16- to 32-cell stage and the accumulation of BP10 m-RNA is limited to a short period at the blastula stage. Temporarily, the highest BP10 activity is detected approximately 1.5 hours after expression of the sea urchin hatching enzyme (envelysin) reaches a maximum.[5] The BP10 transcripts are spatially expressed and only detected in a limited area of the blastula in the animal half of the embryo. The protein is first detected in early blastula stages. Its level reaches a peak in late cleavage, and declines abruptly before ingression of primary mesenchyme cells and remains constant in late development.[5] The likely role of zymogen activator has been assigned to BP10, since the presence of an EGF domain is a highly conserved motif in proteolytic cascades or activation of precursors.[8] However, it was

accurately described[5] that blocking BP10 activity prior to hatching with the use of an antibody resulted in deformed embryos, whereas after hatching the embryos developed normally when treated with the same antibody, though basal levels of the enzyme can be detected after hatching.

The morphogenetic studies conducted by Runnström and Horstadius determined that developmental processes occur across a gradient in where the ectodermal structures are controlled by the animal axis and the mesodermal (skeleton) is controlled by the vegetal pole. This established model has been challenged by recent studies.[9,10] Hence it becomes clear that sole analysis of gene structure and transcriptional levels is not enough to provide irrefutable evidence about animal development. A multi-disciplinary approach is needed where the skills of a developmental biologist and the detailed information about structure/function of enzymes that a biochemist can provide are needed in order to fully understand such questions.

The BP10 protease is constructed of identical domains as BMP-1 and tolloid, and is described as a factor involved in cell differentiation in mid to late blastula. Human BMP-1 has been characterized as a splice variant of the tolloid gene which is required for correct dorsal-ventral patterning of the *Drosophila* embryo. In preliminary studies, BP10 has not been shown to affect axis formation; hence the structure/function paradox does not hold true for BP10, BMP-1, and tolloid. How do similar global mechanisms of development differ at the molecular level? What are the mechanisms of evolution

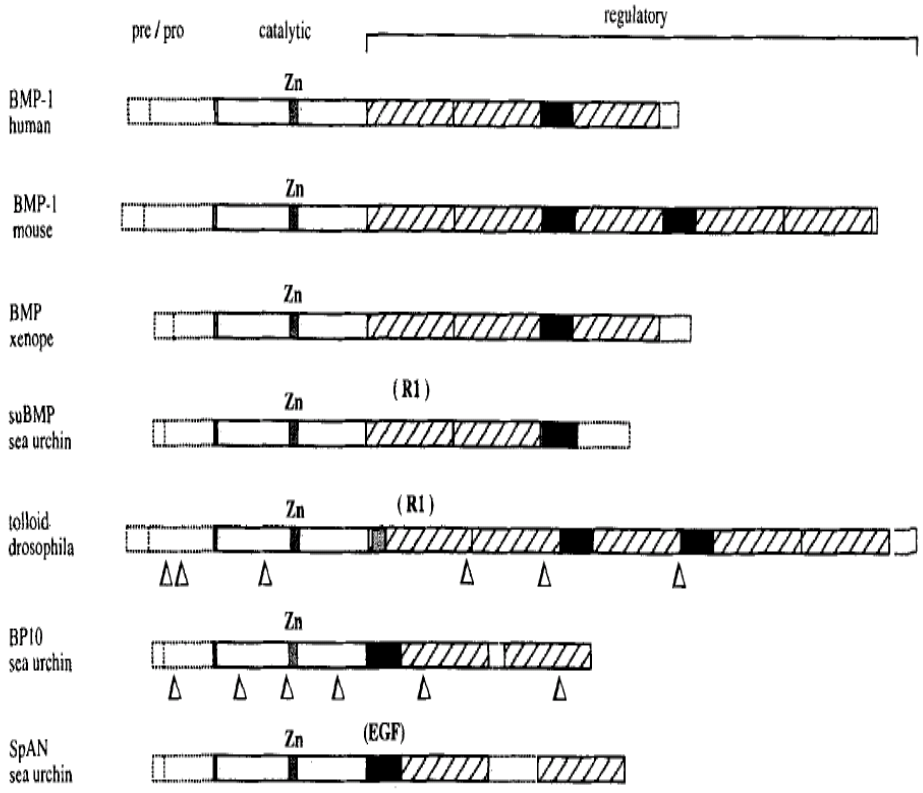

Figure 6.4. Domain organization of proteins from the astacin/CUB/EGF subfamily.[6]

involved in animal development across the deuterostomes? And finally, what are the regulatory networks during embryogenesis in humans, sea-urchins, and *Drosophila*?

BMP-1 has been assigned the role of a procollagen C-protease and its minimal domain structures necessary for activity and secretion have been identified.[11] However BMP-1 is also able to cleave non-collagenous substrates such as dentin and laminin, hinting at a wide distribution of biological regulation factors that may be attributed to this enzyme.[12-15] BP10 may serve a similar purpose in the sea urchin embryo. The developmental regulation of BP10 expression shows that it is an important and necessary event in embryogenesis.[5] Recent studies have also shown that another astacin family enzyme found in sea urchins, SpAN, is able to regulate BMP signaling.[16] BP10 may be part of the signaling events which involve the enzymes suBMP, SpAN and BP10 itself, or perhaps play the role as a less discriminate activator of other important molecular events.

Since BP10 is homologous to tolloid and BMP-1 (Figure 6.4), it is possible that the sea urchin enzyme is part of a regulatory set of interactions with polypeptides of the TGF-β family. The involvement of BP10 in a process similar to that of BMP-1 is unlikely and most likely resembles tolloid in function.[5] However, the high similarity in sequence and structural motifs makes BP10 an important comparison model in a lower species. The mammalian BMP-1-related proteases are all capable of activating the TGF-β protein growth differentiation factor (myostatin), by freeing it from a noncovalent latent complex with its cleaved prodomain.[17] Similarly, BMP-1 and the splice variant mTLL-1 but not tolloid or TLL-2 is able to free the TGF-β morphogens BMP-2 and BMP-4 from latent complexes with the extracellular antagonist chordin.[18] Thus, BMP-1/tolloid-like

proteases may orchestrate formation of the ECM with signaling by various TGF-β-like proteins in morphogenetic events.

BP10 is also a unique system that may contribute important information about the relationship of structural features such as EGF-Ca^{2+} binding domain and its CUB domains and the catalytic domain of these proteases (Figure 6.2). It is unique to BP10 that the EGF-Ca^{2+} domain is located between the catalytic domain and the proposed regulatory sequences of CUB1 and CUB2. Often, these EGF-Ca^{2+} domains are located between CUB sequences. CUB domains have been implicated both in activity and regulation in BMP-1.[11] The kinetic properties of BP10 should then compare and contrast nicely with those of other BMP-1 and tolloid-like proteins. Ca^{2+} may have a synergistic effect on the reaction catalyzed by BP10 due to its close proximity to the catalytic domain.

From a protein evolution viewpoint, BP10 contains modules proposed to be involved in the domain shuffling (i.e evolution through exon shuffling). Characterization of BP10 with simultaneous analysis of its gene structure will add further insight into this mechanism. Moreover, once other sea urchin enzymes involved in embryogenesis, such as SPAN and suBMP are overexpressed and characterized, and their gene structures fully characterized, a better model of module domain shuffling protein evolution can be presented, since BP10, SPAN and suBMP are part of the same family of enzymes, acting in the same organism, and involved in some functional role during embryogenesis.

In the case of astacin, BMP-1, tolloid, and BP10, the presence of a metal-coordinated tyrosine is a rather unusual mechanistic motif due to the reduction of Lewis

acidity induced by the coordination of a negatively charged phenolate to the metal center.[19, 20] This is not the case in astacin where the coordination of the Tyr-phenolate under physiological conditions does not affect its catalysis under neutral conditions.[21,22] A metallotriad mechanism has been proposed based on kinetic, optical, and EPR studies on the Cu^{2+} derivatives of astacin and serralysin.[21, 22] Further analysis of the physical characteristics of astacin-type enzymes using spectroscopically-active metal substitutes in concert with classical enzyme kinetics (i.e. pH profiles, inhibition studies, etc.) analysis of splice variants of recombinant BP10 (whole enzyme and astacin domain truncation) will add further insight into the catalytic mechanism of these enzymes. Concomitant with physical studies on the native system, active site mutants will allow for comparison both in kinetic parameters and the physical properties of BP10. Previous site directed mutagenesis studies have been conducted; however, the choice of mutations have shed no actual mechanistic insight toward the catalytic mechanism of astacins, other than establishing that the conserved glutamate and tyrosine residues are catalytically important.[23] The status of the coordinated tyrosine has been proposed to be an inhibitory process in the metal centered hydrolysis of peptide bonds.[22] In this proposed metallotriad mechanism (Figure 6.5), the active-site Zn^{2+} coordinated by three His, tyrosine, and a water molecule can be activated via detachment of the phenolate with a concomitant

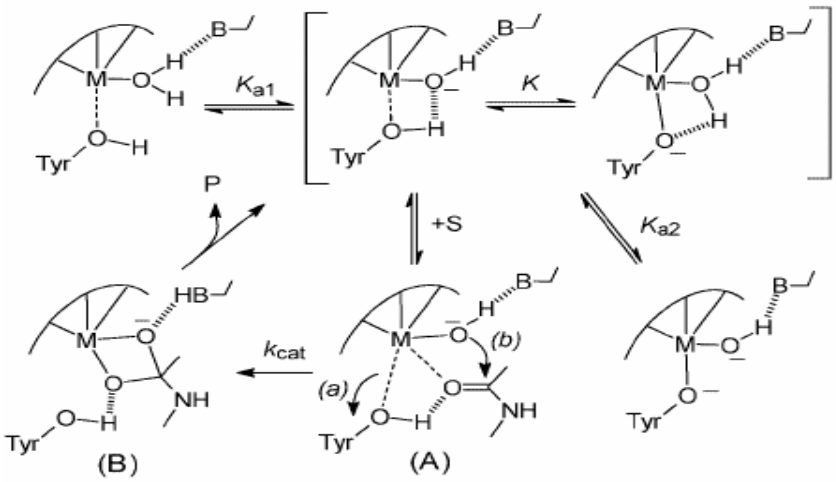

Figure 6.5. Proposed metallotriad mechanism in astacin and serralysin.[22]

general base deprotonation via a glutamate residue. The metal bound OH^- is able to attack and hydrolyze the scissile bond after Zn^{2+} creating electrostatic strain in the peptide bond by interaction with the carbonyl of the scissile bond. The confirmation of this mechanism can shed valuable insight into numerous enzymatic processes across all members of the astacin family, from the numerous astacin-like enzymes in *C.elegans* to the astacin/EGF/CUB members in higher organisms.

IV. LIST OF REFERENCES

1) J.S. Bond, R.J. Beynon, The astacin family of metalloendopeptidases. *Prot. Sci.* (1995), 4, 1247-1261.

2) F. Moehrlen, H. Hutter, R. Zwilling, The astacin protein family in *Caenorhabditis elegans*. *Euro. J. Biochem.* (2003), 270, 4909-4920.

3) F.X. Gomis-Rüth, W. Stöcker, H. Huber, R. Zwilling, W. Bode, Refined 1.8 Å X-ray crystal structure of astacin, a zinc-endopeptidase from the crayfish *Astacus astacus* L.: Structure determination, refinement, molecular structure amd comparison with thermolysin. *J. Mol. Biol.* (1993), 229, 945-968.

4) V.D. Vacquier, Isolation and preliminary analysis of the hyaline layer of sea urchin eggs. *Exp. Cell Res.*, (1969), 54, 140-2.

5) T. Lepage, C. Ghiglione, C. Gache, Spatial and temporal expression pattern during sea urchin embryogenesis of a gene coding for a protease homologous to the human protein BMP-1 and to the product of the Drosophila dorsal-ventral patterning gene tolloid. *Development* (1992), 114, 147-163.

6) T. Lepage, C. Ghiglione, C. Gache, Structure of the gene encoding the sea urchin blastula protease 10 (BP10), a member of the astacin family of Zn^{2+}-metalloproteases. *Eur. J. Biochem.* (1996), 238, 744-751.

7) S.F. Gilbert, Developmental Biology, 6th Ed., Sinauer, Sunderland, MA, (2000).

8) E. Appella, I.T. Weber, F. Blasi, Structure and function of epidermal growth factor-like regions in proteins. *FEBS letters* (1988), 231, 1-4.

9) E.H. Davidson, Lineage Specific gene expression and the regulative capacities of the sea urchin embryo: aproposed mechanism. *Development* (1989), 105, 421-445.

10) F.H. Wilt, Determination and morphogenesis in the sea urchin embryo. *Development* (1987), 100, 559-576.

11) N. Hartigan, L. Garrigue-Antar, K.E. Kadler, Bone morphogentic protein-1 (BMP-1): Identification of the minimal domain structure for procollagen C-proteinase acivity. *J. Biol. Chem.* (2003), 278, 18045-18049.

12) E. Kessler, K. Takahara, L. Biniaminv, M. Brussel, D.S. Greenspan, Bone morphogentic protein-1: the type I procollagen C-proteinase. *Science* (1996), 271, 360-362.

13) A. Borel, D. Eichenberger, J. Farjanel, E. Kessler, C. Gleyzal, D.J. Hulmes, P. Sommer, B. Font, Lysyl-oxidase-like protein from bovine aorta. Isolation and maturation to to an active form by bone morphogenetic protein-1. *J. Biol. Chem.* (2001), 276, 48944-48949.

14) S. Amano, I.C. Scott, K. Takahara, M. Koch, M.F. Champliaud, D.R. Gerecke, D.L. Hudson, T. Nishiyama, S. Lee, D.S. Greesnpan, Bone morphogenetic protein 1 is an extracellular processing enzyme of the 5γ2 chain. *J. Biol. Chem.* (2000), 275, 22728-22735.

15) N. Suzuki, P.A. Labosky, Y. Furuta, L. Hargett, R. Dunn, A.B. Fogo, K. Takahara, D.M. Peters, D.S. Greenspan, B.L.Hogan, Failure of ventral body wall closure in mouse embryos lacking a procollagen C-proteinase encoded by Bmp1, a mammalian gene related to Drosophila tolloid. *Development* (1996), 122, 3587-3595.

16) F.C Wardle, L.M. Angerer, R.C. Angerer, L. Dale, Regulation of BMP signaling by the BMP1/TLD-related metalloprotease, SpAN. *Develop. Biol.* (1999), 206, 63-72.

17) N. Wolfman, A.C. McPherron, W.N. Papppano, M.V. Davies, K. Song, K.N. Tomkinson, J.F. Wright, L. Zhao, S.M. Sebald, D.S. Greenspan, S.J. Lee, Activation of latent myostatin by the BMP-1/tolloid family of metalloproteinases. *Proc. of the Natl. Acad. Sci. USA* (2003), 100, 15842-15846.

18) I.C. Scott, I.L. Blitz, W.N. Pappano, Y. Imamura, T.G. Clark, B.M. Steiglitz, C.L. Thomas, S.A. Maas, K. Takahara, K.W.Y. Cho, D.S. Greenspan, Mammalian BMP-1/Tolloid-Related Metalloproteinases, Including Novel Family Member Mammalian Tolloid-Like 2, Have Differential Enzymatic Activities and Distributions of Expression Relevant to Patterning and Skeletogenesis. *Develop. Biol*. (1999), 213, 283-300.

19) E. Kimura, Macrocyclic Polyamine Zinc(II) Complexes as Advances models for Zinc(II) enzymes. *Prog. Inorg. Chem*. (1994), 41, 443.

20) E. Kimura, T. Koike, Intrinsic Properties of zinc(II) ion pertinent to zinc enzymes. *Adv. Inorg. Chem.* (1997), 44, 229.

21) H.I. Park, L.J. Ming, The mechanistic role of coordinated tyrosine in astacin. *J. Inorg. Biochem.* (1998), 72, 57-62.

22) H.I. Park, L.J. Ming, Mechanistic studies of the astacin-like Serratia metalloendopeptidase serralysin: highly active (>2000%) Co(II) and Cu(II) derivatives for further corroboration of a "metallotriad" mechanism. *J. Bio. Inorg. Chem*. (2002), 7, 600-610.

23) I. Yiallouros, B.E. Grosse, W. Stöcker, The roles of Glu93 and Tyr149 in astacin-like zinc peptidases. *FEBS Letters* (2000), 484, 224-228.

CHAPTER VII. OVEREXPRESSION AND CHARACTERIZATION OF BLASTULA PROTEASE 10 (BP10) FROM *PARACENTROTUS LIVIDUS*[1]

I. INTRODUCTION

Blastula Protease 10 (BP10) is a metalloenzyme assigned to the astacin family of Zn-dependent endopeptidases involved in sea urchin embryogenesis. It contains conserved structural motifs consistent with astacin, tolloid, and bone morphogenetic protein 1 (BMP-1). Astacin, a gut enzyme, and serralysin, a bacterial enzyme, have been proposed to carry out hydrolysis via a "metallotriad" mechanism that involves a metal-coordinated tyrosine. It has not been determined if the more structurally complex members of this family involved in eukaryotic development share this mechanism. The recombinant BP10 has been overexpressed in *E.coli*, its metalloenzyme nature confirmed, and its catalytic properties characterized through kinetic studies. BP10 shows significant

[1] This work has been published: G.F.Z. da Silva, R.L. Reuille, L.-J. Ming, B.T.Livingston *J. Biol. Chem.* **2006** 281, 10737-10744.

hydrolysis toward gelatin both in its native Zn-containing form and copper derivative. The copper derivative of BP10 shows a remarkable 960 % rate-acceleration toward the hydrolysis of the synthetic substrate N-benzoyl-arginine-p-nitroanilide when compared to the Zn form. The enzyme also shows calcium-dependent activation. These are the first thorough mechanistic studies reported on BP10 as a representative of the more structurally complex members of astacin-type enzymes in deuterostomes which can add supporting data to corroborate the metallotriad mechanism proposed for astacin.

The astacin family of zinc-dependent endopeptidases is a class of enzymes ubiquitously distributed across all phyla and part of the superfamily of metzincins.[1] Approximately thirty members of the astacin family have been characterized at the protein level;[2] including meprins, bone morphogenetic protein-1 (BMP-1), and tolloid, while several others have been identified through gene sequencing, including a large number in *Caenorhabditis elegans*.[3] The signature of the primary sequence active site motif for this family of enzymes is **H**EXX**H**GFX**H**EXXRXDR, where one Zn^{2+} ion coordinates with three histidines, a tyrosine, and a water molecule.[4, 5] Most members of this family share common domain structures such as the pre- and pro-enzyme sequences immediately located N-terminal to the protease domain. Several members contain one or two copies of epidermal growth factor EGF-like domains, and complement-like domains (Clr, Cls) near the C-terminus.[2] The shuffling of different domains in relation to the catalytic protease domain creates a variety of proteins with different structures and functions.

Originally isolated and characterized as a developmentally regulated gene in sea urchin embryos,[6,7] BP10 protein has remained uncharacterized. It shares sequence similarity with other members of the astacin family of enzymes. The simplest member of the family, astacin from crayfish digestive fluid is a digestive enzyme and hence a novel prototype in catalytic mechanism important in development such as BMP-1 in vertebrates and tolloid in *Drosophila*. Whereas BP10 is a good candidate as a functional model system of BMP-1 and tolloid. The BP10 protease is constructed of identical domains as BMP-1 and tolloid, but has different arrangement of these domains. The transcription of the BP10 gene is transiently activated around the 16- to 32-cell stage and the accumulation of BP10 mRNA is limited to a short period at the blastula stage. Temporarily, the highest BP10 activity is detected approximately 1.5 hours after expression of the sea urchin hatching enzyme (envelysin) reaches a maximum.[6] The BP10 transcripts are detected in a limited area of the blastula. The protein is first detected in early blastula stages, its level peaks in late cleavage, declines abruptly before ingression of primary mesenchyme cells, and remains invariable in late development.[6] A likely role of zymogen activator has been suggested for BP10, since the presence of an EGF domain is a highly conserved motif in proteolytic cascades or activation of precursors.[8] Blocking BP10 activity prior to hatching with the use of an antibody resulted in abnormal embryos.

BP10 has a unique arrangement of structural features[6, 7] such as EGF-Ca^{2+} binding domain, two adjacent CUB domains, and a catalytic domain that is highly homologous to astacin. In particular, the EGF-Ca^{2+} domain is located between the

catalytic domain and the proposed regulatory CUB sequences. More often, these EGF-Ca^{2+} domains are located between CUB sequences. CUB domains have been implicated in activity and regulation in BMP-1.[9] Astacin family enzymes and serine proteases have been implicated in remodeling the pericellular space in sea urchin embryos, which is composed of the extracellular matrix and transmembrane proteins.[10, 11] Moreover, several studies have reported gelatinase and collagenase activities from enzymes located in the sea urchin egg and embryo which were characterized as metalloenzymes due to inactivation with EDTA and 1, 10-phenanthroline.[12-15]

Beside the interesting distribution of astacin-like enzymes across phyla and the numerous functional roles of these enzymes, mechanistic questions about these highly conserved hydrolases domains still remain to be answered. Within the metzincin superfamily of enzymes, minor differences of active site function have been observed, which are likely to account for different substrate specificities.[16] In the case of astacin as well as BMP-1, tolloid and BP10, a metal-coordinated tyrosine is a rather unusual metal-binding motif due to the reduction of Lewis acidity induced by the coordination of the negatively charged phenolate to the metal center.[17, 18] However, the coordination of the Tyr-phenolate does not seem to affect astacin catalysis under neutral conditions. The status of the coordinated tyrosine has been proposed to be an inhibitory process in the metal centered hydrolysis of peptide bonds.[5] A metallotriad mechanism has been proposed for astacin and serralysin based on kinetic and spectroscopic studies of the native enzymes and their Cu^{2+} derivatives.[5,19] In the proposed metallotriad mechanism, the active-site Zn^{2+} coordinated by three His, a tyrosine, and a water molecule can be

activated via detachment of the Tyr-phenolate with a concomitant deprotonation of the coordinated water assisted by a glutamate residue. The metal-bound OH^- is able to hydrolyze the scissile bond with Zn^{2+} creating electrostatic strain in the peptide bond by interaction with the carbonyl group of the scissile bond. I discuss in this chapter the overexpression and thorough mechanistic study of recombinant BP10, a model system for astacin-type developmentally regulated metalloenzymes. Further analysis of BP10 will add insight into the catalytic mechanism of members of the astacin family of enzymes, and the degree to which the mechanism is conserved among the enzymes found in deuterostomes.

II. EXPERIMENTAL

The expression vector pQE30Xa, Ni-NTA agarose, mouse anti-His primary antibody were from Qiagen (Valencia, CA), XL1-Blue chemically competent *E. coli* from Invitrogen (Carlsbad, CA), Rosetta Blue chemically competent *E. coli* and Factor Xa removal kit were from Novagen (San Diego, CA), all primers were from Integrated DNA Technologies (Coralville, IA), all modifying and restriction enzymes were from Promega (Madison, WI), Eppendorf Perfect plasmid preparation kit was from Eppendorf (Westbury, NY), BM purple phosphatase substrate was from Roche (Indianapolis, IN), EDTA, $ZnCl_2$, $Cu(NO_3)$, $Ca(NO_3)_2$, glycerol, ninhydrin, guanidine hydrocholoride, bovine serum albumin, sodium dodecyl sulfate, Triton X-100, Tween 20, imidazole, NaH_2PO_4, Na_2HPO_4, Tris-HCl, acrylamide, bis-acrylamide, TEMED, ammonium

persulfate, NaN_3, dimethyl sulfoxide (Me_2SO), sodium citrate, acetic acid, guanidine hydrochloride, and propanol were from Fisher (Swanee, GA), Type A porcine gelatin 300 bloom, N-benzoyl-arginine-*p*-nitroanilide (BAPNA), urea, isopropyl-β-thiogalactopyronoside (IPTG), phenylmethyl sulfonyl fluoride (PMSF), benzamidine, urea, lysozyme, bicinchoninic acid, arginine-hydroxamate, and HEPES, CAPS, TAPS, and MES buffers were from Sigma-Aldrich (St. Louis, MO), 1,10-phenanthroline was from Acros (Fairlawn, NJ). All reagents were of enzyme or molecular biology grade when available, all others were reagent grade. All glassware and plasticware were extensively rinsed with EDTA to remove metal contaminants and thoroughly washed with 18 MΩ water to remove the chelator. All buffers contained Chelex resin to remove metal contaminants. All spectrophotometric measurements were performed on a Varian CARY 50 Bio-Spectrophotometer equipped with a PCB-150 water Peltier thermostable cell holder.

Overexpression, purification, and refolding of recombinant BP10: The cDNA coding for *Paracentrotus lividus* BP10 cloned into the pBluescript plasmid (pBP10) was a generous contribution from Christian Gache and Thierry Lepage (Unité de Biologie Cellulaire, Center National de la Recherche Scientifique et Université de Paris VI, Station Marine, 06230 Villefranche-sur-Mer, France). PCR primers coding for both 5' and 3' regions were designed according to the proposed full length BP10 to subclone the cDNA into the pQE30Xa overexpression vector. The 5' primer: 5'-PO_4-AAACTAATACTTTCCCTTTCGGGATTG-3' codes for the first 9 codons in the proposed nucleotide sequence in BP10 and is 5' phosphorylated for blunt-end cloning

using the *Stu*I restriction site in pQE30Xa; 3' primer was designed for cloning into the *Xma*I restriction site 5'-**AATT**<u>CCCGGG</u>**<u>TTA</u>**GTTCAGACGAGGATCTC GGGT-3' (bold = extra base pairs for melting temperature optimization, underlined = *Xma*I restriction site, bold underlined = stop codon). The PCR product coding for BP10 was digested with *Xma*I and cloned into the pQE30Xa vector. The BP10 construct was transformed into Rosetta Blue competent cells. The colonies overexpressing recombinant BP10 were screened using a colony lift protocol according to Qiagen without modifications, where the production of BP10 was monitored using a mouse anti-His tag primary antibody. The active colonies were picked, propagated in liquid media to OD_{600} = 0.4. IPTG was added to a final concentration of 1.0 mM and the culture grown at 30 °C and 300 rpm for 4.5 hours. The bacteria containing recombinant BP10 were pelleted at 4,000×g at 4 °C and resuspended in cell wall lysis buffer (50.0 mM NaH_2PO_4, 100.0 mM NaCl, 10.0 mM imidazole, 2.0 mM benzamidine, 2.0 mM PMSF, pH 8.0) containing 1.7 mg/mL lysozyme and incubated on ice lightly shaking for 60 minutes, then sonicated 6 × 10 seconds with 10 second intervals. The cultures were pelleted at 10,000×g at 4 °C for 20 minutes and the inclusion bodies were resuspended in an urea buffer (8.0 M urea, 10.0 mM Tris, 100.0 mM NaH_2PO_4, 1.0 % Triton X-100, 2.0 mM benzamidine, 2.0 mM PMSF, pH 8.0) and incubated at 37 °C at 200 rpm for 60 minutes. The solubilized inclusion bodies were pelleted at 10,000×g at 4 °C for 20 minutes, and 1.0 mL of Ni-NTA agarose was added to the supernatant. The Ni-NTA slurry was gently shaken at room temperature for 45 minutes then added to a gravity fed column and the recombinant BP10 eluted using a pH gradient, with buffers containing 6.0 M urea, 10.0 mM Tris,

100.0 mM NaH_2PO_4, at pH's 6.3, 5.9, and 4.5. The recombinant BP10 was completely eluted at pH 4.5 and was immediately titrated to pH 7.4 using 0.5 M NaH_2PO_4. Overexpression and purification were monitored on a time-dependent basis using 12.5 % SDS-PAGE according to Laemmli and Western blot techniques using the anti-His-tag antibody.

The concentration of recombinant BP10 was determined using standard BCA assay with a BSA standard curve. The recombinant protein was diluted 40 times by volume using 50.0 mM Tris with 50 mM NaCl then dialyzed extensively with several changes against phosphate buffered saline (PBS) containing 50 μM $ZnCl_2$ for 48 hours at 4 °C. Recombinant BP10 was concentrated either under 18 psi N_2 using an YM3 Amicon membrane or an Amicon Centricon YM3. Final BP10 concentrations were checked using BCA. The His-tag fusion was removed using a Factor Xa His-tag removal kit from Novagen according to instruction.

Circular Dichroism (CD) studies: CD spectra of urea-denatured, and folded Zn-BP10 and Cu-BP10 were collected in PBS using a 0.1 cm cell with a resolution of 0.5 nm. All absorbance readings were converted to molar ellepticity and the percent helicity and sheet content calculated. The α-helical content was calculated according to published methods.[20]

Preparation of the copper derivative of BP10: During the refolding of urea-denatured BP10, 1.0 mM 1,10-phenanthroline was added to the 50.0 mM Tris 50.0 mM NaCl pH 7.5 buffer, then extensively dialyzed against PBS containing 0.5 M guanidine. The guanidine-containing buffer was exchanged through dialysis with PBS buffer, and

then with PBS containing 50 μM $Cu(NO_3)_2$. Protein concentrations were determined with BCA assay.

Gelatin Zymogram: Gelatin was incorporated into a polyacrylamide gel matrix according to standard protocols with modifications to fit current studies as listed below.[21] A volumeof 1.25 mL of 1.4 M Tris at pH 8.8, 0.50 mL of 5.0 mg/mL gelatin solution in water, 25.0 μL 10 % (w/v) APS, 200 μL 10% (w/v) SDS, 25.0 μL TEMED, 2.0 mL water, and 1.25 mL 30:1 acrylamide:bis-acrylamide were mixed and allowed to polymerize in a mini-gel minus a stacking gel. Several concentrations of BP10 were mixed with non reducing gel-loading dye and incubated for 15 minutes at room temperature (standard Laemmli protocol minus mercaptoethanol or dithiothreitol[22]). These BP10 samples were loaded into each lane of the gel and run at 200 V and 4 °C until the dye front reached the bottom of the plate. The running buffer did not contain SDS. The gel was washed two times in 0.25 % Triton X-100 for 15 minutes with gentle shaking, then incubated for 10 hours in 50.0 mM Tris pH 7.50, 1.0 μM $ZnCl_2$ 0.5% Triton X-100, 0.02 % NaN_3, and 2.0 mM $CaCl_2$. After ten hours the gels were stained with 0.1% Coomassie brilliant blue in 40% propanol for 1.0 hour. The gel was destained in a 7% acetic acid solution to reveal the digestion, and then photographed on a light table with a digital camera. The enzyme with gelatinase activity is shown as unstained bands.

Gelatinase Assay: The gelatinase activity of recombinant BP10 was monitored using a detection method for α- amino groups with ninhydrin as an indicator of peptide hydrolysis according to a standard protocol with modifications to fit current studies as

described below.[23] A 5.0 mg/mL gelatin solution was prepared in H_2O and heated to 55 °C for 15 minutes until completely dissolved. A ninhydrin detection solution was prepared by mixing 9.0 mL glycerol, 3.0 mL of 0.5 M sodium citrate at pH 5.50, and 3.75 mL of 1.0% (w/v) ninhydrin solution in 0.5 M sodium citrate buffer. Gelatin and 1.0 μM BP10 were mixed in PBS and incubated at room temperature. A 50.0 μL sample was taken from the reaction at several time points and mixed with 950 μL of ninhydrin detection solution then boiled for 12.0 minutes. The absorbance at 570 nm was determined using a sample containing undigested stock gelatin (the same gelatin used for the experiment, incubated under the same conditions minus BP10) mixed with the same detection assay as the blank. The first order rate constant k_{obs} was determined from an exponential curve fit. The molar absorptivity of Ruhemann's purple (ε_{570} = 22,000 $M^{-1}cm^{-1}$)[24] also allowed for monitoring the substrate dependent hydrolysis of gelatin. Several dilutions of a 10.0 mg/mL stock solution of gelatin were used according to the aforementioned protocol and rates were fitted as a function of substrate concentration according to the Michaelis-Menten equation, yielding k_{cat} and K_m parameters.

Hydrolysis of BAPNA by Zn-BP10 and Cu-BP10: BAPNA stock solutions were made in Me_2SO and then diluted with 50.0 mM HEPES 50.0 mM NaCl pH 7.50. Less than 2% Me_2SO by volume was present in each assay and found not to interfere with kinetic measurements. Several concentration of BAPNA were incubated with 2.17 μM BP10 and rates determined colorimetrically from the release of the p-nitroaniline product (ε_{405} = 10,150 $M^{-1}cm^{-1}$). Kinetic parameters were determined by non-linear fitting to the Michaelis-Menten equation.

Calcium activation assays: Gelatin was extensively dialyzed against an EDTA solution and then extensively dialyzed to remove the chelator. Calcium was carefully titrated under substrate saturation conditions to determine its effect on the hydrolysis of gelatin and BAPNA. Once saturating concentrations of calcium were determined, new kinetic parameters were obtained using sufficient (1.0 mM) calcium in all buffers.

Inhibition studies: the effect of two inhibitors, 1,10-phenanthroline (OP) and arginine-hydroxamate (Arg-NHOH) toward the hydrolysis of BAPNA were determined by running Michaelis-Menten kinetics under several concentrations of each inhibitor. Inhibition constants were determined according to the inhibition patterns for OP and Arg-NHOH respectively.

pH profiles: The pH profiles for Zn- and Cu-BP10 catalyses were constructed by monitoring gelatin and BAPNA hydrolysis under several different pH's using 50.0 mM buffers containing 50.0 mM NaCl and 1.0 mM $CaCl_2$. The following buffers were used: acetate (pH 5.0), MES (pH 5.5-6.5), HEPES (pH 7.0-8.0), TAPS (pH 8.5-9.0), CAPS (pH 9.5-11.0). The pH-dependent kinetic parameters were determined by non-linear fitting and pK_a values were obtained from fitting the data to a two-ionization process.

Electronic spectrum of Cu-BP10: The electronic spectrum of a 20.0 μM Cu-BP10 was monitored from 350 to 800 nm and the tyrosine to copper charge transfer transition was observed at 454 nm. The quenching of this ligand to metal charge transfer transition (LMCT) was monitored spectrophotometrically upon addition of Arg-NHOH.

Homology modeling and substrate docking: The primary sequence of BP10 was overlaid over the crystal structure of serralysin (PDB ID 1SAT) using BioCAChe 6.1.10

(Fujitsu, Beaverton, OR). The structure was energy-minimized using MM3 and molecular dynamics calculations in a simulated water box. The substrate BAPNA was docked into the active site using the standard procedure (PF5) in BioCAChe.

III. RESULTS AND DISCUSSION

Overexpression and refolding of recombinant BP10: The recombinant enzyme was efficiently overexpressed, though it was insoluble and contained within inclusion bodies (Figure 7.1, Lane 3). Urea solubilization proved to be an efficient method for extracting the enzyme from inclusion bodies, coupled with a fusion His-tag at the N-terminus to BP10 that allows for efficient purification using Ni-NTA agarose. The overexpression and purification yields an average of 0.7 mg/mL of total recombinant BP10 after a pH gradient elution from the Ni-NTA agarose column (Figure 7.1). The protein overexpression was monitored on a time course using SDS-PAGE and Western blotting (Figure 7.2**B**). The detection of the His-tag using an anti-His antibody upon induction with IPTG proved a sensitive and consistent method for monitoring the overexpression of the recombinant protein.

Upon removal of the chaotropic reagent urea through extensive dialysis, the protein was refolded and activity could be monitored after removal of the His-tag. It was determined empirically that a 40 fold dilution was important since at higher concentrations the protein coagulates and precipitates out of solution. Recombinant BP10 showed no signs of degradation after refolding (Figure 7.2**A**). Upon removal of the

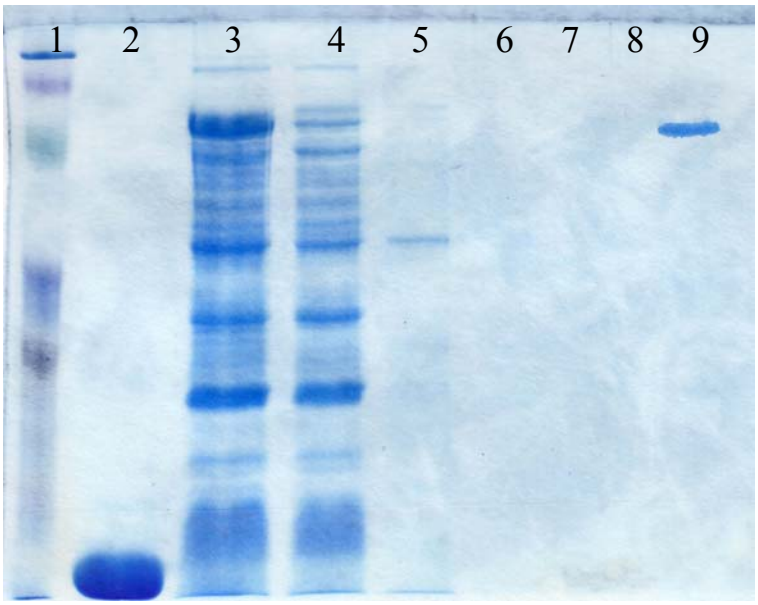

Figure 7.1. SDS-PAGE gel (12.5 %) during purification of recombinant BP10. Lane 1, MW marker; lane 2 total soluble protein after 4 hour induction after lysozyme and sonication; lane 3, total protein solubilized with 8.0 M urea from inclusion bodies; lane 4, flow-thru unbound proteins from Ni-NTA column; lanes 5-6, buffer C wash; lanes 7-9, buffer D at pH's 6.3, 5.9, and 4.5 gradient elution, respectively. Lane 9 shows a homogenous band at 66 kDa, assigned to recombinant BP10.

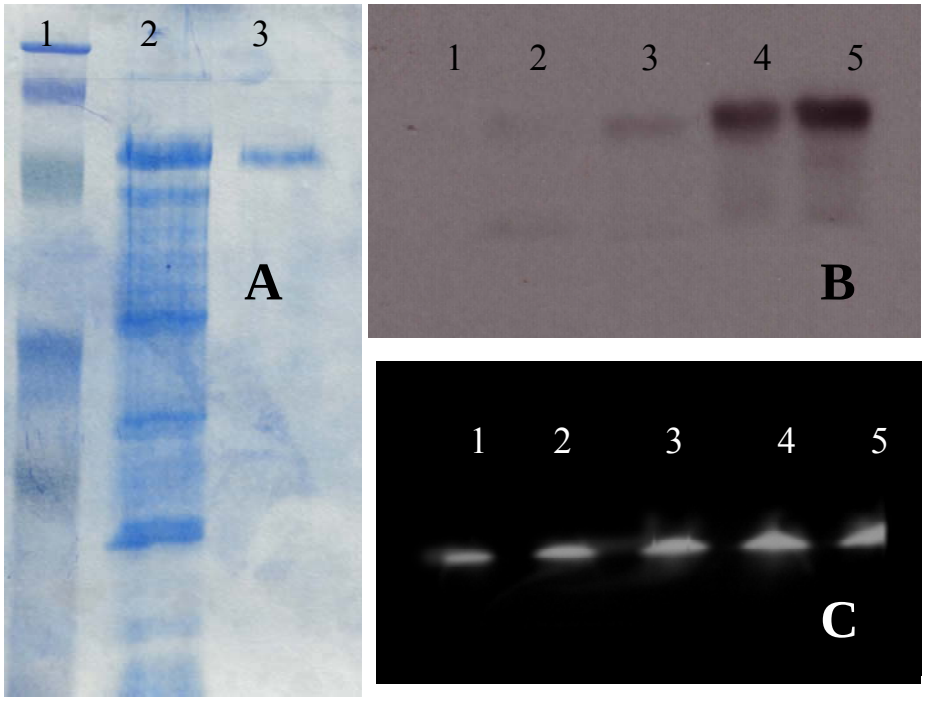

Figure 7.2 (**A**) SDS-PAGE (12.5 %) showing intact BP10 after refolding. Lane 1, MW marker; lane 2, is total urea solubilized protein; lane3, recombinant BP10 after refolding. (**B**) Western blot showing the time course of overexpression. Lane 1, uninduced sample; lane 2, 1.0 hr; lane 3, 2.0 hr; lane 3, 2.0 hr; lane 4, 3.0 hr; lane 5, 4hr. (**C**) Gelatin zymogram showing concentration-dependent substrate hydrolysis by BP10; (Lanes 1-5) 0.25μM, 0.50 μM, 1.0 μM, 1.50 μM , 1.75 μM BP10.

His-tag using a Factor Xa removal kit from Novagen, the protein undergoes autohydrolysis and remained stable only for a few days at 4 °C. However, the protein fused with the His-tag is stable indefinitely at 4 °C. Hence, the His-tag was used as an efficient method for long-term storage of recombinant BP10 and removed only prior to running experiments.

CD Spectra of ZnBP10 and CuBP10: The CD spectrum of urea-denatured BP10 (Figure 3, dotted trace) does not show the random-coil expected in the presence of a high concentration of chaotropic reagents. The CD spectrum of urea-denatured BP10 shows an overall β-sheet-shape with blue shifts observed in the minimum and a red shift in the maximum of the spectrum. The characteristic minimum at 200 nm for random-coil peptides is not present, with only bathochromic shifts resulting in the denaturation of BP10. This resistance to complete denaturation to a random-coil conformation may account for the efficient refolding of BP10 in the absence of reducing agents, due to partially formed secondary structures. The helical content of BP10 is 5.8 % which is consistent with the large content of sheet-like structures (i.e. β-barrel) in CUB domain-containing proteins.[25] According to sequence homology, only the helices present in the astacin-domain shoukd be present accounting for the low helical content of BP10. The CD spectra of Zn-BP10 and Cu-BP10 are virtually identical, suggesting no major conformational change in the overall structure of the protein due to metal substitution.

Kinetics of gelatin hydrolysis: Recombinant BP10 was not able to hydrolyze casein, a commonly used substrate for endopeptidases. Porcine gelatin however proved to be a good substrate to monitor proteolytic activity of BP10 with gelatin zymograms (Figure 7.2C) and a ninhydrin detection protocol (Figures 7.4 and 7.5), establishing the proposed role of BP10 as a protease. The formation of a colored ninhydrin-α-amino acid

conjugate with a known molar absorptivity was a convenient method to monitor gelatin hydrolysis. The saturation kinetics can be fit to the Michaelis-Menten equation, to yield $k_{cat} = 0.013\ s^{-1}$, $K_m = 51.3\ \mu M$, and the second order rate constant $k_{cat}/K_m = 253.4\ M^{-1}s^{-1}$. Interestingly, BP10 shows a Ca^{2+}-dependent activation (Figure 7.5, inset) yielding $k_{cat} = 0.77\ s^{-1}$, $K_m = 46.5\mu M$, and $k_{cat}/K_m = 16{,}740\ M^{-1}s^{-1}$ at saturating [Ca^{2+}]. Other gelatinases found in the sea urchin embryo have shown a Ca^{2+}-dependent activation.[26, 27] However, whether or not the Ca^{2+} bound to the EGF domain is a cofactor in protein-protein interaction or signaling is not known for BP10 and cannot be determined in these studies. Further analysis of the rate constants can shed insight into the role of Ca^{2+} in catalysis. The K_m values are similar in the presence and absence of Ca^{2+}, while the k_{cat} value for the catalysis in the presence of Ca^{2+} is much larger than in the absence of Ca^{2+}. Since K_m is defined as $(k_{-1}+k_{cat})/k_1$, with k_1 and k_{-1} the rate constants for substrate binding and dissociating from the enzyme- substrate (ES) complex, a significant increase in k_{cat} with a constant K_m value in the presence of Ca^{2+} reflects a smaller dissociation k_{-1}/k_1 of the ES complex. This observation reveals that Ca^{2+} affects BP10 catalysis by enhancing substrate binding to the enzyme and by lowering the activation energy (i.e., a larger k_{cat} value). The activation of BP10 by Ca^{2+} is the first report of the effect of Ca^{2+} on the activity of astacin family metalloproteases, although Ca^{2+} dependent gelatinases have been identified[26] in sea urchins; Mg^{2+} showed no effect in activation of BP10. BP10 contains an EGF-Ca^{2+} domain that could mediate the effect of calcium on catalysis.

Elucidation of the role of the EGF domain and Ca^{2+} on BP10 activity may shed interesting insight once similarly functioning and structurally conserved enzymes have been characterized across all phyla.

The kinetic parameters for Zn-BP10 toward gelatin hydrolysis were determined

$$k = \frac{k_{lim}}{\left[\left(1 + H^{+}/Ka_{1}\right)\left(1 + Ka_{2}/H^{+}\right)\right]} \quad \text{Equation (1)}$$

between pH's 4.5-11.0. Plots of k_{cat} and k_{cat}/K_m against pH exhibit bell shaped curves (Figure 7.6 **A,D**) indicating the presence of two ionizable groups in the catalytic mechanism of ZnBP10 and can be fitted to Equation (1). The two ionization constants from the k_{cat} vs. pH profile yield $pK_{a1} = 5.94$ and $pK_{a2} = 10.2$ which can be assigned to the deprotonation of a Zn-bound water and to the coordinated tyrosine respectively upon substrate binding which is consistent with previous reports for serralysin.[5] The role of the coordinated Tyr is further addressed below.

Kinetics of BAPNA hydrolysis: The synthetic substrate BAPNA is a good substrate for BP10. This activity was previously observed for serralysin and is the only synthetic tripeptide of a series of di- and tripeptide mimics, including glycine-, alanine-, valine-, leucine-, glutamate-, lysine-, arginine-, trialanine-, and succinyl-trialanine-p-nitroanilide that was hydrolyzed by BP10. The kinetics of BAPNA hydrolysis (Figure 7.7) fit Michaelis-Menten kinetics to yield $k_{cat} = 0.079\ s^{-1}$ $K_m = 0.66$ mM and $k_{cat}/K_m = 120\ M^{-1}s^{-1}$ in the presence of Ca^{2+}, and $k_{cat} = 1.83 \times 10^{-3}\ s^{-1}$, $K_m = 1.55$ mM and $k_{cat}/K_m = 1.18\ M^{-1}s^{-1}$ in the absence of Ca^{2+} (Figure 7.7 B). Like in gelatin hydrolysis by BP10,

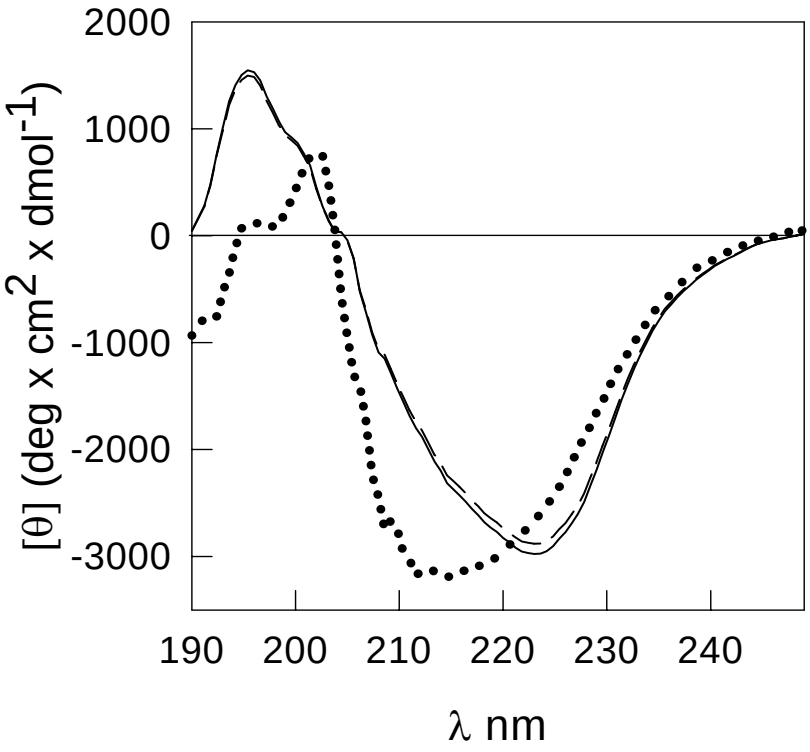

Figure 7.3. CD spectra of Zn-BP10 in PBS with 8.0 M urea pH 7.4 (dotted trace), and renatured Zn- (solid trace) and Cu-BP10 in PBS pH 7.4 (dashed trace).

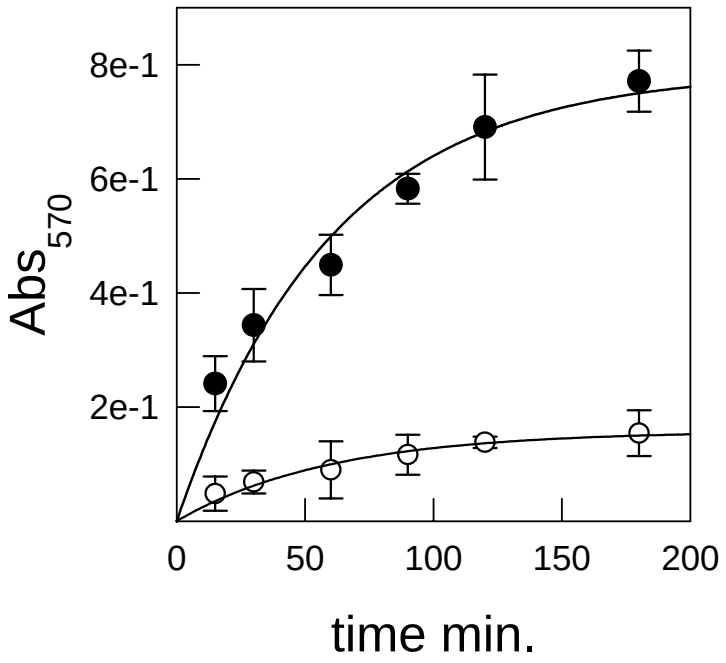

Figure 7.4. First order kinetics of gelatin hydrolysis by Zn^{2+} (•) and Cu^{2+} (o) derivatives of BP10 in the presence of 1.0 mM Ca^{2+} at pH 7.5. The solid traces are the best fit to a pseudo-first-order rate law, which affords the rate constant k_{obs} for each derivative.

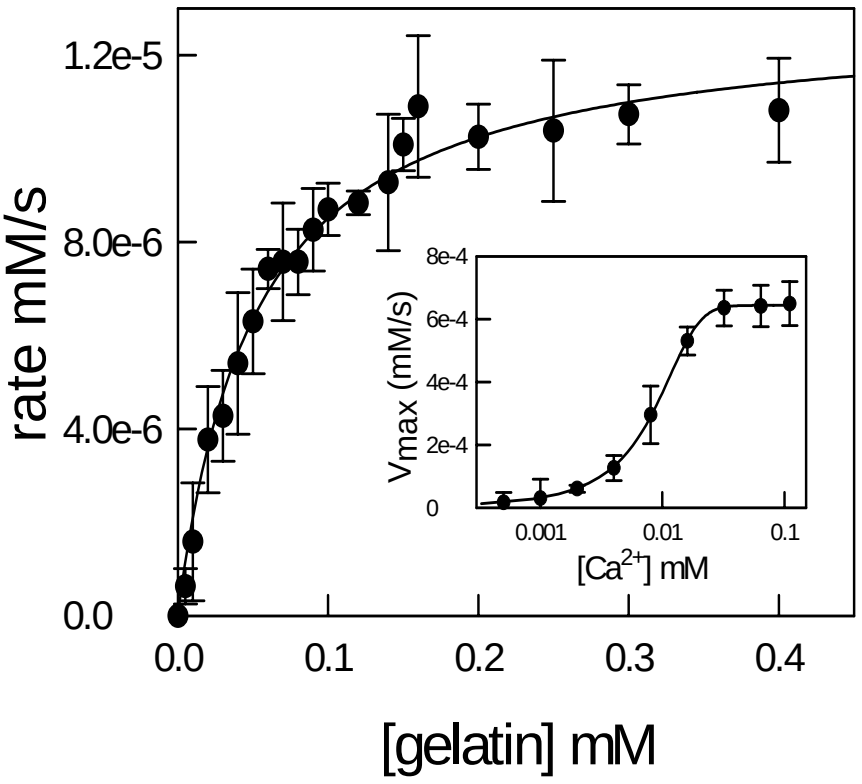

Figure 7.5. Gelatin hydrolysis by 1.0 μM ZnBP10 in 50.0 mM HEPES pH 7.5, 50 mM NaCl, and 1.0 mM $Ca(NO_3)_2$. The solid line is the best fit to the Michaelis-Menten equation. The inset shows a Ca^{2+}-dependent activation upon titration of Ca^{2+} to 60 μM ZnBP10. The solid line in the inset is the best fit to a loose-binding equilibrium.

Ca^{2+} activates BP10 by lowering the activation energy and enhancing substrate binding as reflected in the rate constants and discussed above. The higher k_{cat} and lower K_m for gelatin hydrolysis than BAPNA also indicate a higher affinity of gelatin than BAPNA binding to BP10, reflecting the endopeptidases nature of BP10.

The pH profile for BAPNA hydrolysis by Zn-BP10 (Figure 7.6 B,E) compares well with that of gelatin, showing a bell shaped curve that can be fitted to Equation (1). The ionization constants also fall within experimental range, yielding $pK_{a1} = 5.39$ and $pK_{a2} = 9.18$ for the first order rate constant k_{cat}, and $pK_{a1} = 5.83$ and $pK_{a2} = 8.98$ for k_{cat}/K_m.

The inhibition of Zn-BP10 by the metal chelator 1,10-OP toward the hydrolysis of BAPNA at pH 7.5 shows a noncompetitive pattern which is consistent with metal removal from metalloenzymes and gives $K_i = 7.85$ μM (Figure 7.8). The mixed-type inhibition by Arg-NHOH (Fig. 7.8 B) is a good indication of a combination of specific interaction along with metal chelation afforded by the hydroxamate moiety. The inhibition pattern for Arg-NHOH can be fitted to Equations (2) and (3) to yield $K_{ic} = 0.20$ mM and $K_{iu} = 0.90$ mM, representing the specific inhibition constant for the dissociation of the enzyme-inhibitor complex (EI) and the catalytic inhibition constant for the dissociation of the inhibitor from the enzyme-substrate-inhibitor complex (ESI), respectively.[28]

$$V_{max}^{app}/K_m^{app} = \frac{V_{max}/K_m}{1+[I]/K_{ic}} \quad \text{Equation (2)} \qquad V_{max}^{app} = V_{max}/\left(1+[I]/K_{iu}\right) \quad \text{Equation (3)}$$

Mechanistic studies of the copper derivative of BP10 (Cu-BP10): The spectroscopically inert Zn^{2+} ion found in astacins and several other metallohydrolases offers a poor probe for the metal coordination environment in the active site. Thus spectroscopically active metal derivatives of metalloenzymes can offer detailed insight into the catalytic mechanisms and structure within the active site.[29] The formation of the Cu-BP10 derivative is evident by the intense Tyr-to-Cu^{2+} LMCT at 454 nm, analogous to that in Cu^{2+}-astacin and Cu^{2+}-serralysin. The activity of the Cu^{2+}-substituted BP10 (Cu-BP10) is considerably higher than Zn-BP10 in terms of k_{cat} (0.76 s^{-1}) and k_{cat}/K_m (5430 M^{-1} s^{-1}) toward the hydrolysis of BAPNA, reflecting a ~960 % increase in activity in terms k_{cat} and ~485 % in terms of k_{cat}/K_m. This is a rather unusual characteristic of metal derivatives of Zn enzymes,[29] since most Cu^{2+} derivatives of Zn^{2+}-enzymes are inactive. Increased activity of a Cu^{2+} derivative has been observed in serralysin, another astacin family member able to hydrolyze gelatin and BAPNA.[5] Moreover, the overall proteolytic activity of Cu-BP10 toward gelatin hydrolysis is ~20% of that of the Zn derivative, which is also greater than many metal-substituted metallo-hydrolases previously reported.[29]

Metal-centered hydrolysis relies on the Lewis acidity of metal ions, which can lower the pK_a of metal-bound water molecules by greater than 10^7 fold, generating a metal-hydroxide at neutral pH that can perform nucleophillic attack on the scissile peptide bond. The versatility of metal-centered hydrolysis has been widely demonstrated in synthetic Cu^{2+} model systems which show proficient peptidase activities and phosphodiesterase activities.[30-32] Conversely, Cu^{2+} derivatives of metallohydrolases are generally inactive or exhibit considerably lower activities[29, 33] despite the comparatively

high Lewis acidity of Cu^{2+}. Few examples of metal-substituted metallohydrolases in literature show considerable activation, with serralysin[5] and astacin[34] being the most significant representatives of metal-substituted metallohydrolases that are activated by Cu^{2+}. The poor activation of metallohydrolases observed in Cu^{2+} derivatives may be attributed to Jahn-Teller distortion which can reduce the nucleophilicty of the metal bound water if positioned in the axial coordination of the metal center. The ability to use Cu^{2+} as a viable probe for mechanistic studies is characteristic for the astacin family of metalloenzymes. It is noteworthy that the metal ligands found in the astacin family are a unique example of metal-phenolate coordination in metallohydrolases wherein the coordinated Tyr plays a "switch-off" role in catalysis[5, 19] and may be involved in the unique Cu^{2+}-activation observed in astacin family enzymes thus far characterized. The analysis of BP10 is consistent with this mechanism of hydrolysis discussed below.

From analysis of kinetic parameters k_{cat} and K_m, there is an obvious requirement of the metal center for catalysis. K_m value for the hydrolysis of BAPNA by Cu-BP10 in the presence of Ca^{2+} (K_m = 1.32 mM) is not significantly different (200 %)from the Zn form (0.66mM) when compared to the 960 % increase in k_{cat} of Cu-BP10 compared to the native Zn-BP10. Once again, as previously discussed, a small change in K_m concomitant with a large increase in k_{cat} suggests a lowering of the activation energy and an increase in the affinity for the substrate in the ES complex. The hyperactive Cu-BP10 suggests that the metal center must be involved in catalysis, most importantly in the turnover of the ES complexes to the product with a high k_{cat} value.

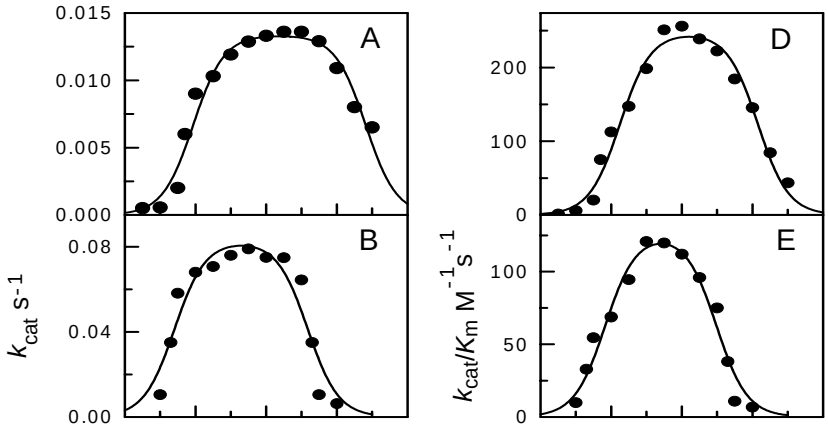

Figure 7.6. pH dependence of k_{cat} and k_{cat}/K_m for the hydrolysis of gelatin by Zn-BP10 (**A**, **D**), hydrolysis of BAPNA by Zn-BP10 (**B**, **E**). The solid traces are the best fit to the equation $k = \frac{k_{lim}}{\left(1 + [H^+]/K_{a1}\right)\left(1 + K_{a2}/[H^+]\right)}$ to afford the two pK_a values reported in the text.

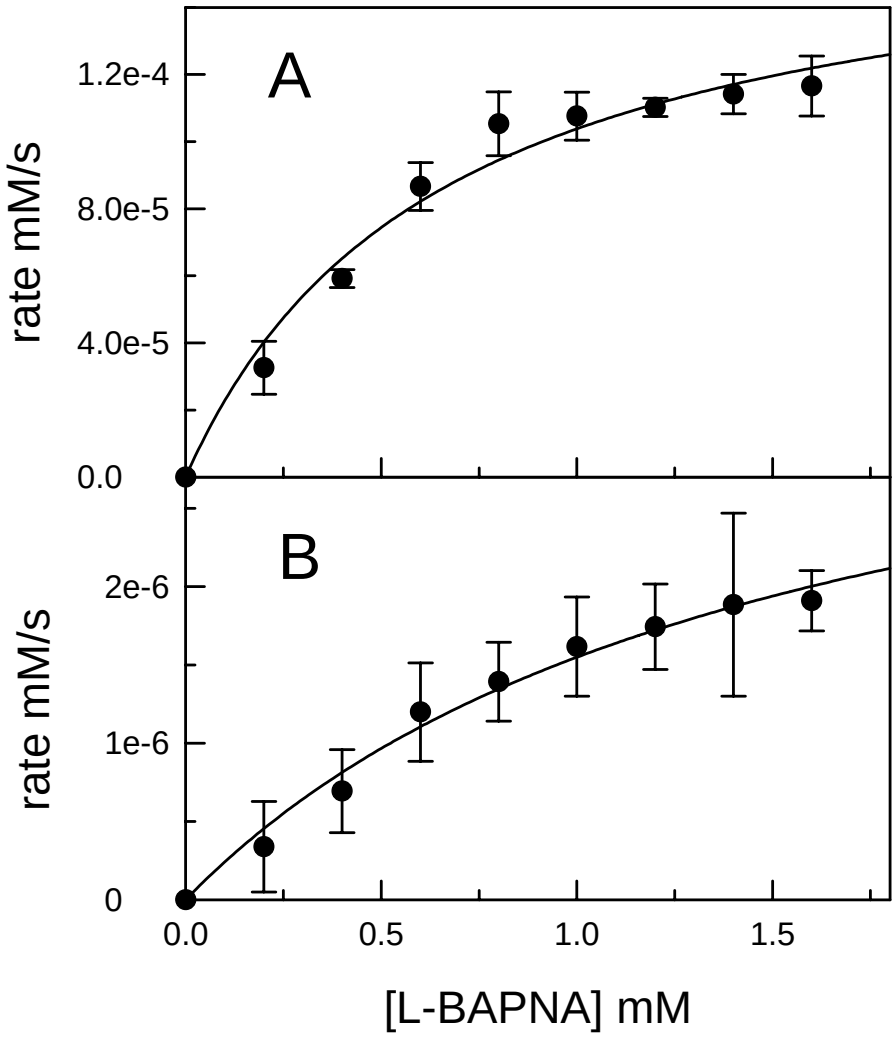

Figure 7.7. (A) Hydrolysis of L-BAPNA by Zn-BP10 in 50.0 mM HEPES, pH 7.5 in the presence of 50mM NaCl, and 1.0 mM $Ca(NO_3)_2$. (B) Same as in (A) in the absence of Ca^{2+}.

Because of the low concentrations available for BP10 (above ~ 70 μM the protein precipitates), electronic spectra of the Cu^{2+} derivative was used to study the metal coordination environment in the active site. Upon substitution of Cu^{2+} during the refolding protocols, a 20 μM sample can show significant ligand to metal charge transfer transition (LMCT) in the visible range. Unfortunately, the low energy d-d transition bands for tetragonally distorted octahedral Cu^{2+} have very low molar absorptivity values (in the order of 100 $M^{-1}cm^{-1}$) and are too noisy to distinguish in the spectrum (Figure 7.9). The large LMCT (ε = 1220 $M^{-1}cm^{-1}$) observed at 454 nm are due to the tyrosinate-to-Cu^{2+} charge transfer transition as determined previously using Cu-astacin.[34] This observation serves as support of EPR studies of Cu-astacin where $g_{//} > g_{\perp}$ spectral features suggests that the metal center is tetragonaly distorted with a weak axial ligand.[19] This is further proof of a similar astacin-like active site structure for BP10.

The inhibition of Zn^{2+} and Cu^{2+} derivatives of BP10 by Arg-NHOH at pH 7.50 (Figure 7.8, 7.10) displays a mixed type pattern as observed in serralysin,[19] wherein the inhibitor is able to bind both the enzyme and the ES complex. The mixed type inhibition yields two different inhibition constants for the dissociation of the inhibitor form the EI and EIS complexes, yielding K_{ic} = 1.58 μM and K_{iu} = 3.93 μM. The significantly different inhibition constants for Zn-BP10 and Cu-BP10 are good evidence that the inhibitor binds directly to the metal center in the active site. Mixed-type inhibition is often a good indicator of an alternative site for inhibitor and substrate binding in the ES complex to afford an ES-I and ES-S ternary complexes.[28]

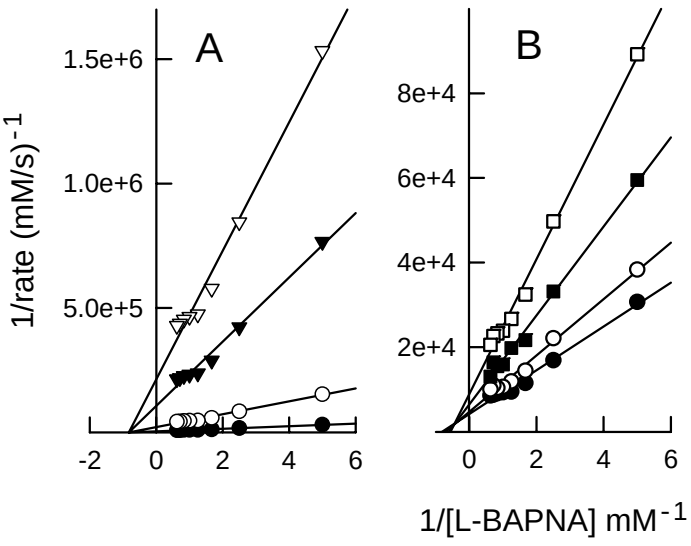

Figure 7.8. Inhibition of Zn-BP10 toward L-BAPNA hydrolysis in 50.0 mM HEPES pH 7.5, 50.0 mM, NaCl, 1.0 mM $Ca(NO_3)_2$ by 1,10 phenanthroline (**A**) and by Arg-NHOH (**B**). Inhibitor concentrations are as follows from bottom to top: (**A**) 0, 0.5, 1.0, and 2.0 mM; (**B**) 0, 0.25, 0.5, and 1.0 mM.

The influence on the LMCT centered at 454 nm can serve as an indicator for inhibitor binding directly to the metal center (Figure 7.9). The quenching of the LMCT band upon inhibitor binding indicates that the metal-coordinated Tyr is detached upon inhibitor binding, a phenomenon observed in the studies of Cu-astacin and Cu-serralysin.[5] The gradual decrease of the LMCT intensity upon inhibitor binding can be described according to Scheme (1), assuming that the binding of one equivalent of inhibitor per active site metal results in concomitant detachment of the coordinated Tyr.

$$\text{BP10(bound Tyr)} + \text{Arg-NHOH} \rightleftharpoons \text{Arg-NHOH-BP10} + \text{detached Tyr}$$

When fitting the quenching of the Tyr-to-Cu^{2+} charge transfer with respect to inhibitor concentration according to Scheme (1) without including $[H^+]$ gives an apparent association constant of 2.9×10^3 M^{-1} for Arg-NHOH binding to Cu-BP10 at pH 8.5 (Figure 7.9, inset). The specific inhibition constant K_{ic} for the inhibition of Cu-BP10 by Arg-NHOH at pH 7.5 (Figure 7.10) can be converted into an apparent association constant of 6.33×10^5 M^{-1}, greater than that at pH 8.5, indicating that the protonation of the metal-coordinated Tyr at lower pH assists the binding of Arg-NHOH.

The kinetic parameters K_m, k_{cat}, and k_{cat}/K_m for the hydrolysis of BAPNA by Cu-BP10 were determined between pH's 5.0-9.5 and exhibit bell shaped curves that can be fitted to Equation (1) to give $pK_{a1} = 5.48$ and $pK_{a2} = 7.98$ for the pH dependence of k_{cat} and $pK_{a1} = 5.83$ and $pK_{a2} = 7.99$ for the pH dependence of k_{cat}/K_m (Figure 7.11). This describes a two ionization mechanism for the catalytic turnover of the substrate by BP10. The similar crystal structures of different metal derivatives of astacin[34] suggest that the

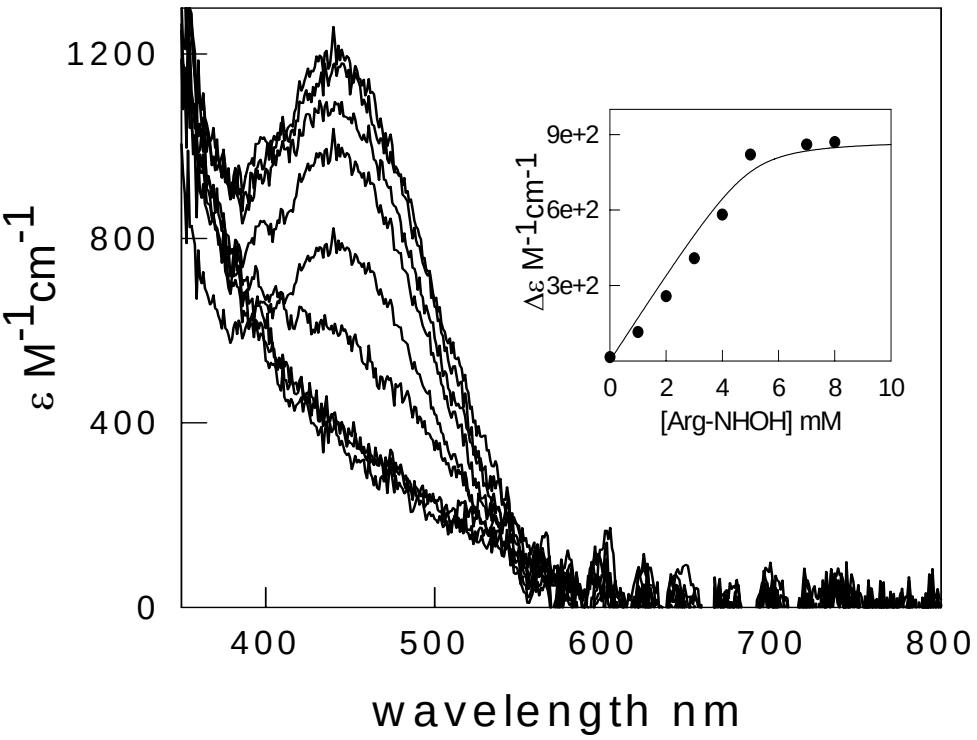

Figure 7.9. Optical titration of Arg-NHOH to Cu-BP10. The inset shows the decrease in the change of the molar absorptivity (Δε) as a function [Arg-NHOH].

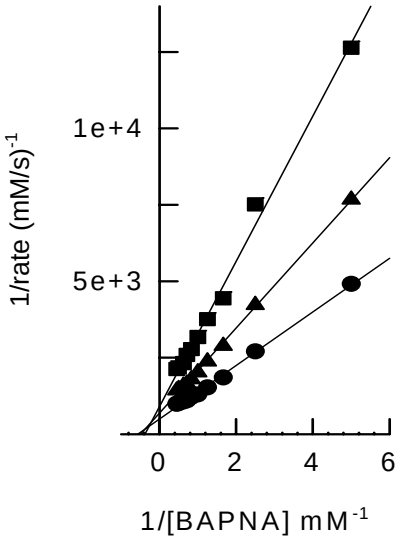

Figure 7.10. Inhibition of Cu-BP10 by Arg-NHOH. Inhibitor concentrations are as follows from bottom to top: 0, 1.5, and 3.0 μM.

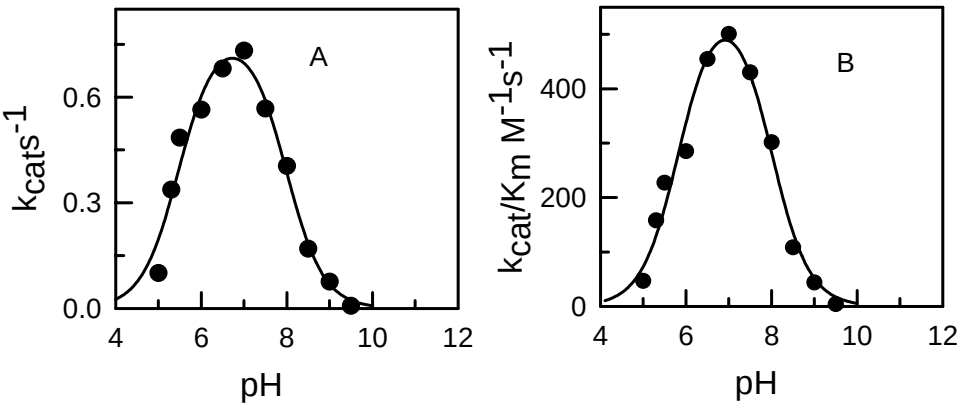

Figure 7.11. pH profile of BAPNA hydrolysis by Cu-BP10.

coordination sphere of Zn^{2+} and Cu^{2+} derivatives of BP10 would be similar. This would possibly attribute the different ionization constants pK_{a1} and pK_{a2} for each metal derivative to the Lewis acidity of each metal, but not due to different metal environments within the active site of BP10. The low pK_{a2} approaching pK_{a1} for Cu-BP10 causes a considerable decrease in the catalytic efficiency, from the intrinsic value of 851 $M^{-1}s^{-1}$ to the maximum fitted value of 580 $M^{-1}s^{-1}$ which means that only 64% of Cu-BP10 is active at pH 7.0. Conversely the intrinsic and fitted values for k_{cat}/K_m of Zn-BP10 differ only slightly with the intrinsic value of 119.7 $M^{-1}s^{-1}$ and the fitted value of 125.1 $M^{-1}s^{-1}$. This is consistent with the coordination sphere of the two metal derivatives of BP10 being similar, and suggest that the differences in ionization constants is due to the effects on the Lewis acidity of each metal.

Ionizable groups must be coordinated or in very close proximity of the metal in the active site of an enzyme to be influenced by the metal ion, as reflected by a change of pK_a values. In astacin the crystal structure suggests that Tyr and Glu as well as a water molecule are bound to the metal center. This "metallotriad" framework of M–$^-$OH…$^-$OOC is similar to the "catalytic triad" of serine proteases Ser–OH…His …$^-$OOC, where the water nucleophile is sandwiched by a Lewis acid (the active site metal) and a Lewis base (the carboxylate in Glu) to serve in a general-acid/general-base catalytic mechanism. This metal-centered triad has also been confirmed in other metallohydrolases including serralysin,[5] thermolysin,[35] matrilysin,[36] and carboxypeptidase A.[37] We utilized the Cu^{2+} derivative of BP10 to determine if a similar mechanism is utilized by this enzyme.

The 454 nm LMCT band does not show full intensity at neutral and lower pH values (~150 $M^{-1}cm^{-1}$ at pH 6.0 versus 1255 $M^{-1}cm^{-1}$ at pH 8.5), indicating that they are pH dependent. The Tyr(phenolate)-to-Cu^{2+} CT in Cu-BP10 changes with pH in a sigmoidal manner (Figure 7.12). Thus, the change can be described by a single ionization process[5] for the ionization of the coordinated Tyr_{249} and simultaneous binding to the active site Cu^{2+} to give $\varepsilon_u = 109$ and $\varepsilon_b = 1182$ $M^{-1}cm^{-1}$ and a pK_a value of 6.87 for the deprotonation of Tyr_{249}, where ε_u and ε_b are the molar absorptivities due to the background and the Cu-bound Tyr_{249}. However, the data do not fit well to a single-ionization model (Fig. 7.10, dotted trace) and the pK_a value of 6.86 is not a close match to the k_{cat}/K_m pK_{a2} value of 7.99.

Since proposed models of astacin-type enzymes show that the Tyr side chain is H-bonded to the metal-coordinated water, the deprotonation of the phenolate moiety and subsequent binding to the active-site metal should be affected by the ionization of the coordinated water and reflected in the CT intensities. The data is much better fitted to a two-ionization process described previously[5] with a fixed $pK_{a1} = 5.83$ (from the k_{cat}/K_m pH profile of Cu-BP10, (Figure 7.11B) to afford $pK_{a2} = 7.42 \pm 0.15$, $\varepsilon_u = 26 \pm 15$, $\varepsilon_W = 591 \pm 33$, and $\varepsilon_b = 1425$ $M^{-1}cm^{-1}$ (Figure 7.10 solid trace). Although the data can be reasonably fitted to a two-ionization process, the similar λ_{max} throughout the titration suggests that it is likely to have only one species that affords the LMCT instead of two. Taken together our data is most consistently described as a single species ionization involved in the LMCT, assigned to a Tyr_{249} to Cu^{2+} charge transfer. Herein, the increase in the LMCT due to Tyr binding corresponds to the decrease in activity, reflecting the

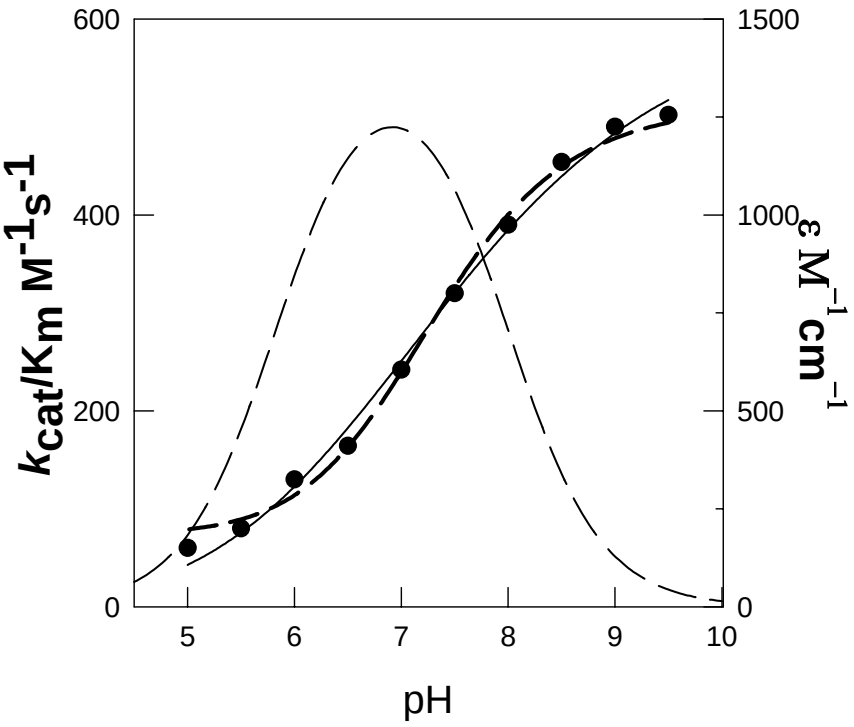

Figure 7.12. The change in intensity of the LMCT transition of Cu-BP10 at 454 nm as a function of pH. The data is much better fitted to a two ionization processes (solid trace) than to a single ionization process (dashed trace). The dashed bell-shaped curve is the best fit for the k_{cat}/K_m vs. pH profile of CuBP10 from Figure 7.11B.

inhibiting role of Tyr249 and its role as a "catalytic switch".

Homology Modeling: The catalytic domain of the astacin family of metallohydrolases is highly conserved across all sequenced enzymes. Because BP10 and serralysin are both able to cleave BAPNA effectively, homology modeling by the use of serralysin as the template for the catalytic domain and substrate binding was performed (Figure 7.11). Molecular mechanics calculations (MM3) and molecular dynamics were used to arrive at the final structure which shows Tyr_{249} within H-bonding distance of the metal-bound water and to the guanidine group of arginine in BAPNA. A predominant hydrophobic interaction is also observed between Trp_{165} and the benzoyl group of the substrate. The p-nitroanilide moiety of BAPNA is exposed to solvent which likely facilitates product release after the cleavage of the substrate.

IV. CONCLUDING REMARKS

BP10 is the first member of the tolloid-like enzymes to be characterized with extensive kinetics and spectroscopic methods. The studies show that BP10 is a metallohydrolase with a hydrolytic mechanism consistent with other astacin-like proteases. The influence of Ca^{2+} toward the catalysis of gelatin and BAPNA by BP10 offers the important insight that Ca^{2+}-signaling can serve an important function in regulation of the proteolytic events in embryogenesis. The studies of the Cu-derivative support the metallotriad mechanism previously proposed for astacin and serralysin, with the involvement of the metal bound Tyr residue in catalysis. Through homology

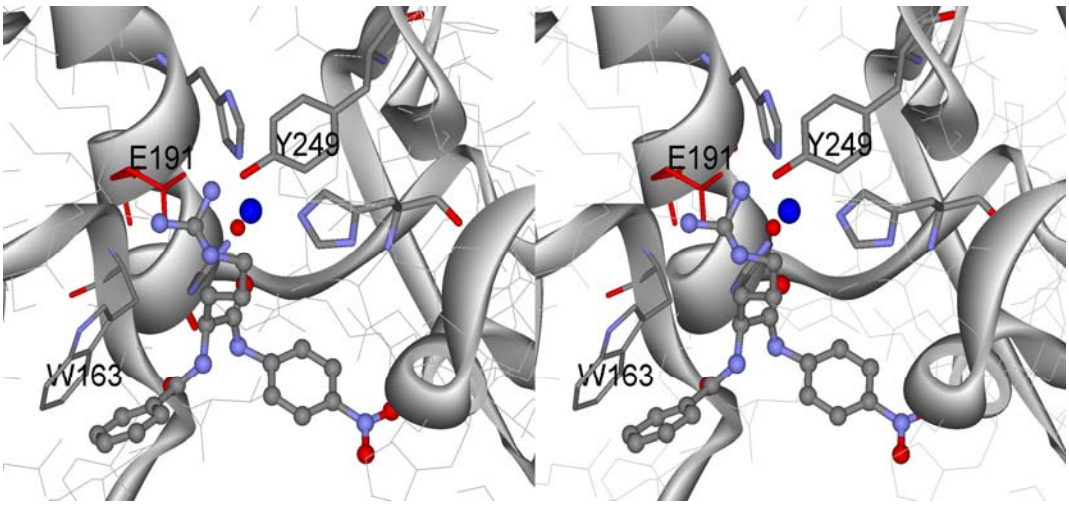

Figure 7.13. Stereo view of the BP10 active site based on the crystal structure of serralysin (PDB ID 1SAT) as the homology template with the use of molecular mechanics (MM3) and molecular dynamics calculations. The substrate BAPNA (ball-and-stick structure) is docked into the active site, with its carbonyl of the scissile bond pointing toward the active site metal (larger sphere), the benzoyl moiety of BAPNA interacting with Trp_{165}, and the guanidinium group of the Arg moiety interacting with Tyr_{249}.

modeling we observed the conserved astacin catalytic motif and that the active-site Tyr may not only play a role in substrate binding via detachment from the metal during a "resting" state, but also may assist in stabilization of the ES complex by directly interacting with the guanidine group of BAPNA via a charge interaction or H-bonding.

The understanding of the detailed mechanism of peptide hydrolysis by BP10 and revealing of the substrate specificity *in vivo* in future studies are important first steps in unraveling the proteolytic events during sea urchin embryogenesis.

IV. LIST OF REFERENCES

1) J.S. Bond, R.J. Beynon, The astacin family of metalloendopeptidases. *Prot. Sci*. (1995) 4, 1247-1261.

2) N.M Hooper, (ed) *Zinc Metalloproteases is Health and Disease*, Chap. 2, Taylor and Francis, Bristol, PA (1996).

3) F. Moehrlen, H. Hutter, R. Zwilling, X-ray absorption spectroscopy study of zinc coordination in tetanus neurotoxin, astacin, alkaline protease and thermolysin. *Euro. J. Biochem*. (2003), 270, 4909-4920.

4) F.X. Gomis-Rüth, W. Stöcker, H. Huber, R. Zwilling, W. Bode, Refined 1.8 .ANG. x-ray crystal structure of astacin, a zinc-endopeptidase from the crayfish Astacus astacus L. Structure determination, refinement, molecular structure and comparison with hermolysin. *J. Mol. Biol*. (1993), 229, 945-968.

5) H.I. Park, L.-J. Ming, Mechanistic studies of the astacin-like Serratia metalloendopeptidase serralysin: highly active (>2000%) Co(II) and Cu(II) derivatives for further corroboration of a "metallotriad" mechanism. *J. Biol. Inorg. Chem*. (2002), 7, 600-610.

6) T. Lepage, C. Ghiglione, C. Gache, Spatial and temporal expression pattern during sea urchin embryogenesis of a gene coding for a protease homologous to the human protein BMP-1 and to the product of the Drosophila dorsal-ventral patterning gene tolloid.

Development, (1992), 114, 147-163.

7) T. Lepage, C. Ghiglione, C. Gache, Structure of the gene encoding the sea urchin blastula protease 10 (BP10), a member of the astacin family of Zn^{2+}-metalloproteases. *Eur. J. Biochem*. (1996), 238, 744-751.

8) E. Appella, I.T. Weber, F. Blasi, F. Structure and function of epidermal growth factor-like regions in proteins. *FEBS letters*, (1988), 231, 1-4.

9) N. Hartigan, L. Garrigue-Antar, K.E. Kadler, Bone Morphogenetic Protein-1 (BMP-1). *J. Biol. Chem*. (2003), 278, 18045-18049.

10) M.D. Sternlicht, Z. Werb, How matrix metalloproteinases regulate cell behavior. *Cell. Dev. Biol.* (2001), 17, 463-516.

11) K. Imai, M. Kusakabe, T. Sakakura, I. Nakanishiki, Y. Okada, Susceptibility of tenascin to degradation by matrix metalloproteinases and serine proteinases. *FEBS Lett.* (1994), 352, 216-218.

12) O. Vafa, D. Nishioka, Developmentally regulated protease expression during sea urchin embryogenesis. *Mol. Reprod. Dev.* (1995), 40, 36-47.

13) G. Karakiulakis, E. Papakonstantinou, M.E. Maragoudakis, G.N. Miservic, Expression of type IV collagen-degrading activity during early embryonal development in the sea urchin and the arresting effects of collagen synthesis inhibitors on embryogenesis. *J. Cell. Biochem.* (1993), 52, 92-106.

14) J.P. Quigley, R.S. Braithwaite, P.B. Armstrong, Matrix metalloproteases of the developing sea urchin embryo. *Differentiation* (1993), 54, 19-23.

15) C. Sharpe, J.J. Robinson, Characterization of matrix metalloprotease activities induced in the sea urchin extraembryonic matrix, the hyaline layer. *Biochem. Cell. Biol.* (2001), 79, 461-468.

16) W. Stöcker, F. Grams, U. Baumann, P. Reinemer, F.X. Gomis-Rüth, D.B. McKay, W. Bode, The metzincins - topological and sequential relations between the astacins, adamalysins, serralysins, and matrixins (collagenases) define a superfamily of zinc-peptidases. *Prot. Sci.* (1995), 4, 823-840.

17) E. Kimura, Macrocyclic polyamine zinc(II) complexes as advanced models for zinc(II) enzymes. *Prog. Inorg. Chem*. (1994), 41, 443.

18) E. Kimura, T. Koike, Intrinsic properties of zinc(II) ion pertinent to zinc enzymes. *Adv. Inorg. Chem*. (1997), 44, 229.

19) H.I. Park, L.-J. Ming, The mechanistic role of the coordinated tyrosine in astacin. *J. Inorg. Biochem.* (1998), 72, 57-62.

20) Y.-H. Chen, J.T. Yang, H.M. Martinez, Determination of the secondary structures of proteins by circular dichroism and optical rotatory dispersion. *Biochemistry* (1972), 11, 4120-4131.

21) G. Murphy, T. Crabbe, Gelatinases A and B. *Methods in Enzymology* (1995) 248, 470-475.

22) U.K. Laemmli, Cleavage of structural proteins during the assembly of the head of bacteriophage T4. *Nature* (1970), 227, 680-685.

23) J.D. Grubb, Purification and assays of bacterial gelatinases. *Methods in Ezymology*, (1994), 235, 602-606.

24) M. Friedman, Applications of the ninhydrin reaction for analysis of amino acids, peptides, and proteins to agricultural and biomedical sciences. *J. Agric. Food Chem.* (2004), 52, 385-406.

25) A.L. Sieron, A.S. Tretiakova, S. Lund-Katz, M.T. Khan, S.-W. Li, W. Stöcker. Structure and Function of Procollagen C-Proteinase (mTolloid) Domains Determined by Protease Digestion, Circular Dichroism, Binding to Procollagen Type I, and Computer Modeling. *Biochemistry* (2000), 39, 3231-3239.

26) J. Mayne, J.J. Robisnon, Calcium-protein interactions in the extracellular environment: calcium binding, activation, and immunolocalization of a collagenase/gelatinase activity expressed in the sea urchin embryo. *J. Cell. Biochem.* (1998), 71, 546-558.

27) C. Calloway, C. Sharpe, J.J. Robinson, Identification and partial characterization of two inducible gelatin-cleavage activities localized to the sea urchin extraembryonic matrix, the hyaline layer. *Biochim. Biophys. Acta* (2003), 1621, 67-75.

28) A. Cornish-Bowden, *Fundamentals of Enzyme Kinetics*, Portland Press, London (1995).

29) I. Bertini, H.B. Gray, S.J. Lippard, J.S. Valentine, (eds) *Bioinorganic Chemistry*, Chap. 2., University Science Books, Sausalito, CA (1994).

30) E.L. Hegg, J.N. Burstyn, Toward the development of metal-based synthetic nucleases and peptidases: a rationale and progress report in applying the principles of coordination chemistry. *Coord. Chem. Rev.* (1998), 173, 133-165.

31) S.T. Frey, N.N. Murthy, S.T. Weintraub, L.K. Thompson, K.D. Karlin, Hydrolysis of Unactivated Esters and Acetonitrile Hydration by a Hydroxo-Dicopper(II) Complex. *Inorg. Chem.* (1997), 36, 956-957.

32) V. Lykourinou-Tibbs, K. Bisht, L.-J. Ming, Effective heterogeneous hydrolysis of phosphodiester by pyridine-containing metallopolymers. *Inorg. Chim. Acta.* (2005), 358, 1247-1252.

33) E. Kimura, T. Koike, Intrinsic properties of zinc(II) ion pertinent to zinc enzymes *Adv. Inorg. Chem.* (1997), 44, 229-261.

34) F.X. Gomis-Rüth, F. Grams, I. Yiallouros, H. Nar, U. Küsthardt, R. Zwilling, W. Bode, W. Stöcker, Crystal structures, spectroscopic features, and catalytic properties of cobalt(II), copper(II), nickel(II), and mercury(II) derivatives of the zinc endopeptidase astacin. A correlation of structure and proteolytic activity. *J. Biol.Chem.* (1994), 269, 17111-17117.

35) B.W. Matthews, Metalloaminopeptidases: Common functional themes in disparate structural surroundings. *Acc. Chem. Res.* (1998), 21, 333-340.

36) J. Cha, D.S. Auld, Site-directed mutagenesis of the active site glutamate in human matrilysin: Investigation of its role in catalysis. *Biochemistry* (1997), 36, 16019-16024.

37) D.W. Christianson, W.N. Lipscomb, Carboxypeptidase A. *Acc. Chem. Res.* (1989), 22, 62-69.

ABOUT THE AUTHOR

Giordano F.Z. da Silva was born in 1977 in the city of Rio de Janeiro, Brazil. Giordano graduated Magna Cum Laude from St. Petersburg High School and attended St. Petersburg Junior College, graduating Magna Cum Laude in 1998 with an Associate of Arts degree with emphasis in the natural sciences. In 1999 he enrolled at the University of South Florida and graduated in 2002 with a Bachelor of Arts. Giordano joined the graduate program in the Chemistry Department at USF in 2002 working in Dr. Li-June Ming's **M**etallo**B**iomolecule **I**nterest **G**roup (MBIG) and Dr. Brian T. Livingston in the Department of Biology. In the five years in the graduate program Giordano has presented his work at the local, state, national, and international levels; taught a bioinorganic workshop at the National Chiayi University in Taiwan; published peer-reviewed top-tier journal articles, and received several awards, including the Theodore Ashford and George Bursa departmental awards and the USF Successful Latino Award.